8-2009

Novel Techniques for The Synthesis of Three-Way Catalytic Converter Support Materials

Prince Anyaba
Clemson University, panyaba@clemson.edu

NOVEL TECHNIQUES FOR THE SYNTHESIS OF THREE-WAY CATALYTIC CONVERTER SUPPORT MATERIALS

A Dissertation
Presented to
the Graduate School of
Clemson University

In Partial Fulfillment
of the Requirements for the Degree
Doctor of Philosophy
Chemical Engineering

---

by
Prince Nwabueze Anyaba
August 2009

Accepted by:
Dr. David A. Bruce, Committee Chair
Dr. Christopher L. Kitchens
Dr. Scott M. Husson
Dr. Stephen E. Creager

ABSTRACT

Current automobiles use catalytic converters, consisting of noble metals on an oxide support, to convert noxious engine exhaust pollutants into less harmful species. The development of mesoporous oxide supports with optimal pore geometries could enable these devises to decrease in size and weight and significantly reduce the metal loadings required to achieve optimal performance. Thus, in this work, I investigated a wide range of techniques for the synthesis of mesoporous oxides to determine if they could be adapted to ceria-zirconia-yttria mixed oxide (CZY) systems, which are the industry standard for the optimal oxide support for catalytic converter applications. Additionally, I compared and critically evaluated the catalytic performance of the CZY mixed oxides, which were synthesized from the various templating techniques. The catalytic performance test was broken up into two: catalyst activity test which was determined based on the light-off temperatures at which 50% conversion of the reacting species have been converted; and resistance to surface area loss under accelerated aging at heating rate of 20 ºC/min form 700 to 1000 ºC, with the final temperature being held fixed for 4 h.

To date, the most cost effective methods for preparing mesoporous materials are via techniques that employ templates or structure directing agents. These templates can be divided into two groups: endo-templates (i.e., soft templates, such as surfactants, dendrimers, and block copolymers) and exo-templates (i.e., hard templates, such as porous carbons and resins). The soft templating techniques generally involve both sol-gel and templating methods, while the hard templates required no sol-gel chemistry to achieve the desired templating effect. The precursors for ceria, zirconia, and yttria used

were cerium (III) nitrate hexahydrate, zirconyl nitrate, and yttrium nitrate hexahydrate, respectively. The mesoporous CZY materials that were synthesized had surface area values that were between 40 and 120 m^2/g and pore diameters that range from 2.2 to 9.0 nm after calcination in air from ambient temperature to 600 °C at heating rates varied from 1 to 20 °C /min, with the final temperature being maintained for 4 h.

The novel CZY oxides that were prepared from the different templating techniques were characterized using nitrogen physisorption to determine the Brunauer–Emmett–Teller (BET) surface area and the Barrett–Joyner–Halenda (BJH) pore size distribution. Samples that showed some promise were further examined by transmission electron microscopy (TEM) to study the morphology of the structure; scanning electron microscopy (SEM) to study the bulk surface structure; thermogravimetric analysis (TGA) and differential scanning calorimetry (DSC) to determine physical and chemical changes occurring during calcination; elemental analysis to determine composition; powder X-ray diffraction (PXD) to determine the existence of crystalline structure; and small angle X-ray diffraction (SAXD) to determine the occurrence of mesoscale ordering of repeating units. Finally, selected samples underwent catalytic testing under simulated exhaust conditions. The results of the tests showed that CZY materials synthesized using sol-gel methods with the Pluronic P123 soft template were the most active (i.e., had the lowest light off temperature), while CZY material with least loss of surface area after accelerated aging from 700 to1000 ºC was the polymeric resin templated CZY materials.

DEDICATION

This work is dedicated to the triune God for guidance, providence, mercies, and grace in my life; to my parents, all my siblings, my wife, uncles and aunties for all their love, support, prayers, and constant encouragement.

ACKNOWLEDGMENTS

My profound gratitude goes to the following for all their contributions in one way or the other towards the completion of my studies. I would like to acknowledge Dr. J.U. Nwalor for believing in me and encouraging me persistently to pursue graduate studies; Dr. K.J. Abiola, for his support in no small measure; Prof. C.T. Ako for his guidance and moral support; and to all the staff and faculty of the Department of Chemical Engineering, University of Lagos, Nigeria for helping me in laying a solid foundation for my professional life.

I am highly indebted to my colleagues, faculty and staff at the Department of Chemical and Biomolecular Engineering, Clemson University, Clemson, South Carolina, for all their support. I am especially grateful to Drs. R.W. Rice, S.M. Husson, G. Harrison, and Prof. J.G. Goodwin, Jr. for the great learning experience at Clemson University. To my wonderful advisor, Dr. David A. Bruce, I would like to say a big thank you for affording me this wonderful opportunity to work on this project and for his support and guidance through it all. To members of my dissertation committee: Drs. S.M. Husson, C.L Kitchens, and S.E. Creager thank you for your support and guidance while I was working on this dissertation.

Lastly, I would like to say thank you to Drs. Paul Fanson and Benjamin Grayson for all their useful suggestions and comments during the experimental stage of the work; and also to Toyota Motor Engineering & Manufacturing North America, Inc. for providing the funds for this project

TABLE OF CONTENTS

Page

TITLE PAGE i

ABSTRACT ii

DEDICATION iv

ACKNOWLEDGMENTS v

LIST OF TABLES ix

LIST OF FIGURES xii

CHAPTER

I. INTRODUCTION 1

II. LITERATURE REVIEW 4

General Applications of Ceria, Zirconia, and Yttria Base Materials 4
Ceria-Zirconia-Yttria Mixed Oxide (CZY) Materials for Automotive Three Way Catalytic Converter Applications 5
Synthesis Techniques for Mesoporous Oxides Materials 9

III. SURFACTANT TEMPLATE TECHNIQUE 16

Synthesis Strategy for Making CZY Mixed oxides Using Surfactant Template Technique 17
Synthesis of CZY Mixed Oxides Using CTAB Template 21
Synthesis of CZY Mixed Oxides Using CTAB/Cosolvent Template 25
Synthesis of CZY Mixed Oxides Using CTAB/Cosolvent/Swelling Agent Template 27
Experimental Methods for Characterizing CZY Mixed Oxides 29
Results and Discussion 30
Conclusion 66

Table of Contents (Continued)

Page

IV. BLOCK COPLOYMER TEMPLATE TECHNIQUE 69

Synthesis Strategy for Making CZY Mixed Oxides Using Surfactant Template Technique 69
Synthesis of CZY Mixed Oxides Using Pluronic P123 Template 71
Results and Discussion 73
Conclusion 92

V. DENDRIMER TEMPLATE TECHNIQUE 94

Synthesis Strategy for Making CZY Using Dendrimer Template Technique 94
Synthesis of CZY Mixed Oxides Using DAB-Am-n Template 96
Results and Discussion 98
Conclusion 112

VI. ACTIVATED CARBON TEMPLATE TECHNIQUE 113

Synthesis Strategy for Making CZY Using Activated Carbon Template Technique 114
Synthesis of CZY Mixed Oxides Using Activated Carbon Template 117
Results and Discussion 119
Conclusion 135

VII. POLYMERIC RESIN TEMPLATE TECHNIQUE 137

Synthesis Strategy for Making CZY Using Polymeric Resin Template Technique 138
Synthesis of CZY Mixed Oxides Using Polymeric Resin Template 140
Results and Discussion 142
Conclusion 155

Table of Contents (Continued)

Page

VIII. EVALUATION OF THE CATALYTIC PERFORMANCE OF THE CZY SAMPLES 156

Methods for Catalytic Performance Evaluation 158
Results and Discussion 160
Conclusion 178

IX. CONCLUSIONS AND RECOMMENDATIONS 179

Conclusions 179
Recommendations 181

REFERENCES 182

VITA 190

LIST OF TABLES

Table		Page
3.1	Typical sample composition of CTAB templated CZY	22
3.2	Typical sample composition of CTAB/1-propanol templated CZY	26
3.3	Typical sample composition for CTAB/1-propanol/benzene templated CZY	28
3.4	Effect of calcination heating rate on the surface area and pore diameter of CTAB templated CZY samples that were calcined in air from 25 to 600 ºC with the final temperature being maintained for 4 h	37
3.5	Effect of synthesis temperature on the physical properties of CTAB templated CZY samples that were calcined in air from 25 to 600 ºC with the final temperature being maintained for 4 h	42
3.6	Effect of varying pH on the surface area and pore diameter of CTAB templated CZY samples that were calcined in air from 25 to 600 °C at a heating rate of 20 ºC/min, with the final temperature being maintained for 4 h	44
3.7	Effect of hydrolysis retarding agents on the surface area and pore diameter of CTAB templated CZY samples. Samples were calcined in air from 25 to 600 °C at a heating rate of 20 ºC/min, with the final temperature being maintained for 4 h	46
3.8	Elemental composition of CTAB templated CZY samples	54
3.9	Variation of surface area and pore volume as a function of aging temperature for CTAB templated CZY samples. Samples were calcined in air to the specified temperature at a heating rate of 20 ºC/min, with the final temperature being maintained for 4 h	63
4.1	Typical sample composition for P123 Templated CZY	71

List of Tables (Continued)

Table Page

4.2 Effect of calcination heating rate on the surface area and pore diameter of Pluronic P123 templated CZY samples that were calcined in air from 25 to 600 ºC with the final temperature being maintained for 4 h 76

4.3 Effect of hydrolysis retarding agents on the surface area and pore diameter of Pluronic P123 templated CZY samples. Samples were calcined in air from 25 to 600 °C at a heating rate of 20 ºC/min, with the final temperature being maintained for 4 h 82

4.4 Elemental composition of Pluronic P123 templated CZY 83

4.5 Variation of surface area and pore volume as a function of aging temperature for Pluronic P123 templated CZY samples. Samples were calcined in air to the specified temperature at a heating rate of 20 ºC/min, with the final temperature being maintained for 4 h 90

5.1 Typical sample composition for DAB-Am-32 Templated CZY 96

5.2 Typical sample composition for DAB-Am-64 templated CZY 97

5.3 Surface area and pore diameter of DAB-Am-n templated CZY samples. Samples were calcined in air from 25 to 600 ºC at a heating rate of 20 ºC/min, with the final temperature being maintained for 4 h 102

5.4 Elemental composition of dendrimer templated CZY 107

5.5 Variation of surface area and pore volume as a function of aging temperature for DAB-Am-32 templated CZY samples. Samples were calcined in air to the specified temperature at a heating rate of 20 ºC/min, with the final temperature being maintained for 4 h 110

6.1 Typical sample composition for activated carbon templated CZY 118

List of Tables (Continued)

Table Page

6.2 Effect of calcination heating rate on the surface area and pore diameter of activated carbon templated CZY samples that were calcined in air from 25 to 600 ºC with the final temperature being maintained for 4 h 124

6.3 Effect of varying precursor concentration on the surface area and pore diameter of activated carbon templated CZY samples. Samples were calcined in air from 25 to 600 ºC at a heating rate of 20 ºC/min, with the final temperature being maintained for 4 h 130

6.4 Elemental composition of activated carbon templated CZY 131

6.5 Variation of surface area and pore volume as a function of aging temperature for activated carbon templated CZY samples. Samples were calcined in air to the specified temperature at a heating rate of 20 ºC/min, with the final temperature being maintained for 4 h 131

7.1 Typical sample composition for polymeric resin templated CZY 140

7.2 Effect of calcination heating rate on the surface area and pore diameter of polymeric resin templated CZY samples that were calcined in air from 25 to 600 ºC with the final temperature being maintained for 4 h 147

7.3 Elemental composition of polymeric resin templated CZY 150

7.4 Variation of surface area and pore volume as a function of aging temperature for polymeric resin templated CZY samples. Samples were calcined in air to the specified temperature at a heating rate of 20 ºC/min, with the final temperature being maintained for 4 h 151

8.1 Effect of thermal aging on the BET surface area and average BJH pore diameter of CZY samples synthesized from various templates. Samples were calcined in air to the specified temperature at a heating rate of 20 ºC/min, with the final temperature being maintained for 4 h 165

LIST OF FIGURES

Figure Page

2.1 Simultaneous catalytic conversions of CO, C_xH_y, and NO_x versus air-fuel ratio in a standard three-way catalytic converter 7

2.2 Mechanistic pathways for the synthesis of MCM-41 type silica based mesoporous oxides. 9

2.3 Illustration of pore generation in an endotemplating technique for synthesizing mesoporous materials using soft templates (e.g. dendrimer)..... 12

2.4 Illustration of pore generation in an exotemplating technique for synthesizing mesoporous materials using hard templates (e.g. activated carbon)..... 13

3.1 Synthesis procedures for mesoporous CZY mixed oxides using Surfactant template 18

3.2 Possible mechanistic pathways for surfactant templated CZY materials. The surfactants are the filled dots with tails..... 24

3.3 Possible mechanistic pathways for surfactant-cosolvent templated CZY The smaller filled dot with shorter tails represents the cosolvent species..... 26

3.4 Possible mechanistic pathways for surfactant-cosolvent-swelling agent templated CZY. The smaller filled dot with shorter tails represents the cosolvent species, while the swelling agents are depicted as tial-less dots that end up in the core of the micellar structure 29

3.5 Differential heat flow to an as-synthesized CZY sample prepared using no SDA upon heating from near ambient temperatures to 600 ºC at different heating rates in a constant flow of air 32

3.6 Thermogravimetric analysis of as-synthesized CZY sample prepared using no SDA upon heating from near ambient temperatures to 600 ºC at heating rates that ranged from 1 to 20 ºC/min 33

List of Figures (Continued)

Figure Page

3.7 Differential heat flow to an as-synthesized CZY sample prepared using CTAB alone as SDA upon heating from near ambient temperatures to 600 ºC at different heating rates in a constant flow of air 34

3.8 Thermogravimetric analysis of as-synthesized CZY sample prepared using CTAB alone as SDA upon heating from near ambient temperatures to 600 ºC at heating rates that ranged from 1 to 20 ºC/min 35

3.9 Nitrogen adsorption (■) /desorption (▲) isotherms and BJH pore size distribution (inset) for a calcined CZY sample prepared using the CTAB template. The sample was calcined in air from 25 to 600 °C at a heating rate of 20 ºC /min, with the final temperature being maintained for 4 h 39

3.10 Nitrogen adsorption (■) /desorption (▲) isotherms and BJH pore size distribution (inset) for a calcined CZY sample prepared using the CTAB/1-propanol template. The sample was calcined in air from 25 to 600 °C at a heating rate of 20 ºC /min, with the final temperature being maintained for 4 h 40

3.11 Nitrogen adsorption (■) /desorption (▲) isotherms and BJH pore size distribution (inset) for a calcined CZY sample prepared using the CTAB/1-propanol/benzene template. The sample was calcined in air from 25 to 600 °C at a heating rate of 20 ºC /min, with the final temperature being maintained for 4 h 41

3.12 Nitrogen adsorption (■) /desorption (▲) isotherms and BJH pore size distribution (inset) for a calcined CZY sample prepared using the CTAB/ACAC template. The sample was calcined in air from 25 to 600 °C at a heating rate of 20 ºC /min, with the final temperature being maintained for 4 h. 48

3.13 Nitrogen adsorption (■) /desorption (▲) isotherms and BJH pore size distribution (inset) for a calcined CZY sample prepared using the CTAB/TEA template. The sample was calcined in air from 25 to 600 °C at a heating rate of 20 ºC /min, with the final temperature being maintained for 4 h. 49

List of Figures (Continued)

Figure Page

3.14 Powder X-ray diffractogram for pure samples of ceria, zirconia, and yttria oxides. Samples were calcined in air from 25 to 600 °C at a heating rate of 20 ºC/min, with the final temperature being maintained for 4 h 51

3.15 Powder X-ray diffractogram for CZY samples prepared using CTAB alone, CTAB/1-propanol, and CTAB/1-propanol/benzene. Samples were calcined in air from 25 to 600 °C at a heating rate of 20 ºC/min, with the final temperature being maintained for 4 h 52

3.16 Powder X-ray diffractogram for CZY samples prepared using CTAB alone, CTAB/ACAC, and CTAB/TEA. Samples were calcined in air from 25 to 600 °C at a heating rate of 20 ºC/min, with the final temperature being maintained for 4 h 53

3.17 Transmission electron micrographs for a calcined CZY mixed oxide prepared using CTAB as the sol gel template. Samples were calcined in air from 25 to 600 °C at a heating rate of 20 ºC/min, with the final temperature being maintained for 4 h 56

3.18 Transmission electron micrographs for a calcined CZY mixed oxide prepared using CTAB/1-propanol as the sol gel template. Samples were calcined in air from 25 to 600 °C at a heating rate of 20 ºC/min, with the final temperature being maintained for 4 h 57

3.19 Transmission electron micrographs of a calcined CZY mixed oxide prepared using CTAB/1-propanol/benzene as the sol-gel template. Samples were calcined in air from 25 to 600 °C at a heating rate of 20 ºC/min, with the final temperature being maintained for 4 h 58

3.20 Transmission electron micrographs for a calcined CZY mixed oxide prepared using CTAB as the sol gel template and ACAC as the hydrolysis retarding agent. Samples were calcined in air from 25 to 600 °C at a heating rate of 20 ºC/min, with the final temperature being maintained for 4 h 59

List of Figures (Continued)

Figure Page

3.21 Transmission electron micrographs for a calcined CZY mixed oxide prepared using CTAB as the sol gel template and TEA as the hydrolysis retarding agent. Samples were calcined in air from 25 to 600 °C at a heating rate of 20 ºC/min, with the final temperature being maintained for 4 h 60

3.22 Proposed mechanistic pathways for CZY mixed oxides prepared via sol gel technique that employ the CTAB surfactant template 62

3.23 Powder X-ray diffractogram (PXD) for CTAB templated CZY samples. Samples were calcined in air to the specified temperature at a heating rate of 20 ºC/min, with the final temperature being maintained for 4 h 65

3.24 Proposed structure for all CZY mixed oxides materials prepared via sol gel techniques that employ CTAB surfactant template 67

4.1 Mechanistic pathways for block copolymer templated CZY synthesis. 72

4.2 Thermogravimetric analysis of as-synthesized CZY sample prepared using Pluronic P123 SDA upon heating from near ambient temperatures to 600 ºC at different heating rates in a constant flow of air. 73

43 Differential heat flow to an as-synthesized CZY sample prepared using Pluronic P123 alone as the SDA upon being heated in air from near ambient temperatures to 600 ºC, at heating rates that ranged from 1 to 20 °C/min 74

4.4 Nitrogen adsorption (■) /desorption (▲) isotherms and BJH pore size distribution (inset) for a calcined CZY sample prepared using the Pluronic P123 template. The sample was calcined in air from 25 to 600 °C at a heating rate of 20 ºC /min, with the final temperature being maintained for 4 h 79

List of Figures (Continued)

Figure Page

4.5 Nitrogen adsorption (■) /desorption (▲) isotherms and BJH pore size distribution (inset) for a calcined CZY sample prepared using the Pluronic P123/ACAC template. The sample was calcined in air from 25 to 600 °C at a heating rate of 20 ºC /min, with the final temperature being maintained for 4 h 80

4.6 Nitrogen adsorption (■) /desorption (▲) isotherms and BJH pore size distribution (inset) for a calcined CZY sample prepared using the Pluronic P123/TEA template. The sample was calcined in air from 25 to 600 °C at a heating rate of 20 ºC /min, with the final temperature being maintained for 4 h 81

4.7 Powder X-ray diffractogram (PXD) for CZY prepared using Pluronic P123 alone, Pluronic P123/ACAC, and Pluronic P123/TEA. Sample were calcined in air from 25 to 600 °C at a heating rate of 20 ºC /min, with the final temperature being maintained for 4 h 84

4.8 Transmission electron micrographs of a calcined CZY mixed oxide prepared using Pluronic P123 block copolymer as the sol gel template Samples were calcined in air from 25 to 600 °C at a heating rate of 20 ºC/min, with the final temperature being maintained for 4 h 86

4.9 Transmission electron micrographs of a calcined CZY mixed oxide prepared using Pluronic P123 block copolymer as the sol gel template and TEA as the hydrolysis retarding agent. Samples were calcined in air from 25 to 600 °C at a heating rate of 20 ºC/min, with the final temperature being maintained for 4 h 87

4.10 Transmission electron micrographs of a calcined CZY mixed oxide prepared using Pluronic P123 block copolymer as the sol gel template and ACAC as the hydrolysis retarding agent. Samples were calcined in air from 25 to 600 °C at a heating rate of 20 ºC/min, with the final temperature being maintained for 4 h 88

4.11 Powder X-ray diffractogram (PXD) for Pluronic P123 templated CZY samples. Samples were calcined in air to the specified temperature at a heating rate of 20 ºC/min, with the final temperature being maintained for 4 h 91

List of Figures (Continued)

Figure Page

5.1 Mechanistic pathway for dendrimer templated CZY synthesis 98

5.2 Thermogravimetric analysis of as-synthesized CZY sample prepared using DAB-Am-32 dendrimer as SDA upon heating from near ambient temperatures to 600 ºC at different heating rates in a constant flow of air. 99

5.3 Differential heat flow to as-synthesized CZY sample prepared using DAB-Am-32 dendrimer as the SDA upon heating from near ambient temperatures to 600 ºC at different heating rates in a constant flow of air 100

5.4 Nitrogen adsorption (■) /desorption (▲) isotherms and BJH pore size distribution (inset) for a calcined CZY sample prepared using the DAB-Am-32 template. The sample was calcined in air from 25 to 600 °C at a heating rate of 20 ºC /min, with the final temperature being maintained for 4 h. 104

5.5 Nitrogen adsorption (■) /desorption (▲) isotherms and BJH pore size distribution (inset) for a calcined CZY sample prepared using the DAB-Am-64 template. The sample was calcined in air from 25 to 600 °C at a heating rate of 20 ºC /min, with the final temperature being maintained for 4 h. 105

5.6 Powder X-ray diffractogram (PXD) for CZY prepared using DAB-Am-32 and DAB-Am-64 templates. Sample were calcined in air from 25 to 600 °C at a heating rate of 20 ºC /min, with the final temperature being maintained for 4 h 106

5.7 Transmission electron micrographs of a calcined CZY mixed oxide prepared using DAB-Am-32 dendrimer as the sol gel template Samples were calcined in air from 25 to 600 °C at a heating rate of 20 ºC/min, with the final temperature being maintained for 4 h 108

5.8 Transmission electron micrographs of a calcined CZY mixed oxide prepared using DAB-Am-64 dendrimer as the sol gel template Samples were calcined in air from 25 to 600 °C at a heating rate of 20 ºC/min, with the final temperature being maintained for 4 h 109

List of Figures (Continued)

Figure Page

5.9 Powder X-ray diffractogram (PXD) for DAB-Am-32 templated CZY samples. Samples were calcined in air to the specified temperature at a heating rate of 20 ºC/min, with the final temperature being maintained for 4 h 111

6.1 The mechanism for creating the pore structure for activated carbon templated porous oxides..... 115

6.2 Schematic representation of the synthesis steps for making non-siliceous mesoporous materials using activated carbon template 116

6.3 Thermogravimetric analysis of as-synthesized CZY sample prepared using activated carbon as SDA upon heating from near ambient temperatures to 1000 ºC at different heating rates in a constant flow of air. 120

6.4 Differential heat flow to as-synthesized CZY sample prepared using activated carbon as the SDA upon heating from near ambient temperatures to 1000 ºC at different heating rates in a constant flow of air..... 121

6.5 Nitrogen adsorption (■) /desorption (▲) isotherms and BJH pore size distribution (inset) for a calcined activated carbon templated CZY sample prepared using 0.50 M solution of precursors. The sample was calcined in air from 25 to 600 °C at a heating rate of 20 ºC /min, with the final temperature being maintained for 4 h 125

6.6 Nitrogen adsorption (■) /desorption (▲) isotherms and BJH pore size distribution (inset) for a calcined activated carbon templated CZY sample prepared using 1.00 M solution of precursors. The sample was calcined in air from 25 to 600 °C at a heating rate of 20 ºC /min, with the final temperature being maintained for 4 h..... 126

6.7 Nitrogen adsorption (■) /desorption (▲) isotherms and BJH pore size distribution (inset) for a calcined activated carbon templated CZY sample prepared using 1.50 M solution of precursors. The sample was calcined in air from 25 to 600 °C at a heating rate of 20 ºC /min, with the final temperature being maintained for 4 h 127

List of Figures (Continued)

Figure Page

6.8 Powder X-ray diffractogram (PXD) for activated carbon templated CZY prepared using 0.5 M, 1.0 M, and 1.5 M solution of precursor salts. Sample were calcined in air from 25 to 600 °C at a heating rate of 20 ºC /min, with the final temperature being maintained for 4 h 129

6.9 Powder X-ray diffractogram (PXD) for activated carbon templated CZY samples. Samples were calcined in air to the specified temperature at a heating rate of 20 ºC/min, with the final temperature being maintained for 4 h 133

6.10 Transmission electron micrographs of a calcined CZY mixed oxide prepared using activated carbon template. Samples were calcined in air from 25 to 600 °C at a heating rate of 20 ºC/min, with the final temperature being maintained for 4 h 134

7.1 Schematic representation of the synthesis procedure for non-siliceous mesoporous materials prepared using polymeric resin template. 138

7.2 Illustration of the synthesis steps for preparing polymeric resin templated non-siliceous mesoporous materials 139

7.3 Photograph of polymeric resin templated CZY material after calcination in air at 600 ºC for 4 h at a heating rate of 20 ºC/min with a penny as the reference scales. The mesoporous CZY materials are approximately spherical in shape with a lot of broken fragments 141

7.4 Thermogravimetric analysis of as-synthesized CZY sample prepared using polymeric resin as SDA upon heating from near ambient temperatures to 1000 ºC at different heating rates in a constant flow of air. 143

7.5 Differential heat flow to an as-synthesized CZY sample prepared using polymeric resin as the SDA upon heating from near ambient temperatures to 1000 ºC at different heating rates in a constant flow of air..... 144

List of Figures (Continued)

Figure Page

7.6 Nitrogen adsorption (■) /desorption (▲) isotherms and BJH pore size distribution (inset) for a calcined CZY sample prepared using polymeric resin template. The sample was calcined in air from 25 to 600 °C at a heating rate of 20 ºC /min, with the final temperature being maintained for 4 h. 148

7.7 Powder X-ray diffractogram (PXD) for CZY synthesized using polymeric resin. Samples were calcined in air from 25 to 600 °C at a heating rate of 20 ºC/min, with the final temperature being maintained for 4 h 149

7.8 Powder X-ray diffractogram (PXD) for polymeric resin templated CZY samples. Samples were calcined in air to the specified temperature at a heating rate of 20 ºC/min, with the final temperature being maintained for 4 h 152

7.9 Transmission electron micrographs of a calcined CZY mixed oxide prepared using polymeric resin template. Samples were calcined in air from 25 to 600 °C at a heating rate of 20 ºC/min, with the final temperature being maintained for 4 h 153

7.10 Mechanistic pathway for pore generation within polymeric resin templated mesoporous CZY mixed oxides 154

8.1 Plot of conversion versus temperature for NO_x, C_xH_y, and CO reactant species 158

8.2 NO_x , C_xH_y, and CO light-off temperature for different templated CZY materials after aging in air at 800 ºC 161

8.3 Correlation between light-off temperature, T_{50} (catalytic activity) and surface area of CZY catalyst support system 162

8.4 Correlation between light-off temperature, T_{50} (catalytic activity) and pore size of CZY catalyst support system. 163

8.5 Pore size variation with aging temperatures for CZY mixed oxides 166

8.6 Surface area variation with aging temperatures for CZY mixed oxides 167

List of Figures (Continued)

Figure Page

8.7 Nitrogen adsorption-desorption isotherms of CTAB templated CZY mixed oxides during thermal aging. Samples were aged in air to the specified temperature at a heating rate of 20 ºC/min, with the final temperature being maintained for 4 h 168

8.8 BJH pore size distribution of CTAB templated CZY mixed oxides during thermal aging. Samples were aged in air to the specific temperature at a heating rate of 20 ºC/min, with the final temperature being maintained for 4 h 169

8.9 Nitrogen adsorption-desorption isotherms of Pluronic P123 templated CZY mixed oxides during thermal aging. Samples were aged in air to the specified temperature at a heating rate of 20 ºC/min, with the final temperature being maintained for 4 h 170

8.10 BJH pore size distribution of Pluronic P123 templated CZY mixed oxides during thermal aging. Samples were aged in air to the specific temperature at a heating rate of 20 ºC/min, with the final temperature being maintained for 4 h 171

8.11 Nitrogen adsorption-desorption isotherms of DAB-Am-32 templated CZY mixed oxides during thermal aging. Samples were aged in air to the specified temperature at a heating rate of 20 ºC/min, with the final temperature being maintained for 4 h 172

8.12 BJH pore size distribution of DAB-Am-32 templated CZY mixed oxides during thermal aging. Samples were aged in air to the specific temperature at a heating rate of 20 ºC/min, with the final temperature being maintained for 4 h 173

8.13 Nitrogen adsorption-desorption isotherms of activated carbon templated CZY mixed oxides during thermal aging. Samples were aged in air to the specified temperature at a heating rate of 20 ºC/min, with the final temperature being maintained for 4 h 174

8.14 BJH pore size distribution of activated carbon templated CZY mixed Oxides during thermal aging. Samples were aged in air to the specific temperature at a heating rate of 20 ºC/min, with the final temperature being maintained for 4 h 175

List of Figures (Continued)

Figure Page

8.15 Nitrogen adsorption-desorption isotherms of polymeric resin templated CZY mixed oxides during thermal aging. Samples were aged in air to the specified temperature at a heating rate of 20 ºC/min, with the final temperature being maintained for 4 h 176

8.16 BJH pore size distribution of polymeric resin templated CZY mixed oxides during thermal aging. Samples were aged in air to the specific temperature at a heating rate of 20 ºC/min, with the final temperature being maintained for 4 h 177

9.1 Agglomeration of oxide particles into (a) closed packed arrangement and other (b) more open secondary structures. 180

CHAPTER ONE

INTRODUCTION

High surface area mesoporous ceria and zirconia based oxides continue to be in great demand for applications that include emissions abatement, solid oxide fuel cells, electronics, sensors and catalysis. Despite this demand, significant challenges in the area of materials synthesis have limited the availability of materials that are optimally suited for these varied applications. Though the ground breaking work of researchers at the Mobil Research and Development in the early 1990s and subsequent advances in the synthesis of mesoporous silica based oxides might lead a novice to suspect that these materials could be easily prepared, progress in the synthesis of mesoporous non-silica based oxides has left much to be desired. This is not to say there has not been progress made in the last almost two decades or so, but there is great room for improvement indeed.

In this work, I do not attempt to fully chronicle the advances that have been made in porous material synthesis thus far, but instead my focus is two-fold: first, I want to bring to the fore the published techniques that exist for the synthesis of mesoporous non-silica based oxides; second, I also want to highlight ways in which the draw backs that hinder the successful synthesis of mesoporous non-silica based oxides can be mitigated.

To date, the most cost effective methods for preparing mesoporous oxide materials are via solution or sol-gel techniques that employ organic templates or structure directing agents. These templates can be divided into two groups: endo-templates (i.e., soft templates, such as surfactants, dendrimers, and block copolymers) and exo-templates

(i.e., hard templates, such as porous carbons and resins). With all of these templates, mesoporous oxides are prepared via solvothermal processes that involve heating mixtures of the template with soluble oxide precursors, often salts, solvents (e.g., water or alcohols) and/or an acid or base hydrolyzing agent. The result of this thermal treatment is the formation of porous oxides.

The major draw backs associated with the synthesis of mesoporous non-silica based oxides are rapid metal oxide crystallization, very rapid rates of hydrolysis during the sol-gel process that do not allow for the self-assembly of the supramolecular templates to occur in sync with the condensation of the metal oxides, and lastly, the rapid collapse of the mesostructure upon heating to temperatures of 800 °C or higher

This work provides a unique opportunity to compare and critically evaluate the effectiveness of all known methods for synthesizing highly stable mesoporous ceria-zirconia-yttria (CZY) mixed oxides with high surface areas and pore structures that can be classified as being mesoporous (i.e., pore diameters from 2 to 50 nm). Specifically, CZY materials were prepared from sol-gel mixtures of the appropriate metal salts using a range of endo-templating techniques, while adsorption based techniques were used with the exo-templates. The resulting oxides were evaluated using nitrogen physisorption to determine the Brunauer–Emmett–Teller (BET) surface area and the Barrett–Joyner–Halenda (BJH) pore size distribution. Transmission electron microscopy (TEM) and scanning electron microscopy (SEM) were used to study the surface morphology and ascertain particle size distributions. Thermogravimetric analysis (TGA) and differential scanning calorimetry (DSC) were employed to quantify the amount of combustibles,

volatile compounds, decomposable hydrates, nitrates, and carbonates present in the as-synthesized CZY samples as well as help determine physical and chemical changes that may be occurring during calcination or prolonged exposure to high temperatures (as is the case with some catalytic converter operating conditions). Elemental analysis using ionization (ICP-EOS methods described later) and Energy Dispersive X-ray analysis (EDX) helped to determine the overall composition of the final oxide samples as well as verify the homogeneity of the oxide phases present. Finally, powder X-ray diffraction (PXD) was used to determine the existence of crystalline structure, while small angle X-ray diffraction (SAXD) helped to identify the presence of long range within the 3 dimensional structures that was created during the synthesis process. Finally, catalyst testing of metal doped CZY materials was undertaken to evaluate the effects of different pore geometries and surface morphologies. These tests compared the overall C_xH_y, NO_x and CO conversion rates to those of an established standard catalyst that is representative of the state-of-the-art for catalytic converter materials.

CHAPTER TWO

LITERATURE REVIEW

General Applications of Ceria, Zirconia, and Yttria Based Materials

Ceria, zirconia and yttria based oxides are known to exhibit properties that afford them widespread use in varied applications. Ceria, for example, is highly sought after for use in emission abatement control because of its high oxygen storage/supply capacity (OSC)[1,2]. It is also a good catalyst for the water gas shift reaction[1,2]. Recently, it has been widely used as an electrode component in solid oxide fuel cells[3]. Zirconia is a high density ceramic material that has useful chemical and physical properties[1]. In its crystalline form, it can withstand high temperatures (the monoclinic phase is stable to 1170 °C); thus, it often used in making thermal barrier coatings[4]. It is also commonly found in solid oxide fuel cells[5] and electrochemical sensors,[6] because it readily allows oxygen ions to move through the structure at high temperatures but has a low electronic conductivity. Yttria is an important stabilizing agent for mixtures of oxides.[7] It is frequently used in combination with other metal oxides (e.g., ceria and zirconia) as thermal barrier coatings, heterogeneous catalyst supports, and electrodes for solid oxide fuel cells.[3,8-13] In order to fully utilize potentials properties (i.e. oxygen storage/release capability of ceria, thermal stability of zirconia, and the stabilizing effects of yttria) that are associated with these oxides-ceria, zirconia, and yttria; they are frequently used in a combinatorial sets of binary or ternary mixed oxides, including yttria stabilized zirconia (YSZ), ceria-zirconia (CZ), ceria-yttria (CY) and ceria-zirconia-yttria (CZY)[10,13-15].

Ceria-Zirconia-Yttria Mixed Oxide (CZY) Materials for Automotive Three Way Catalytic Converter Applications

A key application for CZY materials is as the porous oxide support material for noble metals in the classic "three-way catalyst", which is the industry standard material for converting hazardous exhaust gases from combustion engines (e.g., C_xH_y, CO and NO_x) into more environmentally safe species (e.g., CO_2 and N_2)[16-22]. For this application, noble metals (primarily Pt, Pd, and Rh) are deposited on the surface of CZY materials having moderately high surface areas. These mixtures of precious metal groups and the CZY materials are deposited onto either alumina pellets or incorporated into an alumina wash coat that is later deposited on a monolithic substrate. These alumina supported catalysts are commonly called "three-way catalysts" or TWC because they simultaneously oxidize hydrocarbons and CO to CO_2 and reduce NO_X species to N_2, see Equations 2.1 - 2.3.

$$2CO + O_2 \rightarrow 2CO_2 \quad \text{(oxidation)} \tag{2.1}$$

$$2C_xH_y + (2x+y/2)O_2 \rightarrow 2xCO_2 + yH_2O \quad \text{(oxidation)} \tag{2.2}$$

$$2NO_x \rightarrow N_2 + xO_2 \quad \text{(reduction)} \tag{2.3}$$

While the noble metal components effectively catalyze all of the necessary chemistry for emissions abatement, the CZY support material acts as an oxygen sink/source, which enables the catalyst to work under a greater variety of engines conditions.

When the internal combustion engine of a car or truck is running fuel lean, the air to fuel ratio is greater than the stoichiometric amount, which is 14.6. In other words, the air is in excess of the fuel. Under these conditions, there is sufficient oxygen to readily

combust CO and C_xH_y compounds into CO_2, which optimizes fuel efficiency. However, the increased levels of combustion raise engine temperature, which causes greater amounts of N_2 in the inlet air to be converted to harmful and corrosive NO_x species. In contrast, when engines run fuel rich (i.e., the air to fuel ratio is less than 14.6) there is an insufficient supply of oxygen for complete combustion, which causes more CO and C_xH_y species to be produced. The presence of these incomplete combustion species help to reduce NO_x species into harmless N_2 in the catalytic converter, but can lead to greater CO emissions. Thus, it has been found that the optimal balance of fuel efficiency, pollution control, and catalytic converter life (which must be 100,000 miles on new vehicles in the U.S.) is achieved when the engine operates at near stoichiometric air to fuel ratios. Figure 2.1 shows conversion versus air to fuel ratio (A/F) for a typical three-way catalyst.

Despite modern engine designs incorporating highly accurate and durable oxygen sensors that help to maintain the air to fuel ratio at near stoichiometric levels, rapid engine acceleration/deceleration can lead to conditions where the system operates at rich air to fuel ratios (i.e., there is insufficient air for complete combustion). In order to prevent the emission of unacceptable levels of CO and unburned C_xH_y species, modern catalytic converter materials employ oxygen storage materials (OSM) with the unique ability to store oxygen under normal engine operating conditions and rapidly release or supply oxygen to help compensate for the momentary shortfall in oxygen supply to the catalytic converter. The discovery that ceria has the ability to rapidly absorb and loose framework oxygen led to the development of the first TWC in the early 1980s[23].

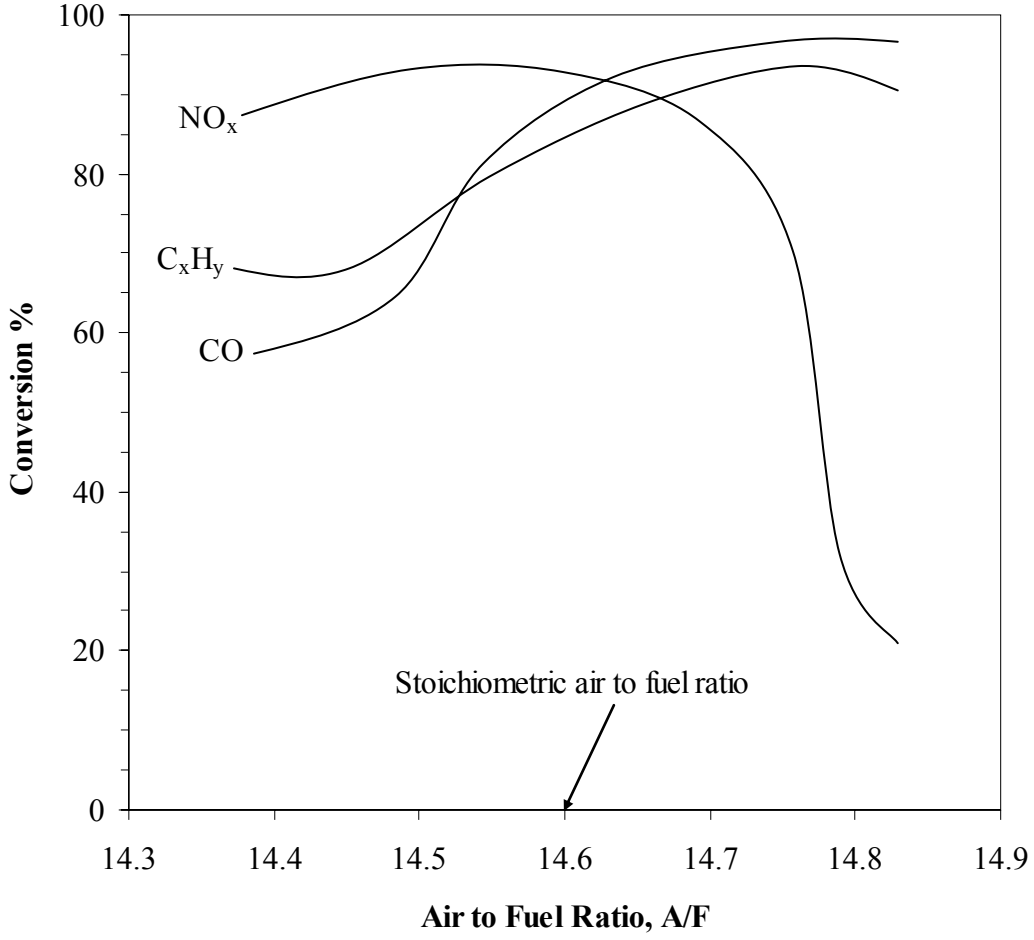

Figure 2.1 Simultaneous catalytic conversions of CO, C_xH_y, and NO_x versus air-fuel ratio in a standard three-way catalytic converter.

However, since it was discovered that adding other rare earth oxides like zirconia and yttria improved the oxygen storage capability of the ceria-containing TWC, use of CZY materials as oxygen storage materials in TWC is now a common practice [24].

To date, significant efforts have been put forth to optimize TWC materials, but they still undergo a significant loss of catalytic activity during prolonged use via a range of chemical and mechanical pathways. Thus, the quantities of expensive noble metals

present in a new catalytic converter are in great excess of that required for initial use, simply so that it will meet those same performance requirements after the vehicle has traveled a significant distance (e.g., 100,000 miles by U.S. standards). Some of this loss in activity is caused by metal sintering at high temperatures (800 – 900 °C), which is the process where well dispersed metals on a catalyst surface begin to agglomerate into larger clusters that reduce the total number of accessible metal sites available for catalysis. Additionally, the high temperatures experienced by the catalytic converter can cause the CZY catalyst support to undergo structural changes via crystallite migration or solid-solid phase transitions that lead to a significant loss in catalyst surface area, which further reduces catalyst activity. Finally, TWC catalyst can be deteriorated via poisoning from impurities in the fuel or engine lubricants (e.g., calcium, magnesium, phosphorus, sulfur, and zinc).

The question remains, can more be done to lower the cost and improve the performance of TWCs? To this end, it has recently been suggested by colleagues at Toyota and elsewhere that higher activity, increased resistance to noble metal sintering, and reduced loss in catalyst surface area might be achieved with a CZY support material that had a significant fraction of its available surface area in the form of mesopores (i.e., pores with diameters from 2-50 nm); however, synthesis strategies for achieving this goal have not been well addressed in the literature.

Synthesis Techniques for Mesoporous Oxide Materials

Overview of Synthesis Techniques for Mesoporous Silica Based Materials

Until the latter part of the 20th century there were no economical ways of producing mesoporous oxide materials of any composition, because most of the strategies for making porous materials employed the use of small molecule organic templates (or structure directing agents) that yielded products with micropores and macropores, but very little mesoporosity. Therefore, the successful synthesis of silica based mesoporous materials by researchers[25] at Mobil Research and Development Corporation in 1992 completely opened a new field of research, the synthesis of mesoporous oxides. Since that time, there has been an explosion in this field of research, and significant progress has been made not just in the area of synthesis of silica based mesoporous materials but also in the understanding of the formation mechanism. Figure 2.2 shows the mechanistic pathway for the synthesis of early silica based mesoporous materials.

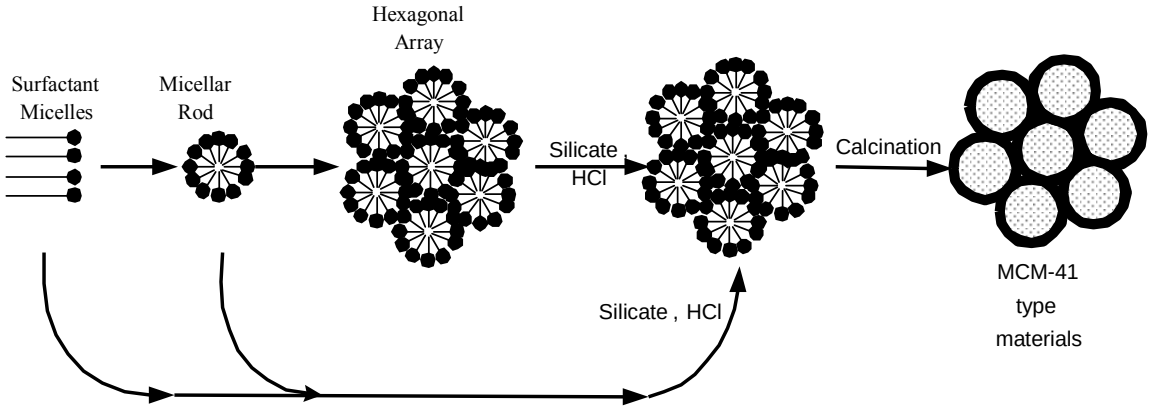

Figure 2.2 Mechanistic pathways for the synthesis of MCM-41 type silica based mesoporous oxides.

In Figure 2.2, there are two possible mechanistic pathways: one involves the self-assembly of the surfactant micelles first into micellar rods, them followed by another self-organization into a supramolecular structure made up of a combination of micellar rods into a hexagonal array of cylindrical rods. After the tertiary structure has been formed, the silicate precursor under an acidic medium would polymerize into a large network of oxides and finally condense around the tertiary supramolecular structure. On calcining the solid precipitate that is formed, the surfactant micelles are burnt-off leaving behind a porous array of cylindrical structures arranged in a honey comb structure. The second pathway suggests that the order in which the self-assembly takes place is irrelevant, that is, the cylindrical honey comb structure with surrounding condensed silicates may be formed in the presence of micelles, micellar rods, and the silicate precursors.

As a result of the success achieved with this mesoporous oxide synthesis technique, the idea has been extended to other varieties of surfactants. Pinnavaia et al. [26]first reported the use of neutral surfactants like alkylamines in the synthesis of silica based mesoporous material. Attard et al. [27]and Pinnavaia et al. [28-30] also reported synthesizing silica based mesoporous materials using nonionic surfactants. The use of anionic surfactants in the synthesis of mesoporous silica based materials has also been recently reported[31-35]. There have also been reports of the synthesis of mesoporous silica based materials using mixed surfactants like cationic and non-ionic; cationic and anionic; and anionic and non-ionic surfactants.[26,36-39]

In addition to surfactants, dendrimers and other functionalized organics have been used as templates in the synthesis of silica based mesoporous materials.[40-43] Other less well ordered silica based mesoporous materials have been synthesized using dramatically different routes that involve rigid three dimensional templates. Some early efforts in this area include the use of activated carbons as structure directing agents[44]. Following the reported[45,46] synthesis of ordered mesoporous carbon (OMC) via nanocasting by Ryoo's group, Schüth reported[47] the synthesis of silica based mesoporous materials via a repeated nanocasting technique.

Overview of Synthesis Techniques for Mesoporous Non-silica Based Materials

Significant progress has been made over the years, especially in extending the methods for the synthesis of silica based mesoporous oxides to the synthesis of non-silica based mesoporous materials.[25,48-51] There have been a number of review papers written on the general subject of mesoporous materials synthesis.[47,49,50,52-64] To date, the most cost effective methods for preparing mesoporous materials are via techniques that employ templates or structure directing agents. These templates can be divided into two groups: endo-templates (i.e., soft templates, such as surfactants, dendrimers, and block copolymers) and exo-templates (i.e., hard templates, such as porous carbons and resins).[47,64-66]

The soft templating techniques routinely employ sol-gel processing methods to assemble the appropriate oxide precursors around the selected structure directing agent (SDA), which is most often a surfactant or block copolymer or much less frequently a dendrimer. It has been shown that the surfactant micelles and the block copolymer

templates self-assemble into supramolecular structures of a variety of shapes, including cubic, hexagonal or bilayer[25,27,28,67]; whereas, the dendrimers exist as preformed pseudo-rigid structures that assume a spherical shape.[41-43,68] Because the mesoporous materials condense around these supramolecular frameworks, the technique is also described as endotemplating[47].

On the other hand, the hard templating technique involves the use of semi-rigid or rigid solids with high surface area and pore volume as templates[69]. Frequently used solids are activated carbons, polymeric resins and nanocast carbons[47,69-71]. With this form of templating, the voids or confined spaces of the porous carbon or polymeric resin are filled with solutions of the mixed oxide precursors (often nitrate metal salts or metal alkoxides). The mesoporous solids are formed within these confined spaces, thus, the technique is also called exotemplating. Figures 2.3 and 2.4 illustrate the concepts of endotemplating and exotemplating, respectively.

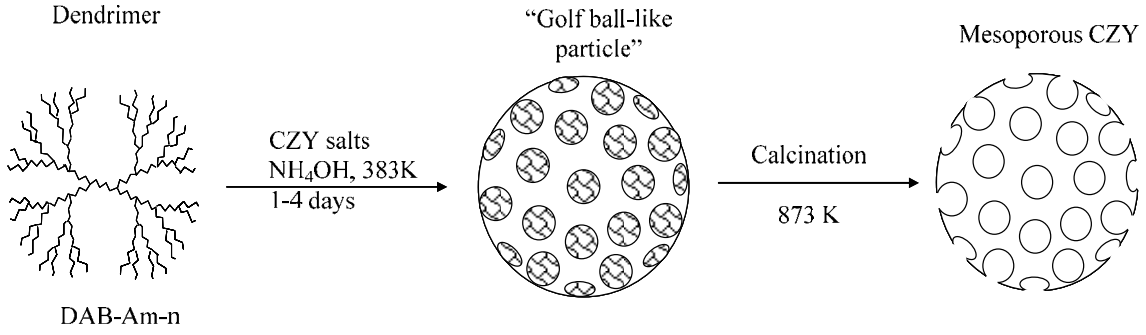

Figure 2.3 Illustration of pore generation in an endotemplating technique for synthesizing mesoporous materials using soft templates (e.g. dendrimer).

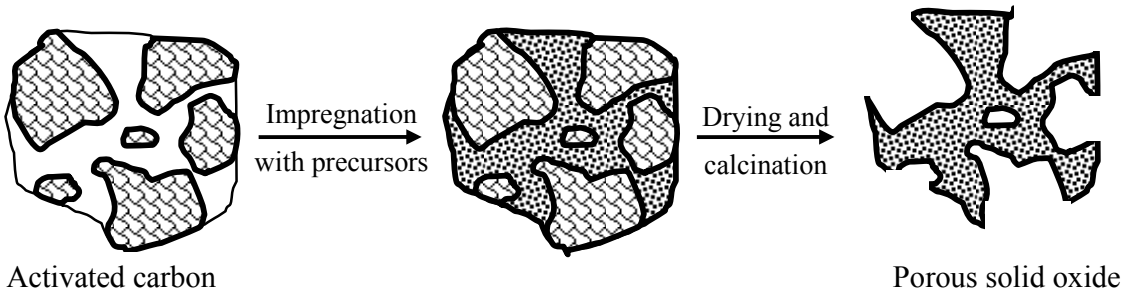

Figure 2.4 Illustration of pore generation in an exotemplating technique for synthesizing mesoporous materials using hard templates (e.g. activated carbon).

The pore structures created using the soft template technique and nanocasting technique lead to the formation of ordered mesoporosity. However, with dendrimers, activated carbon, and polymeric resin templates a non-uniform mesoporosity is created within the materials.

It is no surprise, however, that the synthesis of silica based mesoporous materials has developed much faster than the synthesis of non-silica based mesoporous materials. The following reasons have been adduced by Schüth for this observation[47]. Firstly, most of the research groups that had worked in this area have had a lot of expertise in zeolite (alumino-silicate) synthesis and chemistry. Secondly, silica based mesoporous materials are unique in that the chemistry involving the interaction between the organic based surfactant and the inorganic metal ion source is exceptionally stable. Thirdly, the kinetics of hydrolysis and condensation steps of the metal ion during the sol-gel process occurs at a rate that allows for the self-assembly of the surfactant micelles from spheres to cylindrical rods and finally combining into a stack of hexagonal shaped cylinders. Fourthly, the process of template removal usually leaves the silica walls in an amorphous

state, which enhance the mechanical stability of the resulting honey-comb structure. Lastly, the silicon atoms in silica based mesoporous materials have a stable oxidation state, which does not change during calcination. This stability of the redox state for the silica based materials is important in that it does not lead to crystallization or conformational induced strain in the pore walls during calcination. These general observations illustrate why more success has been recorded with the synthesis of silica based mesoporous materials compared to non-silica based ones.

More recently, there has been a great deal of effort by researchers to overcome the seemingly arduous challenges associated with synthesizing ordered non-siliceous mesoporous materials. Some of these efforts have focused on controlling (or slowing) the hydrolysis and condensation rates of the sol-gel process. Hydrolysis retarding agents, including acetylactetone and triethanol amine, have been used to slow the rate of hydrolysis, so that template (e.g., surfactant micelles) aggregation could occur before condensation processes solidified or locked-in the final oxide structure. The use of condensation retarding agents has also been widely reported. However, the oxides formed were not as readily useful because the synthesis lead to phosphate groups being attached to the surface of the oxides.

Just recently, the first successful synthesis of a ceria-zirconia-yttria mixed oxide (CZY) using CTAB surfactants as the template was reported by Feng et al. [10] The resulting CZY material was heated (at a rate of 1 ºC/min) to 550 ºC and held for 8 h at this temperature. After calcination, the sample was characterized and the specific surface area for the CZY sample was measured to be 139 m^2/g. The average pore diameter

measured by N_2 adsorption was approximately 6.8 nm. Hung et al. [11] also reported the synthesis of yttria stabilized zirconia (YSZ) using only CTAB as the template. Thermal degradation studies on the YSZ sample from 600 ºC to 1200 ºC revealed that the specific surface area significantly reduced from 137 m^2/g to 3.3 m^2/g. Feng et al.[10] also reported synthesizing a zirconia-yttria mixed oxide (ZYO) with a specific surface area of 200 m^2/g. Kapoor et al. in a different synthesis procedure reported[72] synthesizing mesoporous ceria-zirconia mixed oxide (CZO). In their procedure, no basic hydrolyzing agent was used in the synthesis. It is important to note that most transition metal oxide precursor solutions are frequently strongly acidic; thus, the hydrolyzing agent was the acidic nature of the precursor solution. The BET surface area of the CZO samples ranged between 229 and 365 m^2/g depending on the ceria-zirconia mixed oxide composition. These initial efforts at preparing mesoporous CZY samples prove that these materials can be prepared and are stable at moderately high temperatures; however, there has not yet been a systematic investigation of the synthesis parametric space that would allow for a complete analysis of the types of stable mesoporous structures that are possible with the CZY mixed oxide system.

CHAPTER THREE

SURFACTANT TEMPLATE TECHNIQUE

In this chapter, I describe the synthesis of mesoporous ceria-zirconia-yttria (CZY) mixed oxides prepared via sol-gel methods that employ surfactants as structure directing agents. These synthesis efforts were also expanded to include the use of other organic additives, which were chosen to alter the structural characteristics of the primary surfactant templates (e.g., cosolvents and swelling agents) or slow the rate of oxide formation (e.g., hydrolysis retarding agents). In general, the final oxide materials of interest are prepared via the calcination of metal oxide precipitates that are formed by heating aqueous mixtures of metal salts and organic additives. It is the unique interplay among the synthesis conditions, metal oxide precursors, and additives that determines the composition and 3-dimensional structure of the final oxide material. Thus, a comprehensive study of the synthesis parametric space was undertaken, so as to determine the optimal conditions for forming highly stable mesoporous CZY materials.

From these synthesis efforts, the resulting oxide materials were characterized by a range of analytical methods to determine the effects of hydrothermal synthesis temperature, auxiliary templating additives, sol-gel mixture pH, and hydrolysis retarding agent addition on the physical properties of the CZY products. The primary analytical methods used in these studies for material characterization were physisorption techniques (Brunauer-Emmett-Teller (BET) surface area and Barrett-Joyner-Halenda (BJH) pore size distribution), powder X-ray diffraction (PXD), elemental analysis, transmission electron microscopy (TEM), and scanning electron microscopy (SEM). In addition, I

used thermogravimetric and differential scanning calorimetry analysis to determine the optimal calcination protocol for the as prepared mesoporous CZY materials.

Synthesis Strategy for CZY Mixed Oxides Using Surfactant Templates

The synthesis strategy for all soft templated sol-gel techniques is basically the same. Three procedures are involved: synthesis, drying, and template removal. Four types of reagents are required for the synthesis step: metal oxide precursors, a solvent, a hydrolyzing agent or catalyst, and the structure directing agent or template. Figure 3.1 shows the synthesis steps required for making mesoporous CZY mixed oxides using the surfactant template method.

Early efforts to prepare surfactant templated oxide materials used sol-gel methods that required the use of metal alkoxide precursors, which are generally expensive. This high cost prompted our group and others to modify the synthesis method so as to use less expensive metal sources, such as the nitrate salts of the required metals. Therefore, in this study I used cerium (III) nitrate hexahydrate, zirconyl nitrate, and yttrium nitrate hexahydrate as the metal precursors for all surfactant templated CZY materials. The motivation for using nitrate salts, instead of chloride or sulfate salts, is that during calcination, no residual by-products containing nitrogen are formed on the catalyst surface that might alter or inhibit catalyst performance. In general, the thermal decomposition of most transition metal based nitrate salts can be represented as follows:

$$2NO_3^- \rightarrow 2NO_2 + O^{2-} + \tfrac{1}{2} O_2 \text{ (thermal decomposition)} \quad (3.1)$$

Equation 3.1 shows that nitrate thermal decomposition products are nitrogen (IV) oxide, oxygen, and the most stable form of the metal oxide of the transition metal.

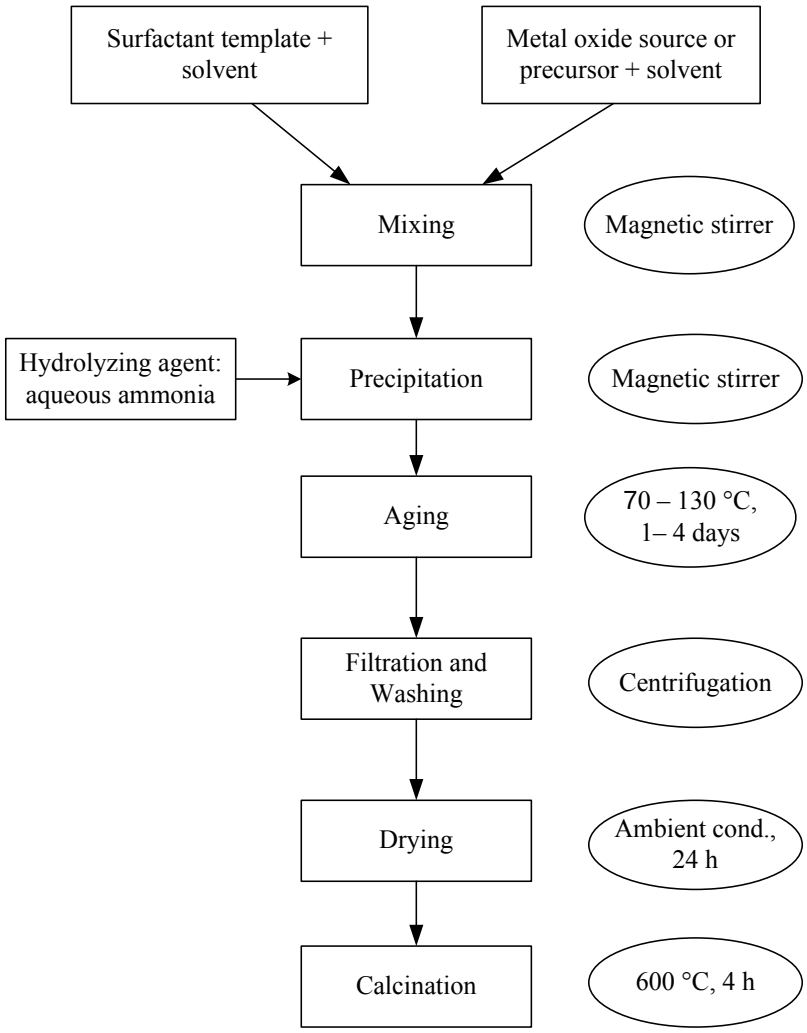

Figure 3.1**:** Synthesis procedures for mesoporous CZY mixed oxides using surfactant template.

The sol-gel solvent is usually water. In addition, alcohols are frequently used as solvents, especially with metal alkoxide precursors. Moreover, certain templates, such as block copolymers and dendrimers, are not readily water soluble; thus, water-alcohol mixtures are used as the sol-gel solvent to improve template solubility. Most salt

precursors can be represented in the general form as MX_n for which n anions of X are linked to the metal, M. In aqueous media, the precursors are dispersed as ions with the metal ion, M^{z+}, being solvated by the water molecules to form the complex ion, $[M(H_2O)_N]^{z+}$, which may or may not associate with the anion, X, depending on the type of metal salt. The type of metal salt determines the type of hydrolysis that would take place. For example, salts that are derived from weak acid conjugates (NO_3^-, SO_4^{2-}, Cl^-), when hydrolyzed in aqueous solution form acidic solution, while salts that are derived from strong acid conjugates (COO^-, CO_3^{2-}) form basic solution when hydrolyzed in aqueous solution. The hydrolyzing agent helps to catalyze the substitution of the aquo groups by the hydroxo group. The presence of the hydroxo group initiates the condensation process, which leads to the formation of M-O-M bridged polyoxides.

$$[M–OH_2]^{z+} \rightarrow [M–OH]^{(z-1)+} + H^+ \rightarrow [M=O]^{(z-2)+} + 2H^+ \text{ (hydrolysis)} \quad (3.2)$$

$$M–OH + M–OH \rightarrow M–OH–M–OH \rightarrow M–O–M + H_2O \text{ (condensation)} \quad (3.3)$$

Equations 3.2, and 3.3 summarizes the sol-gel chemistry for transition metal based salts[73,74]. The pH is crucial because it influences the stability of the oxides, specifically, whether they precipitate out of solution or remain dissolved in the solution. Of all the reagents, the choice of structure directing agent defines each soft templated technique. In this chapter, I focused on the use of surfactant systems as examples of soft template structures. Another important part of the synthesis process is the aging of the sol-gel in the oven. The aging temperature and duration have been found to be vital. The major breakthrough associated with this method is the relatively low synthesis temperature

required, where the usual range has been between 70 and 130 ºC. The thermal aging of the sol-gel also varies from 1 to 4 days.

Following the aging step, the solid oxide products are removed from the sol-gel mother liquor using centrifugation. These solid products are then washed multiple times with fresh solvent to remove any soluble contaminants or residual salts. Once fully washed, the oxides are then dried. There are two ways of carrying out the drying step: evaporative (thermal) drying and supercritical drying. The evaporative drying method is done either at near ambient temperatures with reduced pressure or at elevated temperatures and moderate pressures (often 1 atm). The supercritical drying method uses solvents, such as supercritical CO_2, to extract water and other polar solvents from the catalyst pores. The supercritical solvent (sc CO_2) containing extracted water and organic additives is then separated from the solid products and subsequently allowed to evaporate. Extraction (as opposed to evaporation) of polar solvents from the pores of the catalyst ensures no liquid-vapor phase transitions occur within the pores, which results in the formation low surface tension in the pores. This is advantageous as pore collapse has been shown to occur during the evaporative processing of some catalyst materials due mainly to the effects of surface tension forces.

The final and most delicate step involves template removal. Routinely the organic templates are removed via calcination or various solvent extraction methods. The solvents frequently used for the extraction method of template removal are low boiling organic solvents, such as acetone, or a mixture of an organic solvent with an inorganic acid (e.g., ethanol-HCl mixtures).

Synthesis of CZY Mixed Oxides Using CTAB Alone as Template

All chemicals used in the preparation of surfactant template CZY samples were used as received from their respective manufacturer. The following is a list of the chemicals: yttrium (III) nitrate hexahydrate $Y(NO_3)_3 \cdot 6H_2O$ (Sigma-Aldrich, 99.9% metal basis), cerium (III) nitrate hexahydrate $Ce(NO_3)_3 \cdot 6H_2O$ (Alfa Aesar, ROE 99.5%) and zirconyl (IV) nitrate hexahydrate $ZrO(NO_3)_2 \cdot 6H_2O$ (Sigma-Aldrich, 99%), 1-propanol (Fisher Scientific), hydrogen peroxide (Fisher Scientific, certified ACS 30 wt%), benzene (Fisher Scientific, certified ACS), distilled water, cetyltrimethylammonium bromide (CTAB) (Alfa Aesar, 98%), ammonium hydroxide (Fisher Scientific, certified ACS), triethanolamine (TEA) (Sigma-Aldrich, 98%), and acetylacetone, (ACAC) (Sigma-Aldrich, ≥99.5%). Deionized water was prepared by a combined distillation-filtration system. First, distilled water was produced via a Water Distillation Apparatus Model AG-10 from Corning Glass Works. It was subsequently filtered using a Millipore Milli-Q® Academic (Ultrapure Water Purification) System.

As shown in Figure 3.1, the metal oxide precursors (i.e., cerium (III) nitrate, zirconyl nitrate, and yttrium nitrate) were dissolved in deionized water (~50 mL) to make a homogeneous solution. Then, with vigorous stirring, a small quantity of 30 wt% hydrogen peroxide (~0.3 mL) was added to the salt solution to oxidize Ce (III) species to Ce (IV) ions. Table 3.1 shows a typical sol-gel composition, which includes metal oxide precursors (or salts), hydrogen peroxide, solvent, and the surfactant template, required for the synthesis of mesoporous ceria-zirconia-yttria (CZY) mixed oxides.

Table 3.1 Typical sample composition for CTAB templated CZY.

Reagents	Molar Ratio		Mass (g)
	Sol-gel	Oxide	
$ZrO(NO_3)_2.6H_2O$ (ZrO_2)	9	9	5.000
$Y(NO_3)_3.6H_2O$ ($YO_{1.5}$)	1	1	0.627
$Ce(NO_3)_3.6H_2O$ (CeO_2)	10	10	7.109
CTAB	25		14.917
H_2O_2	5		0.287
water			100.000

In a separate beaker, the surfactant template cetyltrimethylammonium bromide (CTAB), which is by far the most frequently used surfactant for the synthesis of mesoporous materials, was dissolved in the portion of allowed water that was not used to dissolve the metal salts (~50 mL). The surfactant solution was heated to approximately 40 ºC and stirred continuously using a magnetic stirrer until a clear solution was observed. The oxide precursor solution was heated to approximately 40 ºC and stirred continuously using a magnetic stirrer until a homogeneous mixture was obtained. With the oxide precursor solution added gradually at ~5 mL/min to the CTAB solution, and the mixture continuously stirred manual with the aid of a stirrer; the mixture was immediately transformed to a viscous gel. Ammonium hydroxide was added at ~5 mL/min to the gelatinous mixture with vigorous stirring until the pH of the mixture was uniform and approximately greater than 10.0. Upon addition of ammonium hydroxide, the metal oxide precursors rapidly precipitated locally within the sol-gel mixture forming brownish spots amidst the sea of yellow color associated with the sol-gel mixture.

Ammonium hydroxide is preferred to either urea or sodium hydroxide as the hydrolyzing agent source (hydroxide anions are the actual hydrolyzing agent), because urea has a low solubility in the sol-gel mixture and is a weak base, while sodium salts are not easily volatized during calcination and can inhibit catalyst activity. The final gelatinous mixture was poured into a 120 mL Teflon perfluoralkoxy (PFA) reaction vessel (Savillex Corporation) and the vessel sealed. The sealed PFA reaction vessel was put in an oven for 1-4 days at temperatures between 70 and 130 ºC to age. Additionally, the samples were maintained at autogenous pressures for the duration of the heating process.

During the aging process, the gelatinous mixture phase separates into a clear top liquid layer and a dense bottom solid layer. If the gelatinous mixture pH values are less than 9.0 before it is poured into the PFA reaction vessel, the quantity of the bottom solid layer formed after aging is either minimal or non-existent. Once the phase separation has occurred, the sol-gel sample is then removed from the oven, allowed to cool, and residual solvent decanted, leaving behind a solid residue containing a mixture of the organic additives and the metal oxide product. The solid residue was washed thrice with ~40 mL deionized water to remove the CTAB template. Following each washing step, the suspension was centrifuged to separate the solid residue from the top solvent. The washed solid residue was collected in a crucible, and then dried for at least for 12 hours under ambient conditions before it was calcined. Calcination from room temperature to 600 °C was carried out using heating rates ranging from 1 to 20 ºC/min and air purge flow rates between 60 and 100 mL/min, with the final temperature being maintained for 4 h.

Figure 3.2 illustrates the hypothesized mechanistic pathways for the synthesis of surfactant templated CZY with no additional auxiliary templating reagents (i.e., no cosolvents or swelling agents). This mechanistic pathway is a direct extension of the proposed mechanistic pathway developed by researchers at Exxon-Mobil (originally Mobil Oil Co.)[25] for the synthesis of mesoporous silica based oxides. It is important to note from the outset that this model suggests that I hope to synthesize mesoporous CZY materials with regular 3-D pore structures that resemble those found in MCM-41 type silica materials.

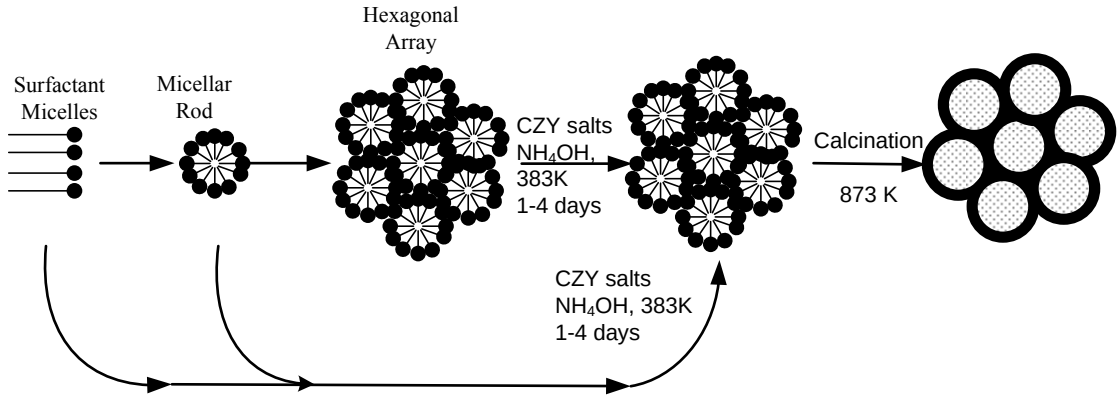

Figure 3.2 Possible mechanistic pathways for surfactant templated CZY materials. The surfactants are the filled dots with tails.

Using a synthesis protocol similar to that described above, I investigated how the addition of hydrolysis retarding agents to the sol-gel synthesis mixture would affect the physical properties of CTAB templated CZY materials. The hydrolysis retarding agents used were triethanolamine (TEA) and acetylacetone (ACAC)[75-77]. These hydrolysis retarding agents also called complexation agents usually form a complex with the central metal ion just like the aquo ligands. The strength of the binding association between the

ACAC and TEA is a measure of the relative ease by which the metal ion would be available for hydroxo ligand substitution. The resulting CZY mixed oxides were characterized using nitrogen physisorption experiment (BET surface area and BJH pore volume distribution), transmission electron microscopy (TEM), scanning electron microscopy (SEM), thermogravimetric analysis (TGA), differential scanning calorimetry (DSC), elemental analysis (using ICP-OES), powder X-ray diffraction (PXD), and catalytic testing.

Synthesis of CZY Mixed Oxides Using CTAB/ Cosolvent as Template

In order to increase the average pore diameter of synthesized mesoporous materials, many researchers have used a cosolvent or cosurfactant in addition to the primary surfactant template to enlarge the size of the micellar aggregates formed during the sol-gel synthesis of silica based mesoporous materials[78-80]. These cosurfactants are often medium chain length alcohols ranging from propanol to octanol. To evaluate whether the same pore size enlargement effect is observed with CZY mixed oxides prepared using cosurfactants, I synthesized CZY mixed oxides samples using CTAB/cosolvent mixtures as structure directing agents (SDA) following the procedure outlined in Figure 3.1. The cosolvents used were 1-propanol or 1-octanol. Table 3.2 shows a typical composition of the precursors, surfactant, cosolvent, and solvent used during the synthesis of mesoporous CZY mixed oxide. The procedure used to synthesize surfactant/cosolvent templated CZY materials was near identical to the procedure shown

in Figure 3.1 and discussed in the preceding section; however, the template solution now contains a mixture of CTAB and 1-propanol, which is present as the cosolvent.

Table 3.2 Typical sample composition for CTAB/1-propanol CZY

	Molar Ratio		
Reagents	Sol-gel	Oxide	Mass (g)
$ZrO(NO_3)_2.6H_2O$ (ZrO_2)	9	9	5.000
$Y(NO_3)_3.6H_2O$ ($YO_{1.5}$)	1	1	0.627
$Ce(NO_3)_3.6H_2O$ (CeO_2)	10	10	7.109
CTAB	25	25	14.917
$CH_3CH_2CH_2OH$			25.000[a]
H_2O_2	5		0.287
water			100.000

a. The cosolvent was measured in mL.

Assuming that the surfactant and cosolvent used during the synthesis of the templated CZY mixed oxides assemble in much the same way as the surfactant and cosolvent mixture used in silica based oxide, then both syntheses would have similar mechanistic pathway for their syntheses[25]. Figure 3.3 illustrates the hypothesized mechanistic pathway for the surfactant-cosolvent templated CZY synthesis.

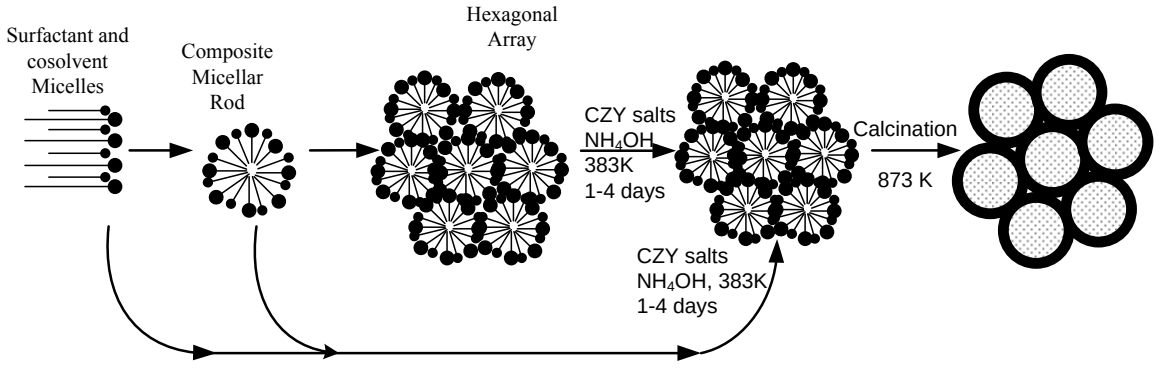

Figure 3.3 Possible mechanistic pathways for surfactant-cosolvent templated CZY. The smaller filled dot with shorter tails represents the cosolvent species.

This mechanistic model holds true for silica based mesoporous materials, but it is only an hypothesized pathway for CZY materials. The results of the TEM analysis and small angle X-ray diffraction pattern would help to confirm or disprove this hypothesis.

Synthesis of CZY Mixed Oxides Using CTAB/Cosolvent/Swelling Agent as Template

In the previous section, I used a mixture of CTAB solution and 1-propanol as SDA during the synthesis of mesoporous CZY mixed oxides. Besides adding a cosolvent to the surfactant solution as a means to increase the diameter of the micellar structure, swelling agents, such as trimethylbenzene and benzene, have also been added to the surfactant cosolvent mixture, so as to further enlarge the diameter of the micellar structure[81-86]. Specifically, this technique was used successfully to synthesize silica based mesoporous materials[82-86]. I extended this same principle to the synthesis of mesoporous CZY mixed oxides using the following swelling agents: benzene and trimethylbenzene (TMB, also known as mesitylene). Using the same general synthesis procedure outlined in Figure 3.1, I made samples of mesoporous CZY mixed oxides using mixtures of CTAB/propanol/benzene and CTAB/propanol/TMB as structure directing agents. Table 3.3 shows the sol-gel synthesis composition of mesoporous CZY mixed oxides prepared using the mixture CTAB/1-propanol/benzene as the SDA.

Table 3.3 Typical sample composition for CTAB/1-propanol/benzene templated CZY

Reagents	Molar Ratio		Salt Mass (g)
	Salt	Oxide	
$ZrO(NO_3)_2.6H_2O$ (ZrO_2)	9	9	5.000
$Y(NO_3)_3.6H_2O$ ($YO_{1.5}$)	1	1	0.627
$Ce(NO_3)_3.6H_2O$ (CeO_2)	10	10	7.109
CTAB	25	25	14.917
$CH_3CH_2CH_2OH$			25.000[b]
Benzene			20.000[b]
H_2O_2	5		0.287
Water			100.000

b. The amount of 1-propanol and benzene are measured in mL

To illustrate how the swelling agent helps to increase the diameter of the hexagonal tertiary structure, I propose the following mechanistic pathway for this synthesis as shown in Figure 3.4, which is an extension of our knowledge of how the silica based MCM-41 family of materials behave[25,86]. The surfactant-cosolvent-swelling agent system is often called a solubilized system. Unlike the surfactant-cosolvent system, the surfactant-cosolvent-swelling agent system creates a supersaturated system with more cosolvents dissolved in the micelle than in the former system. This increased solubility, along with the presence of the swelling agents at the micellar core, helps to enlarge the diameter of the tertiary hexagonal structure formed by the composite micellar rods.

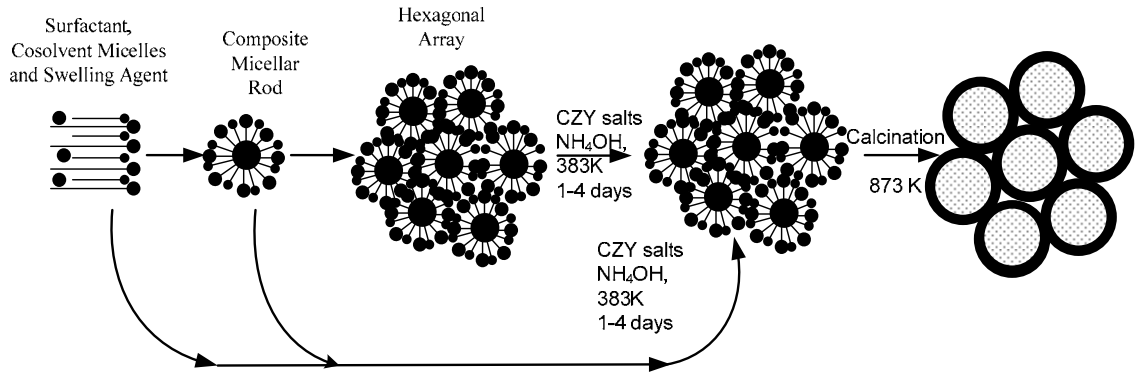

Figure 3.4 Possible mechanistic pathways for surfactant-cosolvent-swelling agent templated CZY. The smaller filled dot with shorter tails represents the cosolvent species, while the swelling agents are depicted as tail-less dots that end up in the core of the micellar structure.

Experimental Methods for Characterizing CZY Mixed Oxides

All synthesized CZY materials were characterized to determine if there were any significant structural or compositional differences among the samples, especially as it pertains to variations in the templates used during the sol-gel synthesis. Phase characterization of the CZY solids was done using powder X-ray diffraction (PXD). The equipment used for carrying out the PXD was a Scintag XDS Model 2000 diffractometer with Cu K α radiation (λ = 1.5406 Å) and Ni filter, operated at 30 kV, 20 mA. A Micromeritics ASAP 2020 volumetric adsorption analyzer was used to measure nitrogen adsorption-desorption isotherms for the as prepared and calcined samples, which were degassed at 473 K for approximately 4 hours before each analysis. These isotherms were then used to calculate the specific surface area (BET technique) and pore size distribution

(BJH technique) of the samples. Particle sizes were estimated using transmission electron microscopy (TEM). The equipment used was a TEM Hitachi H7600T or 9500. Elemental composition of the samples was determined using inductively couple plasma atomic emission spectroscopy (ICP-AES). The equipment used for this experiment was Horiba Jobin Yvon ULTIMA 2. Additionally, more localized compositional differences were investigated using energy dispersive X-ray spectroscopy (EDX). The equipment used for the EXD was the Hitachi S4800 or the SEM 3400. The effects of heat flow, with varying heating rates, on the as-synthesized CZY mixed oxides was studied using thermogravimetric analysis (TGA) and differential scanning calorimetry (DSC). The equipment used for these studies was an SDT Q600 Simultaneous DSC/TGA Analyzer.

Results and Discussion

In order to decide on the best calcination protocol for template removal and oxide sintering, I studied the effects of heat flow on as-synthesized CZY mixed oxides in air at heating rates ranging from 1 to 20 ºC/min from near ambient temperatures to 600 ºC. I used an as-synthesized CZY sample prepared without the inclusion of any structure directing agent as a control or reference sample. In general, the combination of DSC and TGA are better suited than either TGA or DSC alone for studying heat effects associated with the calcination of catalytic materials. The DSC spectra can be used to estimate the loss of materials indirectly (i.e., by equating the heat evolved or absorbed during a process to the known standard condition) from a sample, while TGA is allows for a direct measurement the loss of material that arises from thermal degradation processes (e.g.,

combustion, phase changes-boiling, evaporation, or sublimation). However, DSC is optimally suited for identifying and possibly quantifying processes that involve solid-liquid or solid-solid phase changes (e.g., glass transitions, melting, and crystallization). With the DSC spectra, all of these processes are usually signaled by peaks on the heat flow versus temperature profile. For our purposes, downward peaks indicates endothermic (heat absorbing) processes and upward peaks represent exothermic (heat releasing) processes.

Figures 3.5 and 3.6 show the DSC spectra and TGA of the as-synthesized CZY sample prepared without using an SDA, while Figures 3.7 and 3.8 show the DSC spectra and TGA profile of an as-synthesized CZY sample prepared using CTAB alone as the SDA. The DSC results of Figure 3.5 show that there was moderate heat absorption process occurring between 100 and 200 ºC. This is most probably from the vaporization of physically adsorbed water. On the TGA plot shown in Figure 3.6, the associated weight loss corresponds to about 10%.

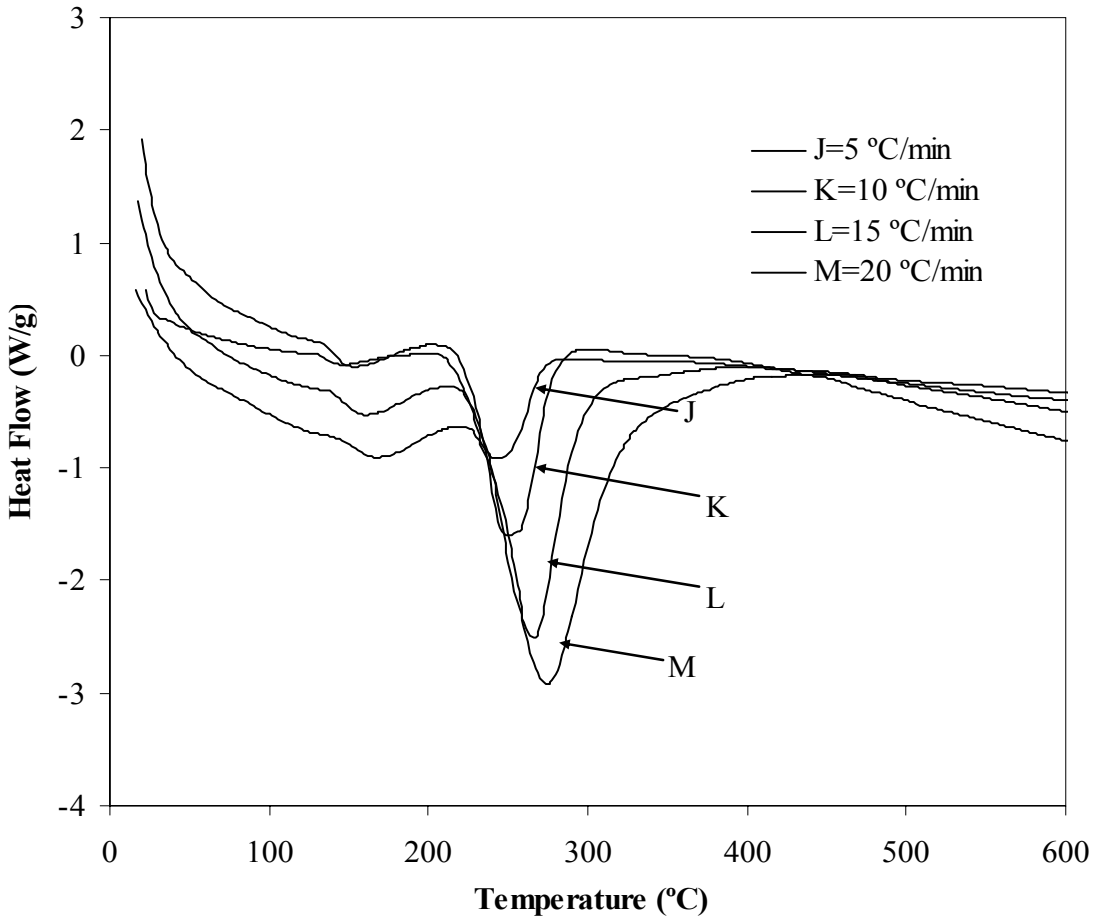

Figure 3.5 Differential heat flow to an as-synthesized CZY sample prepared using no SDA upon heating from near ambient temperatures to 600 ºC at different heating rates in a constant flow of air.

More pronounced endothermic processes are observed at between 200 and 350 ºC. This arises from the thermal decomposition of the nitrate salts. The depth of the downward peak is highest when the heating rate was 20 ºC/min and least when the heating rate was 5 ºC/min.

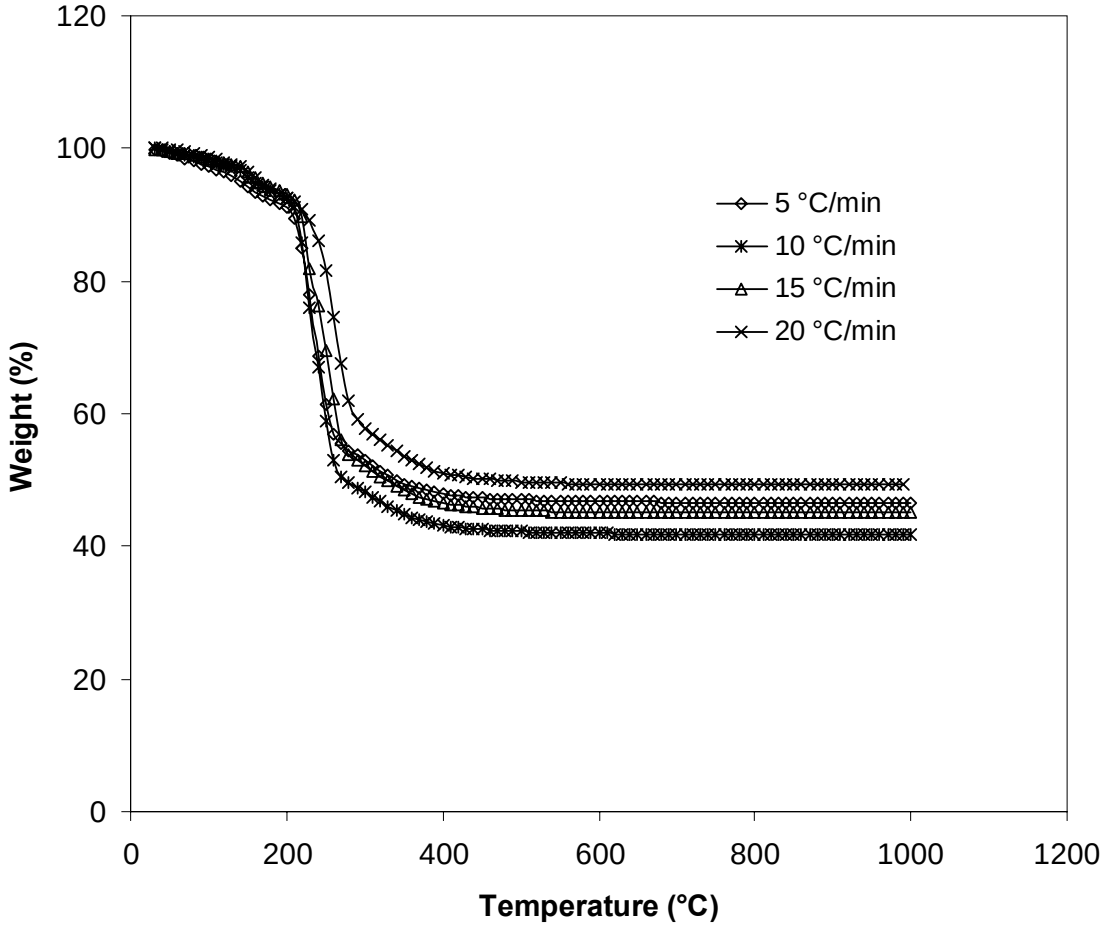

Figure 3.6 Thermogravimetric analysis of as-synthesized CZY sample prepared using no SDA upon heating from near ambient temperatures to 600 ºC at different heating rates in a constant flow of air.

On the corresponding TGA plot (see figure 3.6), the overall weight loss took place between 200 and 400 ºC. This weight loss is equivalent to roughly 50% of the weight of the starting material. Beyond 400 ºC, the sample weight is relatively constant meaning that the decomposition reaction has been completed.

However, with the as-synthesized CZY sample prepared using CTAB alone as the SDA, as shown in Figure 3.7, the results are significantly different. The endothermic processes occurring at the low temperature range of less than 200 ºC are again from the loss of water, but the extent of water loss is significantly greater for the sample containing the surfactant template.

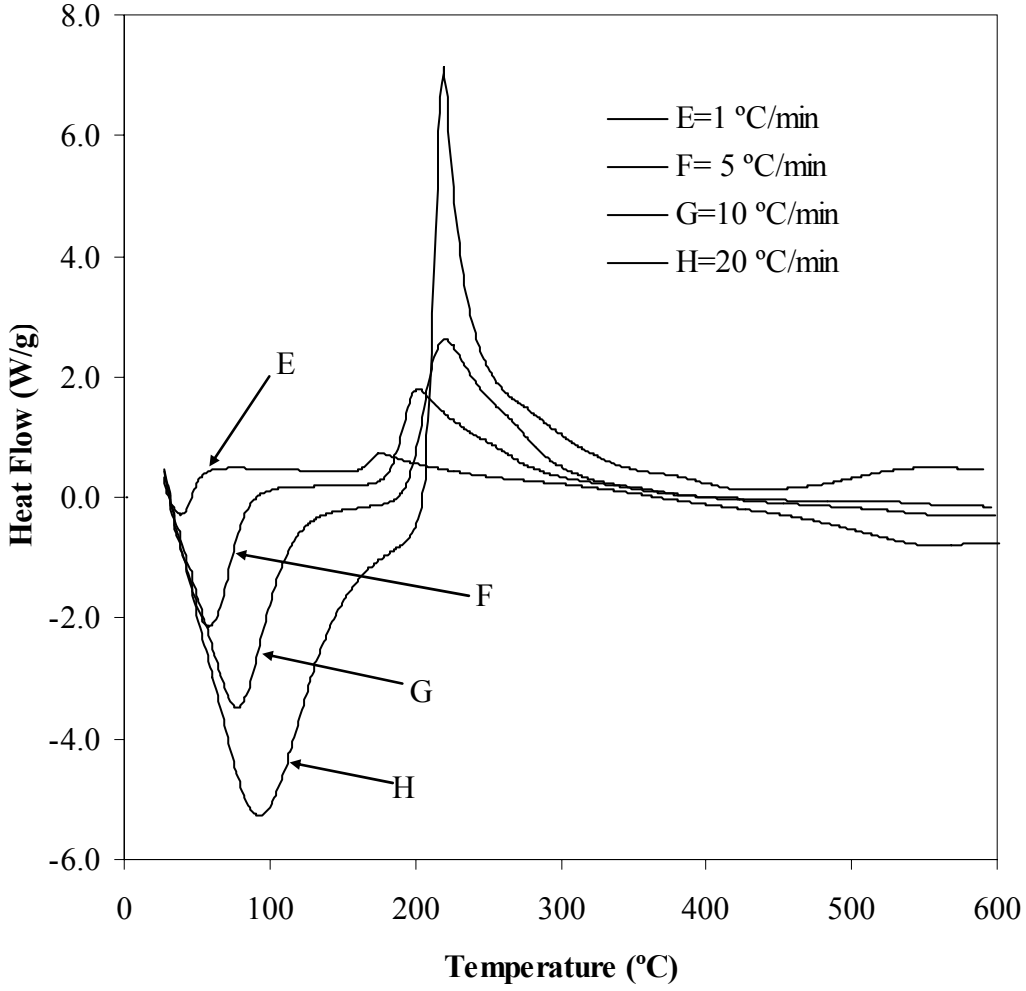

Figure 3.7 Differential heat flow to an as-synthesized CZY sample prepared using CTAB alone as the SDA upon being heated in air from near ambient temperatures to 600 ºC, at heating rates that ranged from 1 to 20 °C/min.

This same observation is clearly depicted in the TGA plot of the same sample shown in Figure 3.8.

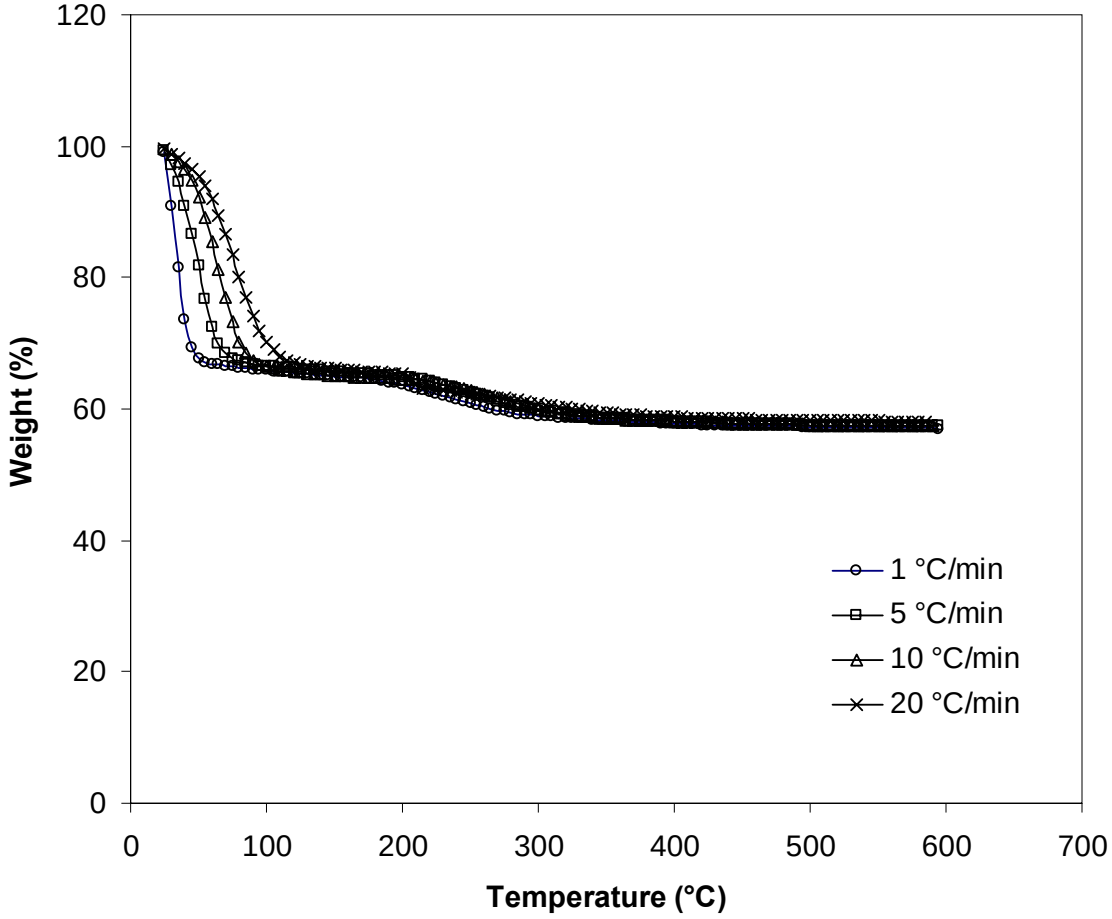

Figure 3.8 Thermogravimetric analysis of as-synthesized CZY sample prepared using CTAB alone as the SDA upon being heated in air from near ambient temperatures to 600 ºC, at heating rates that ranged from 1 to 20 °C/min.

The most important thermal feature in the DSC spectra of the surfactant templated sample (Figure 3.7) occurs between 200 and 300 ºC, where a heat evolution process is

occurring instead of the endothermic process observed with the reference sample that contained no surfactant template. This phenomenon arises because the heat absorbed during the thermal decomposition of the nitrate salts is less than the heat released during the combustion of the organic CTAB template. The TGA plot of Figure 3.8 also shows ~5% weight loss between 200 and 300 ºC. This is most likely the salts and the CTAB being burned off. The combustion of the CTAB template occurred at a relatively low temperature probably as a result of the catalytic activity of the transition metals (e.g., cerium). The amount of CTAB template present in these samples is low.

As shown in Figure 3.7, increasing the heating rate also increases the rate of heat released during the oxidation of the template. This is important because it tells us that carrying out the calcination at low heating rate prevents the occurrence of hot spots within the sample. Hot spots within a sample during calcination could lead to localized melting phenomena that might destroy the structural integrity of the CZY sample and significantly reduce the surface area of the mesopores. Based on the associated heat released during the calcination process, it is obvious that to reduce the possibility of generating hot spots during calcination; the calcination rate would have to be 10 ºC/min or less.

Next, I present results showing the effects of calcination heating rate on the physical properties of the final CZY mixed oxide samples. Specifically, I show in Table 3.4 how the CZY product surface area (BET) and pore size distribution (BJH) are affected by the calcination heating rate for as-synthesized CZY samples prepared using CTAB alone, CTAB/1-propanol, and CTAB/1-propanol/benzene as SDA. These samples were heated from room temperature to 600 ºC in air at heating rates of 1 or 20ºC/min, and

the final temperature of 600 °C was maintained for 4 hrs. These data show that varying the calcination heating rate does not significantly affect the physical properties of CTAB templated CZY samples. The measured values of the BET surface area and average BJH pore diameter of the CZY samples were found to be statistically the same when the error margins are factored in.

Table 3.4 Effect of calcination heating rate on the surface area and pore diameter of CTAB templated CZY samples that were calcined in air from 25 to 600 ºC with the final temperature maintained for 4 h.

	Surface Area m^2/g (Pore Diameter nm)[c]	
Sample	1 ºC/min	20 ºC/min
CZY/CTAB	78 (6.2)	82 (6.2)
CZY/CTAB/ACAC	106 (5.4)	106 (5.3)
CZY/CTAB/TEA	9 (3.8)	14 (3.8)
CZY/CTAB/1-propanol		89 (4.6)
CZY/CTAB/1-propanol/Benzene		92 (5.2)

c. The error margin for the surface area is ±5 m^2/g and for the pore diameter, ±0.5 nm

The total carbon loading for all of the surfactant templated CZY samples tested was so low that the additional heat released as a result of burning off the CTAB template and associated organics could not generate sufficient localized hot spots to damage the structural morphology of the CZY samples. Hence, the values of the BET surface area and BJH pore diameter are statistically unchanged for the two heating rates studied. Earlier in discussing the results of the TGA plots and DSC spectra, I have suggested that a calcination heating rate of 10 ºC/min or less would be sufficient to reduce the

generation of hot spots within the samples during calcination. The results of the effects of varying heating rate on the surface area and pore size shown above are quite contrary. This is so because the amount of combustible materials present in the sample during calcination is also important. Therefore, based on the results shown in Table 3.4, the calcination heating has minimal effects on the surface area and pore size of CTAB templated CZY materials.

Table 3.4 also shows the effects of adding organic additives like cosolvent and swelling agent on the surface area and pore size of the synthesized CZY materials. These additives do not produce the required effect of enlarged pore size to say the least. There are two possible explanations for this observation. It is either the chain length of propan-1-ol used as cosolvent is too short to make any significant effect or no templating effect resulted from using CTAB, 1-propanol, and benzene at all. At the moment, none of the two possible explanations can be ruled out until further results like the TEM images and powder XRD patterns are examined.

Figures 3.9-3.11 show the nitrogen adsorption/desorption isotherms and the BJH pore size distribution of CZY samples synthesized using CTAB alone, CTAB/1-propanol, and CTAB/1-propanol/benzene as structure directing agents. The physisorption isotherms (see Figures 3.9 to 3.11) show the typical hysteresis loop associated with mesoporous materials. This suggests that indeed mesoporous CZY materials were prepared. However, it is impossible to accurately calculate the dimension or shape of the pores present in the sample from simply the adsorption-desorption isotherms.

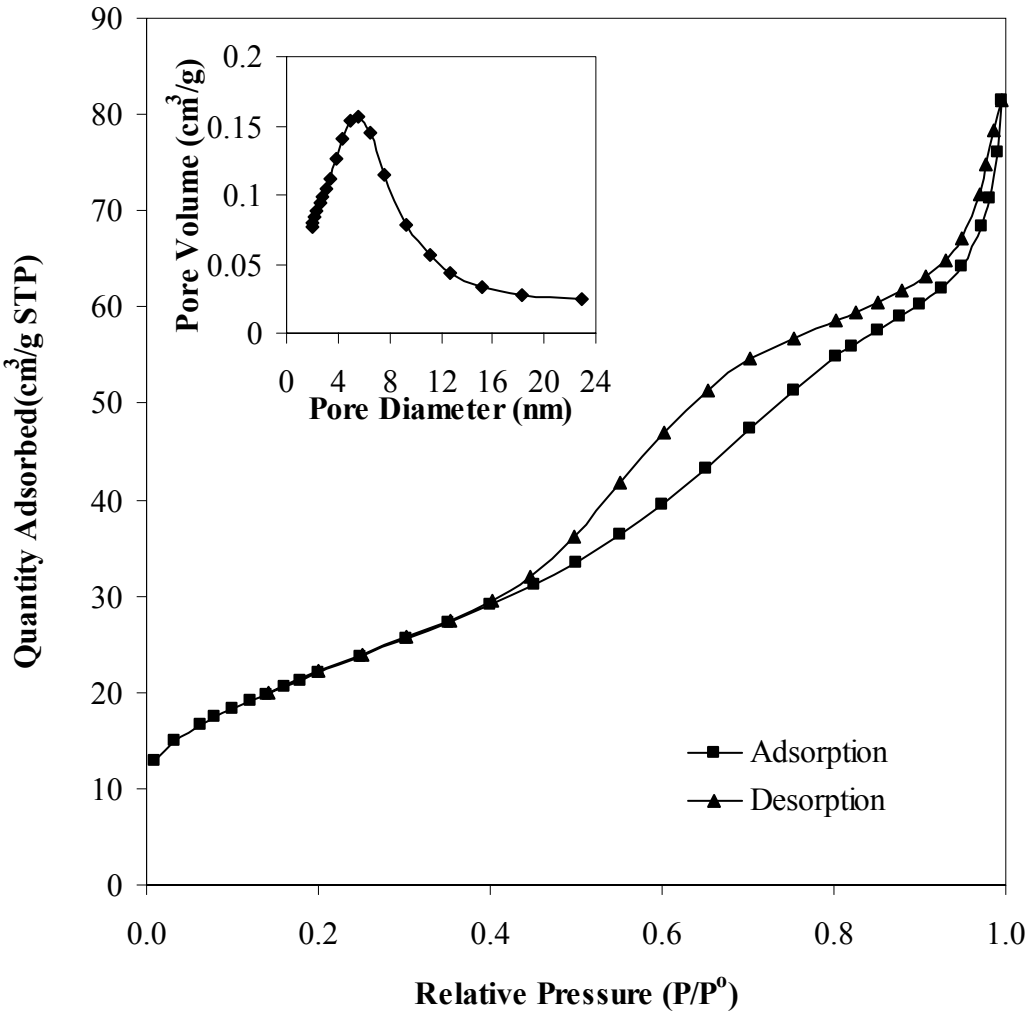

Figure 3.9 Nitrogen adsorption (■) /desorption (▲) isotherms and BJH pore size distribution (inset) for a calcined CZY sample prepared using the CTAB template. The sample was calcined in air from 25 to 600 °C at a heating rate of 20 ºC /min, with the final temperature being maintained for 4 h.

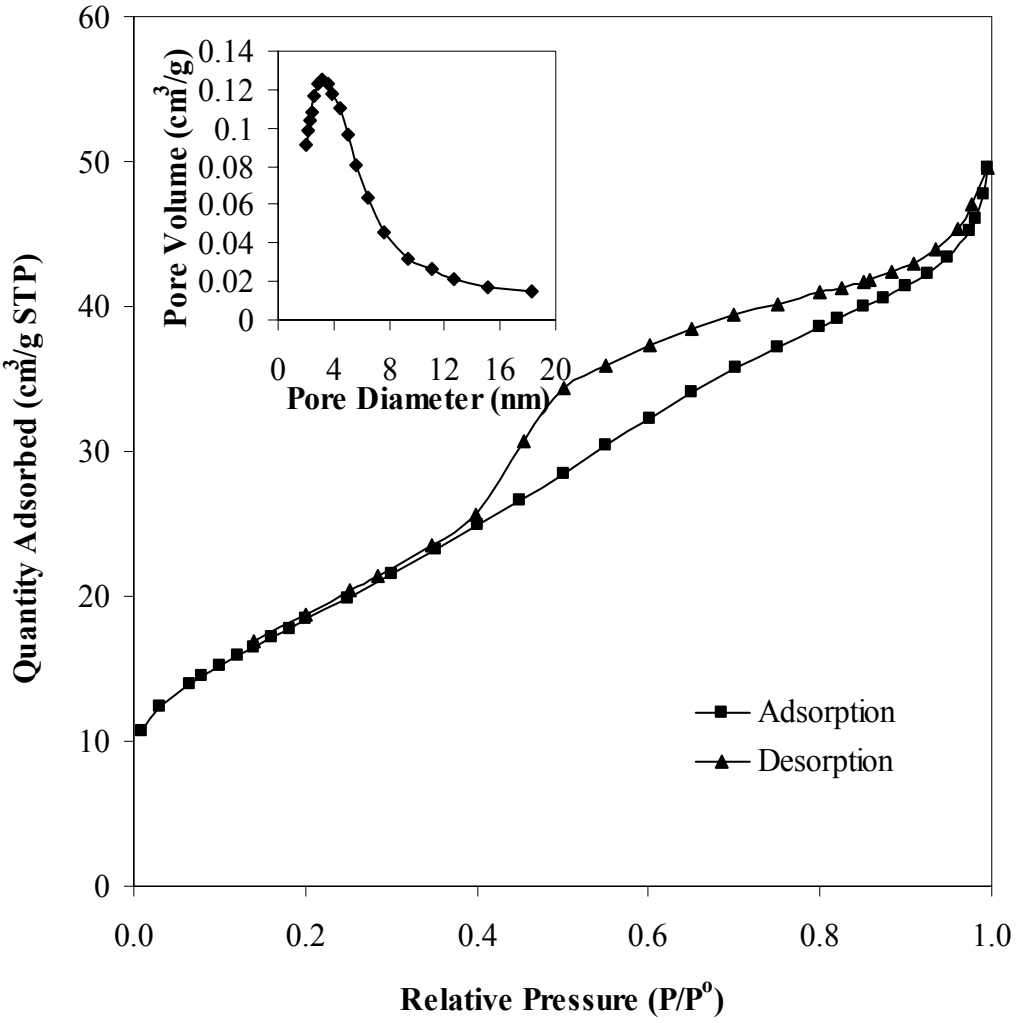

Figure 3.10 Nitrogen adsorption (■) /desorption (▲) isotherms and BJH pore size distribution (inset) for a calcined CZY sample prepared using the CTAB/1-propanol template. The sample was calcined in air from 25 to 600 °C at a heating rate of 20 ºC/min with the final temperature being maintained for 4 h.

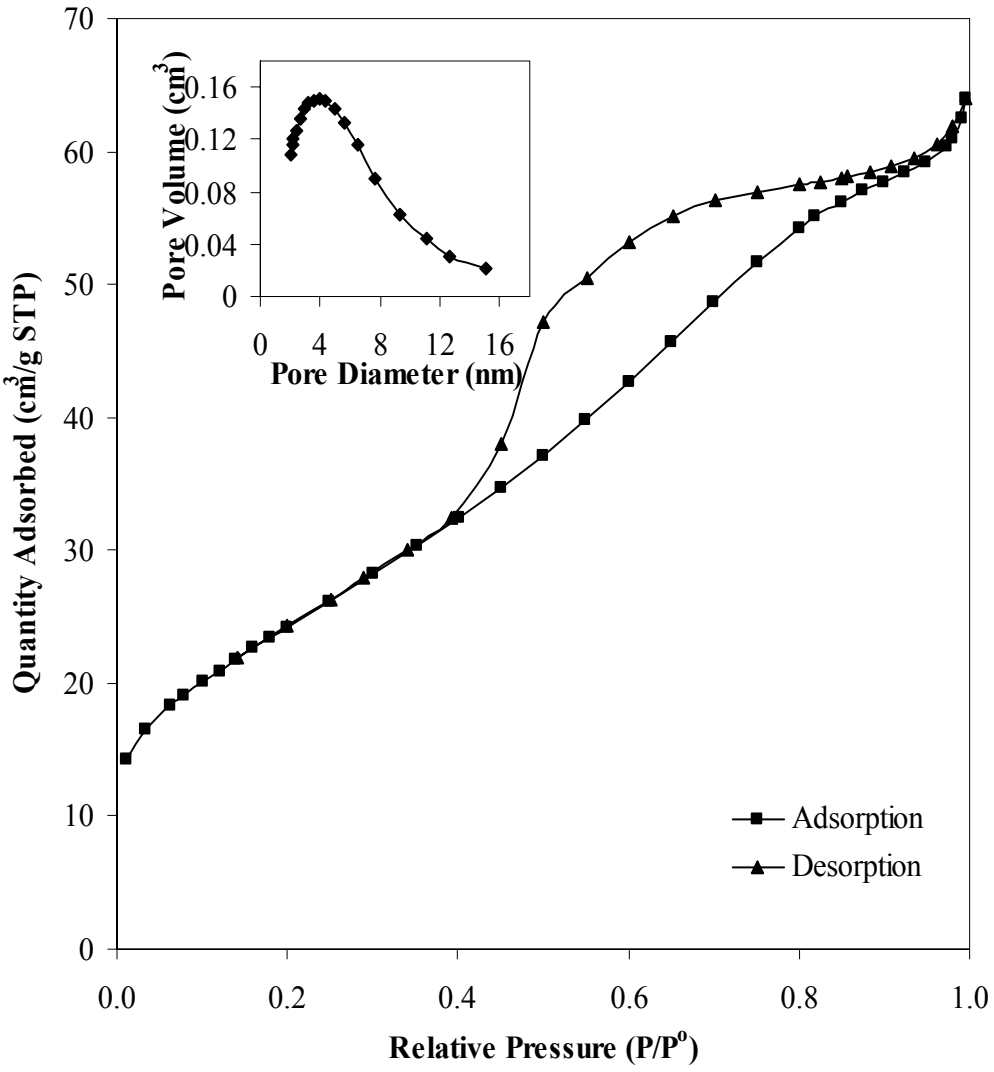

Figure 3.11 Nitrogen adsorption (■) /desorption (▲) isotherms and BJH pore size distribution (inset) for a calcined CZY sample prepared using the CTAB/1-propanol/ benzene template. The sample was calcined in air from 25 to 600 °C at a heating rate of 20 ºC/min with the final temperature being maintained for 4 h.

For our calculations I used the BJH evaporation model to estimate average pore diameters; however, this model assumes that only cylindrical pores are present in the sample[87]. Thus, some inaccuracies could exist with the calculated pore diameters. Despite these possible inaccuracies in absolute pore volume calculations, it is reasonable to expect the BJH model to accurately predict trends with pore diameter for samples having similar pore structures.

An additional synthesis parameter of interest is the sol-gel aging temperature. Table 3.5 shows the effect of varying the synthesis temperature on the physical properties of the calcined CZY samples, such as the BET surface area and average BJH pore diameter.

Table 3.5 Effect of synthesis temperature on the physical properties of CTAB templated CZY samples that were calcined in air from 25 to 600 °C at a heating rate of 20 ºC/min, with the final temperature being maintained for 4 h.

	Synthesis Temperature (ºC)			
	70 ºC	90 ºC	110 ºC	130 ºC
Sample	Surface Area, m^2/g (Pore Diameter, nm)[d]			
CZY/no Template	102 (3.7)	93 (3.7)	101 (4.7)	84 (3.6)
CZY/CTAB	80 (4.7)	94 (4.7)	94 (3.3)	107 (5.4)
CZY/CTAB/1-Propanol	85 (6.3)	87 (5.4)	89 (4.6)	120 (2.2)
CZY/CTAB/1-propanol/benzene	86 (4.7)	98 (4.7)	92(5.2)	95 (3.2)

d. The error margin for the surface area is ±5 m^2/g and for the pore diameter, ±0.5 nm

The three main reactions governing the sol-gel process are the hydrolysis, condensation, and the precipitation (or crystallization) steps. A cursory look at Table 3.5 may be at first misleading. For example, a look at the results for the CTAB/1-propanol templated CZY show that surface area increases while pore size decreases with increasing temperature. This suggests that as the temperature increases the crystal size decreases leading to a decrease in pore size and a corresponding increase in surface area. However, looking at the results a whole, that is, factoring the error margin; my conclusion appears to be different. On the whole, the results revealed that the surface area and pore size of each CZY mixed oxide materials are essentially the same irrespective of the synthesis temperature. This can only be true if the hydrolysis, condensation, and crystallization steps are all very low activation energy processes. This implies that the processes as a whole would come to completion even at low temperature and increasing the temperature would not affect the process.

The sol-gel pH is an important factor that affects metal oxide crystallization rates. The solution of the CZY precursor salts is known to be highly acidic, with a pH generally less than 1.0. This is easily explained as being due to the hydrolysis of the metal ions as discussed in the previous section on synthesis strategy for surfactant template technique. Hence, to bring about the precipitation of the metal oxides, the pH would have to be raised above 6.0, else the metal oxide precursor would permanently exist as stable coordinated cations in solution and no crystallization would occur even after hydrothermal treatment. Table 3.6 shows how the sol-gel pH affects the physical properties (i.e. surface area and pore size) of CZY samples synthesized using CTAB as

the structure directing agent. I observe that as the sol-gel mixture pH increases from near neutral pH values to a pH equal to 10.0, the BET surface area and average BJH pore diameter of the CTAB templated CZY samples also increased. This suggests that at higher pH, smaller size crystals are precipitated resulting in higher surface area but dies not explain the increase in the pore size which is counter intuitive. The reason for this discrepancy might be due to the error margin associated with the reported BJH pore size data. Thus, by putting the reported pore size data into perspective would allow for a proper interpretation of the result, that is, these BJH pore sizes are exaggerated.

Table 3.6 Effect of varying pH on the surface area and pore diameter of CTAB templated CZY samples that were calcined in air from 25 to 600 °C at a heating rate of 20 ºC/min, with the final temperature being maintained for 4 h.

pH of sol-gel mixture	BET Surface Area (m^2/g)[e]	Avg. Pore Diameter (nm)[e]
7.0	79	3.3
8.0	87	3.7
9.0	92	5.2
10.0	96	6.2
11.0	95	6.2

e. The error margin for the surface area is ±5 m^2/g and for the pore diameter, ±2.5 nm

Thus, increasing the pH of the sol-gel mixture would result in an increase in the surface area and a decrease in the pore size of the CTAB templated CZY materials.

As has been mentioned previously, the surfactant templating strategy is known to be highly successful for silica based systems, because the polymeric network of metal-oxygen-metal systems condense into a rigid oxide framework around the self-assembled

surfactant secondary structure at a very slow rate. In contrast, CZY type metal oxide precursors (e.g., hydroxide metal complexes) rapidly agglomerate into larger oxide particles at high pH and are easily crystallized at moderate temperatures. Therefore, it was suggested that the rapid rate of CZY condensation and crystallization might inhibit or hinder the formation of an ordered array of cylindrical mesopores for the CZY system. To address this problem, hydrolysis retarding agents or complexation agents were added to the CZY metal oxide precursor solution, so as to decrease the rate of metal hydroxide complex formation and thus reduce the condensation step. This would allow for sufficient time for surfactant micelles to self assemble to higher order tertiary structure like the hexagonal array structure within the CZY synthesis sol-gel. The retardation agent achieves this effect by becoming a slow to dissociate ligand for the metal ions in solution. In theory, the more strongly the retardation additive binds to the metal ions or hydrated metal complexes in the sol-gel mixture, the slower these metal species can reversibly dissociate the ligands and self assemble into larger oxide particles.

Table 3.7 shows how the physical properties of CTAB templated CZY samples are affected by the addition of hydrolysis retarding agents to the sol-gel mixture during the aging process. Adding acetylacetone (ACAC), a common hydrolysis retarding agent, resulted in a 30% increase in the BET surface area of CTAB templated CZY material. However, adding triethanolamine (TEA), also a hydrolysis retarding agent, resulted in an approximately 90% loss of surface area for the CTAB templated CZY material. Thus, ACAC is a better hydrolysis retarding agent than TEA for improving the BET surface area of the CTAB templated CZY material.

Table 3.7 Effect of hydrolysis retarding agents on the surface area and pore diameter of CTAB templated CZY samples. Samples were calcined in air from 25 to 600 °C at a heating rate of 20 ºC/min, with the final temperature being maintained for 4 h.

CZY Template	BET Surface Area (m^2/g)[f]	Avg. Pore Diameter (nm)[f]
CTAB	78	6.2
CTAB/ACAC	106	5.4
CTAB/TEA	9	3.8

f. The error margin for the surface area is ±5 m^2/g and for the pore diameter, ±2.5 nm

This result suggests that of the two complexation agents, ACAC has a lower binding strength to the metal ions than TEA. This means that with CTAB/ACAC templated CZY mixed oxides, the ACAC ligands are easily replaced by the hydroxo groups than would the TEA in the CTAB/TEA templated CZY mixed oxides. An estimation of the binding strength of ACAC and TEA can be made solely by examining the structures of the compounds as shown below.

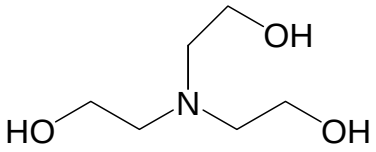

Triethanolamine (TEA)

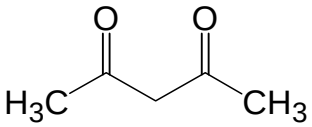

Acetylacetone (ACAC)

Triethanolamine (TEA) is tridentate while acetylacetone (ACAC) is bidentate. Based on rule of thumb, it is expected that TEA would have a stronger binding strength than ACAC because it has 3 binding site while ACAC has two binding sites. This is a

plausible explanation to why both complexation agents behaved the way they did. An actual experiment to determine the binding strength would have to de carried out in order to ascertain the true values. The determination of the binding strength was not explored.

Figures 3.12 and 3.13 show the nitrogen adsorption/desorption isotherms and the BJH pore size distributions of CZY samples synthesized using CTAB/ACAC, and CTAB/TEA. The physisorption isotherm showed typical hysteresis loop associated with mesoporous materials. This suggests that indeed mesoporous CZY materials were prepared. However, the BJH pore size distribution of these samples (CTAB/ACAC templated CZY and CTAB/TEA templated CZY mixed oxides) showed a much narrower pore diameter when compared to the CTAB templated CZY mixed oxides (Figure 3.9-3.11).

The catalytic activity and stability of a support material is closely tied to its composition and three dimensional structures. Thus, energy dispersive X-ray analysis (EDX) was used to examine the homogeneity of the calcined CZY oxide products, and the extent of sample crystallinity (nature and size of crystals present) was determined by powder X-ray diffraction (PXD). Figure 3.14 shows the PXD patterns of pure oxides of ceria, zirconia, and yttria; Figure 3.15 shows the PXD patterns of CZY mixed oxides synthesized using CTAB alone, CTAB/1-propanol, and CTAB/1-propanol/benzene as the structure directing agent; and Figure 3.16 shows the PXD patterns of CZY mixed oxides synthesized using CTAB alone, CTAB/ACAC, and CTAB/TEA as the structure directing agent at 2θ values ranging from 10º to 80º.

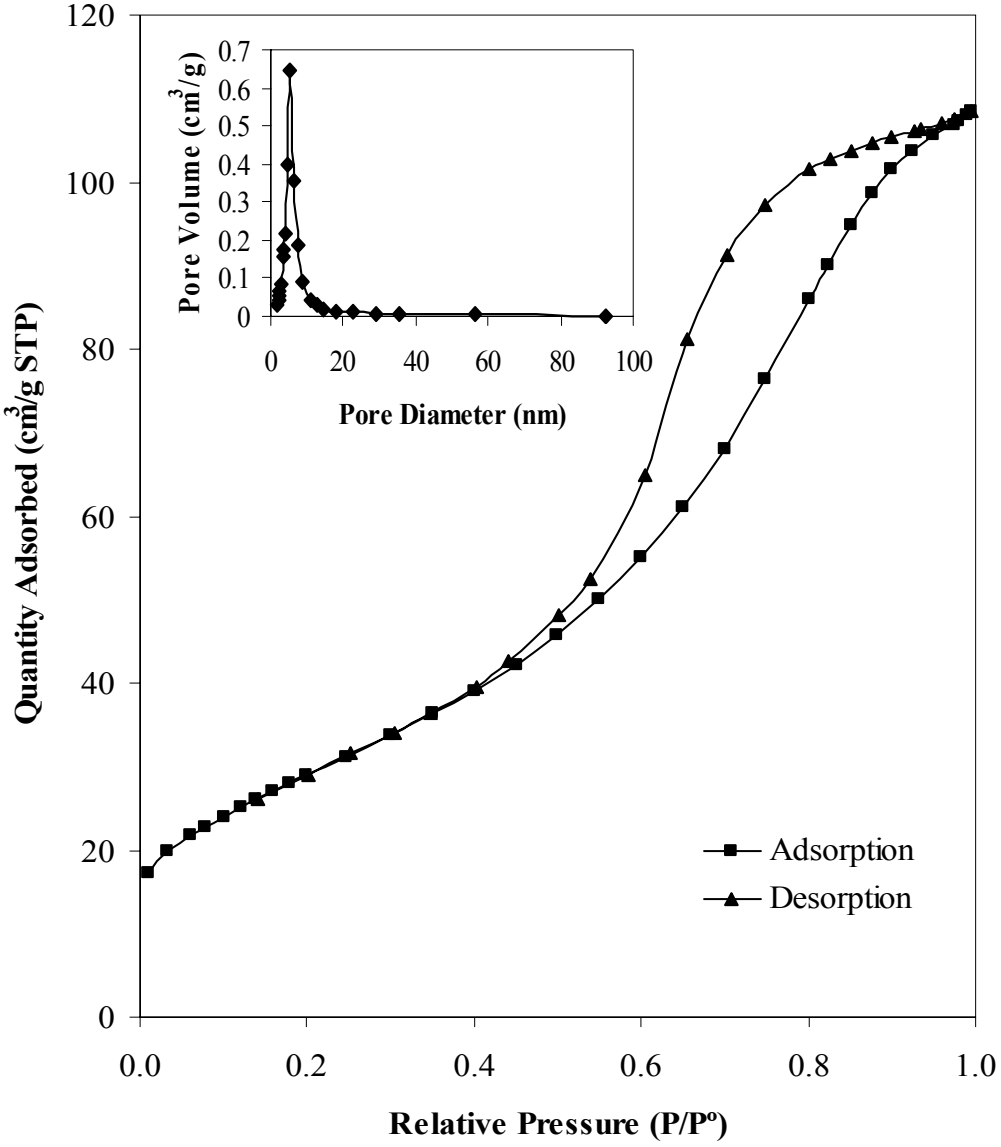

Figure 3.12 Nitrogen adsorption (■) /desorption (▲) isotherms and BJH pore size distribution (inset) for a calcined CZY sample prepared using the CTAB/ACAC template. The sample was calcined in air from 25 to 600 °C at a heating rate of 20 ºC /min, with the final temperature being maintained for 4 h.

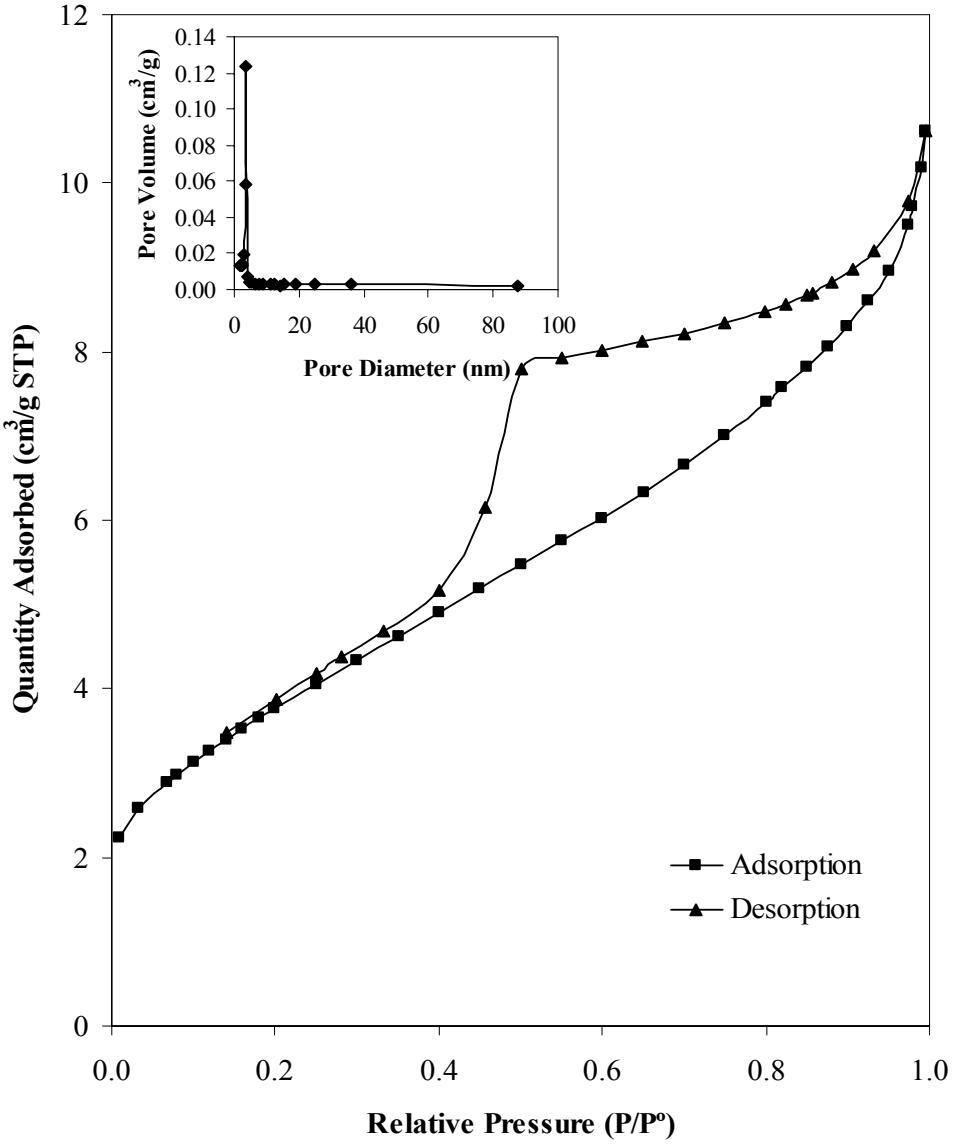

Figure 3.13 Nitrogen adsorption (■) /desorption (▲) isotherms and BJH pore size distribution (inset) for a calcined CZY sample prepared using the CTAB/TEA template. The sample was calcined in air from 25 to 600 °C at a heating rate of 20 ºC /min, with the final temperature being maintained for 4 h.

The small angle X-ray diffraction (SAXD) pattern (not shown) for the same samples at 2θ values ranging from 1º to 10º did not reveal any low angle peaks that are often synonymous with *ordered* mesoporous MCM-41 materials. This suggests that the CZY material synthesized did not consist of an ordered array of mesopores. This conclusion is in agreement with similar observations made by Terribile et al[18,19]. The power XRD patterns for all the CTAB templated CZY samples (see Figure 3.14-3.16) are very similar to that of pure ceria. This means that the CZY samples all have the same cubic fluorite structure of ceria. The absence of split ends at the peaks for the powder XRD patterns of the CZY samples implies that no phase segregation (i.e. ceria rich phase and zirconia rich phase) occurred in the samples. The powder XRD patterns of the CZY samples also reveal the presence of low intensity broad peaks, which indicate the existence of nanocrystallites. By first subtracting out the background noise from the PXD pattern, followed by eliminating all but one peak associated with the first peak position, a curve fitting around this first major peak position that's generally near ~29.0 º 2θ was done automatically. From the results of the fitted curve, the full width at half maximum (FWHM) and the 2θ position for the peak are measured. Using Scherrer's equation, the particle size of the crystallites was estimated to be between 6.0 and 8.0 nm.

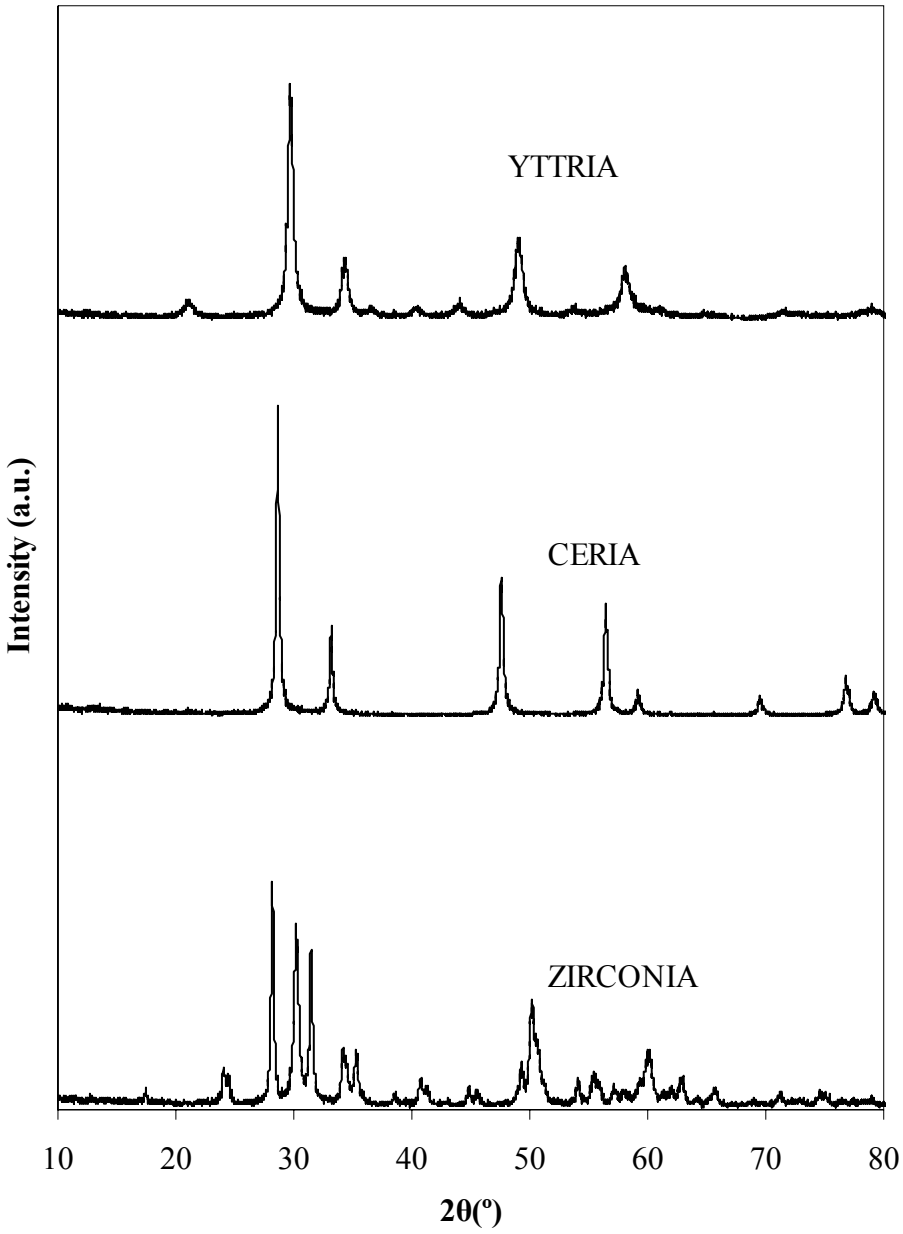

Figure 3.14 Powder X-ray diffractogram for pure samples of yttria, ceria, and zirconia oxides. Samples were calcined in air from 25 to 600 °C at a heating rate of 20 ºC/min, with the final temperature being maintained for 4 h.

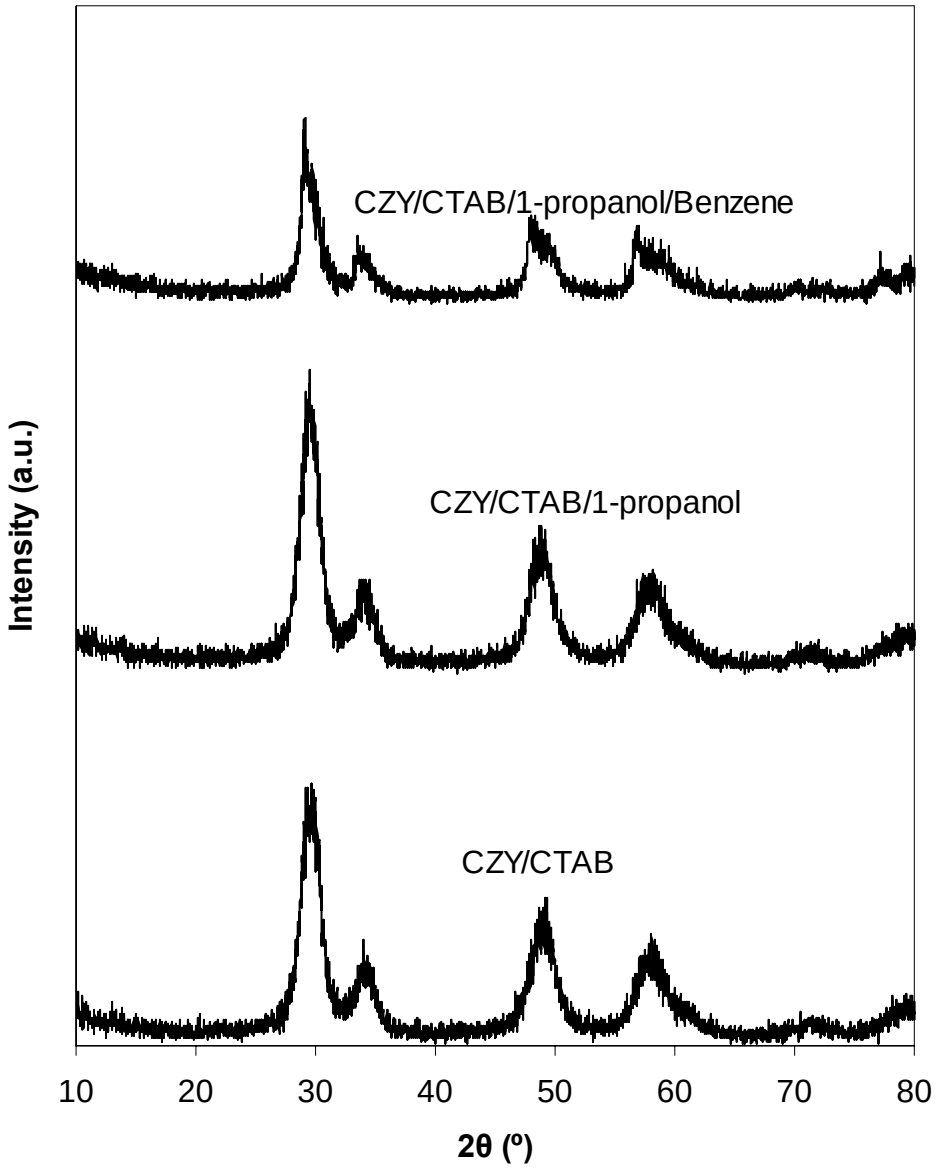

Figure 3.15 Powder X-ray diffractogram for CZY samples prepared using CTAB alone, CTAB/1-propanol, and CTAB/1-propanol/benzene. Samples were calcined in air from 25 to 600 °C at a heating rate of 20 ºC/min, with the final temperature being maintained for 4 h.

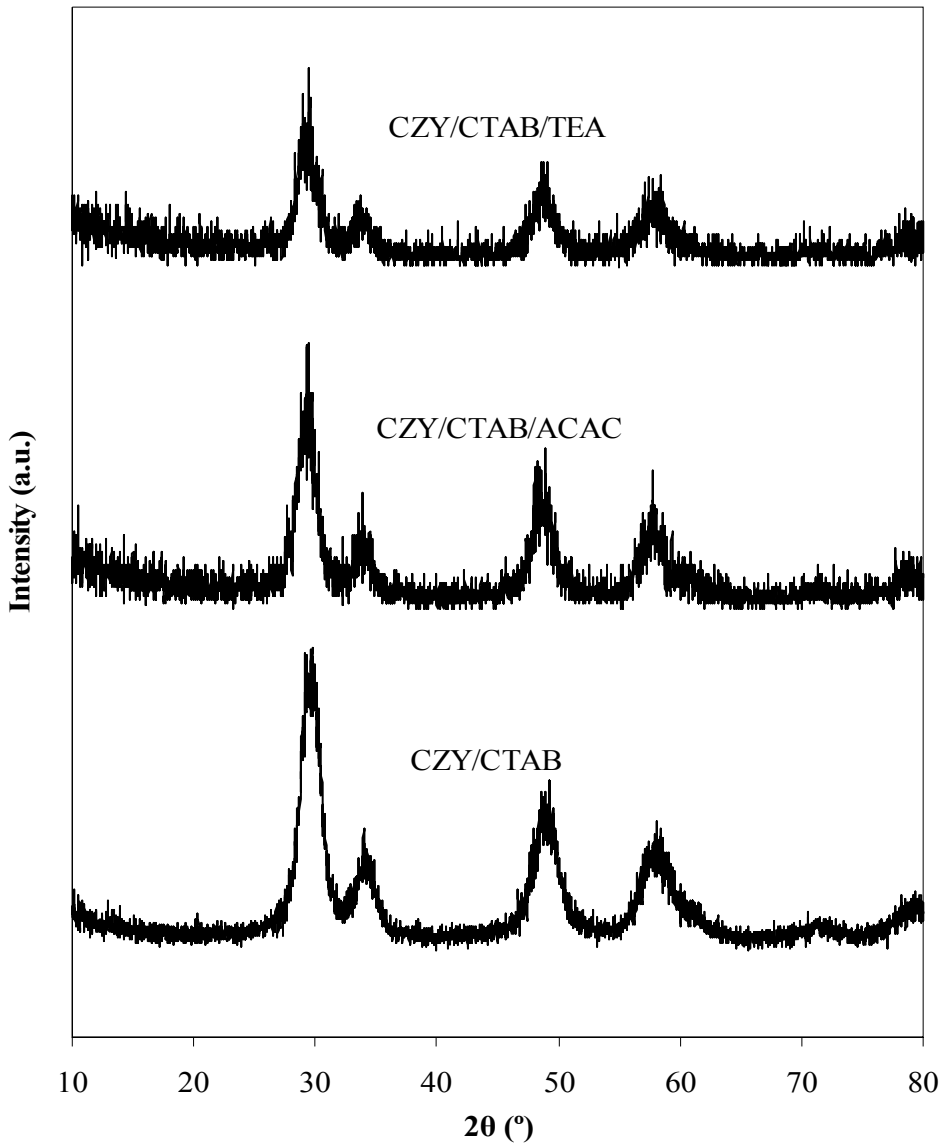

Figure 3.16 Powder X-ray diffractogram for CZY samples prepared using CTAB alone, CTAB/ACAC, and CTAB/TEA. Samples were calcined in air from 25 to 600 °C at a heating rate of 20 ºC/min, with the final temperature being maintained for 4 h.

Prior studies have shown that catalytic converter performance can be significantly enhanced using specific ratios of ceria, zirconia, and yttria oxides as catalyst supports[88-90]. Thus, it was important to test the CZY mixed oxide products to determine if the ratio of salt precursors in the sol-gel corresponded to the ratio of metal oxides found in the calcined CZY materials. In Table 3.8, the predicted oxide composition, as mole percent of ZrO_2, Y_2O_3, and CeO_2, for the family of CTAB templated materials is compared with the experimentally determined compositions that were measured using inductively couple plasma atomic emission spectroscopy (ICP-AES). The expected composition on a mole basis is 45.0 mol%, 5.0 mol%, and 50.0 mol% of ZrO_2, Y_2O_3, and CeO_2, respectively. These results reveal that all the metal oxides are well incorporated into all of the sol-gel prepared CZY materials, and the observed loadings of metal oxide are within the margin of error for the expected amounts.

Table 3.8 Elemental composition of CTAB templated CZY samples

Sample	ZrO_2 (mol %)[g]	$YO_{1.5}$ (mol %)[g]	CeO_2 (mol %)[g]
Theoretical Amount	45.00	5.00	50.00
CZY/CTAB	45.47	4.83	49.70
CZY-CTAB/1-propanol	44.37	4.85	50.79
CZY-CTAB/1-propanol/benzene	45.21	5.14	49.64

g. The error margin for the elemental composition is ±1.0 mol%

Additional efforts were made to observe via electron microscopy the arrangement and size of pore present in the CTAB templated samples. It was also important to ascertain the primary particle size and extent of agglomeration present in these samples; thus, transmission electron miscopy (TEM) was used to examine all CTAB templated materials. Figures 3.14-3.18 show TEM images of CZY materials synthesized via sol-gel methods that employed CTAB alone, CTAB with 1-propanol, CTAB with 1-propanol and benzene, CTAB with ACAC, and CTAB with TEA. All samples were calcined in air from 25 to 600 °C at a heating rate of 20 ºC/min, with the final temperature being maintained for 4 h. The TEM images of all calcined CZY samples prepared from sol-gels that contained CTAB alone, CTAB/1-propanol, CTAB/1-propanol/benzene, CTAB/ACAC, or CTAB/TEA are virtually indistinguishable. They all show similar morphology, that is, they are basically an agglomeration of nanosized primary particles that are approximately 5 nm in diameter and exhibit some crystallinity. Further, there did not appear to be any ordered array of mesopores within any of the samples as is commonly observed with silica materials prepared in a likewise fashion. Thus, surfactant templating strategies have been shown to be ineffective for making cylindrical mesopores similar to those predicted (see Figures 3.2 - 3.4).

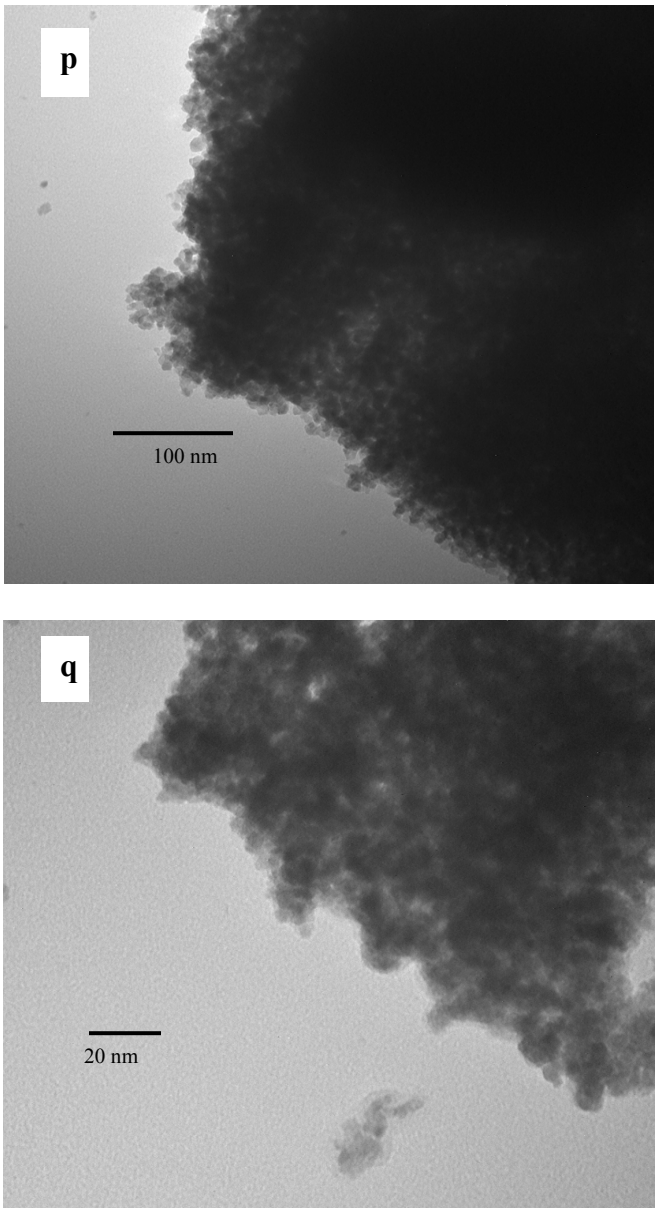

Figure 3.17 Transmission electron micrographs for a calcined CZY mixed oxide prepared using CTAB as the sol-gel template. Samples were calcined in air from 25 to 600 °C at a heating rate of 20 ºC/min, with the final temperature being maintained for 4 h.

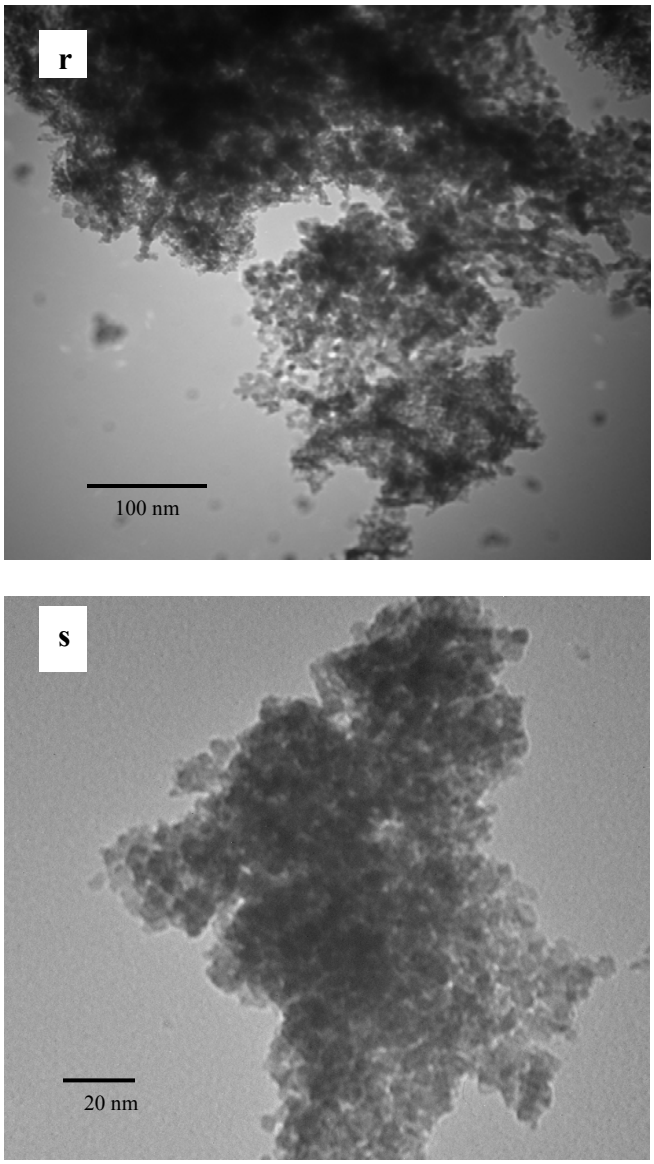

Figure 3.18 Transmission electron micrographs for a calcined CZY mixed oxide prepared using CTAB/1-propanol as the sol-gel template. Samples were calcined in air from 25 to 600 °C at a heating rate of 20 ºC/min, with the final temperature being maintained for 4 h.

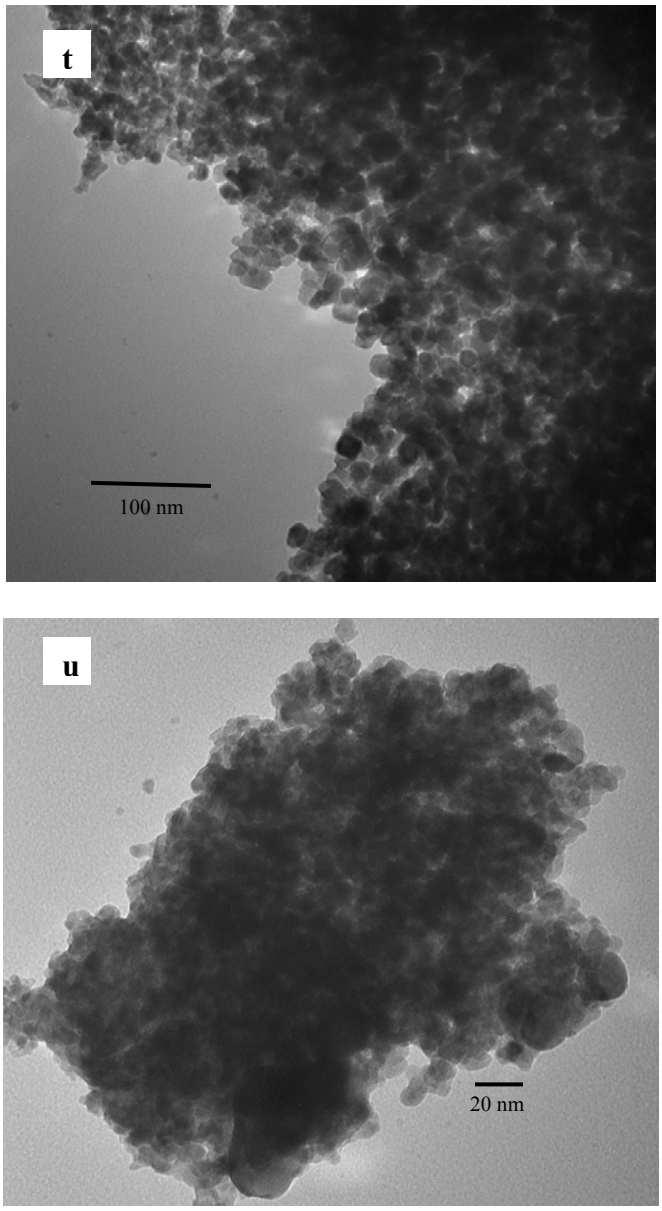

Figure 3.19 Transmission electron micrographs of a calcined CZY mixed oxide prepared using CTAB/1-propanol/benzene as the sol-gel template. Samples were calcined in air from 25 to 600 °C at a heating rate of 20 ºC/min, with the final temperature being maintained for 4 h.

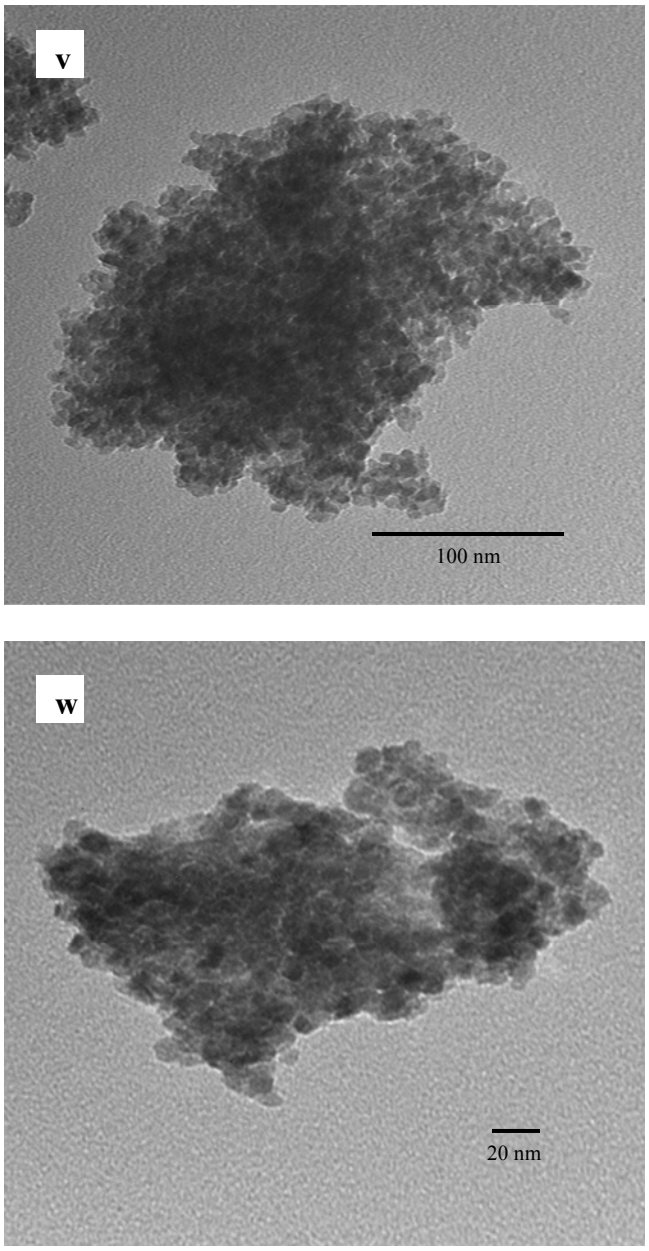

Figure 3.20 Transmission electron micrographs for a calcined CZY mixed oxide prepared using CTAB as the sol-gel template and ACAC as the hydrolysis retarding agent. Samples were calcined in air from 25 to 600 °C at a heating rate of 20 ºC/min, with the final temperature being maintained for 4 h.

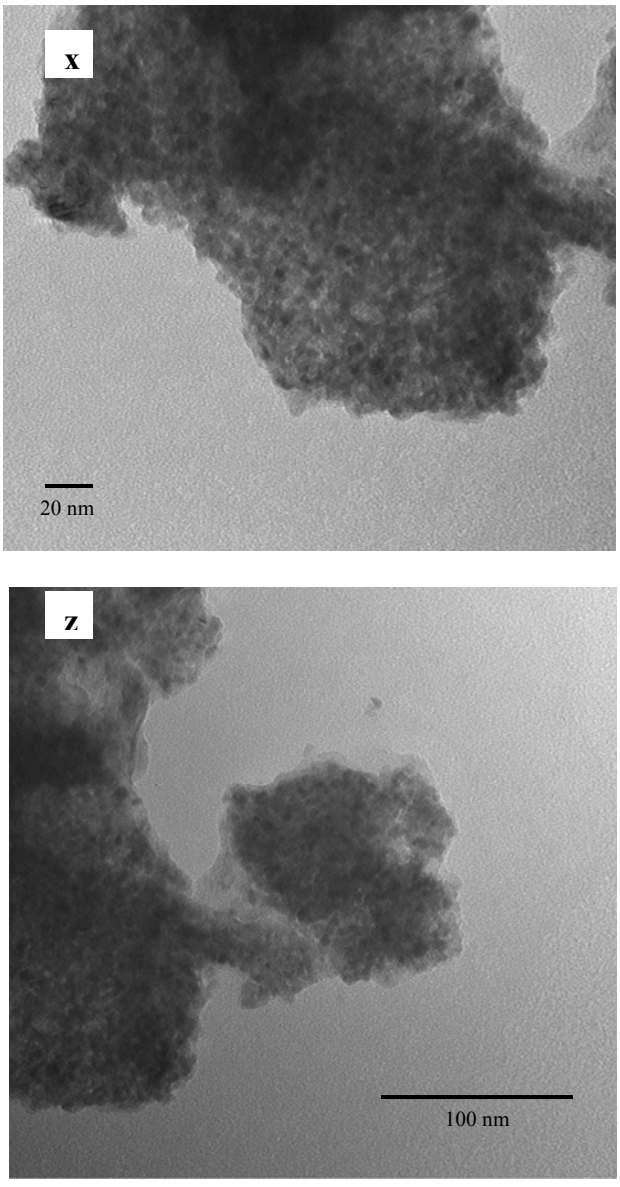

Figure 3.21 Transmission electron micrographs for a calcined CZY mixed oxide prepared using CTAB as the sol-gel template and TEA as the hydrolysis retarding agent. Samples were calcined in air from 25 to 600 °C at a heating rate of 20 ºC/min, with the final temperature being maintained for 4 h.

Although the TEM images showed that ordered mesopores were not formed, yet the nitrogen adsorption experiments showed that all the CZY mixed oxides synthesized contained mesopores. Before proceeding to the out come of the studies on accelerated aging, it is important to re-evaluate the synthesis mechanistic pathways based on the results of the TEM images, powder XRD, and nitrogen sorption experiments. In spite of the shrinking effect which the ethanol solvent may have of CZY samples as they are dried on the carbon grids during the preparatory stages of the sample for TEM imaging, the absence of low angle peaks during the small angle XRD confirms that no long range order exist in any of the samples. Therefore, it can be inferred that the CZY samples followed a completely different mechanistic pathway. Figure 3.22 shows three possible mechanistic pathway that might explain morphology of the CZY samples synthesized using CTAB and additives as structure directing agents. Pathway 1 shows the micelles are assembled into spherical secondary with the oxide particles forming nucleating sites at the interstices between the spherical micelles. On calcination, the micelles are burned off and the oxides particles are eventually left behind. Pathway 2 suggests that the micelles act as reverse micelles. The oxide particles nucleate around the centers of these reverse micelles thus condensing in between them. After calcination, the oxides with different particles sizes are created because of the differences in crystal growth associated with each nucleating sites. Pathway 3 suggests that no self assembly of the micelles into secondary structure has taken place before the metal oxides were precipitated. However, mesopore structures were created within the CZY materials by the micelles that had been trapped between the precipitated oxide particles. After calcination, the micelles are

burned off leaving behind an agglomerated system containing primary sized particles assembled together. This explains why the TEM images looks like an agglomeration of primary particles in general.

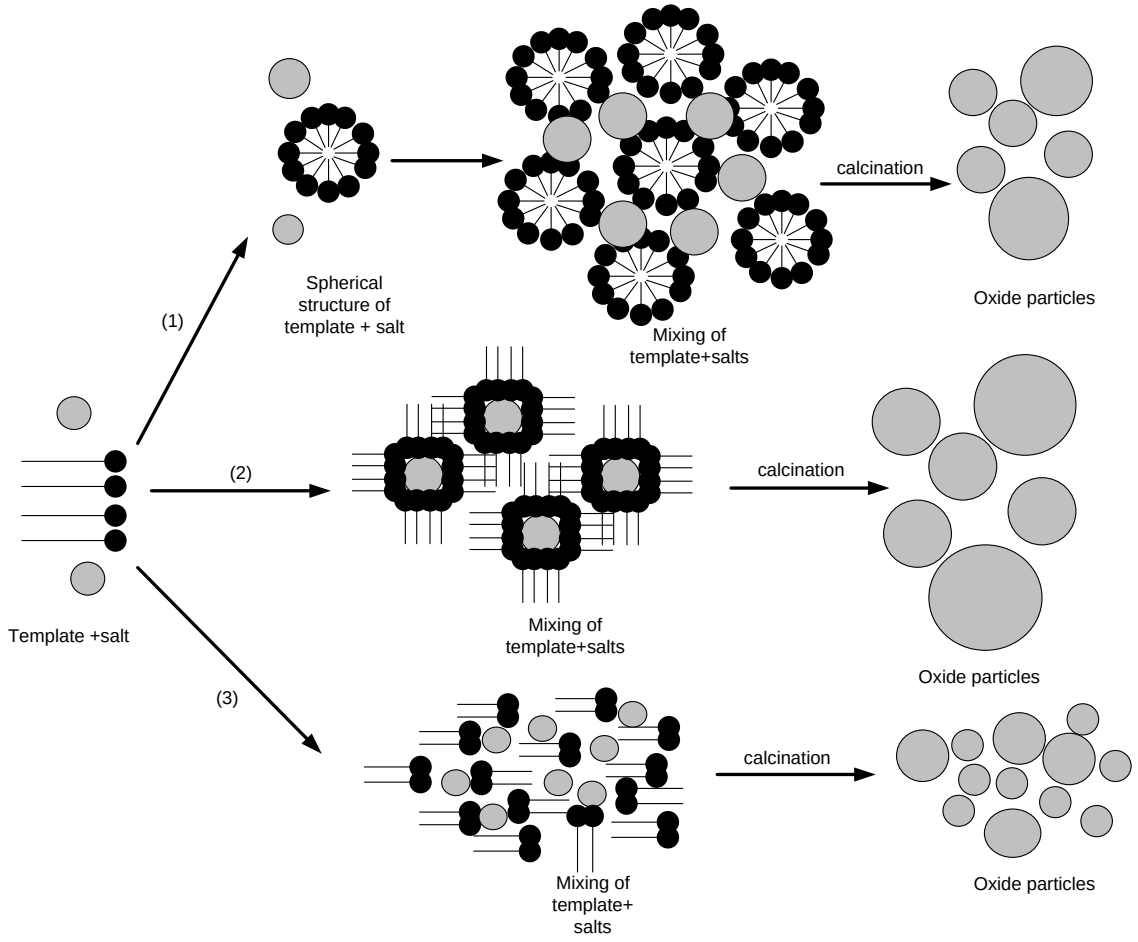

Figure 3.22 Proposed mechanistic pathways for CZY mixed oxides prepared via sol-gel technique that employ CTAB surfactant templated.

It was important to determine the thermal stability of these CZY structures at temperatures above those required to oxidatively remove the templates (i.e., 600 °C). The upper temperature limit for these studies is set by the uppermost temperature they would likely experience under operating conditions as a catalytic converter support material,

which is on occasion as high as 900 to 1000 °C. Therefore, thermal degradation studies of the surfactant templated CZY materials were carried out between 700 and 1000 °C. Table 3.9 shows how the surface area and pore volume of surfactant templated CZY oxides decrease upon calcination to 1000 °C.

Table 3.9 Variation of surface area and pore volume as a function of aging temperature for CTAB templated CZY samples. Samples were calcined in air to the specified temperature at a heating rate of 20 ºC/min, with the final temperature being maintained for 4 h.

Aging Temperature (ºC)	BET Surface Area $(m^2/g)^h$	BJH Pore Diameter $(nm)^h$
700	63	7.5
800	50	11.0
900	30	15.2
1000	13	23.3

h. The error margin for the surface area is ±5 m^2/g and for the pore diameter, ±0.5 nm

The overall loss in surface area from 700 to 1000 ºC is approximately 79.4%. This decrease in surface area is expected because of the enhanced oxide sintering with zirconia and ceria that can occur at temperatures above 800 °C. The trend for surface area and pore size follows the classic trend, that is, as the surface area decreases, the pore size increases.

The nitrogen physisorption experiments for CTAB templated CZY samples that had been calcined to temperatures between 700 and 1000 °C showed a significant loss in porosity. However, what was not known from those studies was the nature of the processes that led

to the decrease in porosity. Namely, did the sample undergo some form of melting that caused the oxide to collapse upon itself or did the sample undergo oxide sintering, which would lead to a decrease in sample surface area as a result of increased oxide crystallinity. The latter sintering process could manifest itself as greater numbers of small crystallites or the growth of existing crystallites into larger crystalline regions, both of which can be quantified by powder X-ray diffraction. Thus, all CTAB templated CZY materials were characterized via PXD, and the resulting spectra are shown in Figure 3.23. The peak positions observed in the powder XRD pattern for all calcined sample were quite similar; however, peak intensity and sharpness increased with increasing calcination temperature. This suggests that the CZY mixed oxides are becoming more crystalline at higher temperatures, and the likely mechanism for this change involves the growth of nanosized oxide crystals formed at lower temperatures (less than 600 °C) via a solid-solid phase change process. This result is supported by Table 3.9. Further, the CZY samples do not show any evidence of phase segregation into a heterogeneous mixture of oxide phases, even at higher temperatures.

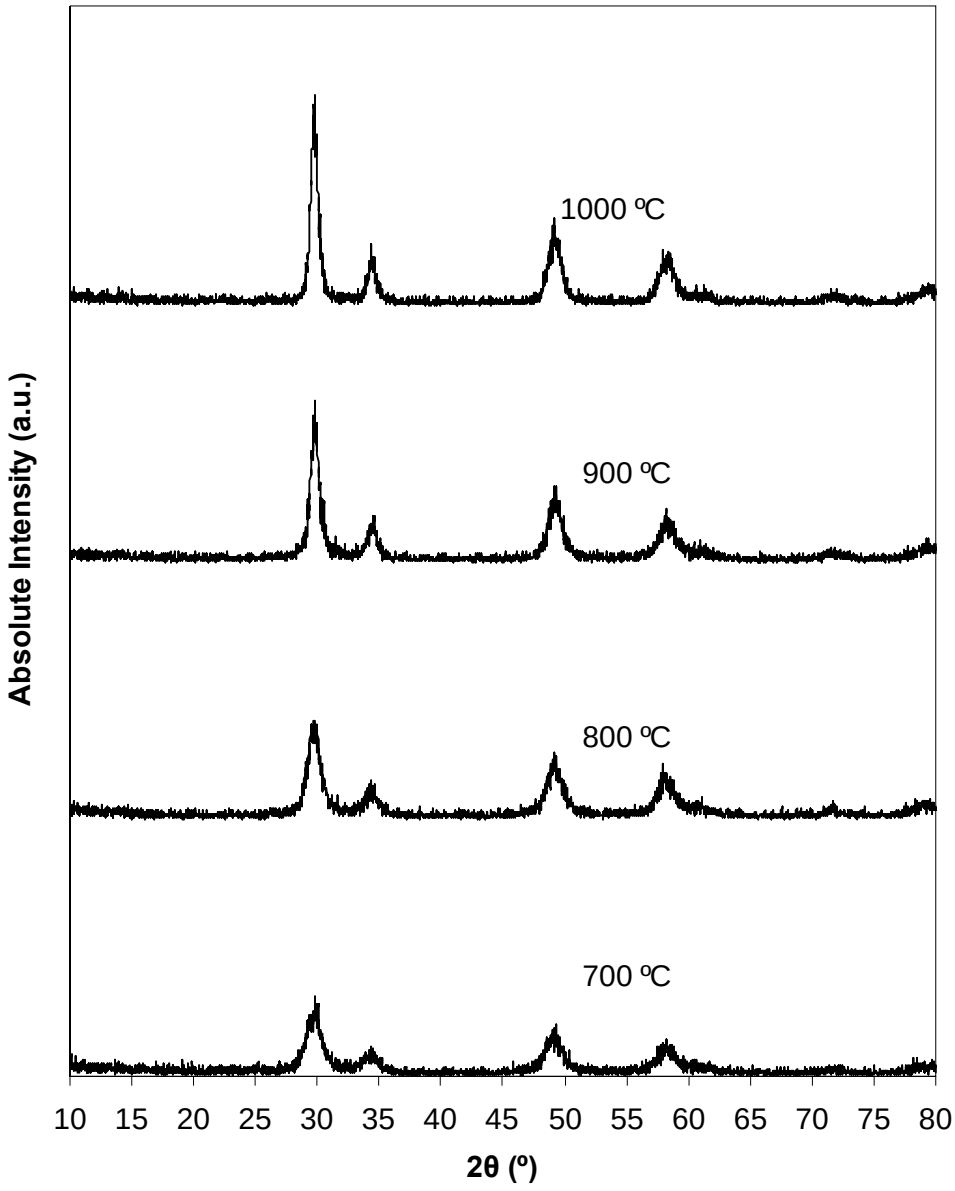

Figure 3.23**:** Powder X-ray diffractogram (PXD) for CTAB templated CZY samples. Samples were calcined in air to the specified temperature at a heating rate of 20 ºC/min, with the final temperature being maintained for 4 h.

Conclusion

In this chapter, I outlined the steps required for synthesizing surfactant (CTAB) templated mesoporous CZY materials. The synthesized CZY materials were characterized via a range of techniques to: ascertain the existence of an ordered mesoporous structure, determine the morphology and homogeneity of the oxide phase, quantify the elemental composition, evaluate the effect of heating rate during calcination, and measure the surface area and the pore size of the calcined material. In addition, the use of auxiliary sol-gel additives, such as cosolvents, swelling agents, and hydrolysis retarding agents, was studied to quantify the effects of each respective additive on the physical properties of the synthesized surfactant templated CZY materials. Ultimately, a range of mesoporous surfactant templated CZY mixed oxides were successfully prepared, although the pore structure exhibited no long range order.

Adding cosolvents and swelling agents did not increase the pore size of the CTAB templated CZY materials, because the templating schemes that were suggested did not occur (refer to Figures 3.2 - 3.4). However, it is proposed that the templating mechanism followed the scheme shown in Figure 3.22 with the third pathway being the most feasible. Further, the use of some hydrolysis retarding agents, e.g., acetylacetone (ACAC), significantly increased the surface area of CTAB templated CZY materials, while other known hydrolysis retarding agents, e.g., triethanolamine, had the opposite effect. The difference between these two hydrolysis retarding agents may have to do with their binding strength to the metals, but this effect was not fully explored.

By combining the results from all of the CZY characterization experiments, it is now believed that the organic additives simply alter the size of the primary oxides particles that are formed in the sol-gel during the thermal hydrolysis stage of sample preparation. The final calcined CZY materials are then simply an agglomeration of these primary particles. Therefore, the mesoporosity observed in the nitrogen physisorption data is likely created by the void space between these agglomerated pseudo-spherical oxide particles shown in Figure 3.24.

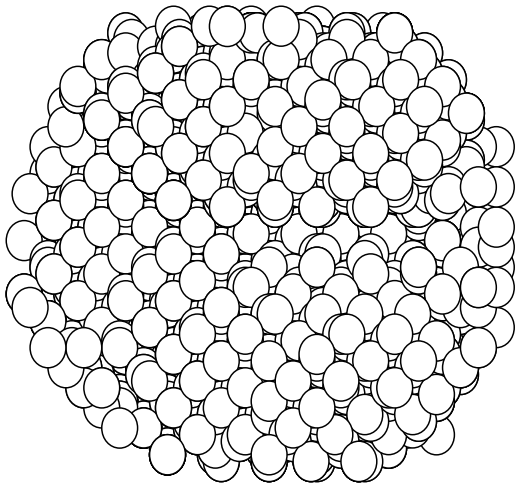

Figure 3.24 Proposed structure for all CZY mixed oxides materials prepared via sol-gel techniques that employ CTAB surfactant template.

Lastly, varying the heating rate during calcination to tempartures as high as 600 °C did not significantly affect the surface area of the surfactant templated CZY materials. This is largely due to the fact that the as-synthesized CZY materials had only moderate loading of organics. It was also observed that all of the CTAB templated materials underwent significant structural changes when heated to temperatures in excess of 800

°C. This suggests that a slow loss of mesoporosity (and thus, a slow decrease in catalytic activity) would likely occur during extended use of the material in catalytic converter applications, but that the observed loss in surface area was still less than that seen with many state-of-the-art CZY materials.

CHAPTER FOUR

BLOCK COPOLYMER TEMPLATE TECHNIQUE

In this chapter, the general synthesis strategy laid out in the previous chapter is extended by using block copolymer template, a soft template, to synthesize mesoporous CZY mixed oxides. The effects of varying calcination heating rate and adding hydrolysis retarding agent on the physical properties of the synthesized mesoporous CZY mixed oxides are investigated. In addition, thermogravimetric analysis (TGA) on the as-synthesized CZY mixed oxides samples are carried out. The information form the TGA will provide key indicators to when the templates and oxide formation reaction is completed. This will be used to plan the temperature at which calcination would be done and best calcination heating rate to adopt for the process too. The characterization of mesoporous CZY mixed oxides would be through the following primary analytical methods: physisorption techniques (Brunauer-Emmett-Teller (BET) surface area and Barrett-Joyner-Halenda (BJH) pore size distribution), powder X-ray diffraction (PXD), elemental analysis, transmission electron microscopy (TEM), and scanning electron microscopy (SEM).

Synthesis Strategy for CZY Mixed Oxides Using Block Copolymer Template Technique

The use of block copolymer template for the synthesis of mesoporous oxides has been reported extensively in the literature.[49,79,91-98] Mesoporous silica based materials synthesized using block copolymer template are known to have silica walls that are

thicker than those made from surfactant template.[51] This is important because it suggests that block copolymer templated CZY mixed oxides would be structurally more stable than surfactant templated CZY mixed oxides. For our work, I used Pluronic P123,, ($PEO_{20}PPO_{70}PEO_{20}$) triblock copolymer as the structure directing agent during the synthesis. Since block copolymer template is an example of a soft template, the general synthesis strategy discussed in detail in the previous chapter can be applied in principle with minor adjustments. The main difference, like in all soft template technique, is the choice of the template. In chapter 3, CTAB, a surfactant, was used as the structure directing agent; but in this chapter, Pluronic 123, a block copolymer, will be used as the soft template. As shown in Figure 3.1, the block copolymer, which replaced the surfactant, is dissolved not in deionized water but in a mixture of ethanol and deionized water. The block copolymer is semi-solid like petroleum jelly. The mixture of block copolymer and the ethanol-deionized water mixture are placed on a hot plate and stirred using a magnetic stirrer. As the mixture is stirred continuously, its temperature is gradually raised to 40 ºC so that the block copolymer would completely be dissolved. The metal oxide precursor salts are prepared in identical fashion as explained in chapter 3. With the block copolymer solution formed, the mixing of the precursor oxide solution and the block copolymer solution follows the exact protocol detailed in chapter 3.The reader is referred to similar section in chapter 3 for more details.

Synthesis of CZY Mixed Oxide Using Pluronic P123 as Template

All chemicals used in the preparation of surfactant template CZY samples were used as received from their respective manufacturer. See chapter 3 for detailed description of the chemical used except Pluronic® P-123 (Sigma-Aldrich, average Mn ~5,800). For the preparation of the metal oxide precursor solution follow the instruction provided in chapter 3. Only the description of how to make the Pluronic P123 solution is provided. In a beaker, some Pluronic P123, a paste or semi solid, was dissolved in a mixture of deionized water (60 vol%) and 1-propanol (40 vol%). 1-propanol is added to improve the solubility of the Pluronic P123. The Pluronic P123 solution is heated on a hot plate to about 40 ºC and stirred continuously for about an hour using a magnetic stirrer until the solution becomes homogeneous. Table 4.1 shows a typical composition of the precursors, solvent, and block copolymer that are used during the synthesis of mesoporous CZY mixed oxide.

Table 4.1 Typical sample composition for P123 Templated CZY

	Molar Ratio		
Reagents	Sol-gel	Oxide	Mass (g)
$ZrO(NO_3)_2.6H_2O$ (ZrO_2)	9	9	4.000
$Y(NO_3)_3.6H_2O$ ($YO_{1.5}$)	1	1	0.502
$Ce(NO_3)_3.6H_2O$ (CeO_2)	10	10	5.687
NH_4OH	30	30	1.377
P123	1	1	7.597
H_2O_2	5		0.223
water			100.00
1-Propanol			25.00[a]

a. The propan-1-ol is measured in volumes (mL)

Forming a sol-gel mixture by mixing the Pluronic P123 solution and the metal oxide precursor solution follows the same procedures outlined in chapter 3.

The hypothesized mechanistic pathway for Pluronic P123 templated CZY synthesis is a direct extension of mechanistic pathway suggested for silica based mesoporous oxides. Figure 4.1 illustrates the mechanistic pathway which is similar to that suggested for surfactant templated silica based mesoporous oxides.[79,92,97,99,100] The lines with the filled dots represent the cosolvent micelles while the curly lines with the thick curly tips represent the block copolymers. The thick curly tips are the hydrophilic end groups e.g. polyethylene oxide and the mid-section of curly line is the hydrophobic group e.g. polypropylene oxide, respectively for the case of Pluronic P123.

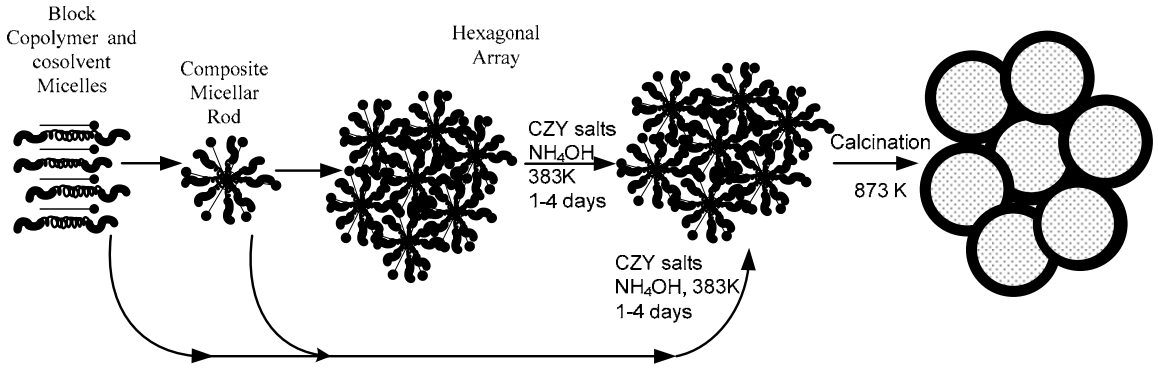

Figure 4.1 Mechanistic pathways for block copolymer templated CZY synthesis.

Following similar procedure as outlined in chapter 3, I investigated the effect of adding hydrolysis retarding agents like ACAC and TEA to the sol-gel mixture with a view to determining how such compounds influence the physical properties of CZY mixed oxide produced. The resulting CZY mixed oxides are characterized using the analytical methods and procedures given in chapter 3.

Results and Discussion

The same convention introduced in chapter 3 still holds true for the discussion of the DSC spectra observed in this chapter. Figures 4.2 and 4.3 show the TGA plot and the DSC spectra of as-synthesized CZY synthesized using Pluronic P123 as SDA, respectively.

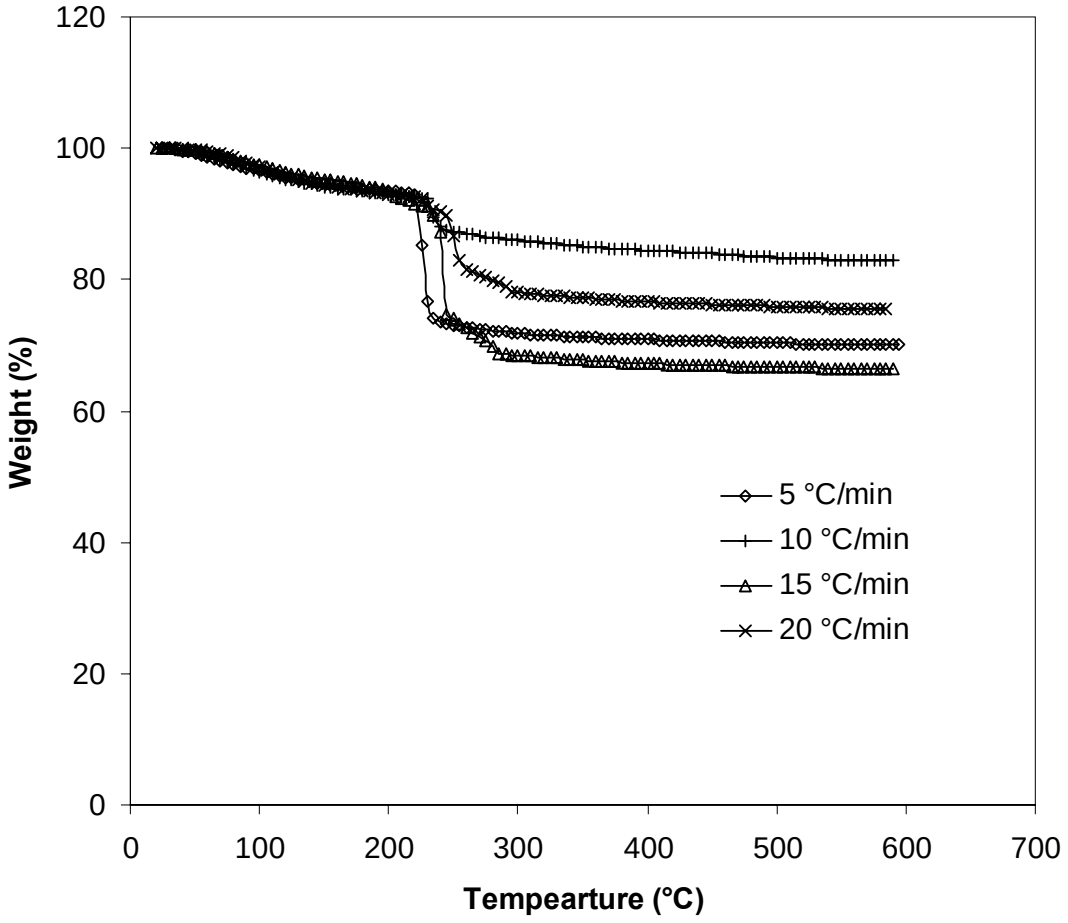

Figure 4.2 Thermogravimetric analysis of an as-synthesized CZY sample prepared using Pluronic P123 alone as the SDA upon being heated in air from near ambient temperatures to 600 ºC, at heating rates that ranged from 5 to 20 °C/min.

The TGA results show that the loss of materials occurred in three steps. First there was the gradual loss of materials between the ambient temperature and 200 ºC. This is most probably the loss of residual and physisorbed water. Following this is the combustion of the block copolymer template that starts at about 200 to 300 ºC.

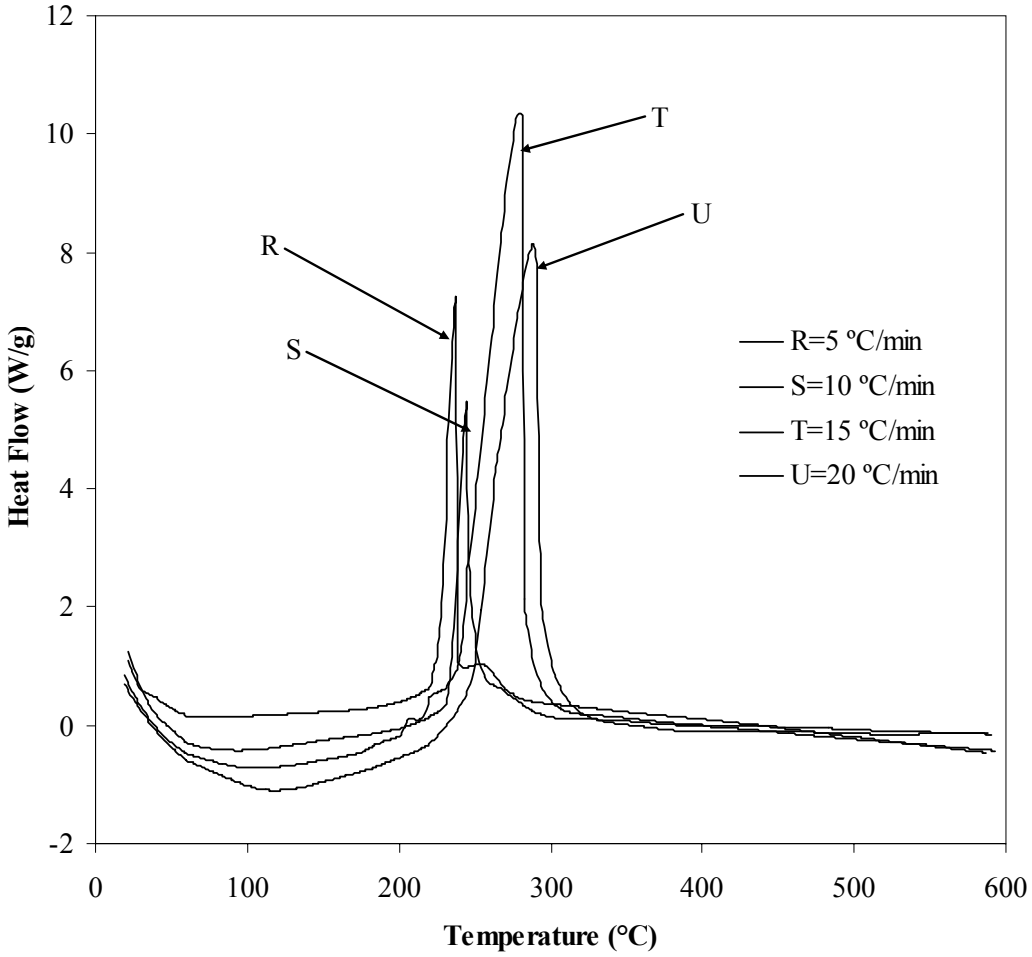

Figure 4.3 Differential heat flow to an as-synthesized CZY sample prepared using Pluronic P123 alone as the SDA upon being heated in air from near ambient temperatures to 600 ºC, at heating rates that ranged from 5 to 20 °C/min.

The chemical decomposition of the metal oxide precursors also takes within the temperature range. The DSC spectra of the Pluronic P123 templated CZY sample (Figure 4.3) show that between 200 and 350 ºC a large heat was released. This observation is different from the heat absorption which occurred within the same temperature range for CZY materials synthesized without the use of structure directing agent (Figure 3.5). This phenomenon can be explained as follows. The heat absorbed during the thermal decomposition of the nitrate salts is less than the heat released during the combustion of the organic P123 template. From the DSC spectra, it is noted that as the heating rate increases the rate of heat released during the oxidation of the template also increased. This is important because it tells us that carrying out the calcination at low heating rate prevents the occurrence of hot spots in the sample, which could lead to localized melting phenomena that might destroy the structural integrity of the CZY sample and significantly reduce the surface area of the mesopores. By looking at both Figures 4.2 and 4.3, it is apparent that beyond 350 ºC, the TGA plot and the DSC spectra both flattens out. This suggests that the decomposition of the template and the metal oxide precursors has already been completed at this temperature. In spite of low percentage weight loss of materials generally between 5 and 20 wt%, the amount of heat released during the DSC was quite large in comparison to the un-templated CZY material and the CTAB templated CZY materials (Figures 3.5–3.7).

As stated in chapter 3, based on the amount of heat released during the heating process, it is recommended that heating rates should be at as low as 10 ºC/min or less in order to prevent the generation of hot spots during calcination of the samples.

Table 4.2 Effect of calcination heating rate on the surface area and pore diameter of Pluronic P123 templated CZY samples. Samples were calcined in air from 25 to 600 °C at a heating rate of 1 and 20 ºC/min, with the final temperature being maintained for 4 h.

	BET Surface Area (m^2/g)[b]		Avg. Pore Diameter (nm)[b]	
	Heating rate (ºC/min)		Heating rate (ºC/min)	
CZY Template	1	20	1	20
P123+ACAC	96	78	3.8	3.6
P123+TEA	50	44	3.8	3.6

b. The error margin for the surface area is ±5 m^2/g and for the pore diameter, ±0.5 nm

From the TGA plot the percentage loss in weight of Pluronic P1213 templated CZY materials was less than 20 wt%. This value suggests that the amount of carbon loading in the form of template was quite low like the CTAB templated CZY materials. However, the large heat released during calcination of the Pluronic P123 templated CZY suggests that the total carbon loading for all of the block copolymer templated CZY samples were significant. The large heat evolved meant that sufficient localized hot spots to damage the structural morphology of the CZY may ensure. The changes in the BET surface area and the BJH pore diameter values did not change drastically for this sample during calcination at slow heating or at high heating rate.

Earlier in discussing the results of the TGA plots and DSC spectra, I have suggested that a calcination heating rate of 10 ºC/min or less would be sufficient to reduce the generation of hot spots within the samples during calcination. The results of the effects of varying heating rate on the surface area and pore size shown above are quite

contrary. This is so because the amount of combustible materials present in the sample during calcination is also important. Therefore, based on the results shown in Table 4.2, the calcination heating has minimal effects on the surface area and pore size of CTAB templated CZY materials.

The results of nitrogen adsorption-desorption experiments CZY samples synthesized using pluronic P123 alone, pluronic P123/ACAC, and pluronic P123/TEA as structure directing agent are presented next. All the CZY samples made using these templates (pluronic P123 alone, pluronic P123/ACAC, and pluronic P123/TEA) were calcined in air at heating rate of 20 ºC /min from ambient temperature to 600 ºC, with the final temperature held constant for 4 h. Figures 4.4–4.6 show the nitrogen adsorption/desorption isotherms and the BJH pore size distribution of CZY sample synthesized using pluronic P123 alone, pluronic P123/ACAC, and pluronic P123/TEA as structure directing agent. The physisorption isotherms (see Figures 4.4–4.6) show the typical hysteresis loop associated with mesoporous materials. The hysteresis loop arises from the condensation within the mesopore of the adsorbing gas in this case liquid nitrogen. This suggests that indeed mesoporous CZY materials were prepared. However, it is impossible to accurately calculate the dimension or shape of the pores present in the sample from simply the adsorption-desorption isotherms. For our calculations I used the BJH evaporation model to estimate average pore diameters; however, this model assumes that only cylindrical pores are present in the sample.[87] Thus, some inaccuracies could exist with the calculated pore diameters. Despite these possible inaccuracies in absolute

pore volume calculations, it is reasonable to expect the BJH model to accurately predict trends with pore diameter for samples having similar pore structures.

The inclusion of hydrolysis retarding agents or complexation agents caused a subtle difference in the shape of the hysteresis loops. The hysteresis loop for the Pluronic P123/ACAC templated CZY materials looked slightly enlarged while that of the Pluronic P123/TEA templated CZY materials looked distended a bit at the center. The pore size plots generally showed a narrowing of the pore size distribution plots for the ACAC and TEA modified CZY samples than the just Pluronic P123 templated CZY sample. These changes are attributed to the varying binding strength of the complexation agents used during the synthesis. The fact that TEA is tridentate while ACAC is bidentate is another reason why TEA might have a stronger binding strength than ACAC. A quantitative measurement of the binding strength for both ligands was not explored.

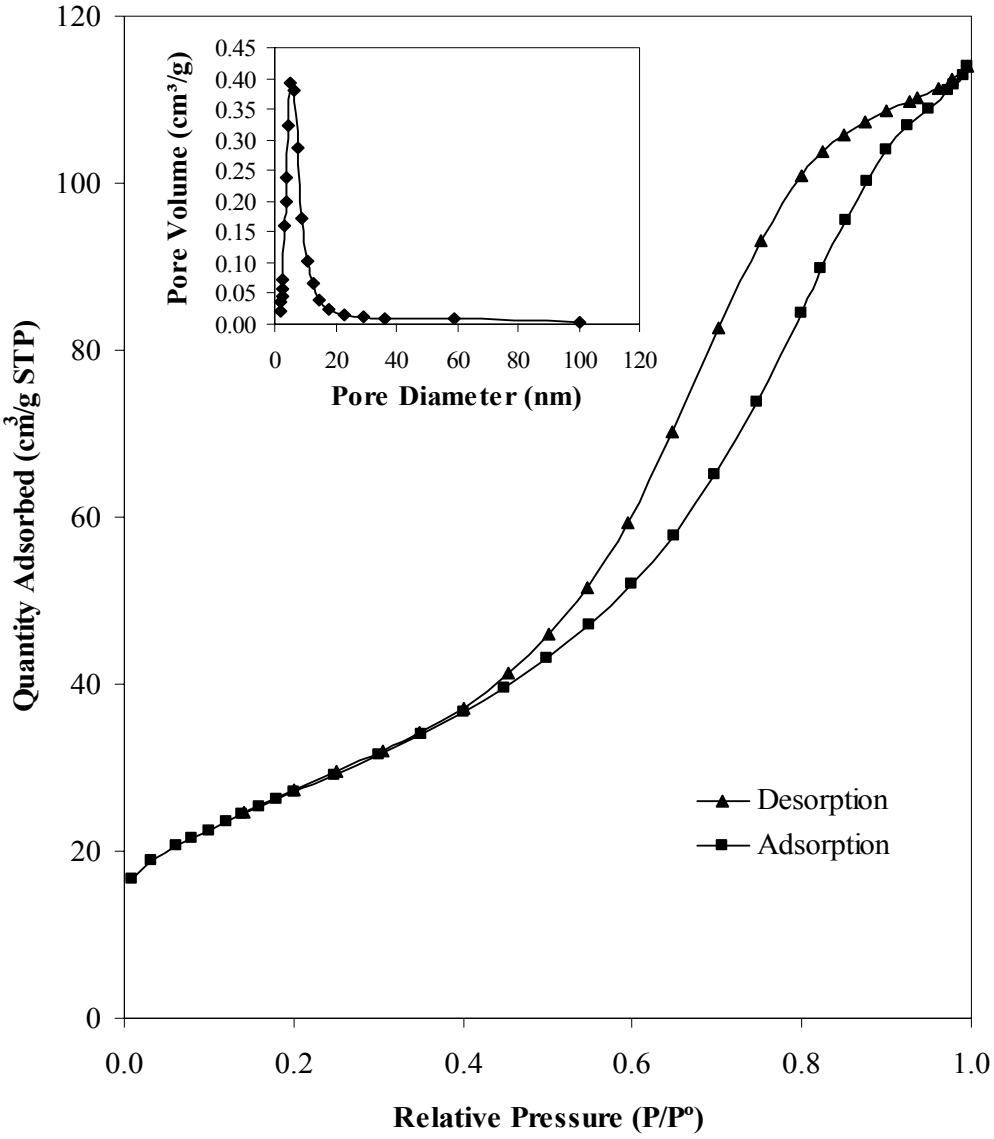

Figure 4.4 Nitrogen adsorption (■) /desorption (▲) isotherms and BJH pore size distribution (inset) for a calcined CZY sample prepared using the Pluronic P123 template. The sample was calcined in air from 25 to 600 °C at a heating rate of 20 ºC /min, with the final temperature being maintained for 4 h.

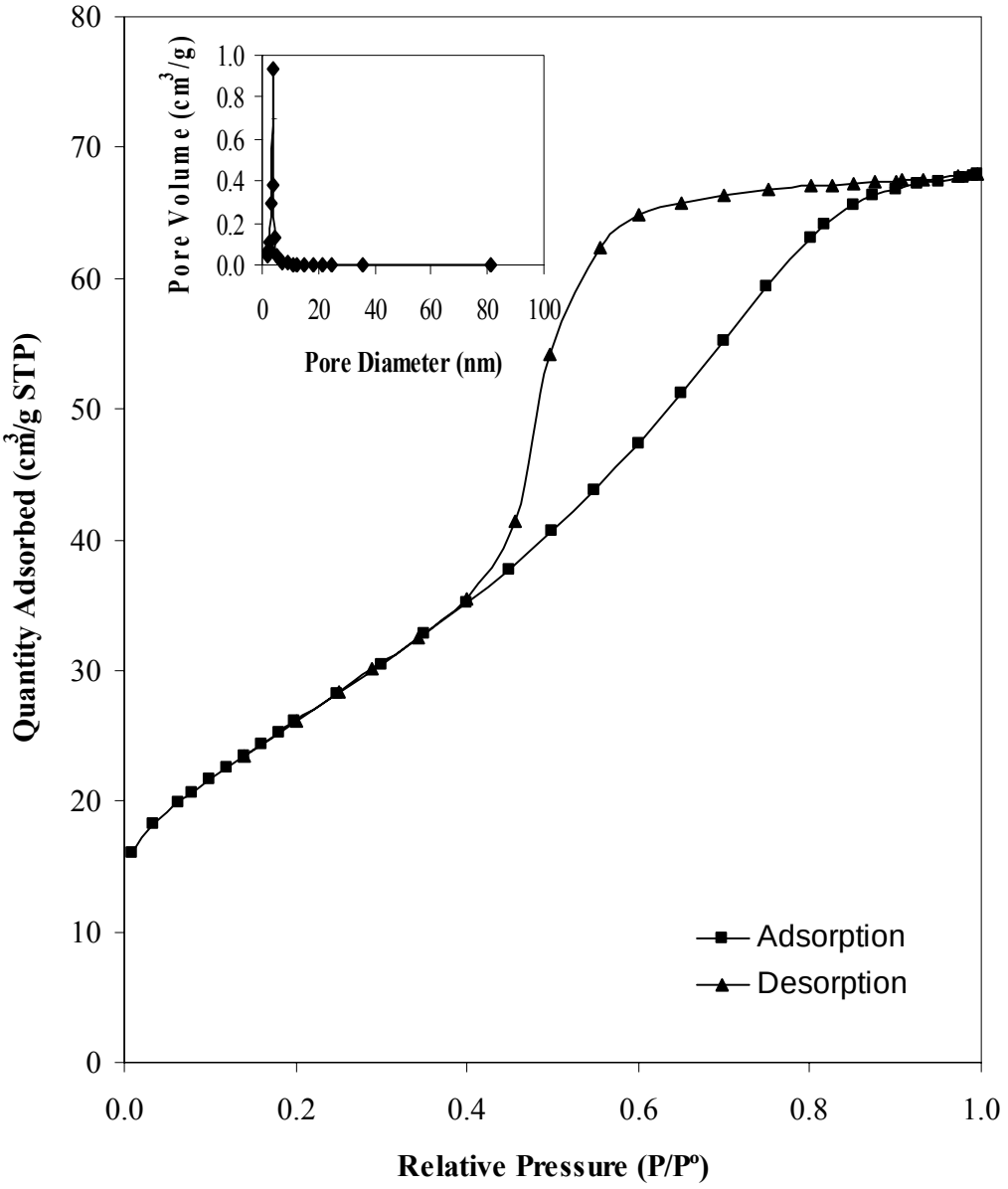

Figure 4.5 Nitrogen adsorption (■) /desorption (▲) isotherms and BJH pore size distribution (inset) for a calcined CZY sample prepared using the Pluronic P123/ACAC template. The sample was calcined in air from 25 to 600 °C at a heating rate of 20 ºC /min, with the final temperature being maintained for 4 h.

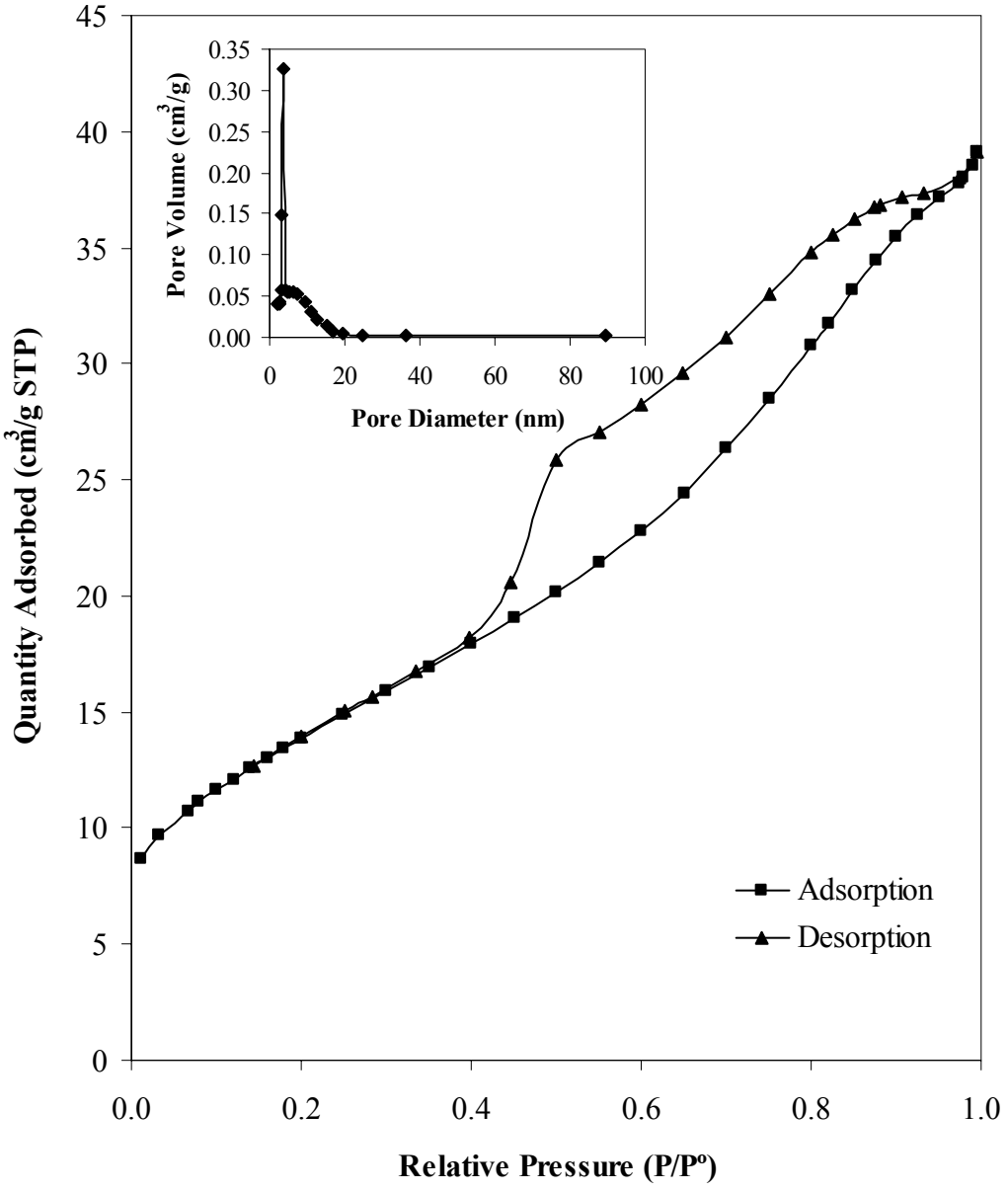

Figure 4.6 Nitrogen adsorption (■) /desorption (▲) isotherms and BJH pore size distribution (inset) for a calcined CZY sample prepared using the Pluronic P123/TEA template. The sample was calcined in air from 25 to 600 °C at a heating rate of 20 ºC /min, with the final temperature being maintained for 4 h.

Table 4.3 shows the effect of adding hydrolysis retarding agents to the CZY sol-gel mixture during synthesis of CZY. Adding ACAC as the hydrolysis retarding agent resulted in over 30% increase in the BET surface area of CZY synthesized using pluronic P123 as the SDA while adding TEA had a contrary effect in that the CZY samples lost a significant amount of its BET surface area. Thus, ACAC is a better hydrolysis retarding agent than TEA for improving the BET surface area of the pluronic P123 templated CZY materials.

Table 4.3 Effect of hydrolysis retarding agents on the surface area and pore diameter of Pluronic P123 templated CZY samples. Samples were calcined in air from 25 to 600 °C at a heating rate of 1 ºC/min, with the final temperature being maintained for 4 h.

CZY Template	BET Surface Area (m^2/g)[c]	Avg. Pore Diameter (nm)[c]
P123	58	2.3
P123/ACAC	96	3.8
P123/TEA	50	3.8

c. The error margin for the surface area is ±5 m^2/g and for the pore diameter, ±1.0 nm

This result is in agreement with the results from chapter 3 (Table 3.7) on the effects of ACAC and TEA on the surface area and pore size of the synthesized CZY materials. The increment of surface area resulting from the use of ACAC suggests as mentioned in chapter 3 that the binding strength of ACAC is weaker than that of TEA. The discrepancies in the pore size are as a result of the effects of the error margin associated with measurement. The pore size of the ACAC modifies samples should be less than the

pore size of the TEA modified CZY sample. See discussion on this section in chapter 3 for more details.

The catalytic activity and stability of a support material is closely tied to its composition and three dimensional structures. Table 4.4 shows the theoretically expected molar percentage, and the measured molar percentage of metal oxides in the CZY materials synthesized using pluronic P123 as SDA. These results reveal that all the metal oxides are well incorporated into the CZY materials. They are well within the margin of error for the theoretically expected molar percentage.

Table 4.4 Elemental composition of Pluronic P123 templated CZY

Sample	ZrO_2 (mol %)[d]	$YO_{1.5}$ (mol %)[d]	CeO_2 (mol %)[d]
Theoretical Amount	45.00	5.00	50.00
CZY/P123	47.52	4.47	48.01

d.The error margin for the elemental composition is ±2.0 mol%

Hence, the extent of sample crystallinity (nature and size of crystals present) was determined by powder X-ray diffraction (PXD). Figure 4.7 shows the PXD patterns of CZY synthesized using pluronic P123 alone, pluronic P123/ACAC, and pluronic P123/TEA as structure directing agent at 2θ values ranging from 10º to 80º. However, the small angle X-ray diffraction (SAXD) pattern for the same samples (not shown) at 2θ º values ranging from 1 to 10º does not reveal low angle peaks synonymous with ordered mesoporous MCM-41 materials. This suggests that although the pluronic P123 templated CZY mixed oxides were mesoporous, the mesopore had no long range ordered.

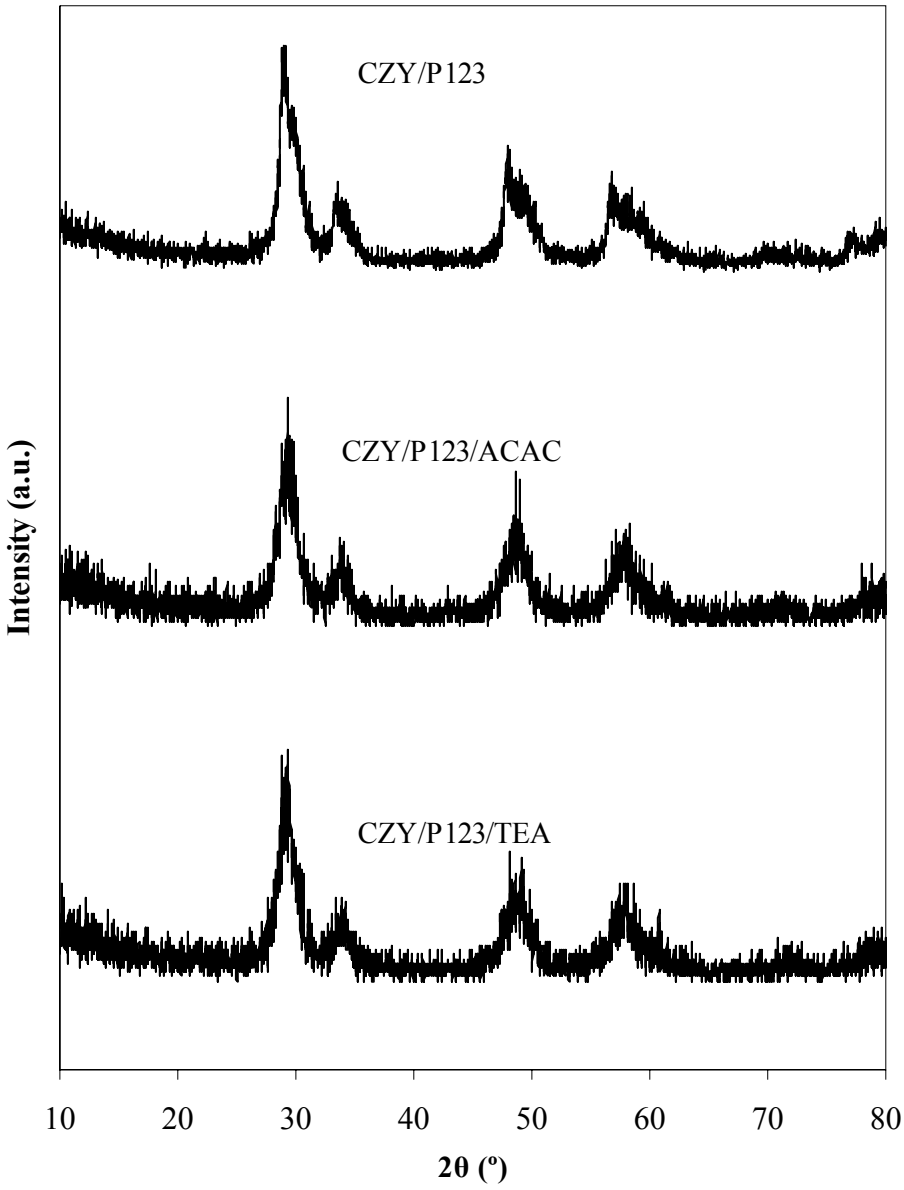

Figure 4.7 Powder X-ray diffractogram (PXD) for CZY prepared using Pluronic P123 alone, Pluronic P123/ACAC, and Pluronic P123/TEA. Samples were calcined in air from 25 to 600 °C at a heating rate of 20 ºC/min, with the final temperature being maintained for 4 h.

The power XRD patterns for all the Pluronic P123 templated CZY samples (see Figure 4.7) show peaks that are slightly broad. The peak positions are very similar to powder XRD patterns of pure ceria (Figure 3.14). This means that the CZY samples all have the same cubic fluorite structure of ceria. The broad peaks suggest that the CZY samples contained nanosized crystallite. The absence of split ends at the peaks for the powder XRD patterns of the CZY samples implies that no phase segregation (i.e. ceria rich phase and zirconia rich phase) occurred in the samples. The powder XRD patterns of the CZY samples also reveal the presence of low intensity broad peaks, which indicate the existence of nanocrystallites. Following similar procedures given chapter 3, the particle size of the crystallites was estimated using the Scherrer's equation to be between 7.0 and 10.0 nm.

Additional information about the arrangement and size of pore present in the pluronic P123 templated samples were observed via electron microscopy. It was also important to ascertain the primary particle size and extent of agglomeration present in these samples; thus, transmission electron miscopy (TEM) was used to examine all pluronic P123 templated materials. Figures 4.8–4.10 show TEM images of pluronic P123 templated mesoporous CZY materials with and without hydrolysis retarding agents after calcination in air at 600 ºC for 4 h at 20 ºC /min. The TEM images are nothing like MCM-41 material in that they do not show any regular hexagonal pore structure.

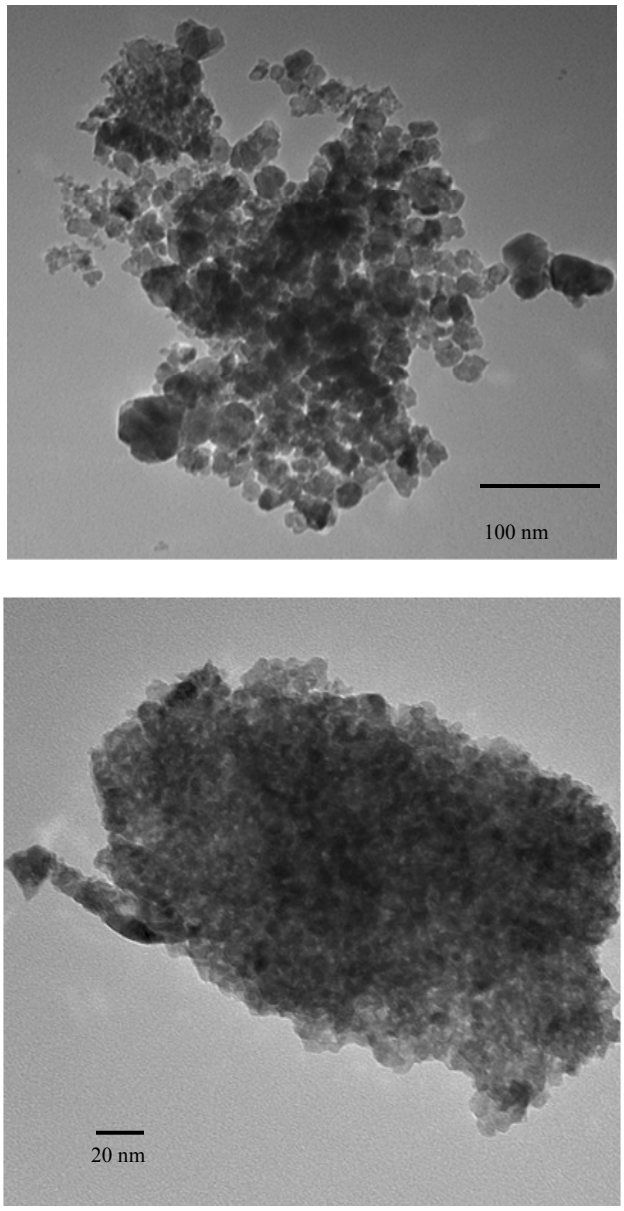

Figure 4.8 Transmission electron micrographs of a calcined CZY mixed oxide prepared using pluronic P123 block copolymer as the sol-gel template. Samples were calcined in air from 25 to 600 °C at a heating rate of 20 ºC/min, with the final temperature being maintained for 4 h.

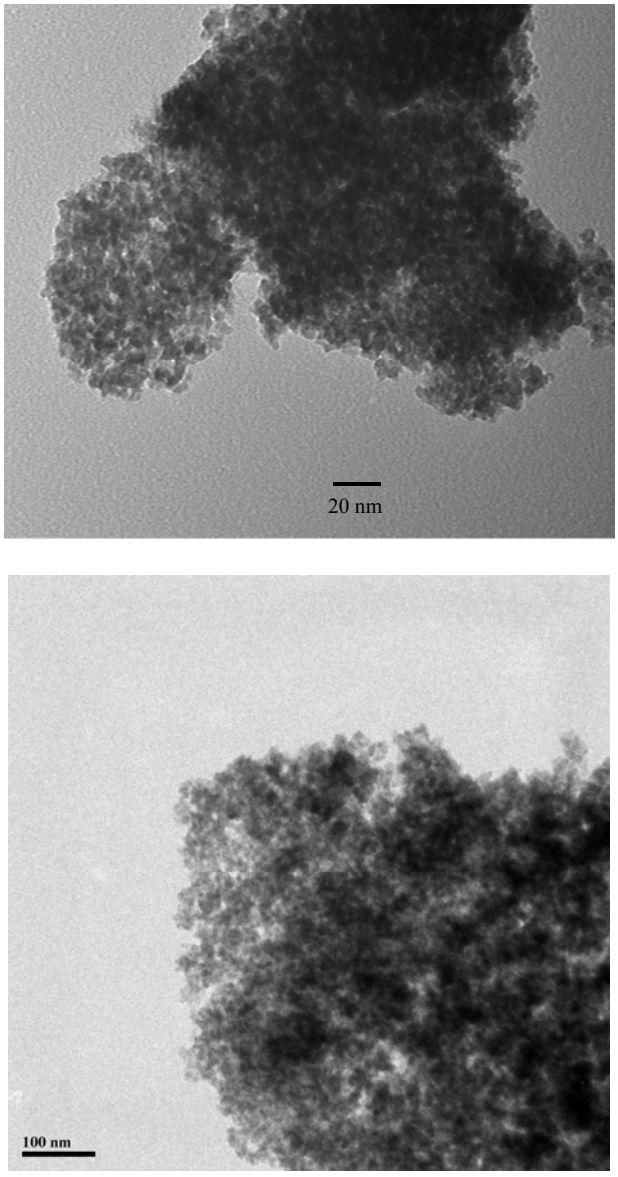

Figure 4.9 T Transmission electron micrographs of a calcined CZY mixed oxide prepared using pluronic P123 block copolymer as the sol-gel template and TEA as the hydrolysis retarding agent. Samples were calcined in air from 25 to 600 °C at a heating rate of 20 ºC/min, with the final temperature being maintained for 4 h.

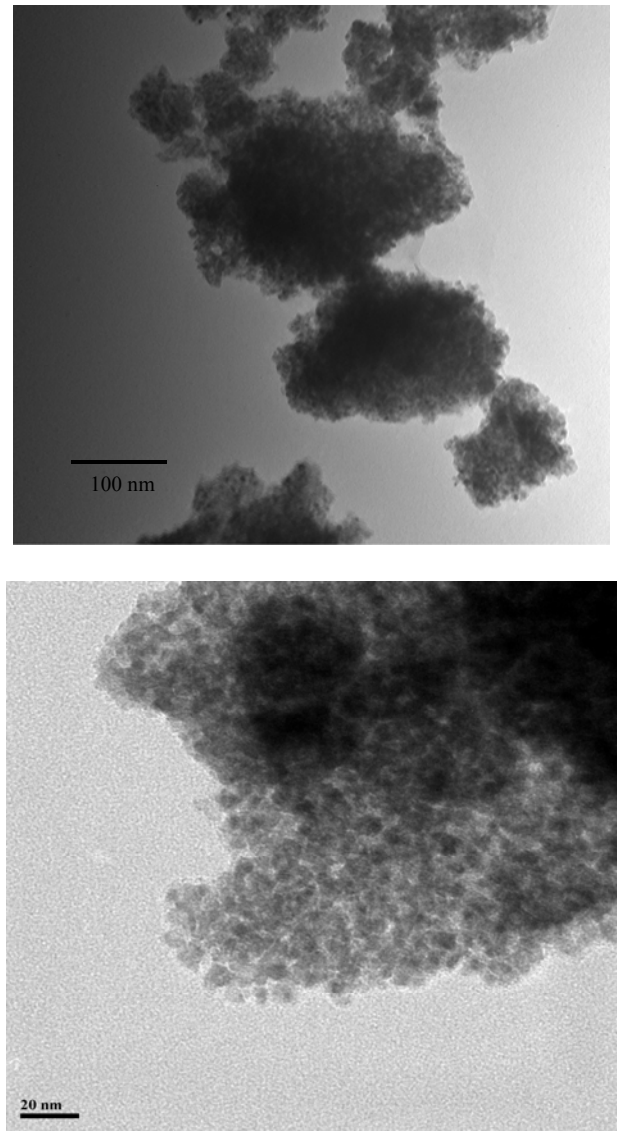

Figure 4.10 Transmission electron micrographs of a calcined CZY mixed oxide prepared using pluronic P123 block copolymer as the sol-gel template and ACAC as the hydrolysis retarding agent. Samples were calcined in air from 25 to 600 °C at a heating rate of 20 ºC/min, with the final temperature being maintained for 4 h.

They are basically an agglomeration of nanosized crystalline particulates, with the diameter of the primary particles being approximately 5 nm in diameter. The absence of an ordered 3-D structure in the TEM images suggested that the synthesized mesoporous CZY material did not have the morphology of MCM-41 type family of materials. This observation is supported by the small angle XRD pattern which did not show any peaks at low values suggesting that no long range order was present in the CZY materials. This observation calls to question the proposed mechanistic pathway that was suggested for the process. Since no long range ordered mesoporous CZY materials were synthesized then, the mechanistic pathway was completely different from the hypothesized pathway. The proposed pathway suggested would be the third pathway. This means that the Pluronic P123 templates were randomly arranged with no specific ordering and the CZY mixed oxides simply condensed in between the Pluronic P123 micelles (Figure 3.22).

Thermal degradation studies of block copolymer templated CZY materials were carried out between 700 and 1000 ºC. Table 4.4 shows the variation of the physical properties of block copolymer templated CZY on calcination temperature. The overall loss in surface area from 700 to 1000 ºC is approximately 87.8%. This decrease in surface area is expected because of the enhanced oxide sintering with zirconia and ceria that can occur at temperatures above 800 °C. The trend for surface area and pore size follows the classic trend, that is, as the surface area decreases, the pore size increases.

Table 4.5 Variation of surface area and pore volume as a function of aging temperature for Pluronic P123 templated CZY samples. Samples were calcined in air to the specified temperature at a heating rate of 20 ºC/min, with the final temperature being maintained for 4 h.

Aging Temperature (ºC)	BET Surface Area (m^2/g)[e]	BJH Pore Diameter (nm)[e]
700	76	6.0
800	48	9.0
900	28	12.8
1000	9.3	24.0

e. The error margin for the surface area is ±5 m^2/g and for the pore diameter, ±0.5 nm

The results of powder XRD patterns after accelerated ageing of the CZY samples from 700 to 1000 ºC for 4 hr are shown in Figure 4.11. The powder XRD pattern are quite similar during each ageing temperature but at higher temperatures the peaks become sharper indicating that the CZY samples are more crystalline and sintered at higher temperature. The lack of peak split in the powder XRD patterns suggests that the CZY samples do not show evidence of phase segregation even at higher temperatures. Phase segregation means there are ceria or zirconia rich phases in the samples after accelerated aging. The aged samples apparently stilled maintained the cubic structure of pure ceria.

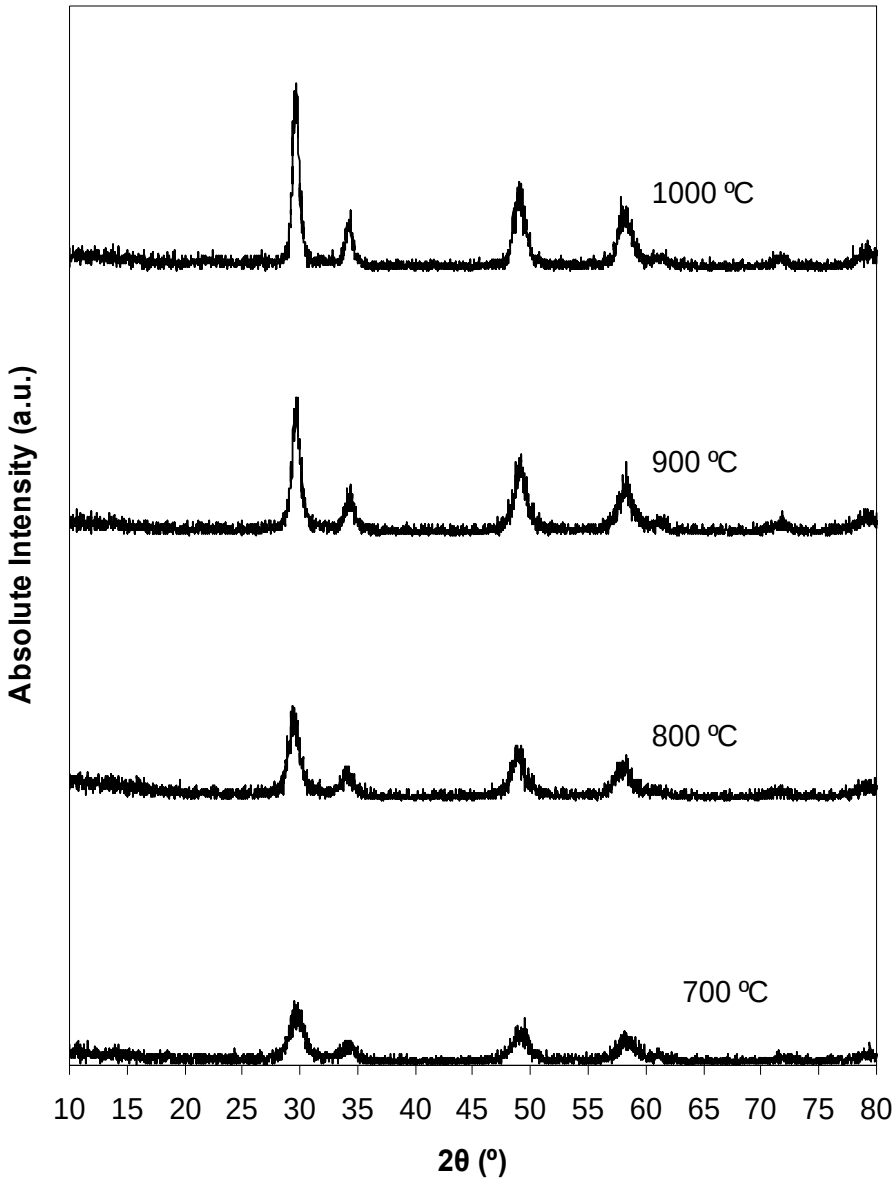

Figure 4.11 Powder X-ray diffractogram (PXD) for Pluronic P123 templated CZY samples. Samples were calcined in air to the specified temperature at a heating rate of 20 ºC/min, with the final temperature being maintained for 4 h.

Conclusion

In this chapter I outlined the synthesis steps for making block copolymer templated mesoporous CZY materials. The synthesized CZY material was characterized to ascertain the existence of mesoporous structure, determine homogeneity of the phase, the elemental composition, the effect of heating rate during calcination, and the morphology of the material. In addition, the effect of adding hydrolysis retarding agents on the physical properties of the synthesized block copolymer templated CZY was determined.

Although a range of mesoporous pluronic P123 templated CZY mixed oxides were successfully prepared, yet the pore structure exhibited no long range order. Further, the use of some hydrolysis retarding agents, e.g., acetylacetone (ACAC), significantly increased the surface area of pluronic P123 templated CZY materials, while other known hydrolysis retarding agents, e.g., triethanolamine, had the opposite effect. The difference between these two hydrolysis retarding agents may have to do with their binding strength to the metals, but this effect was not fully explored.

By combining the results from all of the CZY characterization experiments (i.e. the PXD, TEM, and nitrogen adsorption experiments), I can hypothesize that the final calcined CZY materials are simply an agglomeration of primary particles. Therefore, the mesoporosity observed in the nitrogen physisorption data is likely created by the void space between these agglomerated pseudo-spherical oxide particles, see Figure 3.24.

Lastly, varying the heating rate during calcination to temperatures such as 600 °C did not significantly affect the surface area of the surfactant templated CZY materials.

This is largely due to the fact that the as-synthesized CZY materials had only moderate loading of organics. It was also observed that all of the Pluronic P123 templated CZY materials underwent significant structural changes when heated to temperatures in excess of 800 °C. This suggests that a slow loss of mesoporosity (and thus, a slow decrease in catalytic activity) would likely occur during extended use of the material in catalytic converter applications, but that the observed loss in surface area was still less than that seen with many state-of-the-art CZY materials.

CHAPTER FIVE

DENDRIMER TEMPLATE TECHNIQUE

In the preceding chapters, I have considered two of the most common types of soft templates used in the synthesis of mesoporous materials, that is, the surfactant and block copolymer templates. I now conclude my discussion of soft template technique used in the synthesis of mesoporous materials by looking at dendrimer template. Detailed outline of the synthesis strategy would not be provided because they are similar to those developed for surfactant templated technique (Figure 3.1). The primary focus of this chapter is to ascertain if there is any templating effect associated with the use of polypropyleneimine dendrimers in the synthesis of CZY mixed oxides. The effects of adding hydrolysis retarding agents would not be covered. The synthesized CZY materials are characterized using the primary analytical methods given in chapter 3.

Synthesis Strategy for Making CZY Using Dendrimer Template Technique

The use of dendrimer templates for the synthesis of mesoporous materials has been widely reported in the literature.[40,41,43,68,101-103] Dendrimers are quite different from the previously considered amphiphilic compounds (i.e. surfactant and block copolymer) in chapters 3 and 4. Unlike surfactants and block copolymers that are capable of self-assembly into supramolecular structures of various forms and shapes; for example, the hexagonal structure of MCM-41, the cubic structure of MCM-48and the bilayer structure of MCM-50 depending on the critical micelle concentration and the pH of the surfactant

or block copolymer solution; the 4th and 5th generation polypropyleneimine dendrimers, also known as DAB-Am-32 and DAB-Am-64, respectively, and 5th generation polyamidoamine (PAMAM) dendrimers are unique in that they do not self-assemble like the surfactants and block copolymers. They have a preformed pseudo-spherical structure with the polypropyleneimine dendrimers being more rigid than the polyamidoamine dendrimers. DAB-Am-32 and DAB-Am-64 have been successfully used as structure directing agents (SDA) for the synthesis of silica based mesoporous materials by Larsen et al.[103] The reason for using DAB-Am dendrimers over PAMAM dendrimers was that Larsen et al. found that the pseudo-rigid structure of DAB-Am dendrimers enabled them to maintain their overall structure better than the more flexible and more common polyamidoamine (PAMAM) dendrimers.

Polypropyleneimine (DAB-Am) dendrimers are currently quite expensive, so their use for the large scale synthesis of porous catalysts is very unlikely; however, the unique pore structure which they generate makes them interesting structure directing agents. Like in all soft template techniques, the general synthesis strategy developed in chapter 3 is also applicable. The only difference is the type of the template which in this case are DAB-Am-32 and DAB-Am-64 dendrimers. As shown in Figure 3.1, the DAB-Am-32 or DAB-Am-64, which replaced the surfactant, is dissolved not in deionized water but in a mixture of 1-propanol (40 vol%) and deionized water (60 vol%). The DAB-Am-32 and DAB-Am-64 dendrimers are viscous liquids. The mixture of the dendrimer and the ethanol-deionized water mixture are placed on a hot plate and stirred using a magnetic stirrer. As the mixture is stirred continuously, its temperature is

gradually raised to 40 ºC so that the dendrimer would completely be dissolved. The metal oxide precursor salts are prepared in identical fashion as discussed in chapter 3. With the dendrimer solution formed, the mixing of the precursor oxide solution and the dendrimer solution follows the same exact procedure detailed in chapter 3.

Synthesis of CZY Mixed Oxide Using DAB-Am Template

All chemicals used in the preparation of surfactant template CZY samples were used as received from their respective manufacturer. See chapter 3 for detailed description of all the chemicals except polypropyleneimine dendrimer (DSM). For the preparation of the metal oxide precursor solution follow the instruction provided in chapter 3. Only the description of how to make the Pluronic P123 solution is provided Tables 5.1 and 5.2 show the typical composition of the precursors, solvent, and the dendrimer that are used during the synthesis of mesoporous CZY mixed oxide.

Table 5.1 Typical sample composition for DAB-Am-32 Templated CZY

	Molar Ratio		
Reagents	Sol-gel	Oxide	Mass (g)
$ZrO(NO_3)_2.6H_2O$ (ZrO_2)	9	9	5.000
$Y(NO_3)_3.6H_2O$ ($YO_{1.5}$)	1	1	0.627
$Ce(NO_3)_3.6H_2O$ (CeO_2)	10	10	7.109
DAB-Am-32	0.5	0.5	2.934
H_2O_2	5		0.278
water			100.000
Propan-1-ol			25.000[a]

a. Propan-1-ol is measured in mL

Weigh out ~3.00 g of say DAB-Am-32, a highly viscous liquid, in a beaker. Add ~60.0 g of a mixture of deionized water (60 vol%) and 1-propanol (40 vol%) into the beaker containing the DAB-Am-32.

Table 5.2 Typical sample composition for DAB-Am-64 templated CZY

Reagents	Molar Ratio		Mass (g)
	Sol-gel	Oxide	
$ZrO(NO_3)_2.6H_2O$ (ZrO_2)	9	9	5.000
$Y(NO_3)_3.6H_2O$ ($YO_{1.5}$)	1	1	0.627
$Ce(NO_3)_3.6H_2O$ (CeO_2)	10	10	7.109
DAB-Am-64	0.25	0.25	2.934
H_2O_2	5		0.278
water			100.000
Propan-1-ol			25.000[b]

b. Propan-1-ol is measured in mL

1-propanol was added to improve the solubility of the dendrimer. The DAB-Am-32 solution was heated on a hot plate to about 40 ºC and stirred continuously for about an hour using a magnetic stirrer until the mixture is homogeneous. Afterward, the solution containing metal oxide precursors was added at ~5 mL/min to the DAB-Am-32 solution and the mixture immediately turned brownish suggesting that the metal oxides were precipitated. This precipitation of the metal oxide precursors resulted from the alkaline nature of the DAB-Am-n32 solution owing to the presence of the amine functional groups. The mixture was stirred continuously even as it gradually transformed into a viscous gel. Approximately 2 mL ammonium hydroxide solution was added intermittently to the gelatinous mixture with vigorous stirring to raise its pH above 10.0. The aging of the sample in the oven, filtration, washing, drying, and calcination steps all

followed the same procedures discussed in the relevant section of chapter 3. The synthesized CZY mixed oxides were characterized using the analytical methods and procedures given in chapter 3.

Figure 5.1 illustrates the mechanistic pathway for dendrimer templated mesoporous non-silica material synthesis.

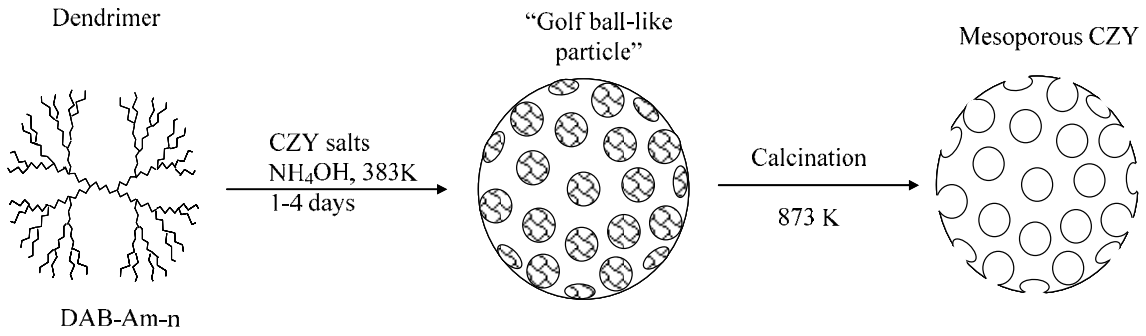

Figure 5.1 Mechanistic pathway for dendrimer templated CZY synthesis.

The hypothesized mechanistic pathway for the synthesis of mesoporous CZY materials using dendritic template follows the model that has been used successfully to describe mesoporous silica based materials.

Results and Discussion

In order to decide on the best calcination protocol to use during the calcination in air, we studied the effects of heat flow on as-synthesized dendrimer templated CZY mixed oxides at different heating rates ranging from 1 to 20 ºC/min. The DSC spectra showed the result from ambient temperature to 600 ºC and the TGA plots showed results from ambient temperature to 1000 ºC. As a form of control, I used as-synthesized CZY synthesized without using any structure directing agent. The TGA plot and DSC spectra

of as-synthesized DAB-Am-32 templated CZY mixed oxides are shown in Figure 5.2 and 5.3, respectively.

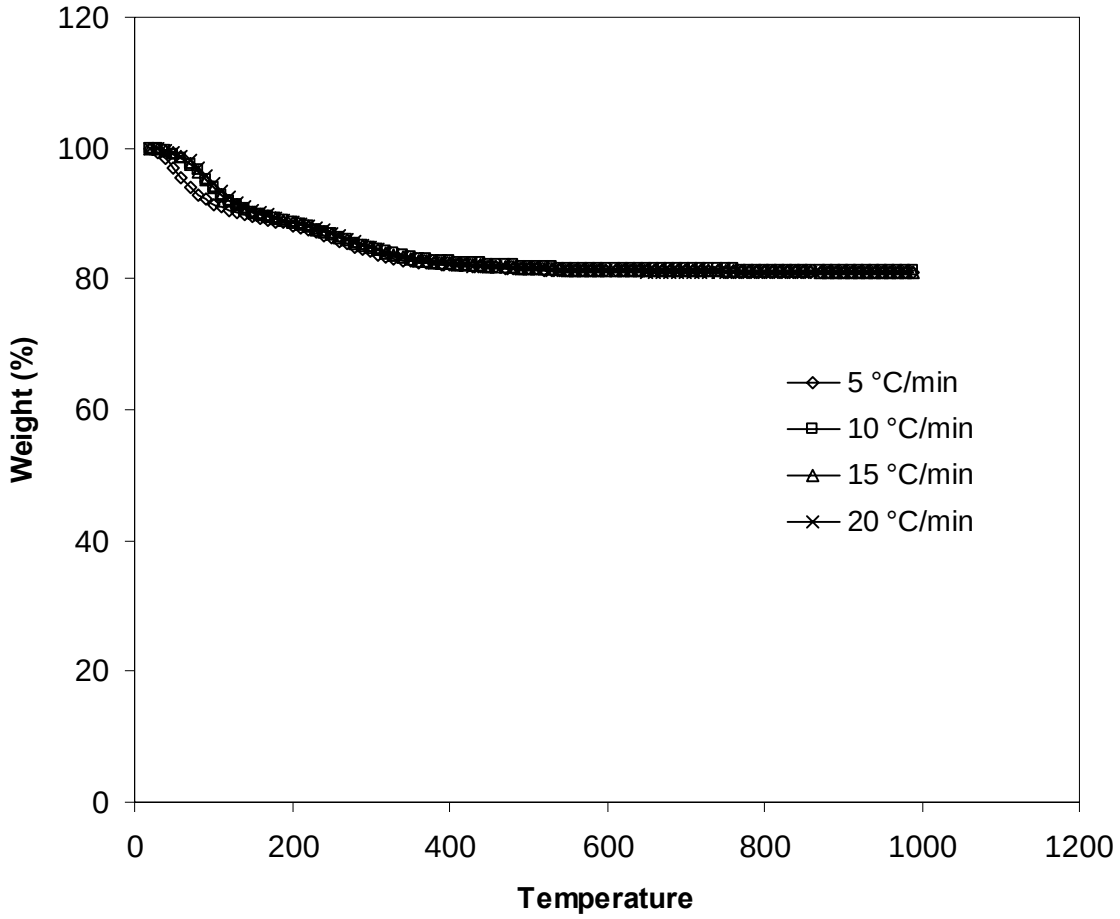

Figure 5.2 Thermogravimetric analysis of as-synthesized CZY sample prepared using DAB-Am-32 dendrimer as SDA upon heating from ambient temperature to 600 ºC at different heating rates in constant flow of air.

As shown in Figure 5.2, the heating rates used did not change the profile of the TGA plots for the samples. The weight loss during the TGA-DSC processes was in two stages. The first stage occurred between ~20 and 120 ºC with all the samples losing ~10 wt%.

This is the weight loss associated with water. The second stage of weight loss started between 120 and 400 ºC. Beyond the 400 ºC, the dendrimer templates and the transformation of the oxide precursors to the CZY were almost completed.

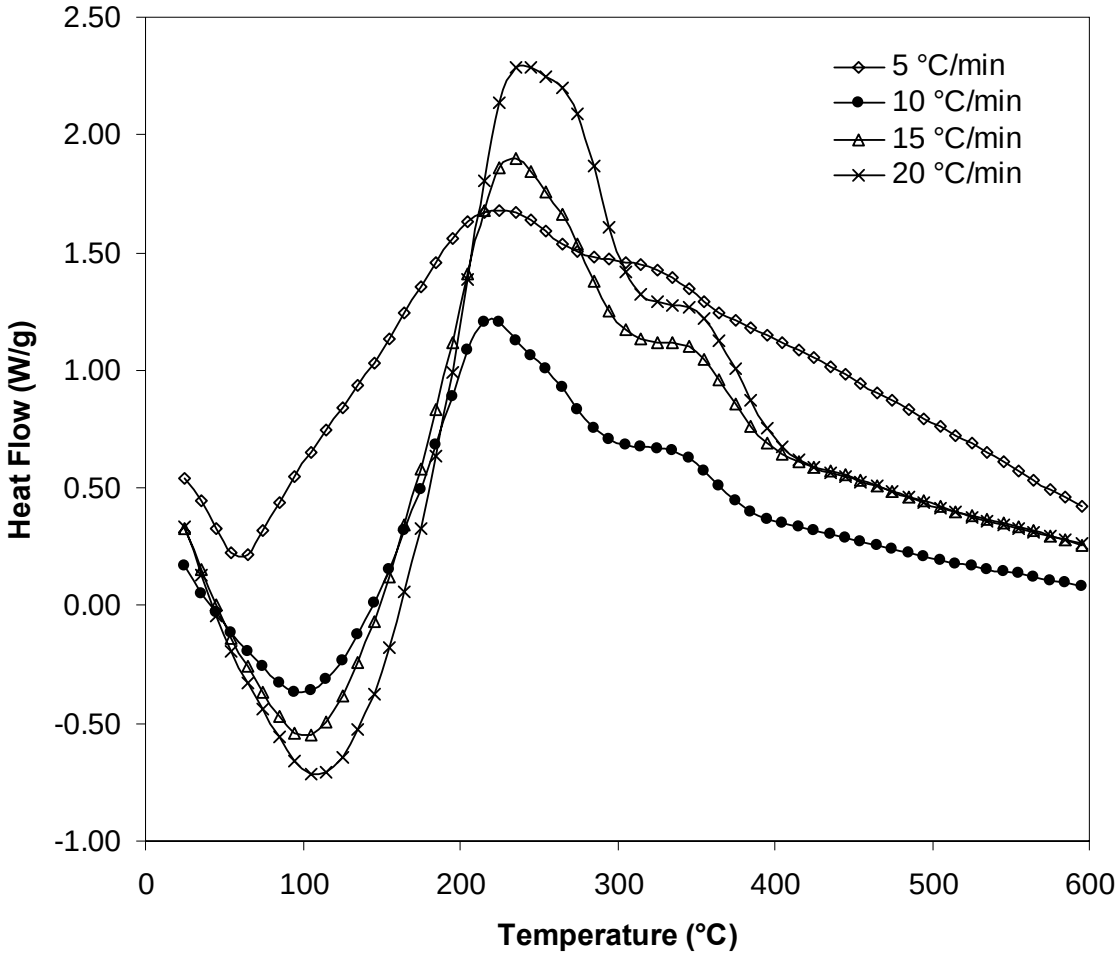

Figure 5.3 Differential heat flow to as-synthesized CZY synthesized using DAB-Am-32 dendrimer as SDA upon heating from ambient temperature to 600 ºC at different heating rates in a constant flow of air.

The sign convention adopted for DSC remains unchanged, that is, the downward peak indicates endothermic (heat absorbing) processes and upward peak exothermic (heat

releasing) processes. Figure 5.3 shows the DSC profile of as-synthesized CZY made using DAB-Am-32 dendrimer as SDA.

The DSC spectra in Figure 5.3 shows the heat flow versus temperature for as-synthesized CZY synthesized using DAB-Am-32 dendrimer as SDA. The downward peaks at the low temperature range of less than 200 ºC indicates water loss. The most interesting feature of the DSC spectra is evolution of heat occurring between 200 ºC and 400 ºC. This same feature was encountered with all the other soft templated CZY mixed oxides. This masking of the decomposition of the metal salts as noted in the chapters 3 and 4 was as a result of the combustion of the dendrimer. The various heating rates showed different heat flow profiles for the DAB-Am-32 templated CZY materials. When the heating rate was 20 ºC/min, the heat evolved for DAB-Am-32 templated CZY was ~2.5 W/g, however, for CTAB and Pluronic P123 templated CZY, at the same heating rate the heat evolved was ~7 and ~8 W/g, respectively. Since with CTAB and Pluronic templated CZY heating rate did not reasonably affect the surface area and the pore size of the CZY, it follows then that DAB-Am-32 templated CZY would also be unaffected by varying heating rates. In addition, the heating rate during calcination of the CZY sample would be unimportant.

Table 5.3 shows the results of the BET surface area and BJH pore average pore diameter of the calcined CZY materials synthesized using DAB-Am-32 and DAB-Am-64 dendrimers. The surface area for the DAB-Am-32 templated CZY sample is greater than the surface area of DAB-Am-64 templated CZY sample. Using an estimated volume of 10960 and 5054 $Å^3$ for a single molecular unit of DAB-Am-64 and DAB-Am-32,

respectively, the diameter of the unit molecule of DAB-Am-64 and DAB-Am-32 is estimated to be 2.8 and 2.1 nm, respectively.

Table 5.3 Surface area and pore diameter of DAB-AM-n templated CZY samples. Samples were calcined in air from 25 to 600 ºC at a heating rate of 20 ºC/min, with the final temperature being maintained for 4 h

CZY Template	BET Surface Area (m^2/g)[c]	Avg. Pore Diameter (nm)[c]
DAB-Am- 32	76	3.5
DAB-Am-64	39	2.8

c. The error margin for the surface area is ±5 m^2/g and for the pore diameter, ±0.5 nm

The single molecular unit is assumed to be a sphere. Based on the molecular diameter, the surface area data shown in Table 5.3 are perfectly in order. This is because for spheres, surface area is inversely proportional to particle diameter. However, the pore sizes are irreconcilable with the surface area data. The problem with this data appears to be due mainly to its error margin. It is therefore safe to conclude that these values reported above have been highly exaggerated. The pore size for the DAB-Am-64 templated CZY should be a lot higher than 2.8 nm based on similar surface area values obtained from the same equipment. The actual value should be between 8 and 12 nm as shown in Table 5.5 (See the pore size for accelerated aging sample with similar surface area).

Figures 5.4 and 5.5 show the nitrogen adsorption/desorption isotherms and the BJH pore size distribution of CZY sample synthesized using DAB-Am-32 and DAB-Am-64, respectively as structure directing agent. The physisorption isotherm shows typical

hysteresis loop associated with mesoporous materials. This suggests that the synthesized dendrimer templated CZY materials were mesoporous. Figure 5.6 shows the PXD patterns of CZY synthesized using DAB-Am-32 and DAB-Am-64 as the SDA at 2θ values ranging from 10º to 80º. The peak positions for the PXD patterns for the DAB-Am-64 templated CZY materials and the DAB-Am-32 templated CZY materials are similar to those of pure ceria as shown in Figure 3.14. As stated previously this means that the structure of the synthesized CZY materials using DAB-Am-32 or DAB-Am-64 was cubic fluorite like ceria.

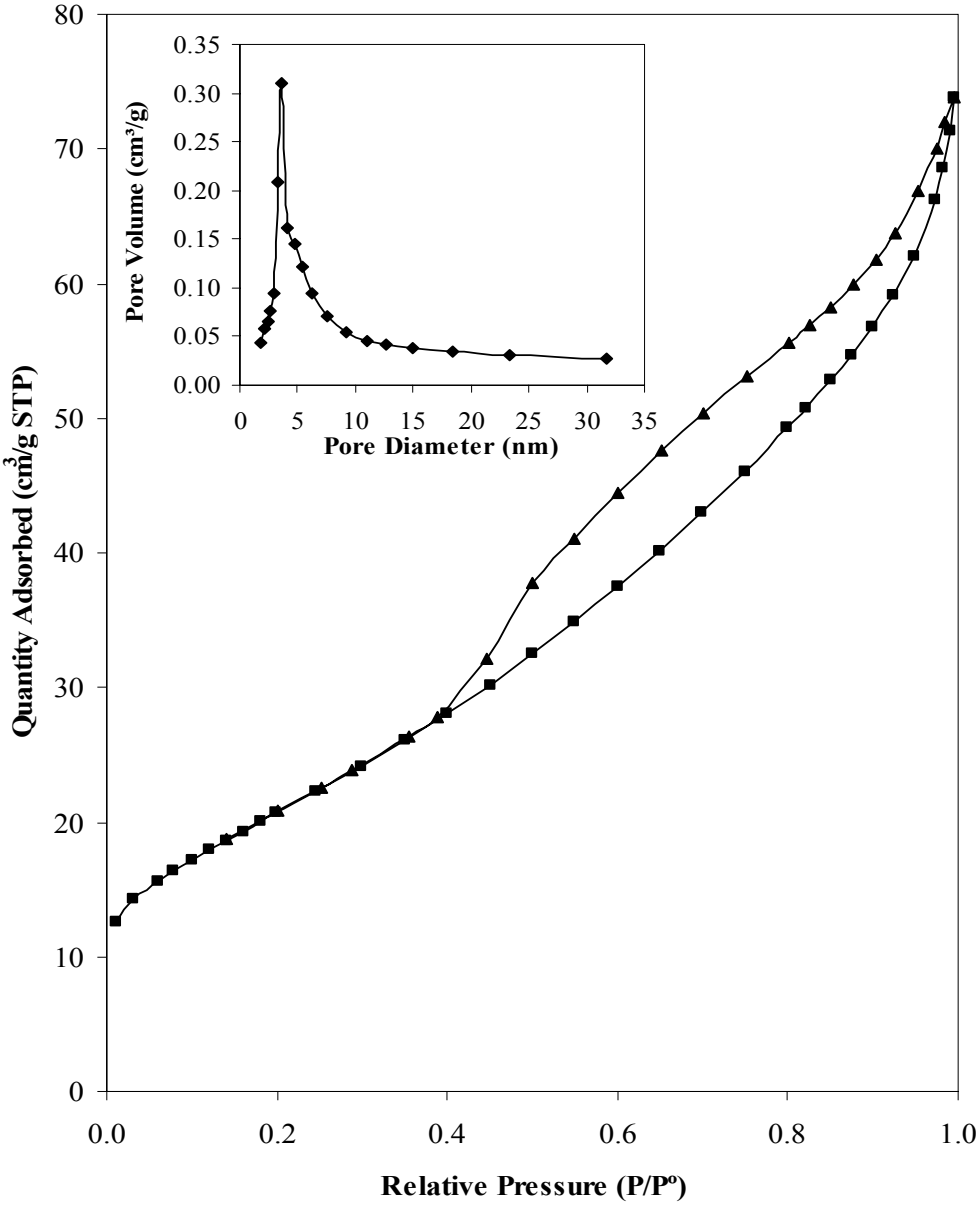

Figure 5.4 Nitrogen adsorption (■) /desorption (▲) isotherms and BJH pore size distribution (inset) for a calcined CZY sample prepared using the DAB-Am-32 template. The sample was calcined in air from 25 to 600 °C at a heating rate of 20 ºC /min, with the final temperature being maintained for 4 h.

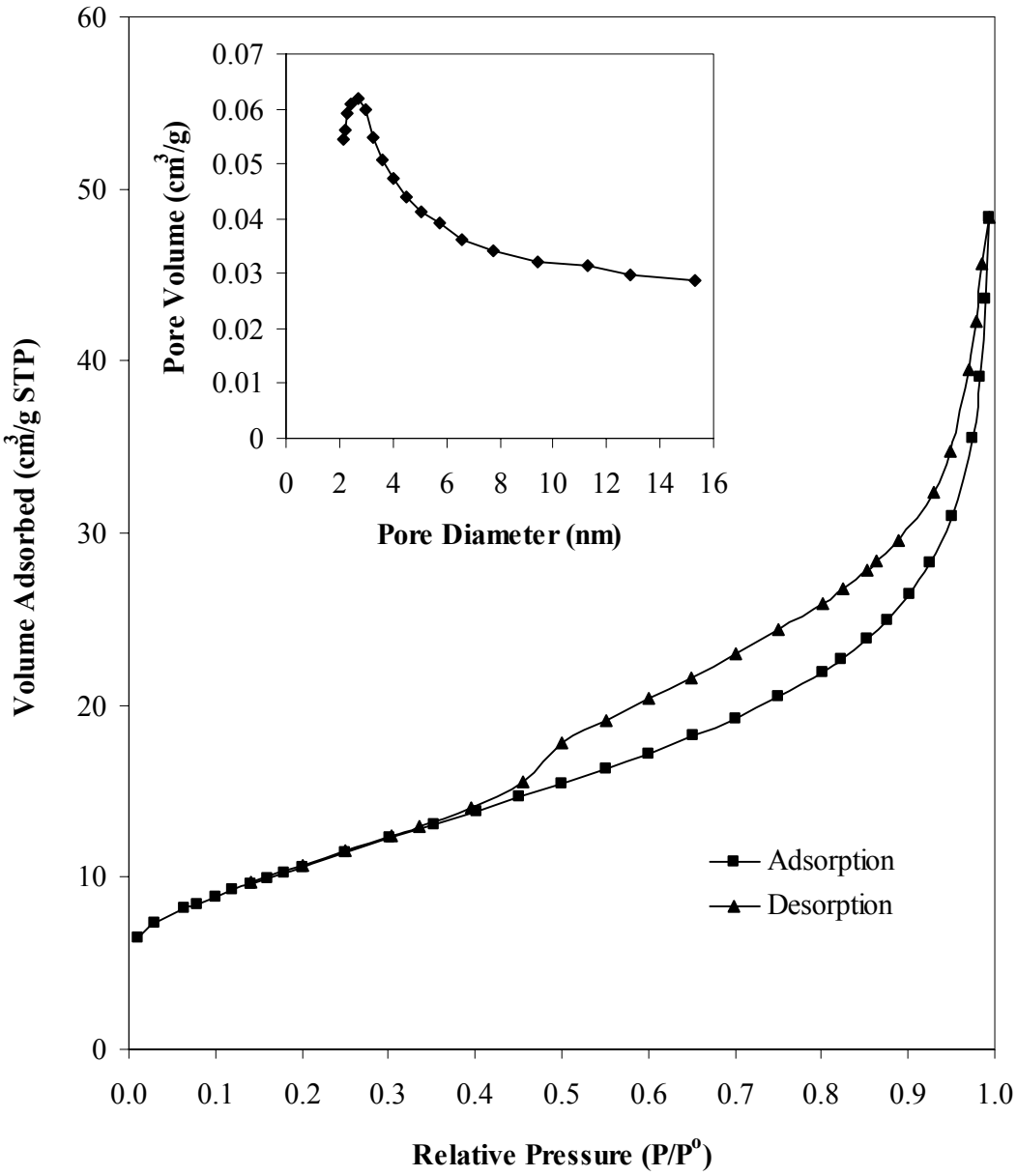

Figure 5.5 Nitrogen adsorption (■) /desorption (▲) isotherms and BJH pore size distribution (inset) for a calcined CZY sample prepared using the DAB-Am-64 template. The sample was calcined in air from 25 to 600 °C at a heating rate of 20 ºC /min, with the final temperature being maintained for 4 h.

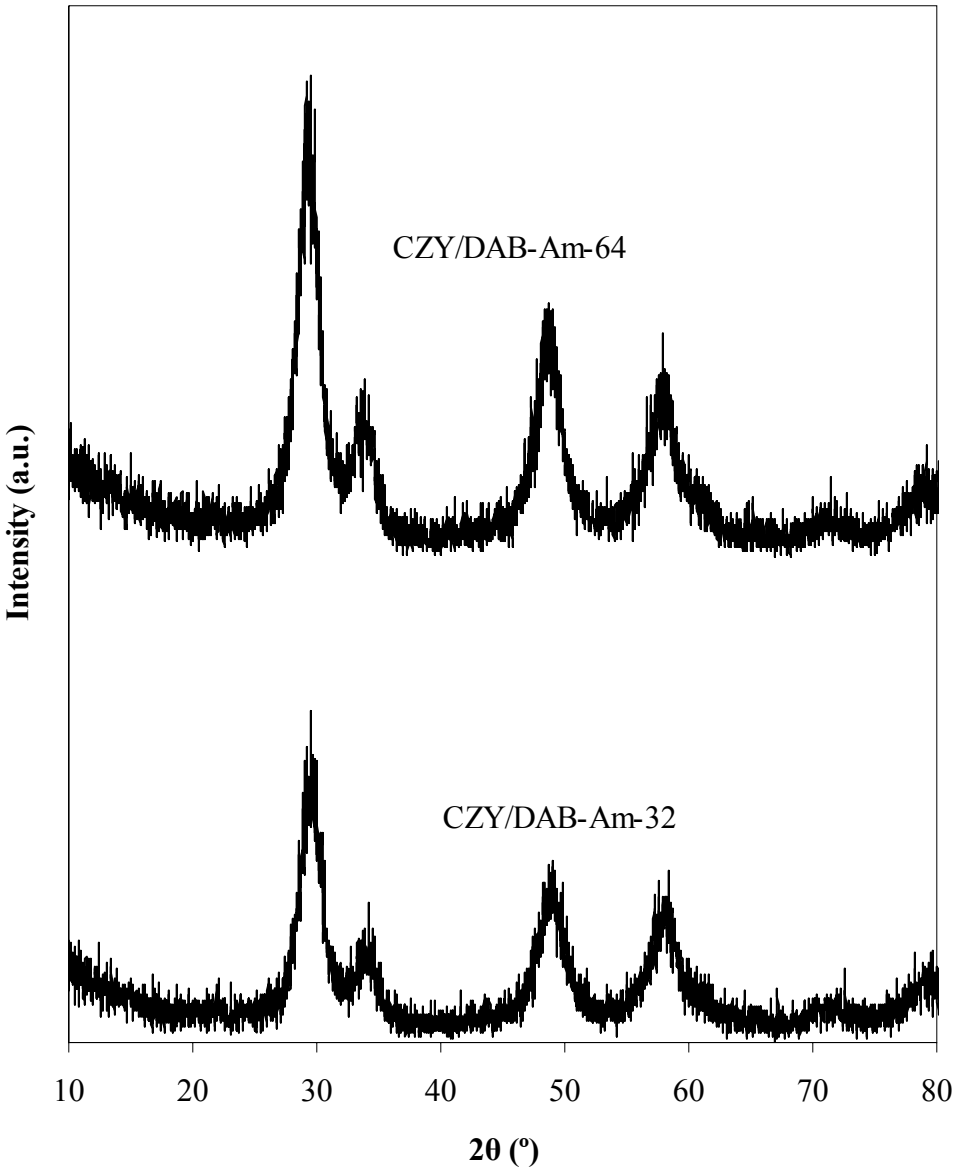

Figure 5.6 Powder X-ray diffractogram (PXD) for CZY samples prepared using DAB-Am-32 and DAB-Am-64 templates. Samples were calcined in air from 25 to 600 °C at a heating rate of 20 ºC/min, with the final temperature being maintained for 4 h.

The peaks do not show split ends which would suggest phase segregation, for example, a ceria or zirconia rich phase. The broadening of the peaks also suggested that crystallites of the dendrimer templated CZY were nanosized. The small angle X-ray diffraction (SAXD) pattern for the same samples at 2θ values ranging from 1 to 10º (not shown) do not reveal low angle peaks synonymous with ordered mesoporous MCM-41 materials. This suggests that the mesoporous CZY materials synthesized using the dendrimer templates did not exhibit long range order.

Table 5.4 shows the estimated molar percentages of metal oxides in the CZY materials synthesized using DAB-Am-32, and DAB-Am-64 as SDA. These results reveal that all the metal oxides are well incorporated into the CZY materials. They are well within the margin of error for the expected molar percentages reported as theoretical amount.

Table 5.4 Elemental composition of dendrimer templated CZY

Sample	ZrO_2 (mol %)[d]	$YO_{1.5}$ (mol %)[d]	CeO_2 (mol %)[d]
Theoretical Amount	45.00	5.00	50.00
CZY/DAB-Am-32	46.23	4.95	48.82
CZY /DAB-Am-64	45.27	5.74	48.98

d. The error margin for the elemental composition is ±1.0 mol%

Figure 5.7 and 5.8 show TEM images of CZY materials synthesized using DAB-Am 32, and DAB-Am-64 template, respectively. The TEM images are virtually indistinguishable. They all show similar morphology, that is, they are basically an agglomeration of nanosized particulates of approximately 5 nm in diameter.

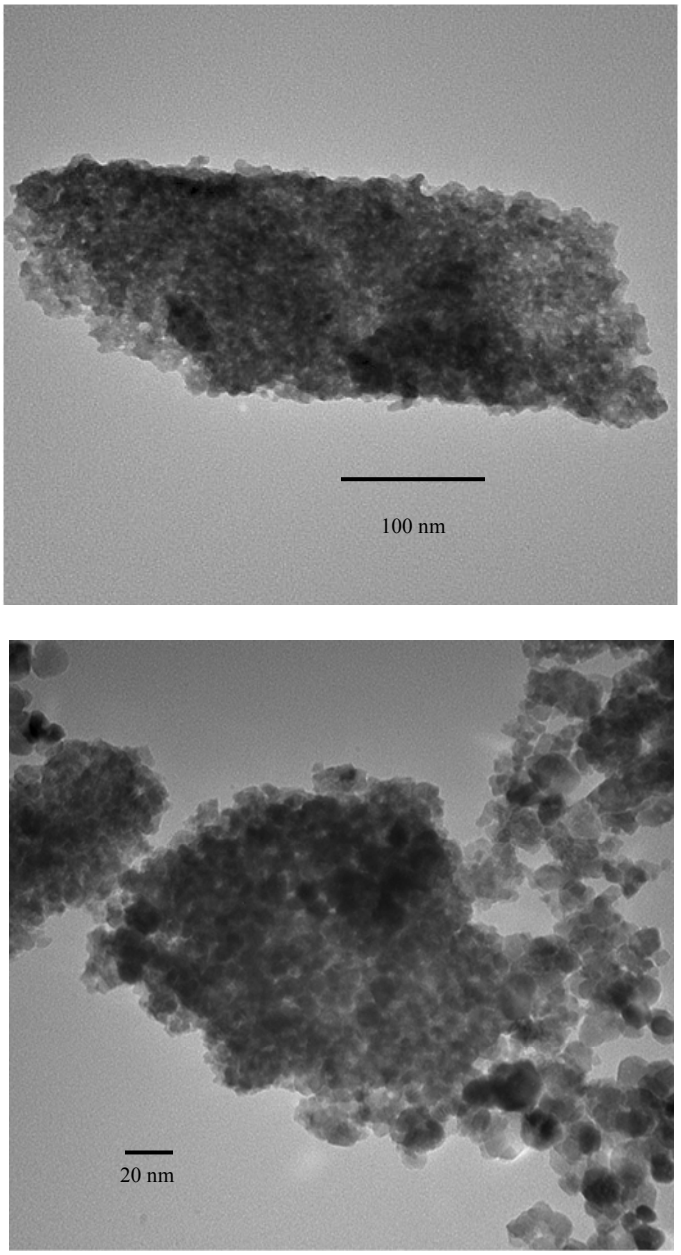

Figure 5.7 Transmission electron micrographs of a calcined CZY mixed oxide prepared using DAB-Am-32 dendrimer as the sol-gel template. Samples were calcined in air from 25 to 600 °C at a heating rate of 20 ºC/min, with the final temperature being maintained for 4 h.

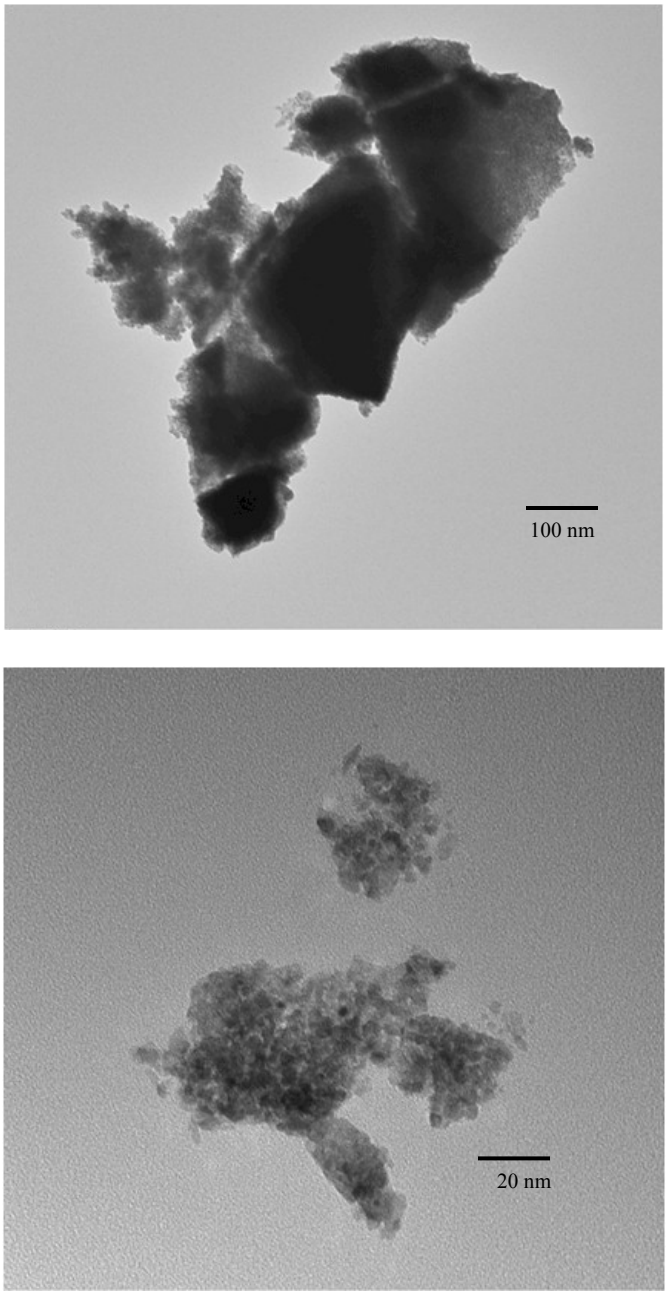

Figure 5.8 Transmission electron micrographs of a calcined CZY mixed oxide prepared using DAB-Am-64 dendrimer as the sol-gel template. Samples were calcined in air from 25 to 600 °C at a heating rate of 20 ºC/min, with the final temperature being maintained for 4 h.

This suggests that adding templates has not significantly imparted the structural morphology of the CZY material. Thermal degradation studies of surfactant templated CZY materials were carried out between 700 and 1000 ºC. Table 5.5 shows the variation of the physical properties of dendrimer templated CZY on calcination temperature. The overall loss in surface area from 700 to 1000 ºC is approximately 82.7%.

Table 5.5 Variation of surface area and pore volume as a function of aging temperature for DAB-Am-32 templated CZY samples. Samples were calcined in air to the specified temperature at a heating rate of 20 ºC/min, with the final temperature being maintained for 4 h.

Aging Temperature (ºC)	BET Surface Area (m^2/g)[e]	BJH Pore Diameter (nm)[e]
700	42.7	3.5, 6.0
800	29.3	10.0
900	13.0	18.0
1000	7.4	30.0

e. The error margin for the surface area is ±5 m^2/g and for the pore diameter, ±0.5 nm

The results of powder XRD patterns after accelerated ageing of the CZY samples after calcining from 700 to 1000 ºC for 4 hr are shown in Figure 5.9. The powder XRD pattern are quite similar during each ageing temperature but at higher temperatures the peaks become sharper indicating that the CZY samples are more crystalline and sintered at higher temperature. The CZY samples do not show evidence of phase segregation even at higher temperatures because there are no peak splits even at higher temperatures.

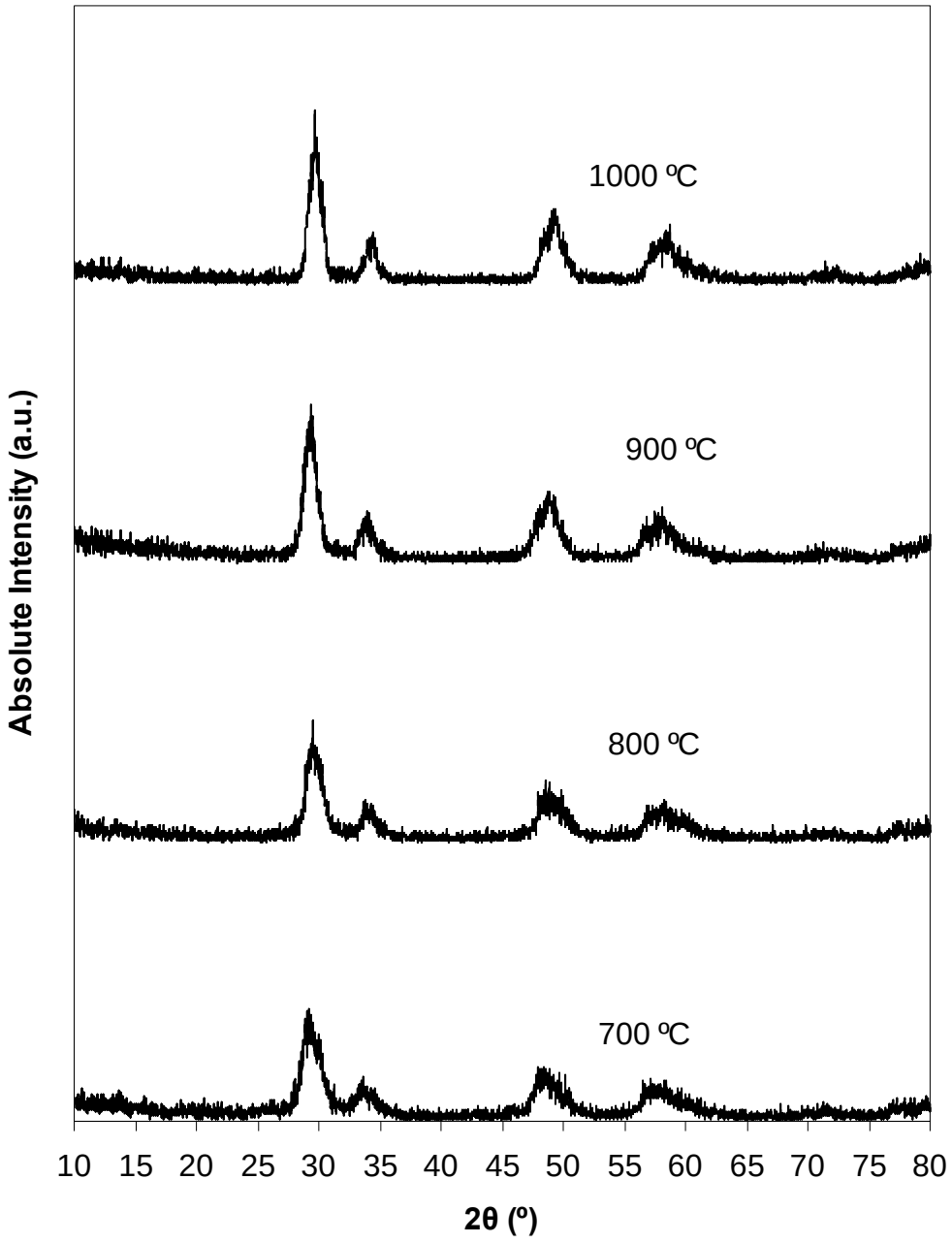

Figure 5.9 Powder X-ray diffractogram (PXD) for DAB-Am-32 templated CZY samples. Samples were calcined in air to the specified temperature at a heating rate of 20 ºC/min, with the final temperature being maintained for 4 h.

Conclusion

In this chapter I describe the synthesis steps for making mesoporous CZY materials using dendrimer as the structure directing agent. The synthesized CZY material was characterized using analytic methods and procedures given in chapter 3. The TEM images and the physisorption isotherm both indicate that the synthesized CZY mixed oxide contained some mesopore structures. The peak broadening shown in the powder XRD patterns showed that the primary particles were nanosized crystallites. In view of all these pieces of evidence, it obvious that the mechanistic pathway for this synthesis was completely different from the golf-ball structure shown in Figure 5.1. It appears that the most appropriate pathway would be pathway 1 as shown in Figure 3.22. The units of the dendrimer are like the spherical micelles shown in Figure 3.22. The precipitated oxides nucleate in the interstice between these dendrimer units. Therefore, the mesoporosity observed in the nitrogen physisorption data is likely created by the void space between these agglomerated pseudo-spherical oxide particles, see Figure 3.24.

CHAPTER SIX

ACTIVATED CARBON TEMPLATE TECHNIQUE

This chapter introduces the first member of a set of CZY templates which are different from the soft templates discussed in the last three chapters: surfactant, block copolymer, and dendrimer templates. The first two examples, surfactant and block copolymer templates, organize by self assembly into larger secondary and tertiary structures. The exact type of secondary and tertiary structures that are formed depends on the concentration of the micelles of the surfactant or block copolymer templates in the sol gel solution, the presence of organic co-additives, the pH of the sol-gel, temperature and the hydrophilicity of the sol gel solvent. The dendrimers are a unique type of soft template in that they exist as pre-formed secondary structures that are not known to readily self assemble into well organized tertiary structures.

The class of templates to be discussed in the next two chapters is called exo-templates or hard templates because they exist as rigid or semi-rigid solids that require no self-assembly in order to generate their supramolecular structure. These porous templates have random arrangements of micro-, meso-, and macro-pores or exhibit porous microstructures that are created by the interstices between primary template particles. The choice of a hard template is driven by the following criteria: ease of availability, low cost, ease with which it can be removed via calcination, and possession of a substantial pore volume. Two very important classes of compounds are activated carbons and polymeric resins. The use of hard templates in the synthesis of both siliceous and non-silica based materials has been reported in the literature[14,44,69-71,104,105]; however, the focus on the use

of hard templates for the synthesis of CZY materials has been limited. Therefore, the discussion that follows will describe the properties of CZY mesoporous materials that were prepared using activated carbon as an exo-template for the generation of a disordered, three-dimensional pore structure in the CZY mixed oxides. In addition, the effects of varying metal oxide precursor solution on the surface area and pore size of the synthesized activated carbon templated CZY will be investigated also.

Synthesis Strategy for Making CZY Using Activated Carbon Template Technique

In general, the synthesis procedure for making mesoporous non-silica based oxides employing hard templates is quite different from that used with the soft templates described previously. The distinction can be viewed more in terms of the mechanism for creating the pore structure. For soft templates, the polymeric hydroxides of the metal are deposited around the soft template. During calcination, the organic soft templates are burned off, leaving a porous metal oxides structure. This has been aptly described as endotemplating. However, with hard templates, the metal oxide precursors are absorbed into the interstices between the hard template particles or into pores within the template structure. For these systems, the porous oxide structure is generated when the rigid template is removed via calcination in air. This has also been aptly described as exotemplating. Figure 6.1 illustrates the mechanism for pore structure generation using an activated carbon template as the structure directing agent.

The earliest reported use of activated carbon as an SDA for the synthesis of mesoporous materials was reported by researchers at the Toyota Central R&D lab in Japan.[105] More recently, the technique has been widely used in the synthesis of a number of metal oxides, including pure single component oxides and mixed oxides containing two or more active metals.[14,47,69-71,104]

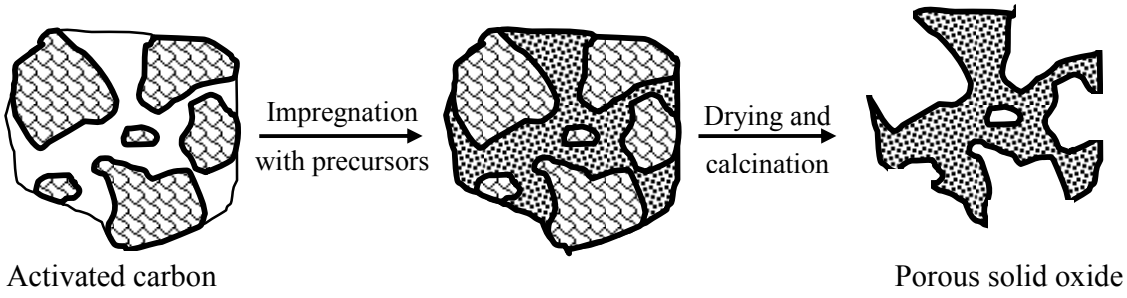

Figure 6.1 Mechanism for creating the pore structure for activated carbon templated porous oxides.

Figure 6.2 shows a schematic representation of the synthesis procedure for mesoporous non-silica based materials using activated carbon as the structure directing agent. The synthesis procedure can be divided into five categories: precursor preparation, impregnation, filtration, drying, and calcination. In the precursor preparation step, the procedures given in chapter 3 are followed in details. To investigate the effect of metal oxide precursor concentration on the surface area and the pore size, different concentrations of the metal oxide precursors in deionized water could be prepared using the same procedures given in chapter 3.

The second step is the impregnation of the activated carbon template with the solution containing the metal oxide precursors. This step is very important. The

impregnation is achieved by the incipient wetness method, which involves adding the metal salt solution to a known quantity of the dried carbon template. The volume of the added solution should closely match the water pore volume (WPV) of the sample, where the WPV is the mass or volume of water a dried sample will absorb without the surface of the sample becoming visibly wet.

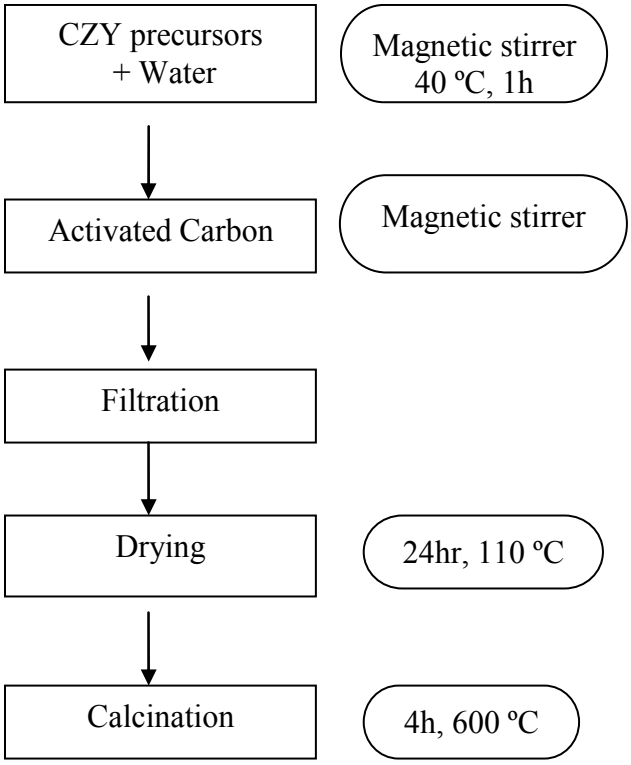

Figure 6.2 Schematic representation of the synthesis procedure for non-siliceous mesoporous materials using activated carbon as the template.

The wet activated carbon is then properly kneaded together to ensure maximum saturation and subsequently vacuum filtered to ensure that only the pores of the activated carbon are filled with the metal oxide precursor solution. After, the filtration step, the metal oxide precursor laden activated carbon is the dried over night under ambient

conditions. Lastly, the dry metal oxide precursors laden activated carbon is then calcined. The calcination process is carried out at a high enough temperature for the complete combustion of the activated carbon template, but at a low heating rate so as to prevent the generation of localized hot spots that could cause pore collapse and oxide sintering.

Synthesis of CZY Mixed Oxide Using Activated Carbon Template

All chemicals used in the preparation of the carbon templated CZY samples were used as received from their respective manufacturer. See chapter 3 for detailed description of all the chemicals except Darco® G-60 Activated Carbon (Sigma-Aldrich, powder, 100 mesh particle size), and ammonium cerium (IV) nitrate (Sigma-Aldrich, 98.5%) which replaced cerium (III) nitrate hexahydrate $Ce(NO_3)_3 \cdot 6H_2O$ (Alfa Aesar, ROE 99.5%) and thus precluded the use of hydrogen peroxide (Fisher Scientific, certified ACS 30 wt%). No additives like cosolvent or swelling agent are required for this technique. For the preparation of the metal oxide precursor solution follow the instruction provided in chapter 3. In a separate beaker, activated carbon (~20 g) was weighed out. Table 6.1 shows the typical quantities of the metal oxide precursors, solvent, and activated carbon that were used during the synthesis of mesoporous ceria-zirconia-yttria (CZY) mixed oxides. Three different levels of metal oxide precursor solution concentration are reported in Table 6.1. The homogeneous solution of metal oxide precursors was then added drop wise to the beaker containing the activated carbon template. Each time after adding the homogeneous solution of metal oxide precursors, the

mixture is stirred continuously using a hand held spatula. The activated carbon/homogenous solution of metal oxide precursors were well kneaded together to ensure complete adsorption of the solution of the metal oxide precursors by the activated carbon.

Table 6.1 Synthesis composition for activated carbon templated CZY samples. Each solution was separately combined with 21.0 g of activated carbon (Darco® G-60).

Sample	$ZrO(NO_3)_2 \cdot 6H_2O$ (g)	$Y(NO_3)_3 \cdot 6H_2O$ (g)	$(NH_4)_2Ce(NO_3)_6$ (g)	Deionized Water (mL)
CZY@ 0.5 M	3.817	0.479	6.853	50.00
CZY @ 1.0 M	7.635	0.958	13.706	50.00
CZY @ 1.5 M	11.452	1.436	20.558	50.00

Subsequently, the wet activated carbon was vacuum filtered. After filtration, the wet mixture of activated carbon and homogenous solution of metal oxide precursors was dried overnight for at least 12 h under ambient conditions. The resulting metal salt laden activated carbon mixture was placed in a ceramic crucible and calcined in air from 25 to 600 °C at heating rates ranging from 1 to 20 ºC/min. The final 600 °C temperature was maintained for 4 hours to ensure that all oxidizable/organic material had been removed. Because the carbon template is removed via calcination, it is very important that the ash content of the activated carbon template be less than 0.2 wt% of the weight of the activated carbon or even ash-free where possible so as to prevent contamination of the final catalyst material. The activated carbon template should also be highly porous (preferably with roughly over 0.7 mL/g pore volume) and have a specific surface area of

over 500 m^2/g. The calcined samples are characterized using the analytical methods and procedures stated in chapter 3.

Results and Discussion

To determine the optimal calcination protocol for carbon template removal and oxide sintering, we studied the effects of heat flow on as-synthesized CZY mixed oxides in air at heating rates ranging from 1 to 20 ºC/min from near ambient temperatures to 600 ºC. We used an as-synthesized CZY sample prepared without the inclusion of any structure directing agent as a control or reference sample. Results from thermal degradation studies for the reference sample and CZY samples prepared using activated carbon as the structure directing agent are shown below. Figure 6.3 shows the TGA plot both activated carbon and as-synthesized CZY oxide sample synthesized using activated carbon template as SDA. The activated carbon samples were heated at 1 and 20 ºC /min form ambient temperature to 600 ºC. At 20 ºC /min heating rates, the activated carbon samples showed a slight weight loss of about 5 wt% of it total weight because of the loss of water. The percentage weight remained stable until 550 ºC at the preceding heating rate before it was completely vaporized. At 1 ºC /min heating rate, the initial percent weight loss was very little. The percentage weight of the activated carbon sample remained stable until about 450 ºC where the combustion of the activated carbon starts and all its contents vaporized at 600 ºC. With the activated carbon templated CZY samples, the TGA plots are quite different. After the weight loss associated with the water loss, the second stage of percentage weight loss started at a much lower

temperature suggesting that the cerium, zirconium, or yttrium might be acting as catalyst for the combustion process. The decomposition of the metal oxide nitrates have been shown to start between 200 and 350 ºC. But for activated carbon templated CZY samples, the temperature exceeded the upper stated above to about 600 ºC.

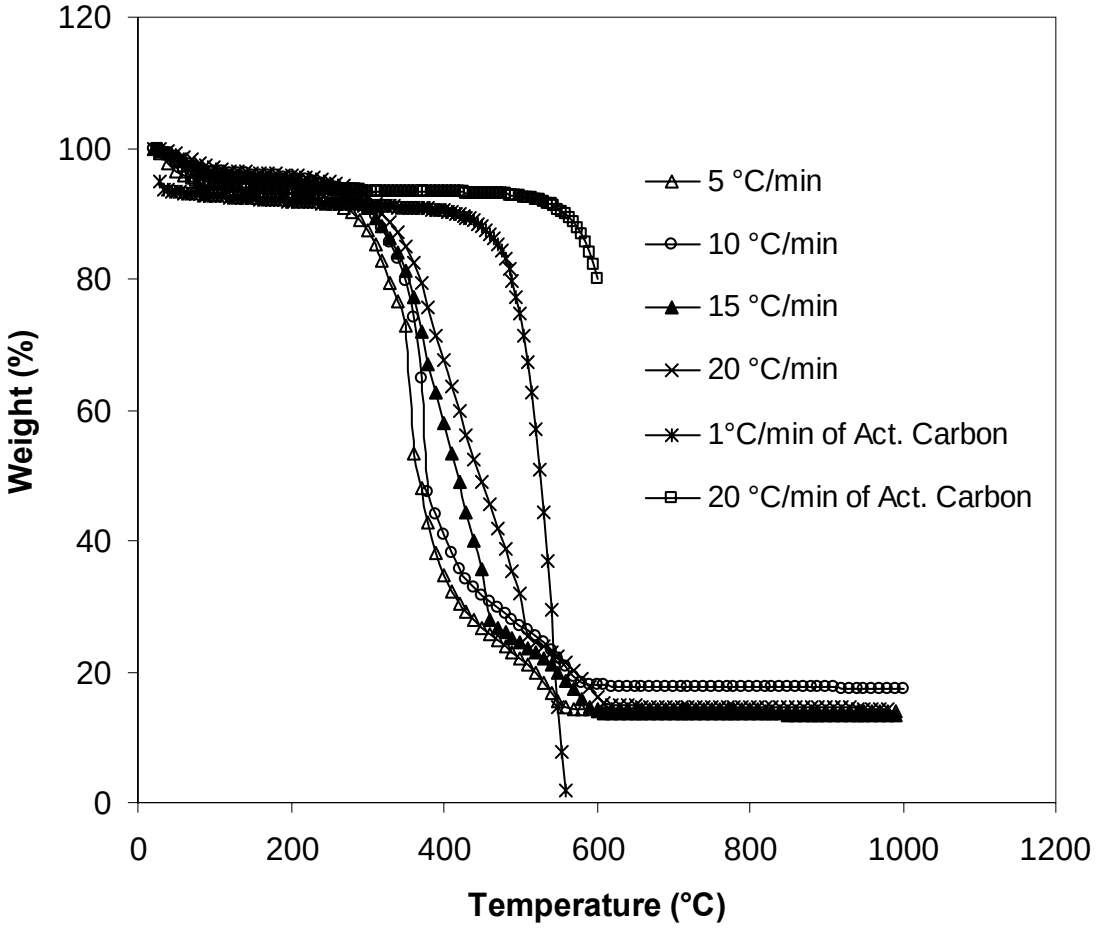

Figure 6.3 Thermogravimetric analysis of activated carbon and as-synthesized CZY sample, prepared using an activated carbon template upon heating from near ambient temperatures to 1000 ºC at different heating rates in a constant flow of air.

This high temperature within the CZY samples was due mainly to the effect called localized heating or hot spots generation. The percentage weight of activated carbon templated CZY samples remained constant beyond 600 ºC for all the samples irrespective of the heating rate used. This suggests that the activated carbon templates are burned off right around 600 ºC.

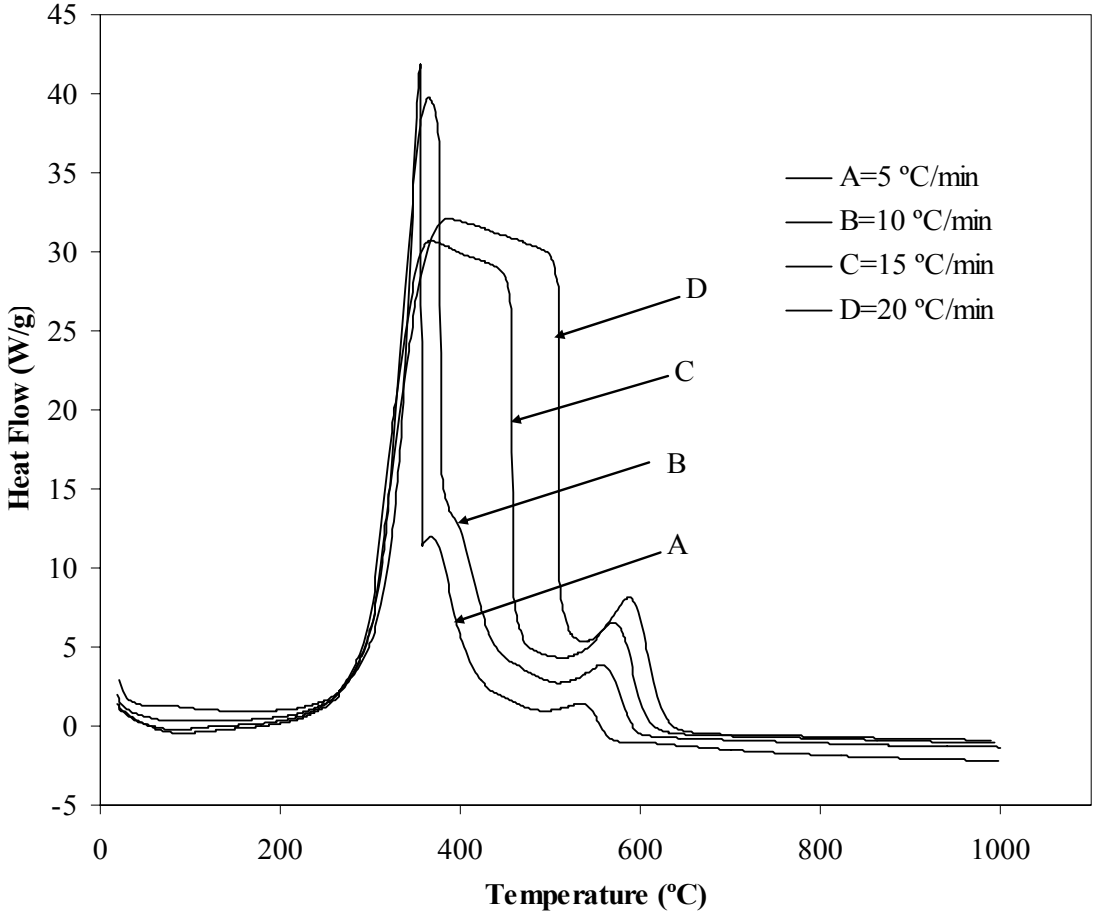

Figure 6.4 Differential heat flow to as-synthesized CZY sample prepared using an activated carbon template upon heating from near ambient temperatures to 1000 ºC at different heating rates in a constant flow of air.

DSC spectra, shown in Figure 6.4, for the as-synthesized CZY sample prepared using activated carbon are significantly different from those observed with the reference CZY material that contained no template (Figure 3.5). At temperatures less than 200 ºC, the endothermic processes appeared non-existent because of the large scale used in making the plot. The TGA plots showed that water loss occurred at this temperature range. However, the most important thermal feature in the DSC spectra of the carbon templated samples (Figure 6.4) occurs between 200 and 700 ºC, where significant heat evolution processes are occurring instead of the endothermic process observed with the reference CZY sample that contained no template (Figure 3.5). This phenomenon arises because the heat absorbed during the thermal decomposition of the nitrate salts is less than the heat released during the combustion of the carbon template.

In Figure 6.4, a significant exotherm was observed for carbon templated CZY samples that were heated at the rate of 10 ºC/min or less was found between 250 and 400 ºC; however, for equivalent samples heated at a rate higher than 10 ºC/min, the exotherm occurred at temperatures between 250 and 550 ºC. Further, a second exothermic process occurred, regardless of the heating rate, at temperatures between 500 and 700 ºC. The exotherm observed at temperatures slightly above 250 °C results from the combustion of the activated carbon templates and the decomposition of the nitrate salts of the precursors. The magnitude of the heat released from the carbon combustion process, because of the high template loading in these samples, very likely causes localized hot spots within the oxide samples. For samples calcined at heating rates above 10 °C/min, these hot spots arising from template combustion are generated at much higher sample

temperatures (up to 550 °C), which suggests that the local sample temperature can exceed the melting point of the oxide. This observation helps to explain why a significant loss in surface area was observed with carbon templated samples that were calcined to 600 °C at a heating rate of 20 °C/min (see Table 6.2). Because the exiting gas flow from the DSC was not characterized, by methods such as IR or mass spectrometry, we were unable to definitively identify the nature of the exothermic degradation process occurring at higher sample temperatures (500 – 700 °C). However, the key aspect of these studies was the conclusion that carbon templated catalysts should be calcined at heating rates below 10 °C/min so as to prevent the occurrence of hot spots in the sample, which lead to localized oxide melting and loss of catalyst surface area.

The effect of calcination heating rate on the surface area and pore diameter of activated carbon templated CZY samples that were calcined in air from 25 to 600 ºC with the final temperature being maintained for 4 h was investigated. The results of the findings are presented in Table 6.2. Table 6.2 shows the effect of calcination heating rates on the surface area and pore diameter of activated carbon templated CZY mixed oxides as they are calcined from ambient temperature to 600 °C at heating rates of 1 and 20 °C/min, while the final temperature is maintained for 4 h. The pore size measure for activated carbon templated CZY describes the external interstitial space between oxide particles or crystallite.

Table 6.2 Effect of calcination heating rate on the surface area and pore diameter of activated carbon templated CZY samples that were calcined in air from 25 to 600 ºC with the final temperature being maintained for 4 h

Heating rate (ºC/min)	BET Surface Area (m^2/g)[a]	BJH Pore Diameter (nm)[a]
1	118	9.0
20	103	9.0

a. The error margin for the surface area is ±5 m^2/g and for the pore diameter, ±1.0 nm

The results are very interesting in that they are supported by the DSC spectra (see Figure 6.4) which shows that as the heating rates are increased from 5 to 20 °C/min, the propensity to produce hot spots within materials increased significantly. Thus, the loss of over 10% of its initial surface area is whole attributable to the effects of hot spots generation within the materials as the heating rates are increased. Besides the effects of hot spots during calcination, the large amount of oxidizable materials present in the form of carbon templates during calcination, could fuel the reaction thus, generating more heat at higher calcination rates. Schuth et al. noted that the combustion of carbon is usually catalyzed by certain transition metals (copper based salts being the most reactive).[70] Although we cannot say for certain if any of the component oxides (ceria, zirconia, or yttria) catalyzes the combustion of carbon yet cannot rule out the possibility either.

Figure 6.5-6.7 show the nitrogen adsorption/desorption isotherms and the BJH pore size distribution of calcined CZY samples that were templated with activated carbon and employed varying concentrations of CZY precursors. For all of the samples studied, the physisorption isotherm shows a hysteresis loop, which is indicative of mesoporous

materials. It is important to note that hysteresis loop for the activated carbon templated CZY starts at a higher relative pressure of ~0.6.

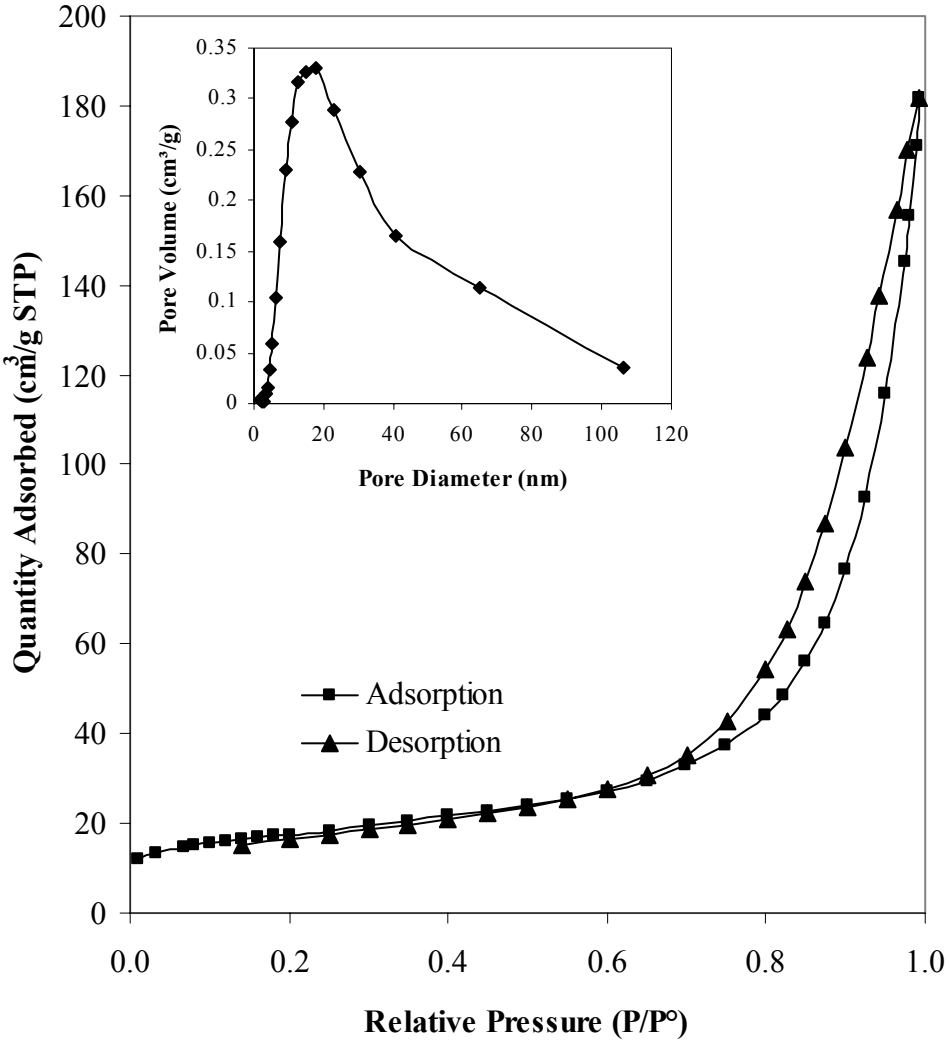

Figure 6.5 Nitrogen adsorption-desorption isotherms and BJH pore size distribution (inset) for an activated carbon templated CZY sample that was prepared using a 0.5 M solution of oxide precursors (CZY salts). The sample was calcined in air from 25 to 600 °C at a heating rate of 20 ºC /min, with the final temperature being maintained for 4 h.

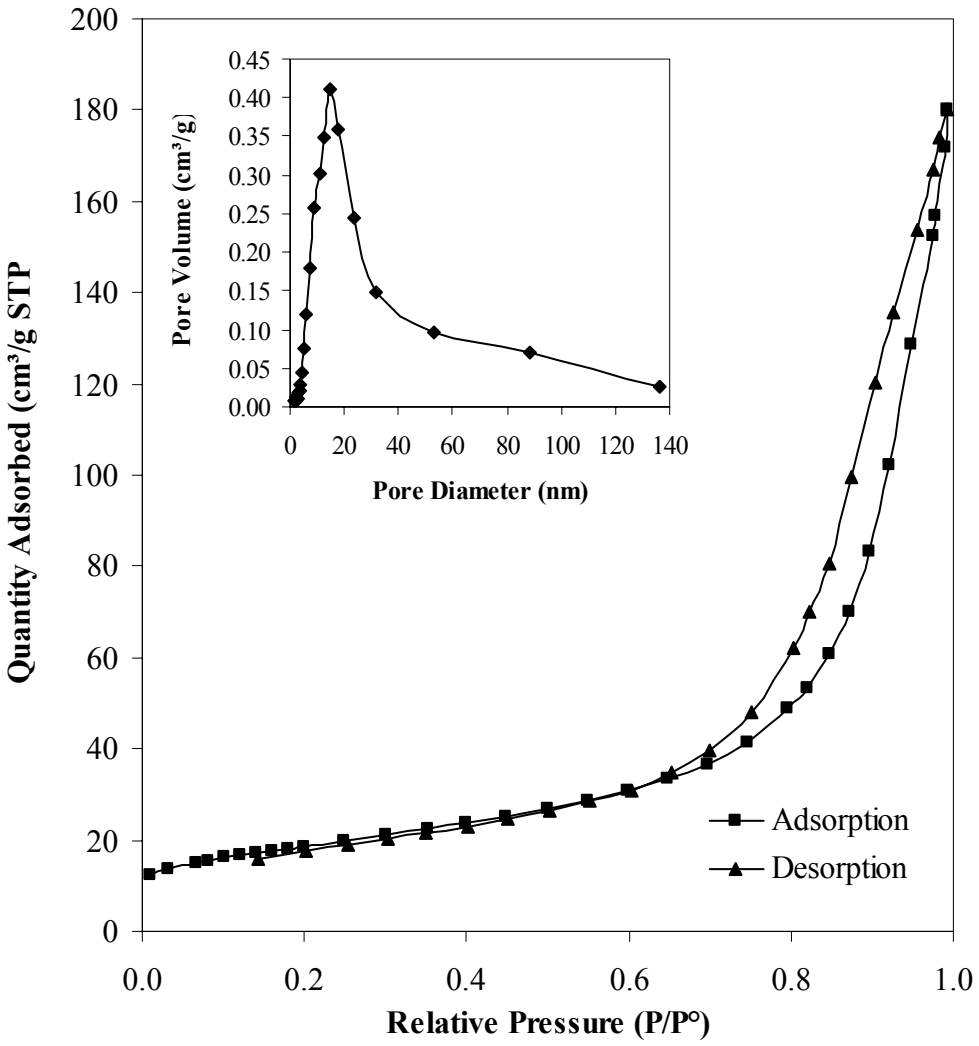

Figure 6.6 Nitrogen adsorption-desorption isotherms and BJH pore size distribution (inset) for an activated carbon templated CZY sample that was prepared using a 1.0 M solution of oxide precursors (CZY salts). The sample was calcined in air from 25 to 600 °C at a heating rate of 20 ºC /min, with the final temperature being maintained for 4 h.

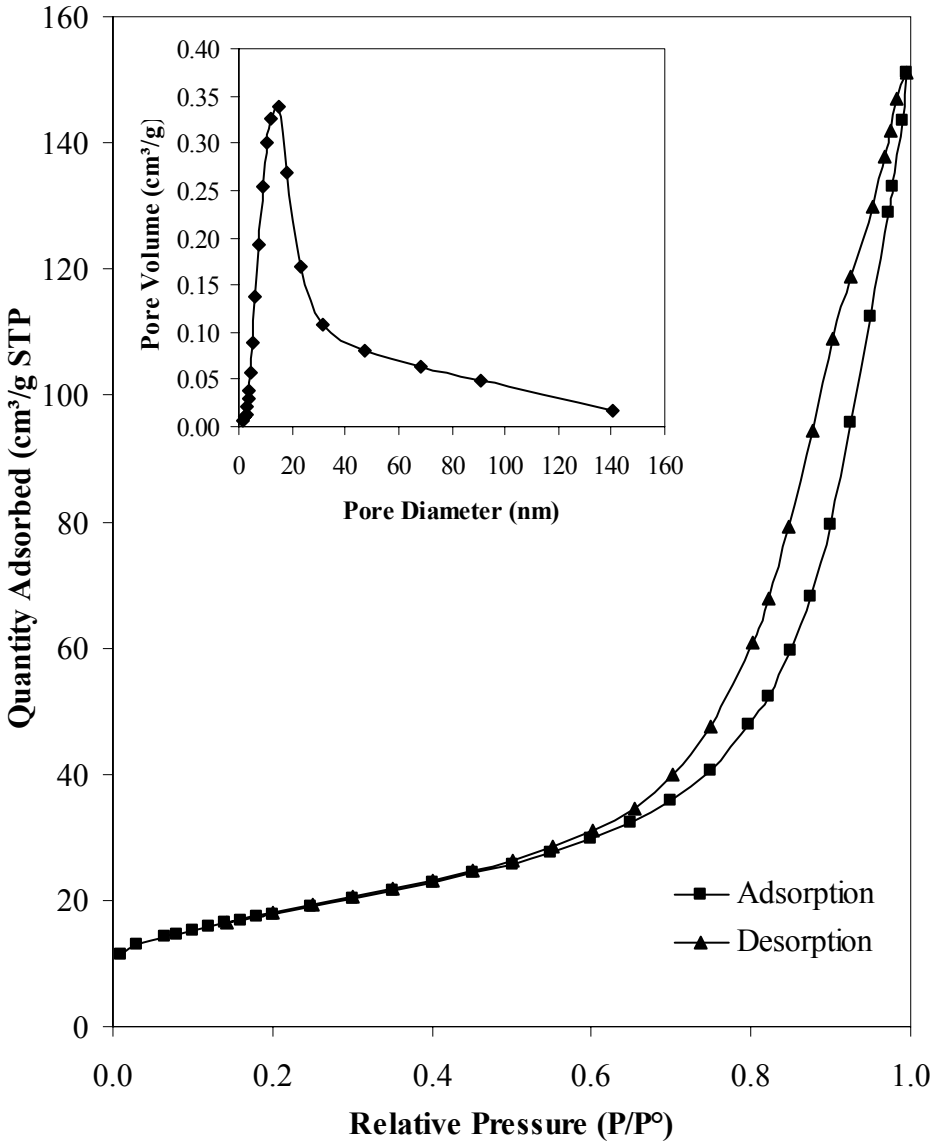

Figure 6.7 Nitrogen adsorption-desorption isotherms and BJH pore size distribution (inset) for an activated carbon templated CZY sample that was prepared using a 1.50 M solution of oxide precursors (CZY salts). The sample was calcined in air from 25 to 600 °C at a heating rate of 20 ºC /min, with the final temperature being maintained for 4 h.

This suggests that the pores contain a significant ratio of macroporosity. This is supported by the BJH pore size distribution plots for the various samples of CZY synthesized using activated carbon (see insets in Figures 6.5-6.7). The pore size distribution show a broadening of the central peak, suggesting the pore size range extends well beyond the mesoporous range.

The powder XRD patterns for multiple CZY samples prepared using activated carbon templates and oxide precursor solutions of varying concentration (0.5 M, 1.0 M, and 1.5 M salt solutions) are shown in Figure 6.7. Examination of the powder XRD patterns for each of the calcined CZY samples reveals that they are homogeneous in nature (i.e., a solid solution is formed) and exhibit a cubic fluorite PXD pattern, with the most intense diffraction peak at 29° 2-theta being attributed to diffraction from the (111) planes of the cubic lattice.[106] In general, the carbon templated powder XRD patterns are very similar to the powder X-ray diffraction pattern of pure ceria and yttria, which are both cubic fluorite structures; however, these PXD patterns clearly differ from that observed for the fluorite-type monoclinic phase of zirconia (see Figure 3.14). The characteristic line broadening associated with the peaks on the synthesized samples is evidence of the existence of nanocrystalline structures. Estimates of the crystallite size obtained from the Scherrer's equation were between 6 and 20 nm and they compared well to those observed via TEM which were between 5 and 15 nm. However, the small angle X-ray diffraction (SAXD) pattern for the same samples at 2θ values ranging from 1º to 10º do not reveal low angle peaks synonymous with ordered mesoporous MCM-41 materials. This suggests that the CZY material synthesized was not an ordered mesopore.

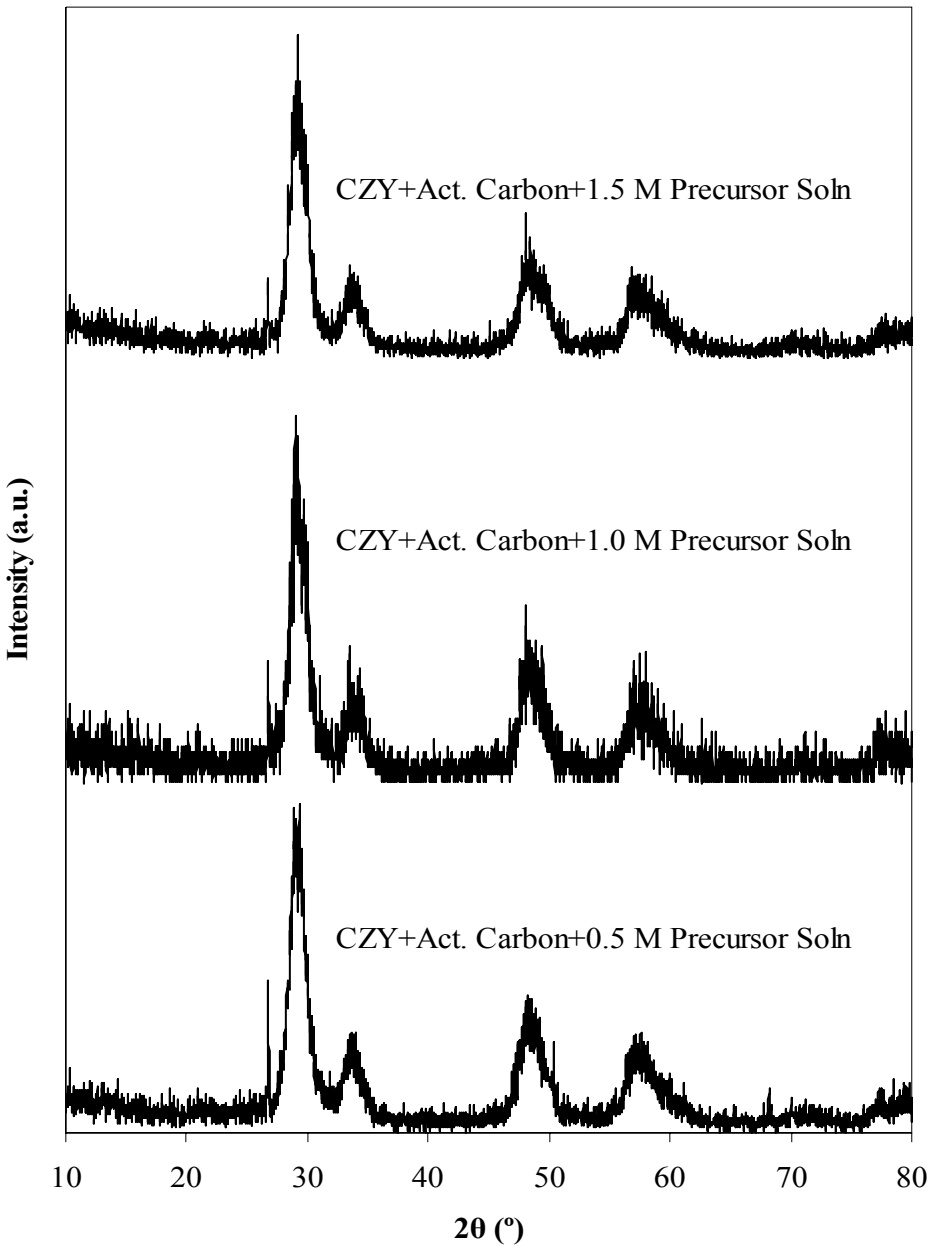

Figure 6.8 Powder X-ray diffractograms for CZY samples prepared using activated carbon templates and oxide precursor solutions of varying concentration (0.5 M, 1.0 M, and 1.5 M salt solutions). All samples were calcined in air from 25 to 600 °C at a heating rate of 20 ºC /min, with the final temperature being maintained for 4 h.

The effect of oxide precursor (salt solution) concentration on the physical properties of carbon templated CZY materials were characterized via nitrogen physisorption, and the results of these experiments are summarized in Table 6.3. Moderate increases in the surface area of the synthesis metal oxides have been reported as the precursor concentration was increased by Schuth et al.[47,69,70]. The results shown in Table 6.3 do not suggest any significant increase in surface area as the precursor concentrations were increased. This may be due to the error margin associated with taking these data. Another reason may be the selected calcination procedure (heating rate of 20 °C/min), which lead to some localized melting of the oxide (i.e., the calcination heating rate was too high to obtain high surface area CZY materials).

Table 6.3 Physical properties of synthesized CZY samples after calcination in air at 600 ºC for 4 h at 20 ºC /min.

Concentration of Precursor in CZY (M)	BET Surface Area (m^2/g)[b]	BJH Pore Diameter (nm)[b]
0.5	60	17.88
1.0	66	14.47
1.5	64	14.75

b. The error margin for the surface area is ±5 m^2/g and for the pore diameter, ±2.5 nm

Table 6.4 shows the elemental composition of a representative sample of an activated carbon templated CZY mixed oxide. These results showed that the estimated molar percentage of CeO_2, ZrO_2, and $YO_{1.5}$ as obtained by ICP-AES were within the margin of error for the expected theoretical values.

Table 6.4 Elemental composition of activated carbon templated CZY

Sample	ZrO_2 (mol %)[c]	$YO_{1.5}$ (mol %)[c]	CeO_2 (mol %)[c]
Theoretical Amount	45.00	5.00	50.00
CZY/activated carbon	48.10	4.29	47.61

c. The error margin for the elemental composition is ±3.0 mol%

Thermal degradation/sintering studies of activated carbon templated CZY materials were carried out between 700 and 1000 ºC in air. Table 6.5 shows the variation of the surface area and pore volume of activated carbon templated CZY with calcination temperature. The overall loss in surface area from 700 to 1000 ºC is approximately 86.5%.

Table 6.5 Variation of surface area and pore volume as a function of aging temperature for activated carbon templated CZY samples. Samples were calcined in air to the specified temperature at a heating rate of 20 ºC/min, with the final temperature being maintained for 4 h

Aging Temperature (ºC)	BET Surface Area (m^2/g)[d]	BJH Pore Diameter (nm)[d]
700	52	18.0
800	22	30.0
900	13	49.0
1000	7	70.0

d. The error margin for the surface area is ±5 m^2/g and for the pore diameter, ±2.5 nm

The effects accelerated aging on CZY sample crystallinity were studied using powder X-ray diffraction, and the results are shown in Figure 6.9. Samples were calcined in air from 700 to 1000 ºC at a heating of 20 °C/min, with the final calcination temperature maintained for 4 h. The peak positions observed in the powder X-ray diffractograms for all thermally aged samples are similar and no diffraction peaks are formed or lost as the calcination temperature is increased. This indicates that the oxide particles form a solid solution and that all samples maintain a fluorite-type cubic structure. However, at higher calcination temperatures the peaks become sharper (i.e., the full width at half height decreases), indicating that the CZY samples become more crystalline at higher temperature. This growth in crystallinity is the product of oxide sintering processes for CZY material that occur at temperature above 600 °C.

In order to examine CZY particle morphology and measure oxide particle sizes directly (as opposed to using PXD and the Scherrer's equation), TEM images of the activated carbon templated CZY materials were collected and are shown in Figure 6.10. These images are similar to those of other templated CZY materials, which were discussed in earlier chapters. They show nanosized crystalline particles that are stuck to one another. However, they do show a somewhat fluffy or powdery CZY samples which other CZY samples synthesized using soft templates do not exhibit. The activated carbon templated CZY samples possess rather low bulk density and mechanical strength. Thus**,** in other to use them industrially there would be need to add binding agents to re-enforce their mechanical strength.

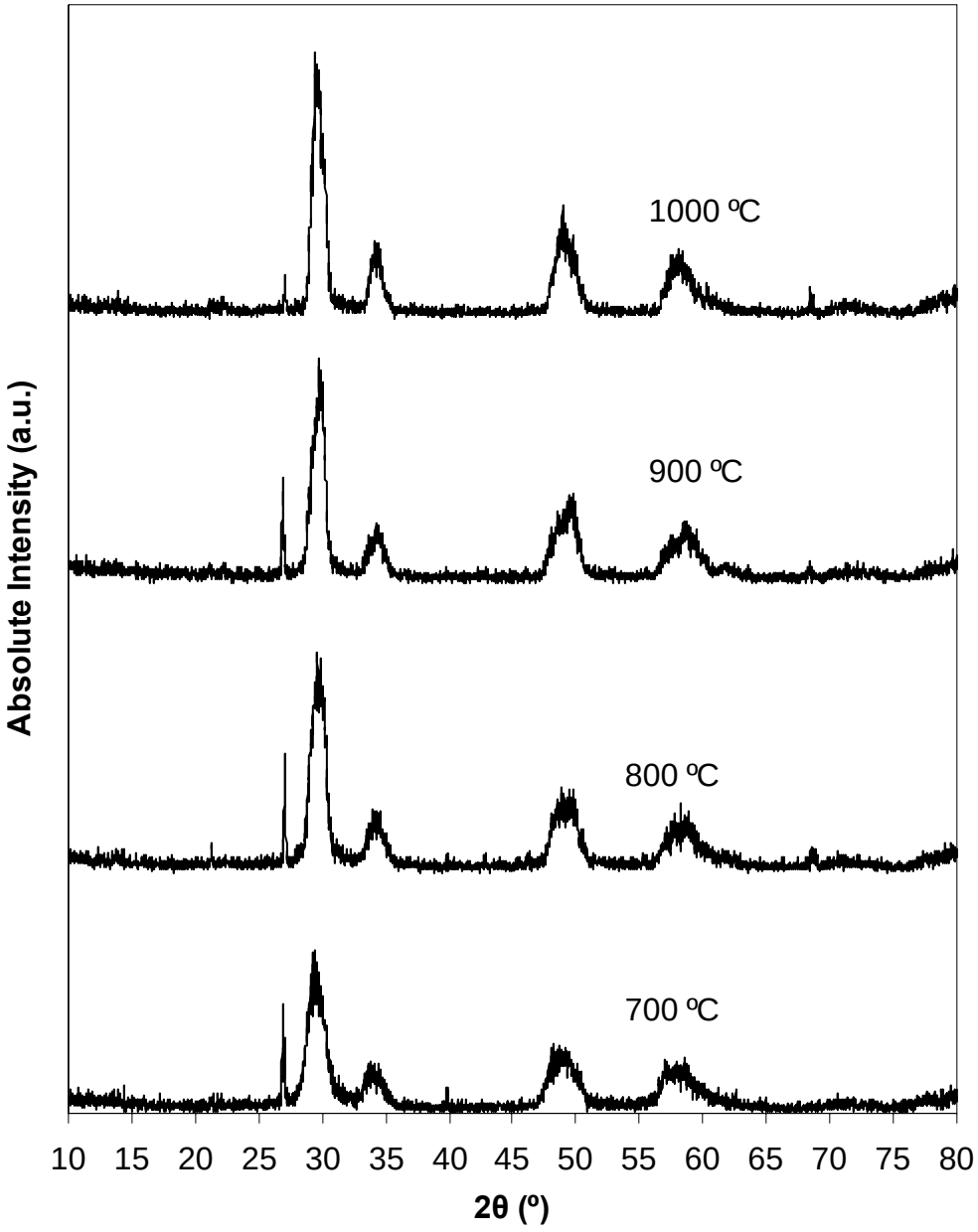

Figure 6.9 Powder X-ray diffractograms (PXD) for activated templated CZY samples. Oxides were calcined from 700 to 1000 ºC at a heating of 20 °C/min, with the final calcination temperature maintained for 4 h.

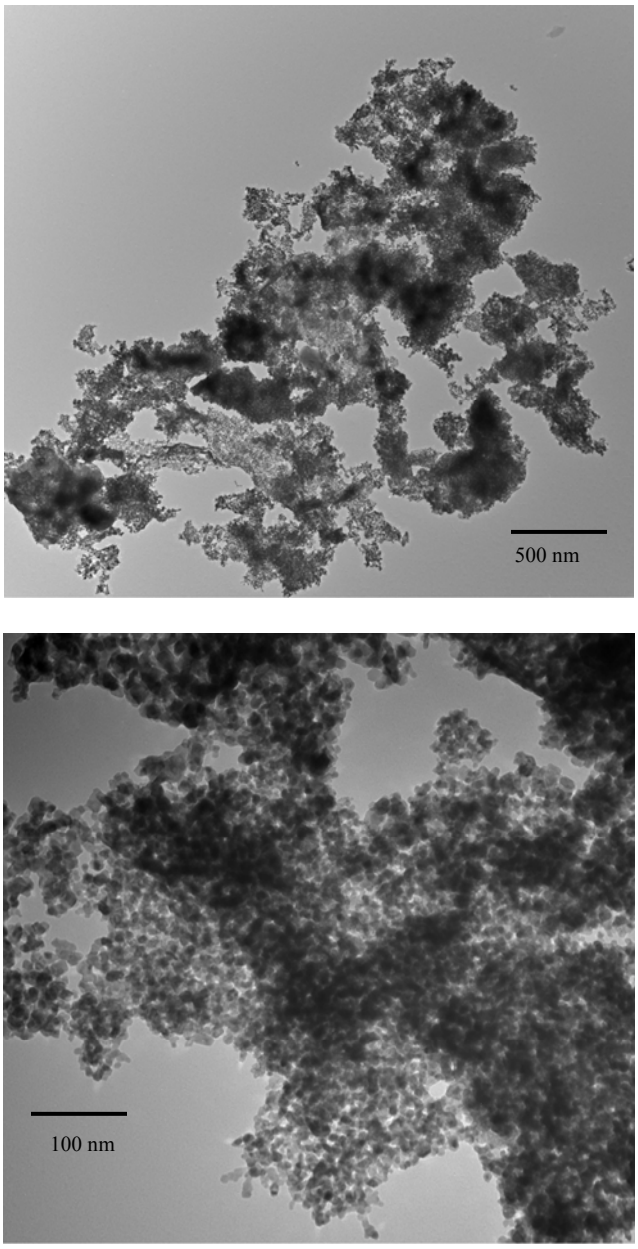

Figure 6.10 Transmission electron micrographs for activated carbon templated CZY at magnifications of 500 nm and 100 nm. All samples were calcined in air from 25 to 600 °C at a heating rate of 20 ºC /min, with the final temperature being maintained for 4 h.

Conclusion

In this chapter I have outlined the synthesis steps for making mesoporous CZY materials using activated carbon as the structure directing agent. The synthesized CZY materials were characterized to ascertain the existence of mesoporous structure, determine homogeneity of the phase, the elemental composition, the effect of heating rate during calcination, and the morphology of the material. In addition, the effects of varying precursor concentration on the physical properties (i.e. surface area and pore diameter) of the synthesized activated carbon templated CZY was determined as well as the effects of thermal ageing was also investigated.

After characterizing the activated carbon templated CZY mixed oxides, the shape of the nitrogen physisorption isotherm, the PXD spectra, and the TEM images, all suggest overwhelmingly that the synthesized materials was mesoporous; however, the absence of low angle peaks for the small angle powder XRD indicated that the mesopores were not ordered.

A huge concern with regards to using activated carbon templates has been the high ash contents associated with the synthesized materials after calcination. This would generally require further separation steps in order to remove them. Hence, the idea carbon template should not only possess high surface area and pore volume but it should be ash free as much as possible. An interesting carbon template candidate would be nanocast carbon. This is because it has well defined geometry and tunable pore structure.

The results of the study of the effects of varying calcination heating rates on the surface area and pore diameter are very revealing. They warn of a significant loss of

surface area when calcination is done at high heating rates. Hence, the ideal heating rate would be say 10 ºC/min or less, so as to preserves the structural integrity of the materials. A more robust calcination protocol such as varying the oxygen/nitrogen ratios during the calcination steps may be necessary.

The accelerated ageing experiments revealed that at higher calcination temperatures the materials lost surface area significantly. This is because of metal oxide sintering which led to growth in crystal size.

CHAPTER SEVEN

POLYMERIC RESIN TEMPLATE TECHNIQUE

In the previous chapter I introduced the concept of hard templating and tried to contrast it to soft templating. It was noted that the main difference between both templating techniques was the mechanism by which pores are generated. The synthesized mesoporous CZY mixed oxides using activated carbon templated CZY materials was described in great details. I examined the effects of varying metal oxide precursor concentration, calcination heating rates, and thermal aging on the physical properties (i.e. surface area and pore diameter) of the activated carbon templated CZY materials, and characterized the activated carbon templated CZY materials. In this chapter I continue my discussion on hard templating techniques by considering the use of polymeric resin as a structure directing agent (SDA). The synthesis strategies for making CZY materials using polymeric resin are very similar to that used for activated carbon templated CZY materials. An important distinction between both templates in terms of synthesis strategies is the mechanism for generating the porosity. While activated carbon templates readily adsorbed the solution of precursor salts, the same is not true of the polymeric resin which is polystyrene based polymer for example Amberlyst A26 OH. Most polymeric resins are rigid solids with little or no internal pore structure. The polymeric resins may or may not be functionalized with hydrophilic or hydrophobic groups. The use of polymeric resins as templates for the synthesis of mixed oxides has been reported in the literature[107-110]. The unique mechanism by which polymeric resins create mesoporous solids is also called the inverse opal technique.[111] This technique is fascinating because

after removing the polymeric resin templates by calcination it confers a negative replica of its structure unto the porous metal oxide that is formed.

Synthesis Strategy for Making Mesoporous CZY Materials
Using Polymeric Resin Template Technique

Figure 7.1 shows a schematic representation of the synthesis steps used when rigid porous materials, which may or may not be functionalized with hydrophilic or hydrophobic groups, are used as structure directing agents.

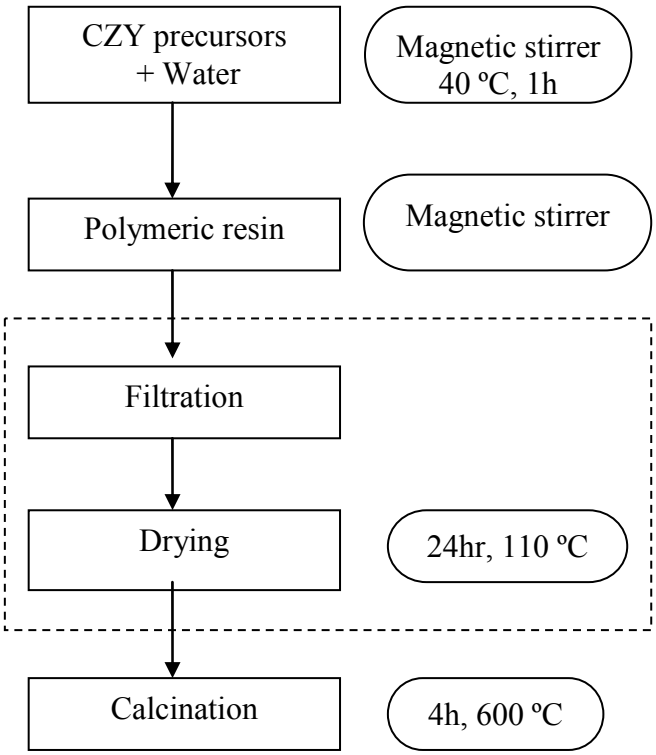

Figure 7.1 Schematic representation of the synthesis procedure for non-siliceous mesoporous materials prepared using polymeric resin template.

The synthesis steps are divided into three categories: precursor preparation, impregnation and calcination. Note that with polymeric resin template technique, both the filtration and drying steps are completely left out as shown in Figure 7.1 by the broken line around both processes. This may or may not be the case with activated carbon template technique covered in the last chapter. During the precursor preparation step, the procedures given in chapter 3 are followed in details.

Following the precursors preparation step, the homogeneous solution of metal oxide precursors is added at ~5 mL/min to polymeric resin templates. This slurry is then directly calcined because neither the filtration nor drying steps are required. The calcination is carried out at a low heating rate, sufficiently high temperature and a duration necessary for the complete combustion of the polymeric resin. The above mentioned synthesis steps for making mesoporous non-silica oxides by using polymeric resin are summarized as shown in Figure 7.2.

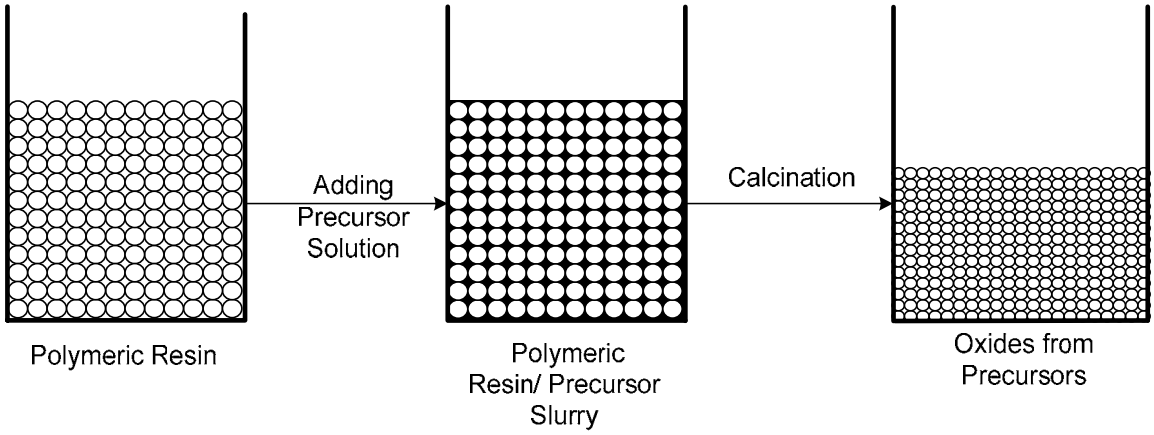

Figure 7.2 Illustration of the synthesis steps for preparing polymeric resin templated non-siliceous mesoporous materials.

Synthesis of CZY Mixed Oxide Using Polymeric Resin as Template

All chemicals used in the preparation of surfactant template CZY samples were used as received from their respective manufacturer. See chapters 3 and 6 for detailed description of all the chemicals except Amberlyst A-26 (OH) ion exchange resin (Sigma-Aldrich). For the preparation of the metal oxide precursor solution follow the instruction provided in chapter 3.

In a separate beaker, some polymeric resin (~15 g) was weighed out. Table 7.1 shows a typical composition of the precursors, solvent, and polymeric resin used during the synthesis of polymeric resin templated mesoporous ceria-zirconia-yttria (CZY) mixed oxide.

Table 7.1 Typical sample composition for polymeric resin templated CZY

	Molar Ratio		
Reagents	Salt	Oxide	Mass (g)
$ZrO(NO_3)_2 \cdot 6H_2O$	9	9	5.000
$Y(NO_3)_3 \cdot 6H_2O$	1	1	0.627
$(NH_4)_2Ce(NO_3)_6$	10	10	8.976
Amberlyst A26 OH			15.00
water			50.000

The homogeneous solution of metal oxide precursors was then added at ~ 5 mL/min to the beaker containing the polymeric resin template The mixture of polymeric resins and the precursor solution both form slurry. Since the polymeric resin is a poor adsorbent, the filtration and the drying steps can be skipped. Subsequently, the slurry was calcined in air from 25 to 600 °C at heating rates ranging from 1 to 20 ºC/min. The final 600 °C

temperature was maintained for 4 hours to ensure that all oxidizable/organic materials had been removed.

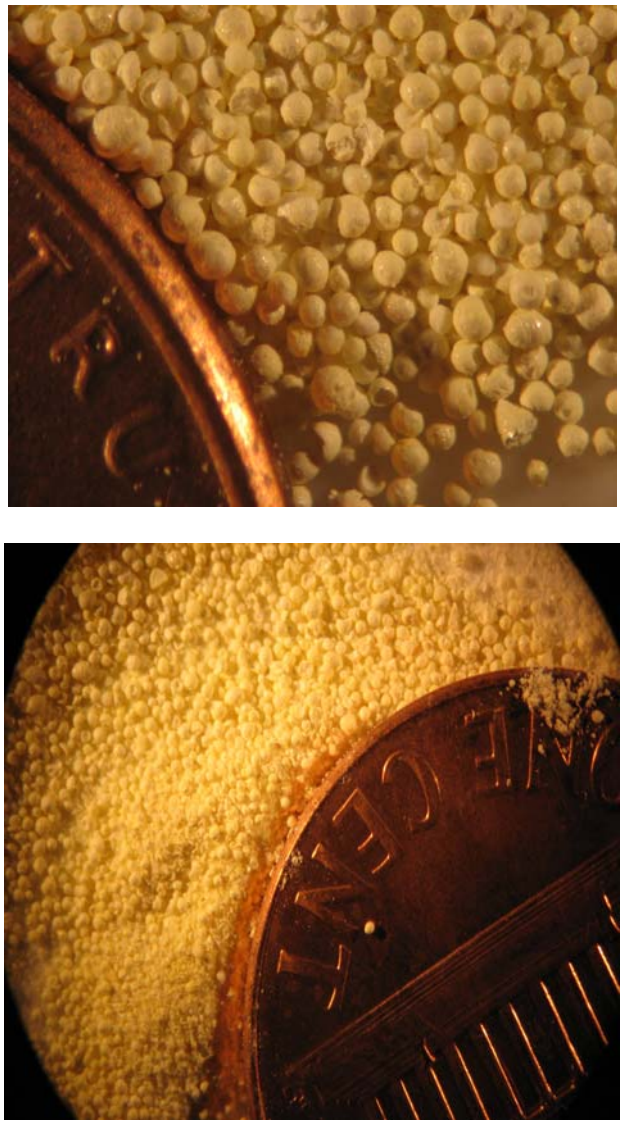

Figure 7.3 Photograph of polymeric resin templated CZY material after calcination in air at 600 ºC for 4 h at a heating rate of 20 ºC/min with a penny as the reference scales. The mesoporous CZY materials are approximately spherical in shape with a lot of broken fragments.

After calcination the polymeric resin templated CZY material is ash-free. The synthesized polymeric resin templated CZY materials were characterized following the analytical methods and procedures given in chapter 3. Figure 7.3 shows the photograph of the polymeric resin templated CZY material after calcination.

Results and Discussion

To determine the optimal calcination protocol for carbon template removal and oxide sintering, we studied the effects of heat flow on as-synthesized CZY mixed oxides in air at heating rates ranging from 1 to 20 ºC/min from near ambient temperatures to 600 ºC. We used an as-synthesized CZY sample prepared without the inclusion of any structure directing agent as a control or reference sample. Results from thermal degradation studies for the reference sample and CZY samples prepared using activated carbon as the structure directing agent are shown below. Figure 7.4 shows the TGA plot of pure polymeric resin and the CZY oxide sample synthesized using polymeric resin as SDA. The polymeric resin samples were heated at 1 and 20 ºC /min form ambient temperature to 600 ºC. At both 1 and 20 ºC /min heating rates, the resin samples showed similar profiles, a slight weight loss of about 10 wt% of it total weight because of the loss of water. The percentage weight rapidly declined afterwards to about 25 wt% when at 200 ºC. The percentage weight remained stable between 200 and 350 ºC at the preceding heating rate before undergoing stepwise weight losses until all the resins were completely burned off at 600 ºC. With the polymeric resin templated CZY samples, the TGA plots are quite different. In spite of the different heating rates, the TGA plots for the resin

templated CZY samples were quite similar in terms of profile. After the weight loss associated with the water loss, the second stage of weight loss started at a much higher temperature about 250 ºC suggesting that the cerium, zirconium, or yttrium did not catalyze the combustion process. The percentage weight remained constant after a series of two more weight losses at approximately 600 ºC and over.

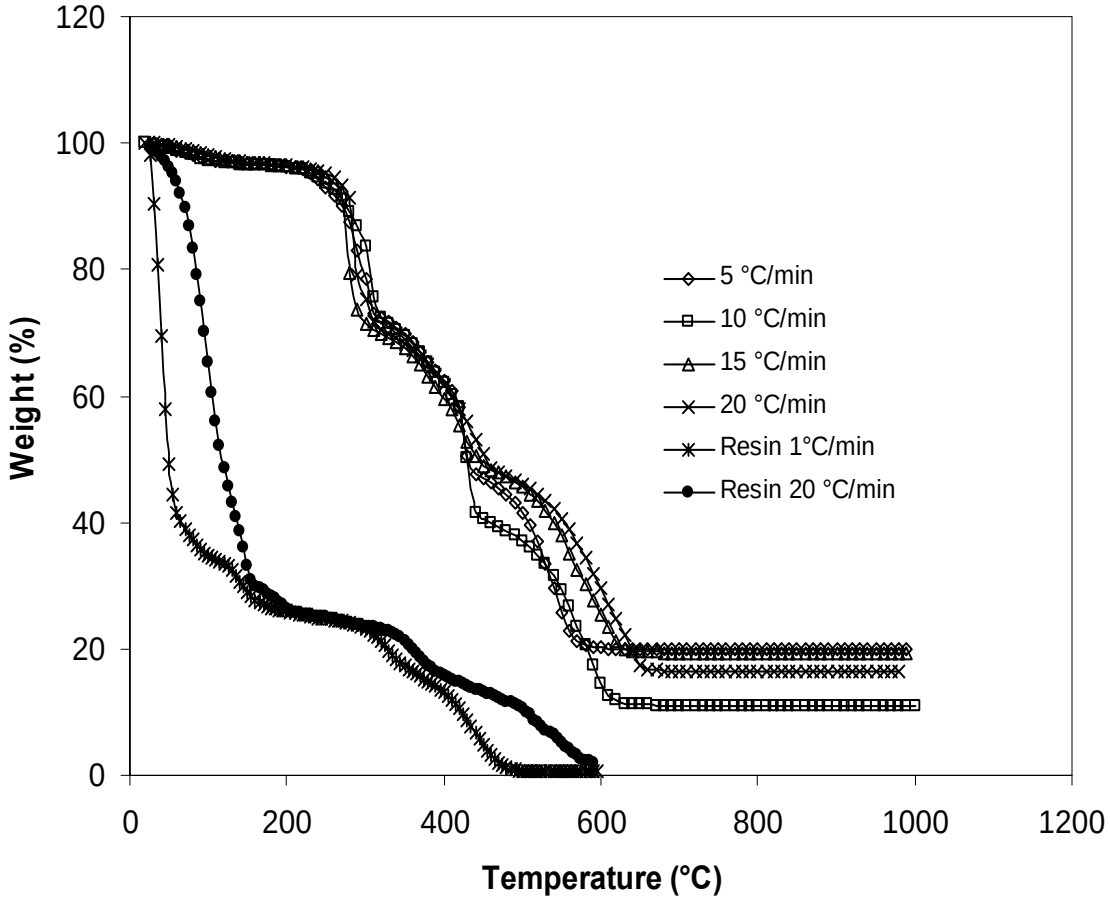

Figure 7.4 Thermogravimetric analysis of as-synthesized CZY sample prepared using no SDA upon heating from near ambient temperatures to 1000 ºC at different heating rates in a constant flow of air.

Figure 7.5 shows the DSC profile of polymeric resin templated CZY materials before the removal of the templates. The downward peaks at temperature range of less than 200 ºC are almost flat because of the scaling of the graph. However, form TGA plots it can be observed that water loss occurred within this temperature range.

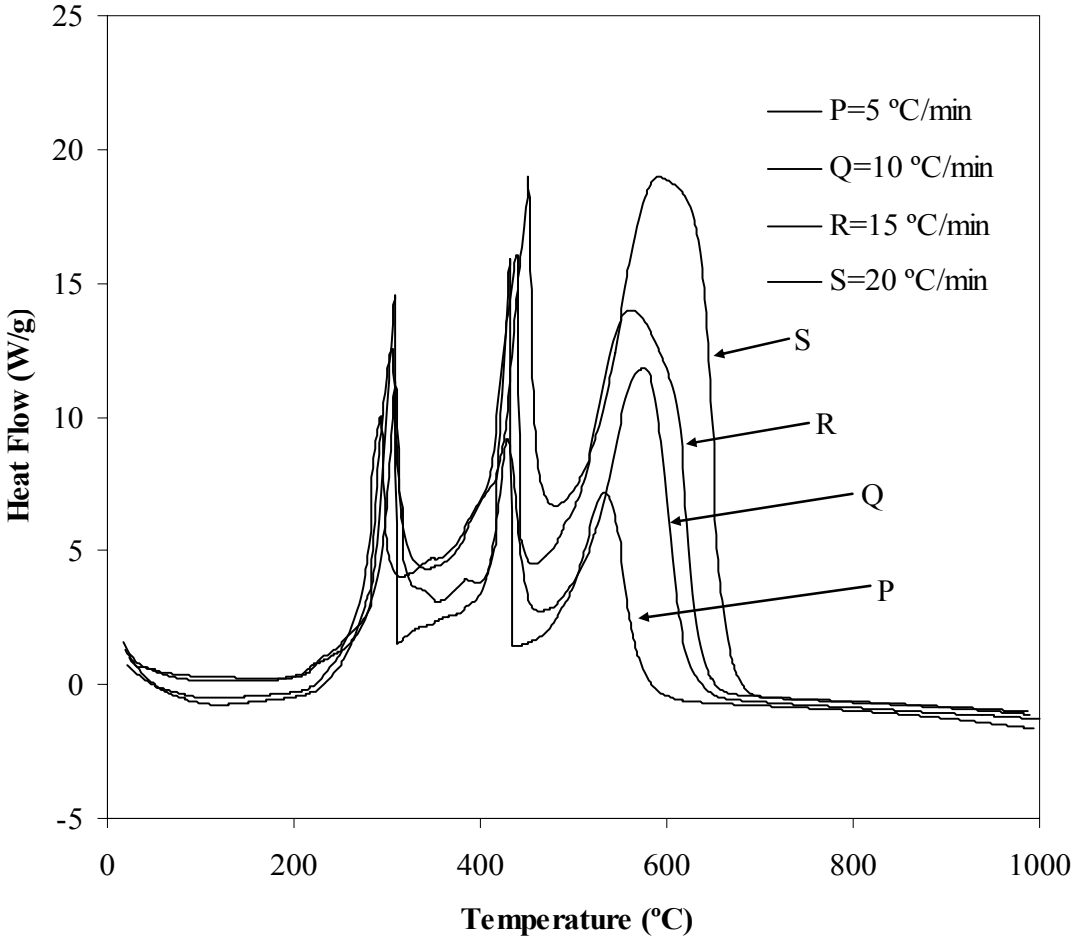

Figure 7.5 Differential heat flow to an as-synthesized CZY sample prepared using polymeric resin as the SDA upon being heated in air from near ambient temperatures to 1000 ºC, at heating rates that ranged from 1 to 20 °C/min.

Another striking feature of this sample is the occurrence of three upward peaks, which has not been observed in other samples previously. The locations of the peaks are as follows: between 250 and 350 ºC, between 400 and 500 ºC, and between 500 and 700 ºC. The DSC spectra show that heat is evolved during these processes because the peaks are upward. The first peak positions for polymeric resin templated CZY samples were found between 250 and 350 ºC irrespective of the heating rate. This temperature interval shows significant heat evolution processes are occurring instead of the endothermic process observed with the reference sample that contained no template. This phenomenon arises because the heat absorbed during the thermal decomposition of the nitrate salts is less than the heat released during the combustion of the polymeric resin template. The second and third upward peaks located at between 400 and 500 ºC, and between 500 and 700 ºC, respectively, suggest the combustion of higher molecular weight components of the polymeric resin. Amberlyst A26 OH polymeric resin is formed by cross linking styrene divinylbenzene copolymer containing quaternary ammonium groups. The peaks observed second and third peaks may correspond to the decomposition of the styrene and divinylbenzene blocks, respectively. Since we did not observe any the fusion of the metal salts while heat treating CZY made without an SDA even beyond the 600 to 1000 ºC , we conclude that the third peak was very unlikely a metal oxide fusion. Because the exiting gas flow from the DSC was not characterized, by methods such as IR or mass spectrometry, we were unable to definitively identify the nature of the exothermic degradation process occurring at higher sample temperatures (500 – 700 °C). On the other hand, were it to be fusion, it would have been an endothermic process and not an

exothermic process as indicated by the third upward peak. Another explanation could be that the magnitude of the heat released from the polymeric resin combustion process, because of the high template loading in these samples, very likely causes localized hot spots within the oxide samples.

For samples calcined at heating rates above 10 °C/min, these hot spots arising from template combustion are generated at much higher sample temperatures (up to 600 °C), which suggests that the local sample temperature can exceed the melting point of the oxide. This observation helps to explain why a significant loss in surface area was observed with polymeric resin templated samples that were calcined to 600 °C at a heating rate of 20 °C/min.

Table 7.2 showed the effects of varying heating rates during calcination on the surface area and pore diameter of a given polymeric resin templated CZY sample. This loss of surface area (~20% of its initial surface area) arising from increasing the calcination heating rates from 1 to 20 ºC/min is attributed to the sintering of the metal oxide particles at high temperatures and exacerbated by the hot spots created within the samples.

Table 7.2 Effect of calcination heating rate on the surface area and pore diameter of polymeric resin templated CZY samples that were calcined in air from 25 to 600 ºC with the final temperature being maintained for 4 h.

Heating rate (ºC/min)	BET Surface Area (m^2/g)[a]	BJH Pore Diameter (nm)[a]
1	98	3.4
20	78	3.4

a. The error margin for the surface area is ±5 m^2/g and for the pore diameter, ±1.0 nm

Figure 7.6 show the nitrogen adsorption/desorption isotherms and the BJH pore size distribution for polymeric resin templated CZY sample. The physisorption isotherm shows a two-step isotherm. The two hysteresis loops suggest a bimodal distribution of pore sizes for the polymeric resin templated CZY materials. The first and second loops correspond to the mesopore and macropore pore ranges in the CZY materials. These two pore size ranges can be attributed to the mechanism by which pores are generated during calcination. This will be elaborated upon in later discussion on proposed mechanistic pathway.

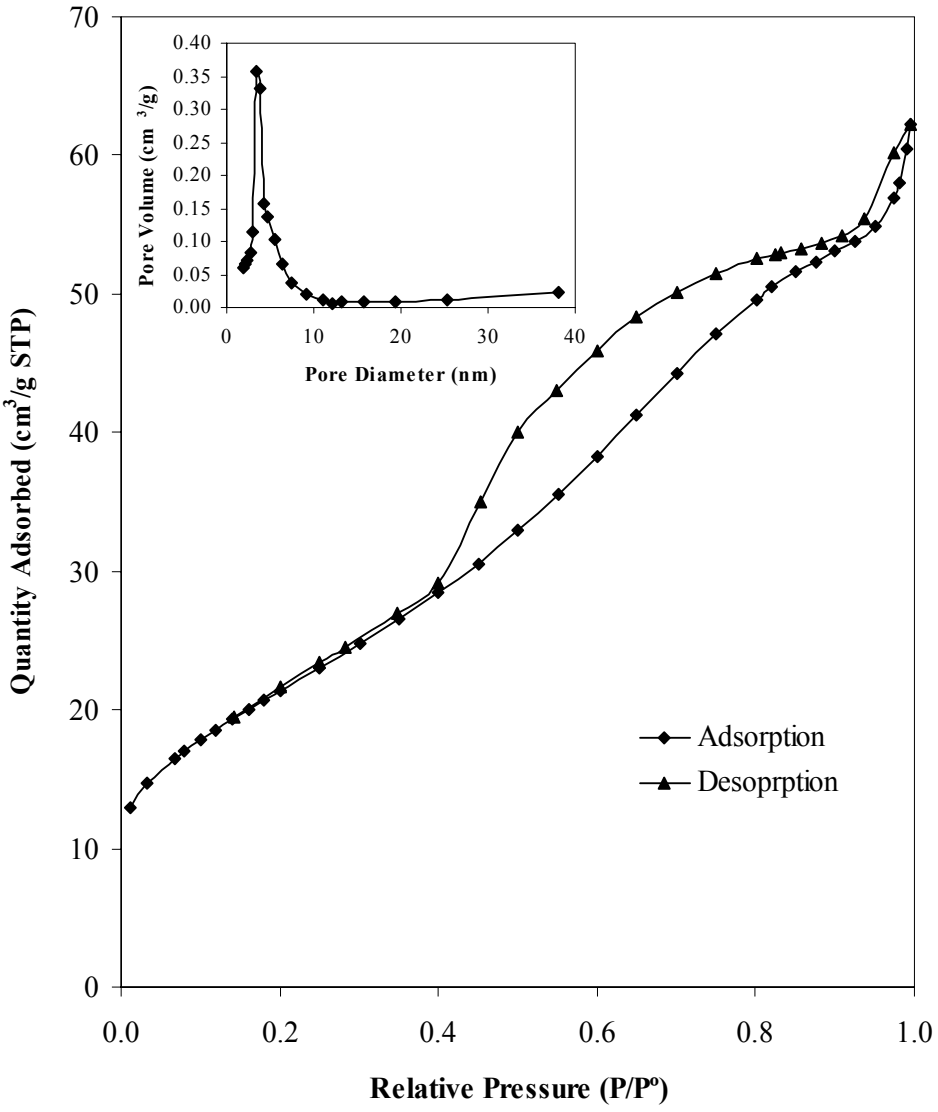

Figure 7.6 Nitrogen adsorption (■) /desorption (▲) isotherms and BJH pore size distribution (inset) for a calcined CZY sample prepared using polymeric resin template. The sample was calcined in air from 25 to 600 °C at a heating rate of 20 ºC /min, with the final temperature being maintained for 4 h.

The powder X-ray diffraction (PXD) patterns reveal slightly broad peaks which indicate the existence nanocrystallites. Figure 7.7 shows the PXD patterns of CZY synthesized using polymeric resin as the SDA at 2θ values ranging from 10 to 80º.

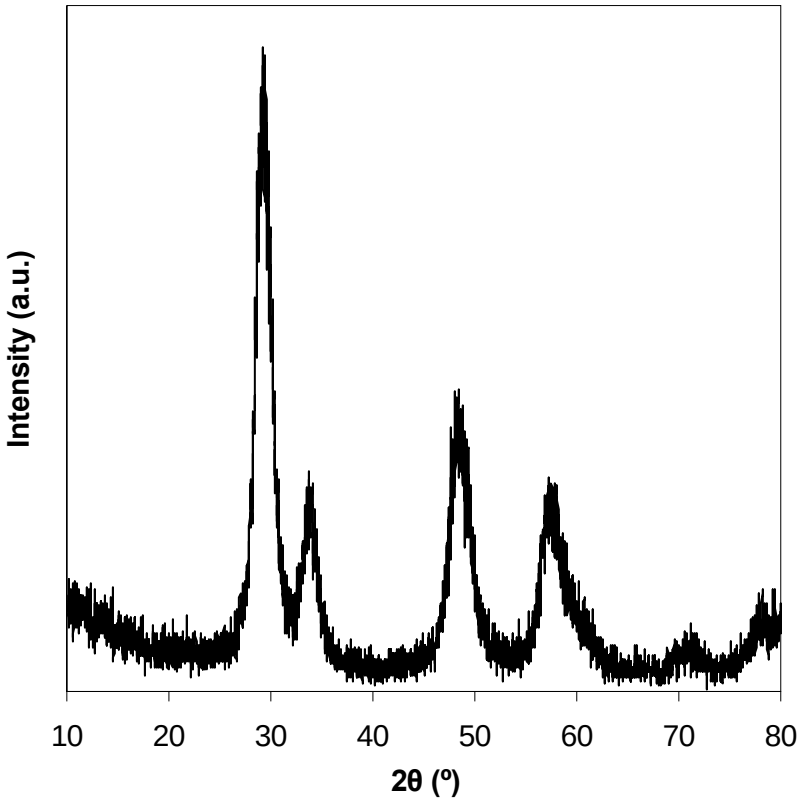

Figure 7.7 Powder X-ray diffractogram (PXD) for CZY synthesized using polymeric resin. Samples were calcined in air from 25 to 600 °C at a heating rate of 20 ºC/min, with the final temperature being maintained for 4 h.

The fact that PXD pattern of the polymeric resin templated CZY is very similar to the PXD pattern of pure ceria (see Figure 3.14) suggests that the CZY mixed oxides are arranged in the cubic fluorite structure. The lack of split peaks means that there are no phase segregation within the sample. Hence, the CZY sample is a homogeneous phase or

solid solution with no ceria or zirconia rich phase. However, the small angle X-ray diffraction (SAXD) pattern not shown for the same samples at 2θ values ranging from 1 to 10º do not reveal low angle peaks synonymous with ordered mesoporous MCM-41 materials. This suggests that the CZY material synthesized do not contain an ordered mesopore.

The results of our study on the level of metal oxide incorporation during polymeric resin templated CZY material synthesis are shown in Table 7.3.

Table 7.3 Elemental composition of polymeric resin templated CZY

Sample	ZrO_2 (mol %)[b]	$YO_{1.5}$ (mol %)[b]	CeO_2 (mol %)[b]
Theoretical Amount	45.00	5.00	50.00
CZY/polymeric resin	46.86	3.72	49.42

b. The error margin for the elemental composition is ±2.0 mol%

Table 7.3 shows the composition of metal oxides in the CZY synthesized using polymeric resin as SDA. These results reveal that all the metal oxides are well incorporated into the CZY materials. They are well within the margin of error for the theoretically expected molar percentages.

Thermal degradation or accelerated aging studies of polymeric resin templated CZY materials were carried out between 700 and 1000 ºC. Table 7.4 shows the variation of the physical properties of polymeric resin templated CZY on calcination temperature. The overall loss in surface area from 700 to 1000 ºC was approximately 74.4%. The loss of surface area is due mainly to sintering CZY mixed oxides. The increase in the pore

size is completely as expected because of the inverse relationship that exists between pore size and specific surface area.

Table 7.4 Variation of surface area and pore volume as a function of aging temperature for polymeric resin templated CZY samples. Samples were calcined in air to the specified temperature at a heating rate of 20 ºC/min, with the final temperature being maintained for 4 h.

Aging Temperature (ºC)	BET Surface Area (m^2/g)[c]	BJH Pore Diameter (nm)[c]
700	39	60.0
800	25	51.9
900	16	51.7
1000	10	73.0

c. The error margin for the surface area is ±5 m^2/g and for the pore diameter, ±1.0 nm

The results of thermal ageing of the CZY samples after calcining from 700 to 1000 ºC for 4 hr are shown in Figure 7.8. The powder XRD spectra are quite similar during each ageing temperature but at higher temperatures the peaks become sharper indicating that the CZY samples become more crystalline at higher temperature. The primary peak at the ~29º peak position show a peak split for all the spectra. This peak split was not observed in Figure 7.7. Hence, we can attribute the splitting of the primary peak to be solely due to the aging at higher temperatures. This means that at higher temperatures the zirconia rich phase becomes segregated from ceria rich phase.

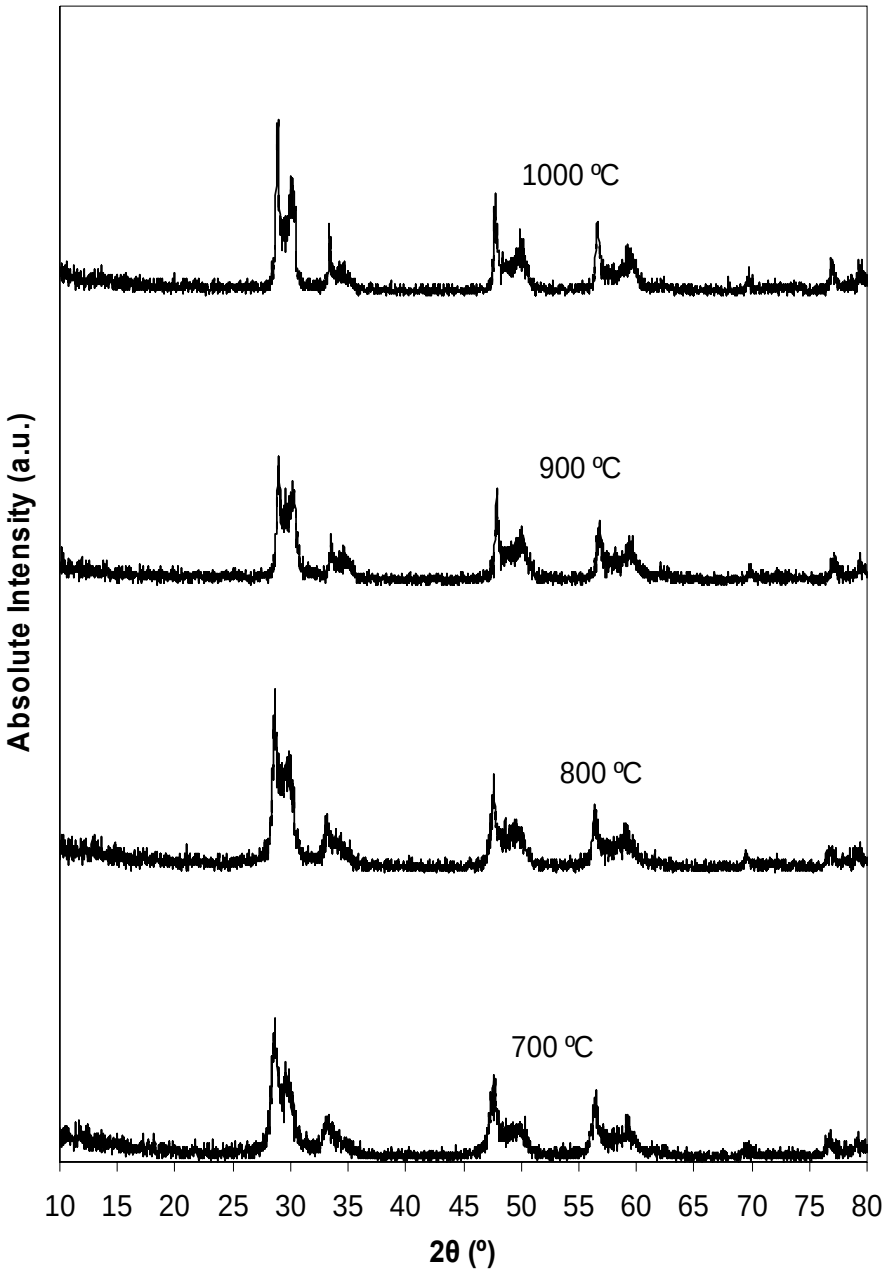

Figure 7.8**:** Powder X-ray diffractogram (PXD) for polymeric resin templated CZY samples. Samples were calcined in air to the specified temperature at a heating rate of 20 ºC/min, with the final temperature being maintained for 4 h.

Figure 7.9 shows TEM images of CZY materials synthesized using polymeric resin template. The CZY samples are nanosized crystals that are appear to be glued together.

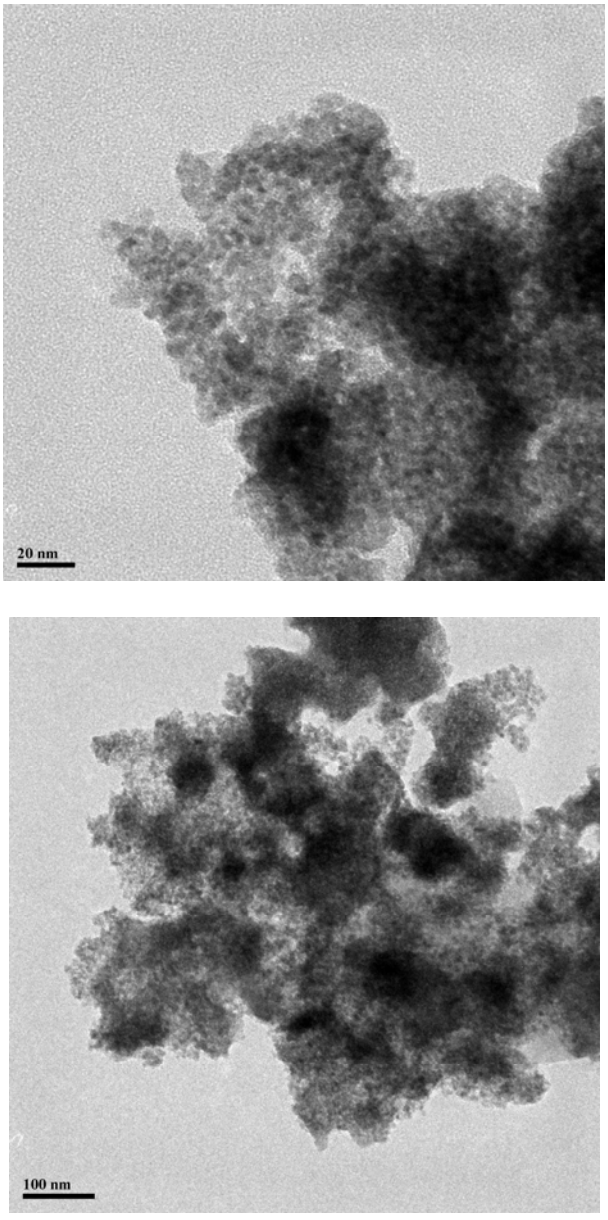

Figure 7.9 Transmission electron micrographs of a calcined CZY mixed oxide prepared using polymeric resin template. Samples were calcined in air from 25 to 600 °C at a heating rate of 20 ºC/min, with the final temperature being maintained for 4 h.

The TEM images do not reveal phase segregation but rather that the samples are homogenous. The particle size of the primary particles is between 5 and 8 nm in size. The bulk material is an agglomeration of these primary particles like all the other CZY samples that I have discussed previously thus far. The TEM images, powder XRD patterns, and the nitrogen adsorption-desorption isotherms all help to explain the mechanistic pathway for this process. Figure 7.10 shows the proposed mechanistic pathway for pore generation in polymeric resin templated CZY mixed oxides.

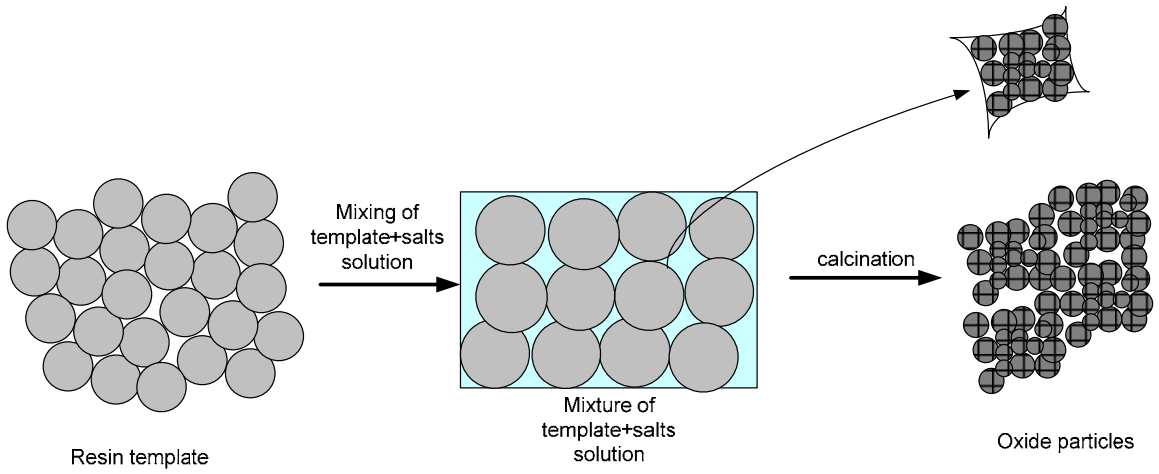

Figure 7.10 Mechanistic pathway for pore generation within polymeric resin templated mesoporous CZY mixed oxides.

During the synthesis procedures, it was noted that the slurry containing the polymeric resin and the precursor solution was calcined. Based on this, the above mechanistic pathway was proposed. It is suggested that during calcination, the CZY mixed oxides are forced to crystallize in the interstices between the resins. Close to the resin, large sized crystal can grow because of surface tension effects while far away from the resin surface smaller sized crystal grow. The combination of small and large sized crystals explains

why the nitrogen isotherms are divided into two-steps. The large and small sized crystals both correspond to the macropore and the mesopore end of the pore size range.

Conclusion

In this chapter I have outlined the synthesis steps for making mesoporous CZY materials using polymeric resin as the structure directing agent. The synthesized CZY material was characterized to ascertain the existence of mesoporous structure, determine homogeneity of the phase, the elemental composition, the effect of heating rate during calcination, and the morphology of the material. The results from the various characterization methods suggest that the synthesized polymeric resin templated CZY mixed oxides contained some mesopores. The physisorption isotherm indicates the existence of double hysteresis loops suggesting a bimodal pore diameter. This is corroborated by the results from the BJH pore size distribution plots for the sample. Interestingly, the CZY samples prepared using polymeric resin template showed the least loss in surface area during thermal aging. The effect of changing the heating rate during the calcination step, once again reiterates the importance of devising a calcination protocol that would preserve the structural integrity of the synthesized materials.

CHAPTER EIGHT

EVALUATION OF THE CATALYTIC PERFORMANCE OF THE CZY SAMPLES

In the preceding chapters, I have looked at the various ways in which mesoporous CZY materials can be synthesized. I specifically looked at the surfactant, block copolymer, dendrimer, activated carbon, and polymeric resin templating techniques. In this chapter, my goal is the evaluation of the catalytic performance of the mesoporous CZY materials that have been synthesized using the various techniques mentioned previously. Though there are several catalytic applications for mesoporous CZY materials, e.g., CO partial oxidation catalysis, fuel cell applications, etc., the focus of this work is on the development of catalytic converter catalysts; thus, I focused on reactions for emission abatement control as applied to three–way catalytic converters.

Many automobile manufacturers now use CZY as a support material in three way catalytic converters, which are used for the control and abatement of emissions generated by combustion engines in cars and trucks. The three oxide components each have a unique purpose, some of which are not catalytic. Specifically, the high oxygen storage capacity (OSC) associated with ceria[16,22,112-114] allows the engine to alternate between fuel rich and lean conditions and still enable the complete combustion of hydrocarbons and CO in the exhaust. Yttria is known to help stabilize the precious metals deposited on the oxide surface (in this case platinum, rhodium, and palladium) by preventing the agglomeration/sintering of the precious metals at elevated temperatures. Yttria is also known to help stabilize grain boundaries in mixed oxide systems, which helps to reduce the loss of catalytic surface area during thermal cycling. Finally, zirconia is known to

provide thermal stability to the catalytic system that makes up the three way catalytic converter devices, i.e., it inhibits oxide sintering and crystal growth phenomena that increase the size of oxide particles that reduce catalytic surface area.

The three-way catalytic converter is designed to depollute the exhaust from cars by the following processes: reduce NO_x species as well as oxidize CO and unburned hydrocarbons, which are also called volatile organic compounds (VOCs). The noble metal components that make up the three-way catalytic converter are: platinum, rhodium, and palladium. Platinum and palladium are both very good reduction-oxidation (redox) catalysts, while rhodium is an oxidation catalyst with high selectivity for CO oxidation. The reactions catalyzed by the active components of the catalyst are shown below:

$$2CO + O_2 \rightarrow 2CO_2 \text{ (oxidation)} \quad (8.1)$$

$$2C_xH_y + (2x+y/2)O_2 \rightarrow 2xCO_2 + yH_2O \text{ (oxidation)} \quad (8.2)$$

$$2NO_x \rightarrow N_2 + xO_2 \text{ (reduction)} \quad (8.3)$$

I evaluated the catalytic performance of the various CZY samples by two simple methods. The first method involves the determination of the catalytic activity or light-off temperature of all the reactant species (CO, C_xH_y, and NO_x) that participate in the redox reactions listed above. The light-off temperature T_{50} is the temperature at which 50% conversion of the reactant species occurs; it is a measure of the catalytic performance of the precious metal loaded CZY materials. Figure 8.1 shows a representative plot of conversion versus temperature from which T_{50} can be measured.

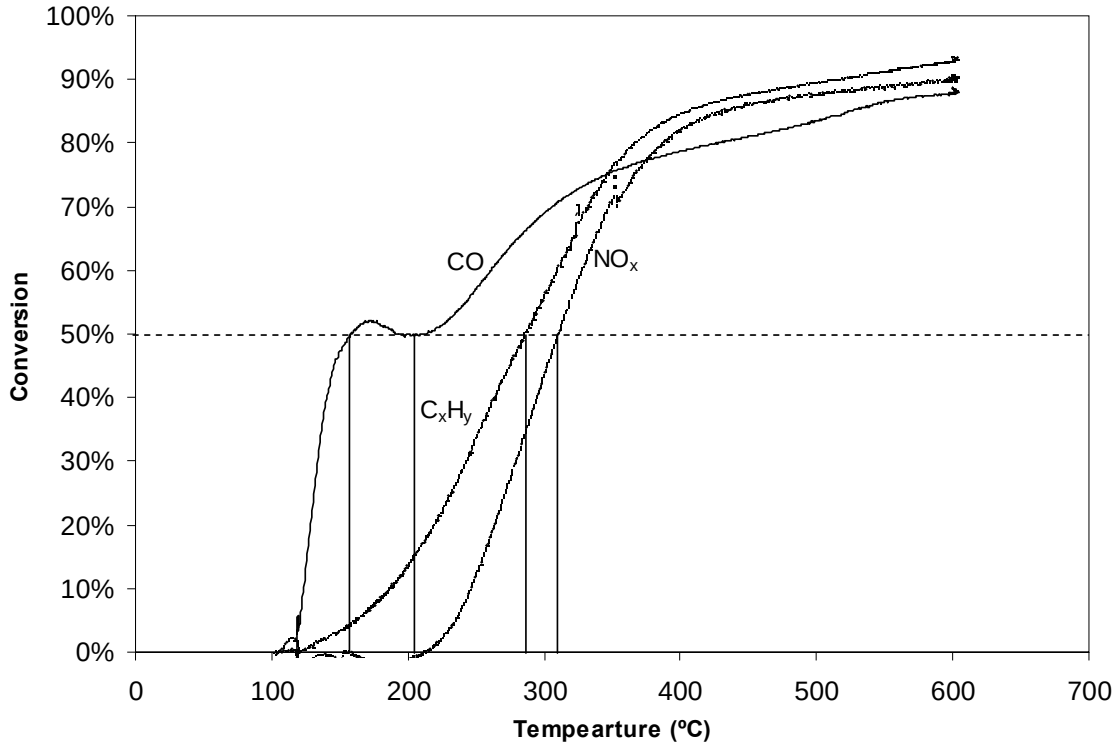

Figure 8.1 Plot of conversion versus temperature for NO_x, C_xH_y, and CO reactant species.

The second method examined the loss of surface area during thermal aging for each CZY sample. These two tests address the critical aspects of ongoing efforts focused on reducing noble metal loadings on three way catalyst and extending their active life. All catalytic testing was carried out at the Toyota Motor Engineering Research Center in Michigan and the thermal aging studies were carried out in laboratories at Clemson.

Methods for Catalytic Performance Evaluation

Catalyst Preparation Steps

To prepare the CZY materials for catalytic testing, a number of pretreatment processes were performed. First, the mesoporous CZY oxide samples were crushed and sieved to a

specified size range. Then they were loaded with precious metal salts using the incipient wetness method, so as to achieve a 1 wt% loading of Pt on the final calcined catalyst (no Rh or Pd were used for these studies). The precious metal loaded CZY samples are later pelletized (without the use of any organic or inorganic binder) and the subsequently calcined at 800 ºC for 2 h so that the precious metal loaded CZY materials can simulate actual catalyst. Lastly, the precious metal loaded CZY samples are placed in a continuous flow fixed bed reactor that acts as the three-way catalytic converter. The precursors of the precious metal groups and their composition cannot be disclosed because of propriety reasons. For the second part of the experiment, I took the CZY samples synthesized that I have synthesized using the different templating techniques and weighed out a small quantity (~2 g) of each in a crucible and calcined the CZY materials in air in the oven using the procedure given in chapter 3. Only this time, the final temperature was between 700 and 1000 ºC.

Emissions Abatement Reaction Studies

Catalytic activity studies were conducted in a plug flow reactor using 3 grams of the selected CZY oxide that had been doped with 1 wt% Pt. The feed to the reactor entered at a total flow rate of 30 L/min (roughly 600,000 hr^{-1} space velocity) and contained 0.21% O_2, 1200 ppm CO, 500 ppm C_3H_6, 1500 ppm NO, 15 vol% CO_2, 10 vol% water, and the balance N_2, which simulated the composition of the engine exhaust leaving a typical Toyota vehicle. The catalyst was then exposed to a linear temperature ramp, and the exhaust gas composition measured, so as to determine the conversion

achieved for Reactions 8.1–8.3 at each reaction temperature. For these studies, it was assumed that negligible catalyst deactivation occurred during the study.

Thermal Aging Studies

For the accelerated aging studies, I calcined the various CZY samples that were previously prepared using different templating techniques at the following temperatures: 700, 800, 900, and 1000 ºC in air. The furnace temperature was increased at the rate of 20 ºC/min from 25 °C to the specified final temperature, which was maintained for 4 hrs.

Results and Discussion

The data shown in Figures 8.2 are the temperatures at which each gas reaches 50% conversion for each platinum loaded CZY material that has been synthesized using the various templates after having been calcined in air at 800 ºC. An equivalent mass (~3 g) of each catalyst was used for this study. Figure 8.2 shows the NO_x light-off temperatures for the polymeric resin, activated carbon, CTAB, dendrimer, and P123 templated CZY materials after each has been loaded with 1 wt% Pt using a proprietary mixture of metal salts. The lowest light-off temperatures were measured for the dendrimer and pluronic P123 templated CZY. Both have a T_{50} value of 317 ºC. Next is the resin templated CZY sample, followed by the CZY material templated with activated carbon, and lastly a CTAB templated CZY sample.

A comparison of the hydrocarbon (C_xH_y) light-off temperature showed that the highest catalytic activity was observed with the dendrimer templated CZY sample with a T_{50} value of 304 ºC. It is closely followed by the P123 templated CZY sample with a T_{50}

of 306 ºC. The three remaining catalysts were all catalytically active, but exhibited lower levels of activity. Specifically, reaction rates were lower for the resin templated, CTAB templated, and activated carbon templated CZY materials, in decreasing order of activity.

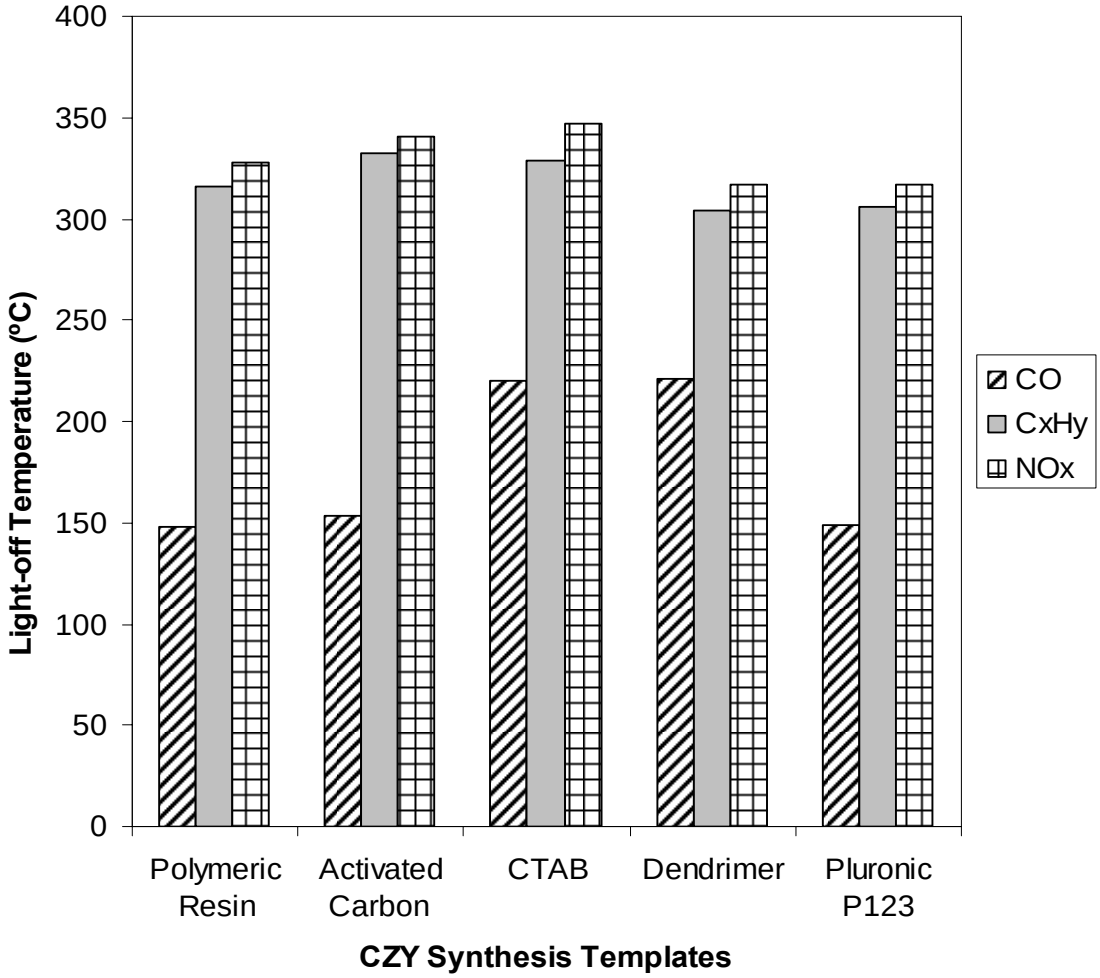

Figure 8.2 NO_x, C_xH_y, CO light-off temperatures for different templated CZY materials after aging in air at 800 ºC.

The CO light-off temperature for Reaction 8.1 showed that the catalyst with the highest activity was the resin templated CZY sample with a T_{50} value of 148 ºC. It was closely followed by P123 templated CZY with a T_{50} of 149 ºC. Next is activated carbon

templated CZY with 153 ºC, followed by CTAB templated CZY, and lastly we have dendrimer templated CZY.A comparison of the T_{50} catalytic results reveals that the most active catalysts, in decreasing order of activity, are the P123 templated, dendrimer templated, and resin templated CZY materials.

Figure 8.3 shows the plot of light-off temperature T_{50} versus surface area.

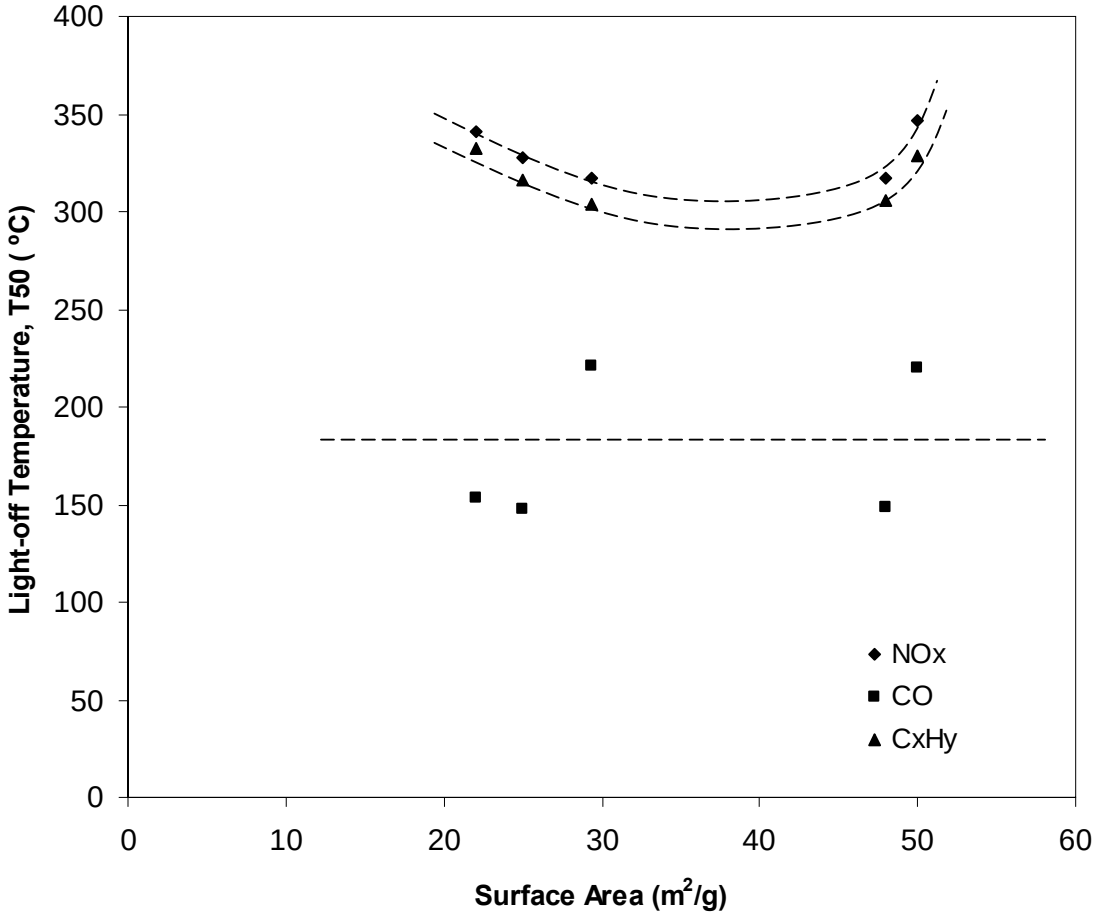

Figure 8.3 Correlation between light-off temperature, T_{50} (catalytic activity) and surface area of CZY catalyst support system.

Figure and 8.4 shows the plot of light-off temperature T_{50} versus pore size for the CZY catalyst support materials, respectively. These figures reveal interesting correlations

among the T_{50} light-off temperatures, the pore size and surface area the CZY catalyst support materials. For both the NOx and CxHy species, the light-off temperatures seems to gradually decrease with increasing pore size and later increases gradually at the other tail end of the graph with a minimum occurring somewhere in the middle. This trend between light-off temperature and surface area suggests that the optimum surface area for the CZY system lies between 30 and 50 m^2/g. However, there was no trend between the light-off temperature of CO and the surface area of the CZY support system.

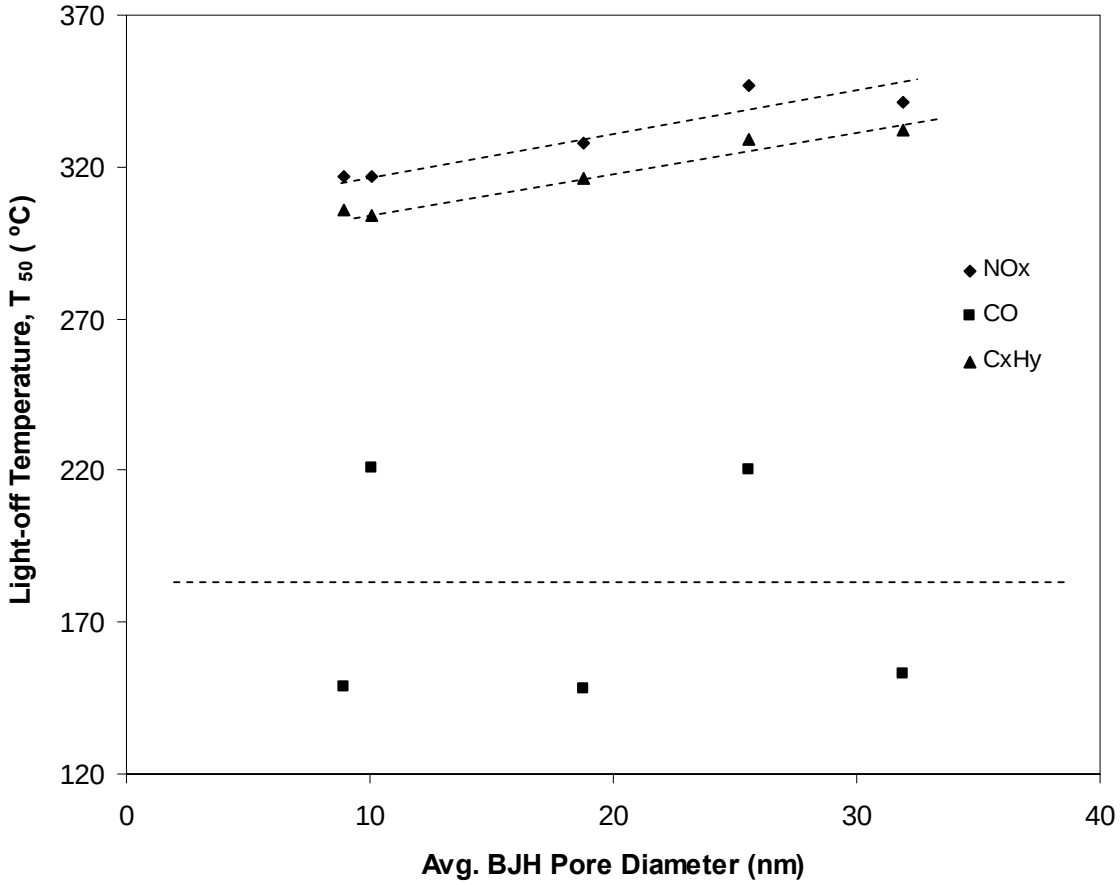

Figure 8.4 Correlation between light-off temperature, T_{50} (catalytic activity) and pore size of CZY catalyst support system.

Figure 8.4 shows a somewhat different correlation between the light-off temperatures of NOx and CxHy and the pore size of the CZY catalyst support system. There appears to be a linear correlation pore size and light-off temperatures for these two reacting species- NOx and CxHy. This suggests that as the pore size gets larger the precious loaded Pt has greater dispersion. The lack of correlation between the light-off temperature for CO and pore size is still not understood. The above correlations between light-off temperature and pore size and between light-off temperature and surface area provide some insight into the catalytic activity of the CZY support system.

The results of the thermal aging studies reveal that each sample of CZY, whatever the choice of template, underwent significant loss of surface area when calcined at temperatures above 600 °C. Table 8.1 shows the BET surface area and average BJH pore diameter for samples that were calcined from 700 to 1000 ºC for 4 h in air using a heating rate of approximately 20 ºC/min. The overall percentage loss in CZY surface area as the calcination temperature was increased was as follows: CTAB templated CZY material lost 79.4%, P123 templated CZY material 87.8%, DAB-Am-32 templated CZY material 82.7%, activated carbon templated CZY material 86.5%, and resin templated CZY material 74.4%. Based on these results, it is apparent that the resin templated CZY material has the greatest resistance to oxide sintering and pore collapse.

Table 8.1 Effect of thermal aging on the BET surface area and average BJH pore diameter of CZY samples synthesized from various templates. Samples were calcined in air to the specified temperature at a heating rate of 20 ºC/min, with the final temperature being maintained for 4 h.

	BET surface area, m^2/g (average BJH pore diameter, nm)[a]				
Aging Temperature (ºC)	CTAB	P123	DAB-Am-32	Activated Carbon	Polymeric resin
700	63 (7.5)	76 (6.0)	42.7 (3.5, 6.0)	52 (18.0)	39 (3.7,60.0)
800	50 (11.0)	48 (9.0)	29.3 (10.0)	22 (30.0)	25 (3.7, 51.9)
900	30 (15.2)	28 (12.8)	13.0 (18.0)	13 (49.0)	16 (3.7, 51.7)
1000	13 (23.3)	9.3 (24.0)	7.4 (30.0)	7 (70.0)	10 (73.0)

a. The error margin for the surface area is ±5 m^2/g and for the pore diameter, ±2.0 nm

The relationship between the pore size and surface area with temperatures are shown in Figures 8.5 and 8.6. Figure 8.5 shows that as aging temperature increases the pore size of the CZY materials also increases. However, Figure 8.6 showed that the surface area decreased as the aging temperature was increased. Both phenomena are due to metal oxide sintering. Figures 8.7-8.16 show both the nitrogen adsorption-desorption isotherms and the BJH desorption pore size distribution of the templated CZY materials as a function of calcination temperature.

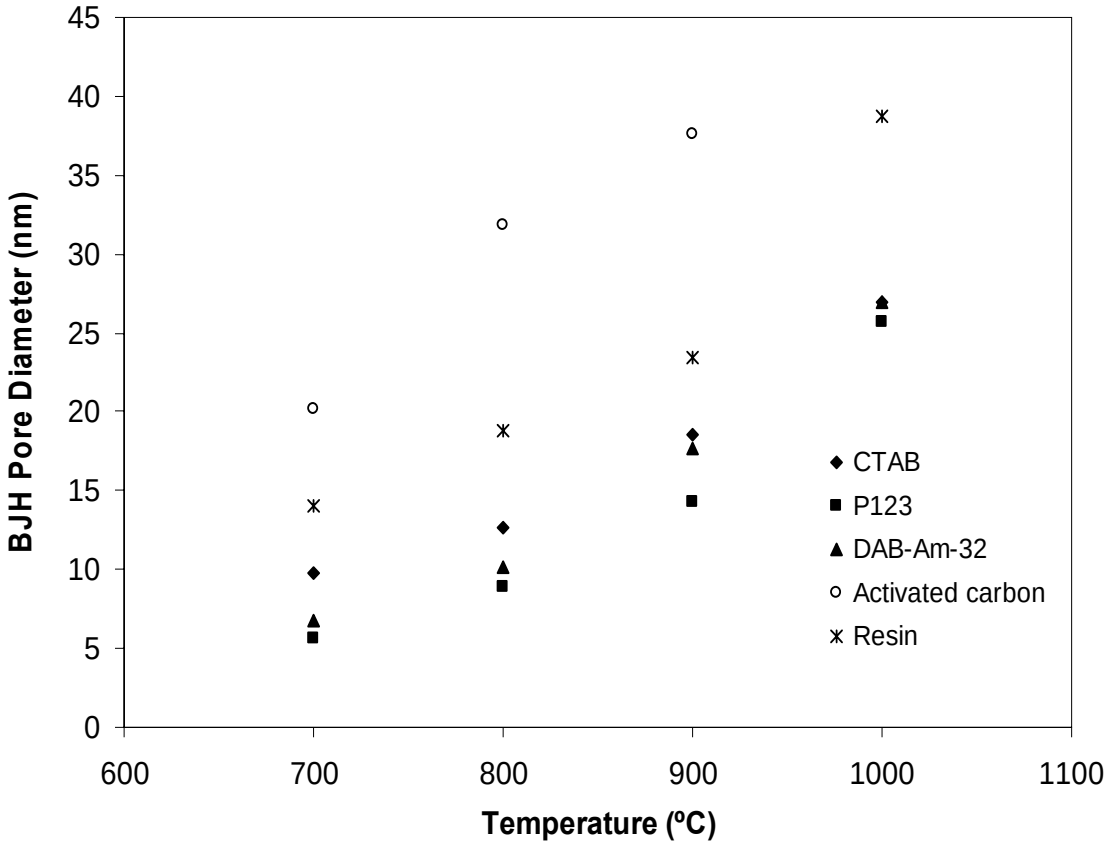

Figure 8.5 Pore size variation with aging temperatures for CZY mixed oxides.

These plots provide unique insight into the effect of aging on the properties of the CZY materials generally. Both the physisorption isotherms and the BJH desorption pore size distribution show a gradual decrease in mesoporosity with a corresponding increase in macroporosity as the CZY materials are calcined at higher temperatures.

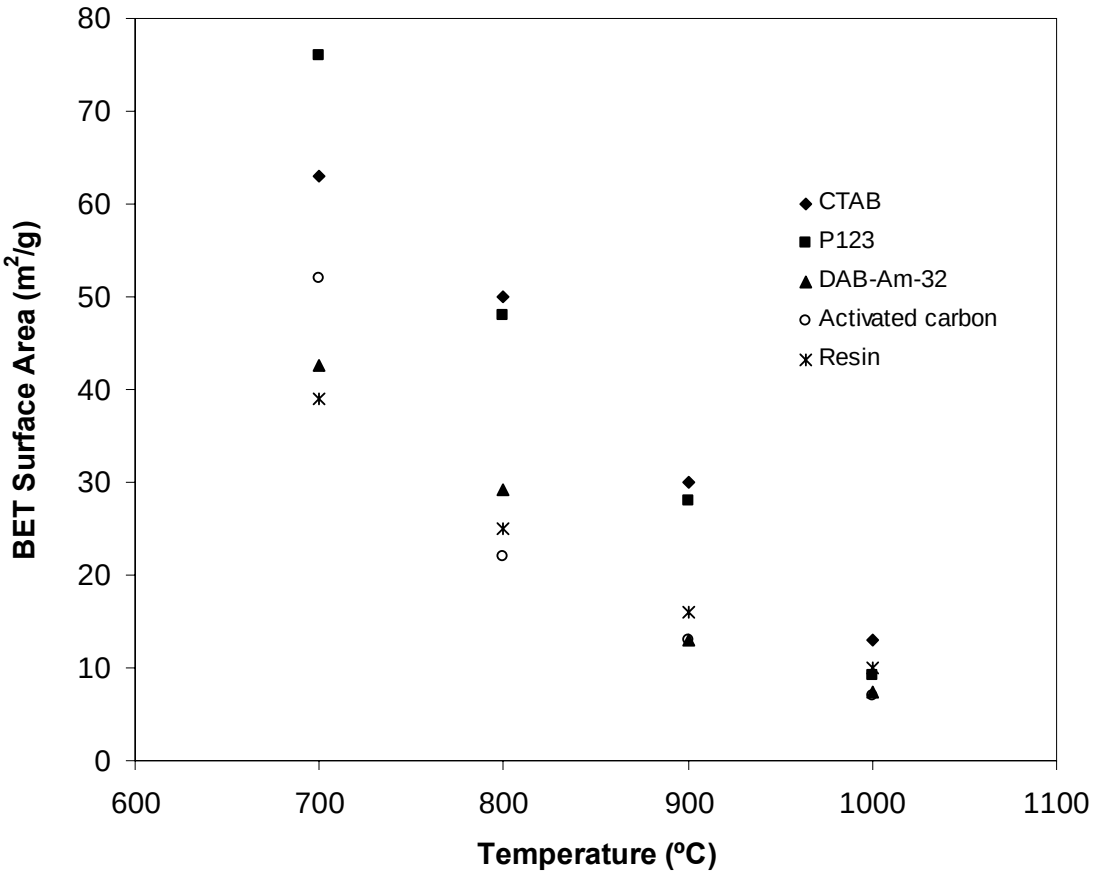

Figure 8.6 Surface area variation with aging temperatures for CZY mixed oxides.

With the nitrogen adsorption-desorption isotherms, the total quantity of nitrogen gas adsorbed decreased as the aging temperature was raised. The mean pore size as shown in the pore size distribution plots was gradually displaced to the right signifying the growth of larger sized crystals due to sintering effects mainly.

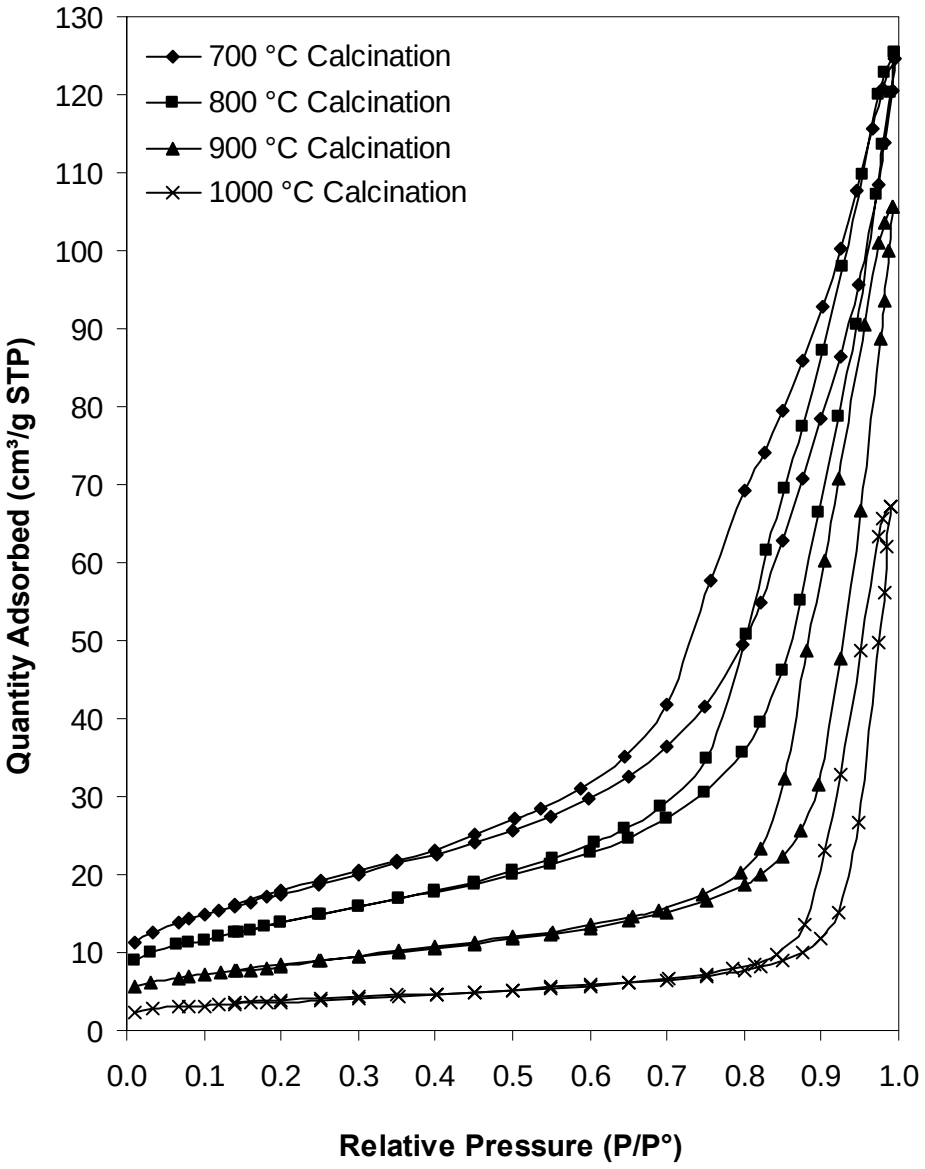

Figure 8.7 Nitrogen adsorption-desorption isotherms of CTAB templated CZY mixed oxides during thermal aging. Samples were aged in air to the specified temperature at a heating rate of 20 ºC/min, with the final temperature being maintained for 4 h.

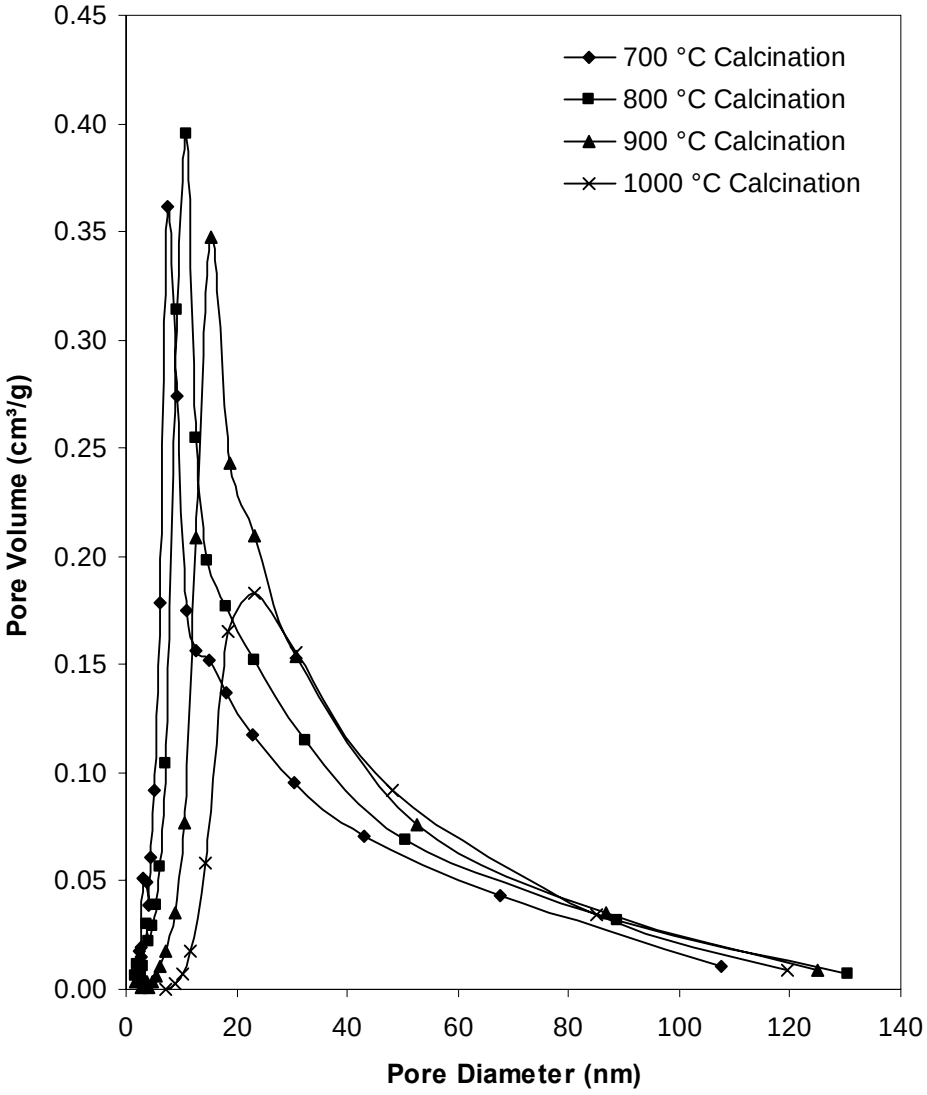

Figure 8.8 BJH pore size distribution of CTAB templated CZY mixed oxides during thermal aging. Samples were aged in air to the specified temperature at a heating rate of 20 ºC/min, with the final temperature being maintained for 4 h.

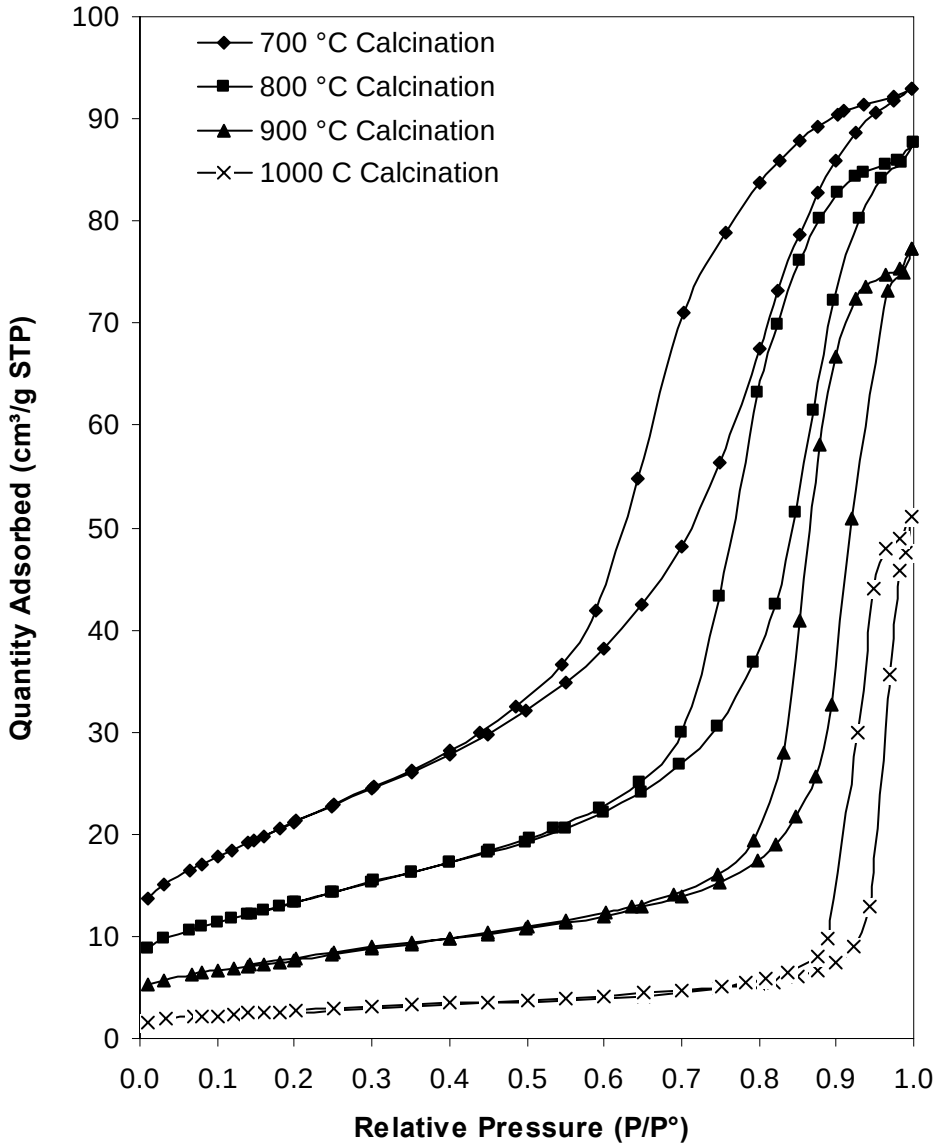

Figure 8.9 Nitrogen adsorption-desorption isotherms of Pluronic P123 templated CZY mixed oxides during thermal aging. Samples were aged in air to the specified temperature at a heating rate of 20 ºC/min, with the final temperature being maintained for 4 h.

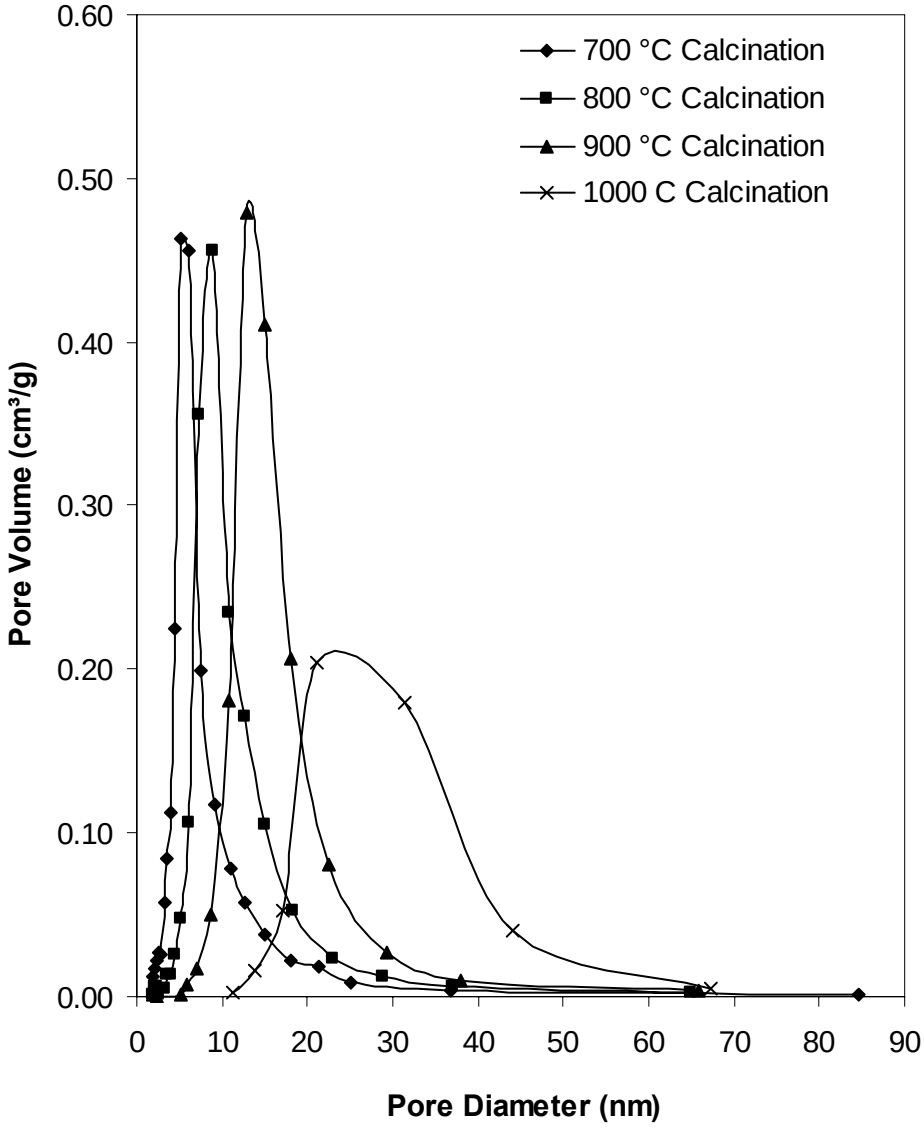

Figure 8.10 BJH pore size distribution of Pluronic P123 templated CZY mixed oxides during thermal aging. Samples were aged in air to the specified temperature at a heating rate of 20 ºC/min, with the final temperature being maintained for 4 h.

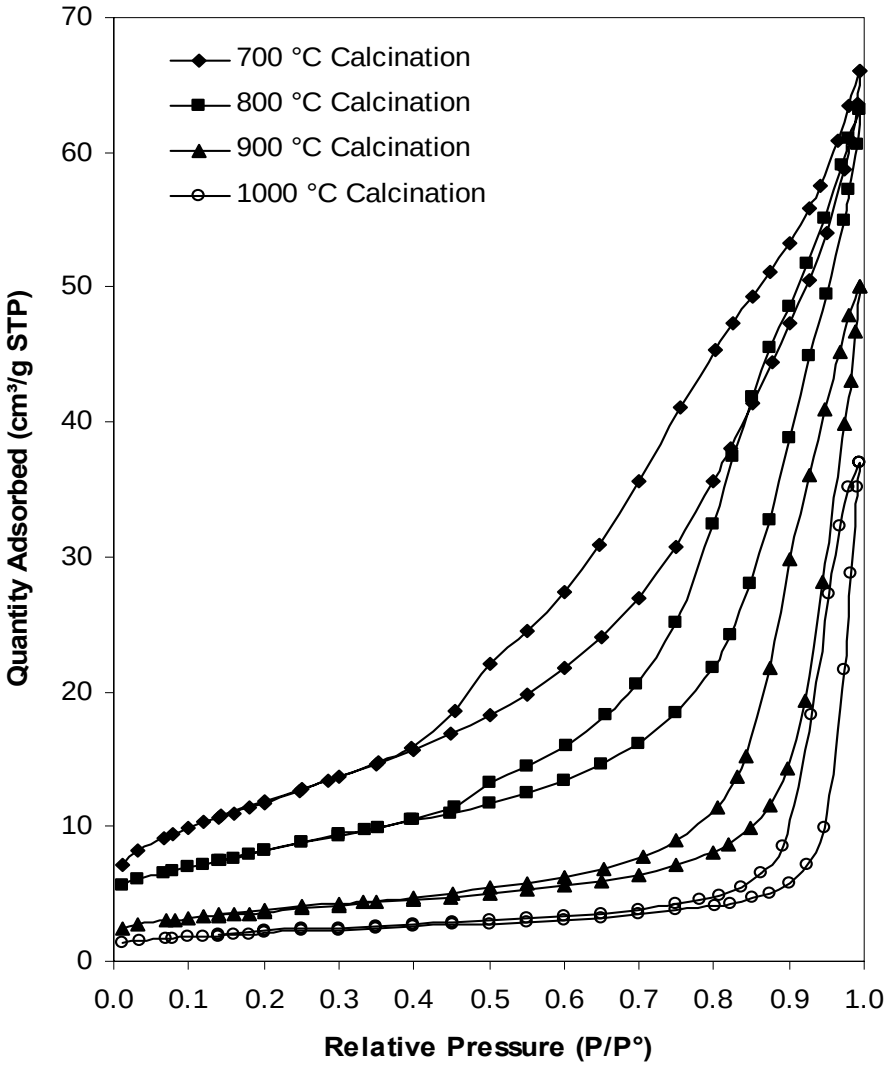

Figure 8.11 Nitrogen adsorption-desorption isotherms of DAB-Am-32 templated CZY mixed oxides during thermal aging. Samples were aged in air to the specified temperature at a heating rate of 20 ºC/min, with the final temperature being maintained for 4 h.

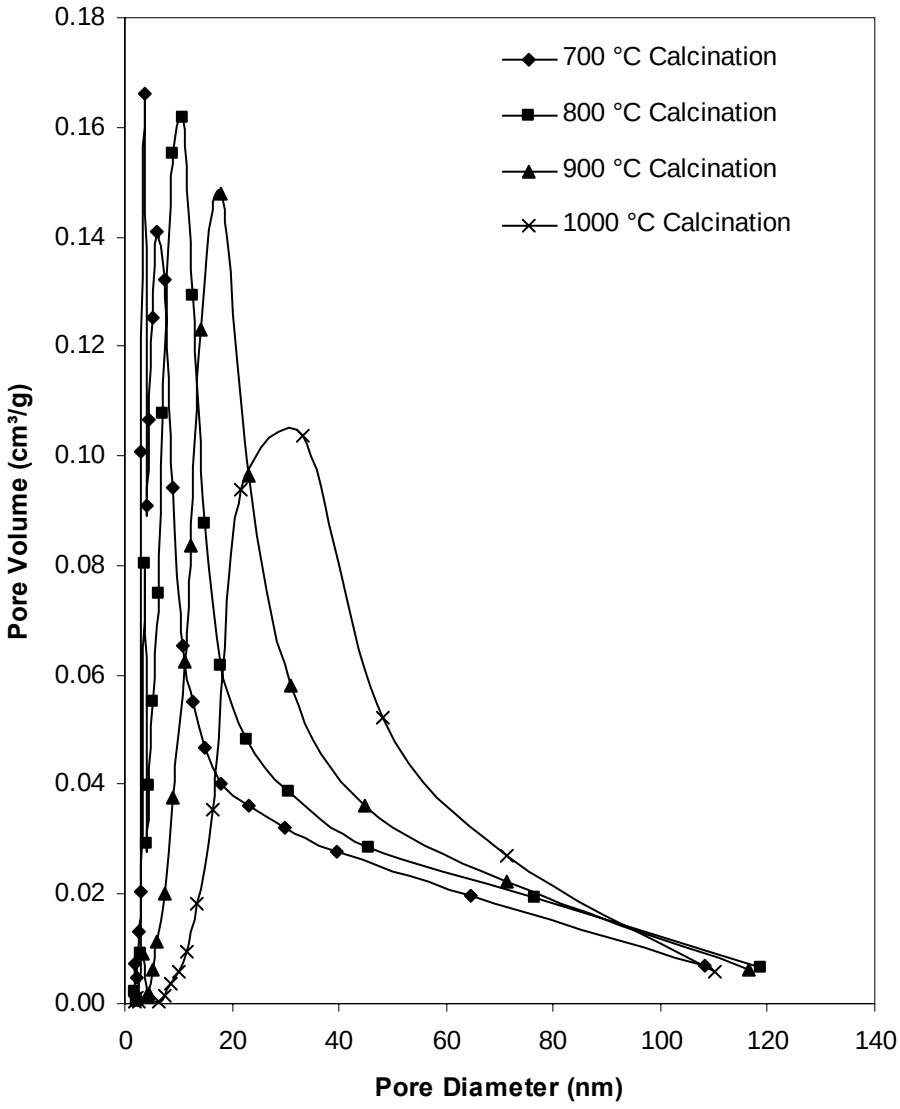

Figure 8.12 BJH pore size distribution of DAB-Am-32 templated CZY mixed oxides during thermal aging. Samples were aged in air to the specified temperature at a heating rate of 20 ºC/min, with the final temperature being maintained for 4 h.

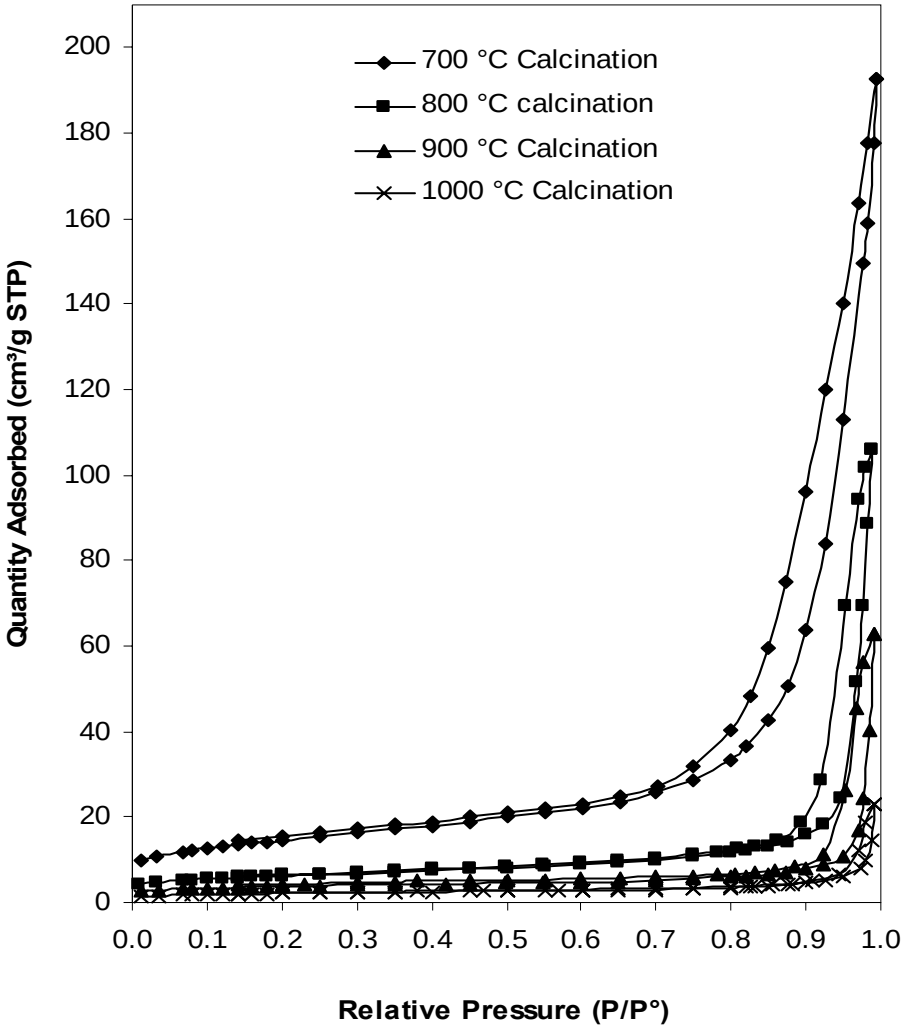

Figure 8.13 Nitrogen adsorption-desorption isotherms of activated carbon templated CZY mixed oxides during thermal aging. Samples were aged in air to the specified temperature at a heating rate of 20 ºC/min, with the final temperature being maintained for 4 h.

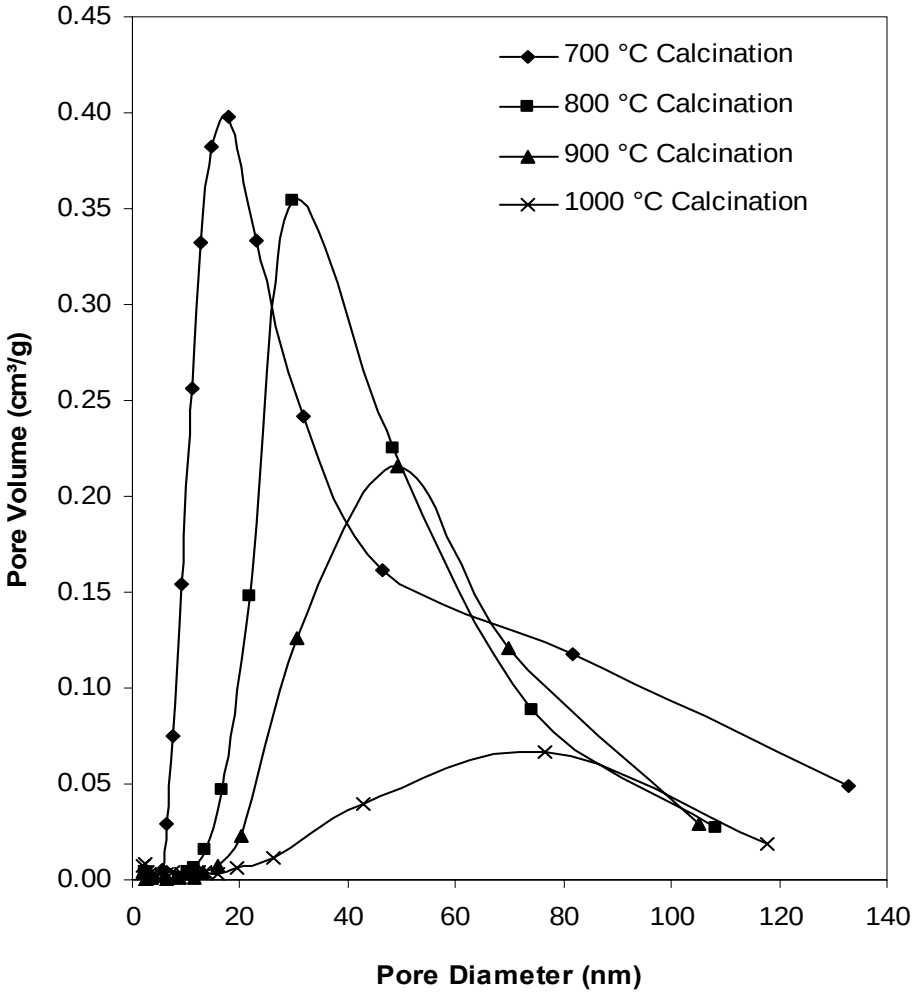

Figure 8.14 BJH pore size distribution of activated carbon templated CZY mixed oxides during thermal aging. Samples were aged in air to the specified temperature at a heating rate of 20 ºC/min, with the final temperature being maintained for 4 h.

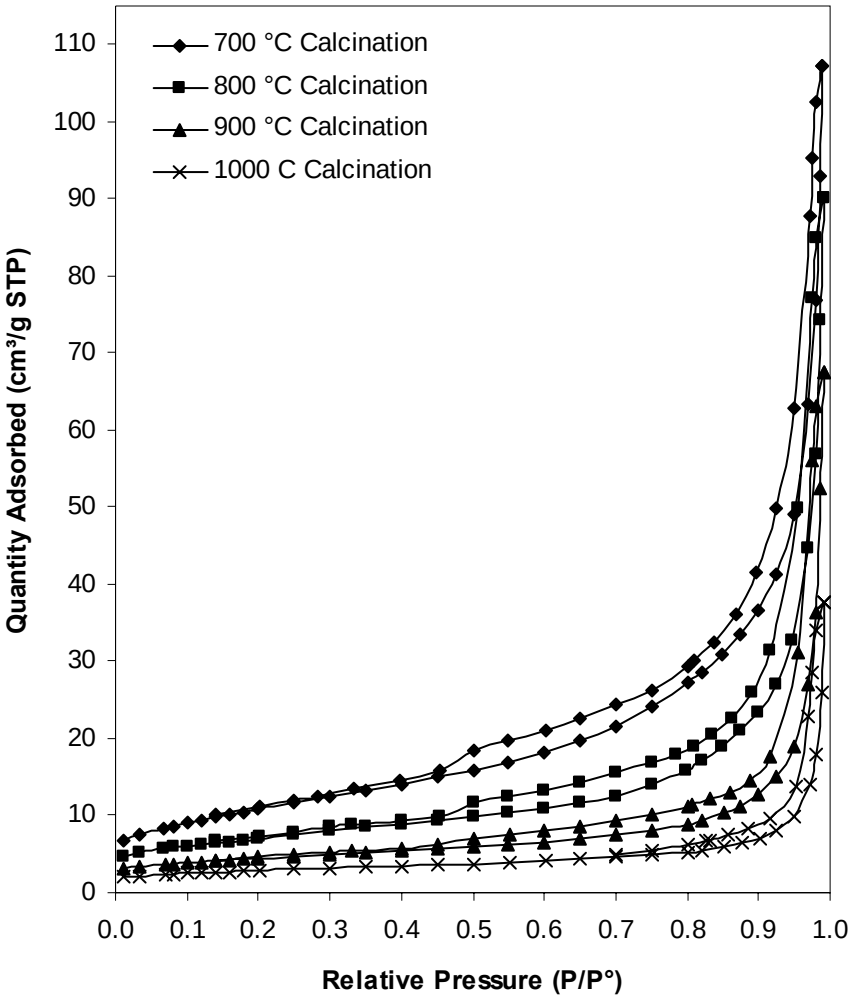

Figure 8.15 Nitrogen adsorption-desorption isotherms of polymeric resin templated CZY mixed oxides during thermal aging. Samples were aged in air to the specified temperature at a heating rate of 20 ºC/min, with the final temperature being maintained for 4 h.

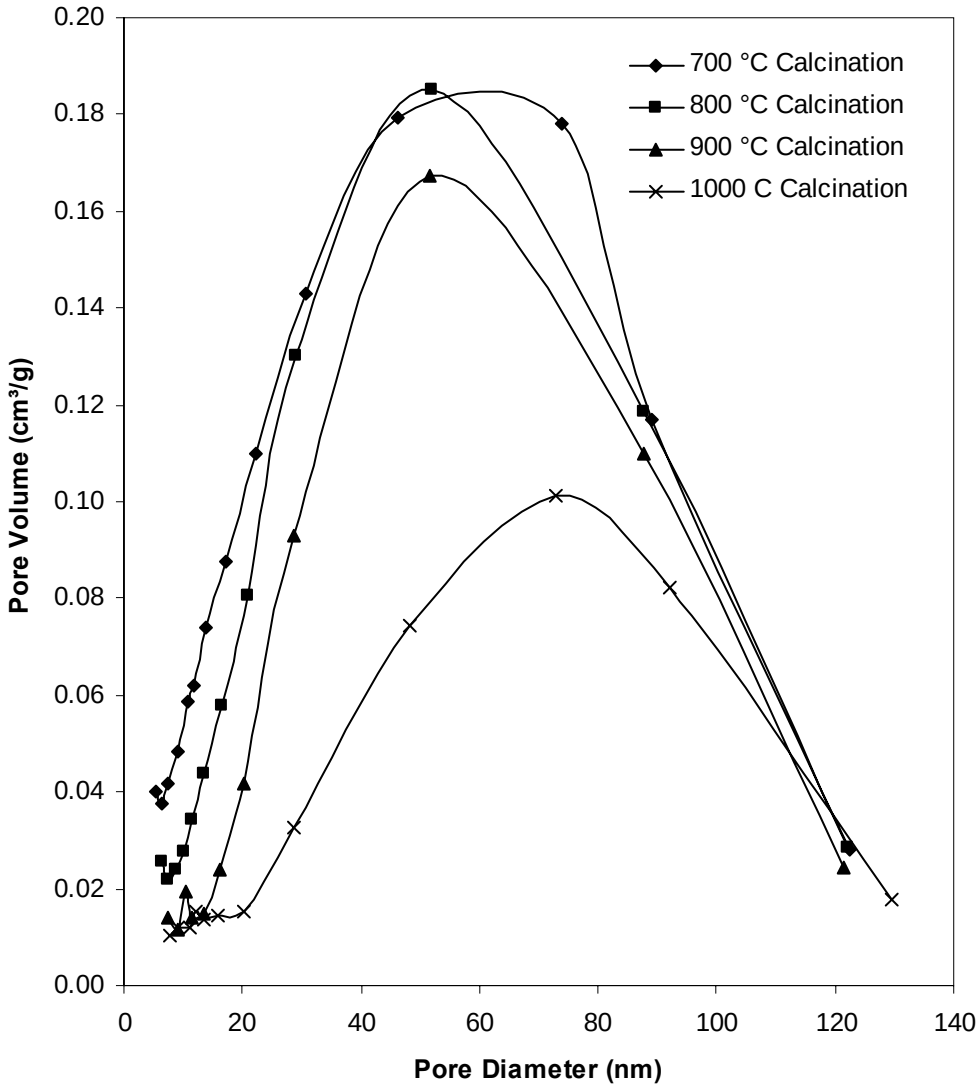

Figure 8.16 BJH pore size distribution of polymeric resin templated CZY mixed oxides during thermal aging. Samples were aged in air to the specified temperature at a heating rate of 20 ºC/min, with the final temperature being maintained for 4 h.

Conclusion

In this chapter, two different parameters were used to evaluate the catalytic performance of the CZY materials that were synthesized using different templates. In the first scenario, the synthesized CZY materials were loaded with 1 wt% Pt. The Pt loaded CZY materials are then used for emission abatement studies where the T_{50} light-off temperatures for the reactant species (NO_x, CO, and C_xH_y) were used as the performance parameter indicator. The second performance parameter used was the resistance to the loss of surface area by the support materials during accelerated thermal aging of the CZY catalyst support system.

Based on light-off temperatures, the Pt metal loaded P123 templated CZY material was found to be the most catalytically active. The trend between surface area and light-off temperature do not support this observation; however, the trend between pore size and light-off temperature do support the observation. It is important to note that catalytic activity of the polymeric resin templated CZY was comparable to those of the industry standard CZY material. The result for the industry standard CZY material was not included for proprietary reasons. The results from the accelerated aging of the CZY materials showed that the resin templated CZY had the most resistance to surface area loss during the aging process.

CHAPTER NINE

CONCLUSIONS AND RECOMMENDATIONS

The goals of this project have been two-fold. On one hand, I have sought to synthesize mesoporous ceria-zirconia-yttria mixed oxide (CZY) materials with varying pore geometries by using a variety of templating techniques. It was hoped that novel CZY materials could be prepared with a well defined 3-D mesoporous structure, exhibit high thermal stability, be low cost and easy to manufacture. I also sought to evaluate the catalytic performance of the CZY materials that were synthesized using all the various templating techniques based on light-off temperatures and thermal stability. Ultimately, the knowledge gained from the CZY mixed synthesis and characterization studies could prove useful to researchers preparing a wide variety of mesoporous oxides, especially those that will be used in high temperature applications.

Conclusion

1. With CZY materials, it was impossible to synthesize 3-D structures that have amorphous walls like the silica based materials. Thus, making CZY materials with a 3-D pore structure like MCM-41 type materials was not possible because of the crystalline nature of the mixed oxide.
2. By using soft and hard template techniques, CZY materials with definite 3-D mesoporous structure were synthesized. In general, the 3-D structures formed by the CZY materials are a combination of a number of secondary structures, as

shown in Figure 9.1. For example, the primary particles can agglomerate into closed packed type structures (see Fig. 9.1-a) as well as more open macroporous structures (see Fig. 9.1-b). The interstices between the particles that make up structures like Figure 9.1-a would give rise to small mesopores (2-10 nm diameter pores), while the trough formed in the secondary structure shown in Figure 9.1-b would yield large mesopores and macropores (20-1000 nm diameter pores).

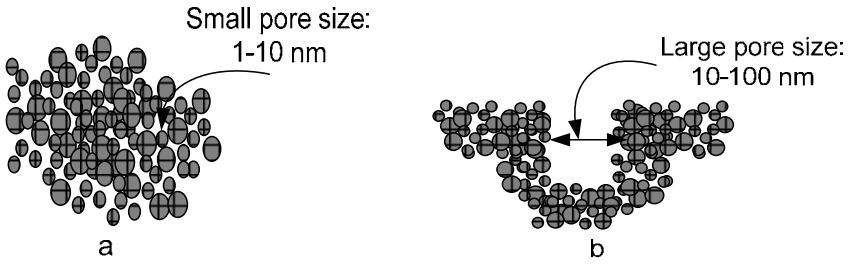

Figure 9.1 Agglomeration of oxide particles into (a) closed packed arrangement and other (b) more open secondary structures.

3. Using hard templating techniques makes it possible to have greater control over the type of particle agglomeration that would result eventually. For instance, with polymeric resin templates larger sized particles of the CZY mixed oxides can be created.
4. The similarities in the TEM images of the soft templated CZY mixed oxides suggests that the templating effect was more localized (i.e., did not participate in the formation of tertiary structures) and that the precipitation of the metal hydroxides was a process that had a very low activation barrier for it to take place.

5. The precious metal loaded CZY materials revealed that the light-off temperatures of C_xH_y, and NO_x were dependent upon pore size and to a lesser extent surface area but that of CO was independent of both the pore size and surface area.

Recommendations

1. To further slow the rate of hydrolysis and condensation during the synthesis of surfactant or block copolymer templated CZY materials, it is recommended that the samples be pre-aged at room temperature for at least 12 h before transferring into the oven for higher temperature processing for approximate 1-4 days.
2. To slow the rate of hydrolysis and condensation, other complexation agents besides acetylacetone or triethanol amine should be explored in the soft template synthesis technique.
3. Since the Pluronic P123 templated CZY material was most reactive during the catalytic activity test, I would recommend that the synthesis conditions, such as the pH, synthesis temperature, and the ratio of salts to block copolymer template, should be optimized in order to make materials with maximum surface area and optimal pore size. In addition, other types of block copolymers should be explored as SDA.
4. In order to shed more light on the effects of pore geometry on the reactivity of the CZY materials, molecular dynamics simulations studies could be used to arrive at the best geometry with the highest catalytic activity.

REFERENCE

1. Di Monte, R.; Kaspar, J. *Topics in Catalysis* **2004**, *28*, 47-57.

2. Kaspar, J.; Fornasiero, P.; Hickey, N. *Catalysis Today* **2003**, *77*, 419-449.

3. M. Mamak, N. C. G. O. *Advanced Materials* **2000**, *12*, 198-202.

4. Chen, L. B. *Surface Review and Letters* **2006**, *13*, 535-544.

5. Jung, G. B.; Lo, K. F.; Chan, S. H. *Journal of Solid State Electrochemistry* **2007**, *11*, 1435-1440.

6. Akbar, S.; Dutta, P.; Lee, C. H. *International Journal of Applied Ceramic Technology* **2006**, *3*, 302-311.

7. Lin, Y. S.; Chang, C. H.; Gopalan, R. *Industrial & Engineering Chemistry Research* **1994**, *33*, 860-870.

8. Chavan, S. V.; Mathews, M. D.; Tyagi, A. K. *Journal of the American Ceramic Society* **2004**, *87*, 1977-1980.

9. Dudek, M.; Molenda, J. *Materials Science-Poland* **2006**, *24*, 45-52.

10. Feng, R. M.; Yang, X. J.; Ji, W. J.; Au, C. T. *Materials Chemistry and Physics* **2008**, *107*, 132-136.

11. Hung, I. M.; Hung, D. T.; Fung, K. Z.; Hon, M. H. *Journal of the European Ceramic Society* **2006**, *26*, 2627-2632.

12. Pandey, R. K.; Kumar, P. *Catalysis Communications* **2007**, *8*, 1122-1125.

13. Viazzi, C.; Deboni, A.; Zoppas Ferreira, J.; Bonino, J.-P.; Ansart, F. *Solid State Sciences* **2006**, *8*, 1023-1028.

14. Crocker, M.; Graham, U. M.; Gonzalez, R.; Jacobs, G.; Morris, E.; Rubel, A. M.; Andrews, R. *Journal of Materials Science* **2007**, *42*, 3454-3464.

15 Lyons, D. M.; Ryan, K. M.; Morris, M. A. *Journal of Materials Chemistry* **2002**, *12*, 1207-1212.

16. Cai, L.; Zhao, M.; Pi, Z.; Gong, M.; Chen, Y. *Chinese Journal of Catalysis* **2008**, *29*, 108-112.

17. Martínez-Arias, A.; Fernández-García, M.; Hungría, A. B.; Iglesias-Juez, A.; Duncan, K.; Smith, R.; Anderson, J. A.; Conesa, J. C.; Soria, J. *Journal of Catalysis* **2001**, *204*, 238-248.

18. Terribile, D.; Trovarelli, A.; Llorca, J.; de Leitenburg, C.; Dolcetti, G. *Catalysis Today* **1998**, *43*, 79-88.

19. Terribile, D.; Trovarelli, A.; Llorca, J.; de Leitenburg, C.; Dolcetti, G. *Journal of Catalysis* **1998**, *178*, 299-308.

20. Wu, X.; Xu, L.; Weng, D. *Applied Surface Science* **2004**, *221*, 375-383.

21. Wu, X.; Yang, B.; Weng, D. *Journal of Alloys and Compounds* **2004**, *376*, 241-245.

22. Fornasiero, P.; Balducci, G.; Kaspar, J.; Meriani, S.; di Monte, R.; Graziani, M. *Catalysis Today* **1996**, *29*, 47-52.

23. Shelef, M.; McCabe, R. W.; Elsevier Science Bv: **2000**, 35-50.

24. C. H. Bartholomew; Farrauto, R. J. In *Fundamentals of Industrial Catalytic Processes*; 2nd Edition ed.; John Wiley-AIChE: **2006**, 714.

25. Beck, J. S.; Vartuli, J. C.; Roth, W. J.; Leonowicz, M. E.; Kresge, C. T.; Schmitt, K. D.; Chu, C. T. W.; Olson, D. H.; Sheppard, E. W.; McCullen, S. B.; Higgins, J. B.; Schlenker, J. L. *Journal of the American Chemical Society* **1992**, *114*, 10834-10843.

26. Tanev, P. T.; Pinnavaia, T. J. *Chem. Mater.* **1996**, *8*, 2068-2079.

27. Attard, G. S.; Glyde, J. C.; Goltner, C. G. *Nature* **1995**, *378*, 366-368.

28. Bagshaw, S. A.; Prouzet, E.; Pinnavaia, T. J. *Science* **1995**, *269*, 1242-1244.

29. Kim, S. S.; Pauly, T. R.; Pinnavaia, T. J. *Chemical Communications* **2000**, 1661-1662.

30. Zhang, W. Z.; Glomski, B.; Pauly, T. R.; Pinnavaia, T. J. *Chemical Communications* **1999**, 1803-1804.

31. Gao, C.; Qiu, H.; Zeng, W.; Sakamoto, Y.; Terasaki, O.; Sakamoto, K.; Chen, Q.; Che, S. *Chem. Mater.* **2006**, *18*, 3904-3914.

32. Garcia-Bennett, A. E.; Terasaki, O.; Che, S.; Tatsumi, T. *Chem. Mater.* **2004**, *16*, 813-821.

33 Mitra, A.; Bhaumik, A.; Paul, B. K. *Microporous and Mesoporous Materials* **2008**, *109*, 66-72.

34. Yokoi, T.; Tatsumi, T. *Journal of the Japan Petroleum Institute* **2007**, *50*, 299-311.

35. Yokoi, T.; Yoshitake, H.; Yamada, T.; Kubota, Y.; Tatsumi, T. *Journal of Materials Chemistry* **2006**, *16*, 1125-1135.

36. Chen, F.; Huang, L.; Li, Q. *Chemistry of Materials* **1997**, *9*, 2685-2686.

37. Chen, F. X.; Song, F. B.; Li, Q. Z. *Microporous and Mesoporous Materials* **1999**, *29*, 305-310.

38. Ohkubo, T.; Ogura, T.; Sakai, H.; Abe, M. *Journal of Colloid and Interface Science* **2007**, *312*, 42-46.

39. Zhao, W.; Kong, L.; Luo, Y. F.; Li, Q. Z. *Microporous and Mesoporous Materials* **2007**, *100*, 111-117.

40. Cho, B. K.; Jain, A.; Nieberle, J.; Mahajan, S.; Wiesner, U.; Gruner, S. M.; Turk, S.; Rader, H. J. *Macromolecules* **2004**, *37*, 4227-4234.

41. Larsen, G.; Lotero, E.; Marquez, M. *J. Phys. Chem. B* **2000**, *104*, 4840-4843.

42. Larsen, G.; Lotero, E.; Marquez, M. *Chemistry of Materials* **2000**, *12*, 1513-1515.

43. Mitra, A.; Bhaumik, A.; Imae, T. *Journal of Nanoscience and Nanotechnology* **2004**, *4*, 1052-1055.

44. Xu, Q.; Fan, H. J.; Guo, Y. Q.; Cao, Y. X. *Materials Science and Engineering a-Structural Materials Properties Microstructure and Processing* **2006**, *435*, 158-162.

45. Ryoo, R.; Joo, S. H.; Jun, S. *Journal of Physical Chemistry B* **1999**, *103*, 7743-7746.

46. Ryoo, R.; Joo, S. H.; Kruk, M.; Jaroniec, M. *Advanced Materials* **2001**, *13*, 677-681.

47. Schuth, F. *Angewandte Chemie-International Edition* **2003**, *42*, 3604-3622.

48. Behrens, P. *Angewandte Chemie-International Edition in English* **1996**, *35*, 515-518.

49. Bhattacharyya, S.; Lelong, G.; Saboungi, M. L. *Journal of Experimental Nanoscience* **2006**, *1*, 375-395.

50. Ciesla, U.; Schuth, F. *Microporous and Mesoporous Materials* **1999**, *27*, 131-149.

51. Di Renzor, F.; Galameau, A.; Trens, P.; Fajula, F. In *Handbook of Porous Solids*; Schüth, F., Sing, K. S. W., Weitkamp, J., Eds.; Wiley-VCH Verlag GmbH & Co. KGaA: Weinheim, Germany, **2002**; Vol. 3, 1311-1395.

52. Carreon, M. A.; Guliants, V. V. *European Journal of Inorganic Chemistry* **2005**, 27-43.

53. Lin, H. P.; Cheng, Y. R.; Lin, C. R.; Li, F. Y.; Chen, C. L.; Wong, S. T.; Cheng, S. F.; Liu, S. B.; Wan, B. Z.; Mou, C. Y.; Tang, C. Y.; Lin, C. Y. *Journal of the Chinese Chemical Society* **1999**, *46*, 495-507.

54. Polarz, S.; Antonietti, M. *Chemical Communications* **2002**, 2593-2604.

55. Sayari, A.; Liu, P. *Microporous Materials* **1997**, *12*, 149-177.

56. Schuth, F. *Chemistry of Materials* **2001**, *13*, 3184-3195.

57. Schuth, F. *Annual Review of Materials Research* **2005**, *35*, 209-238.

58. Valdes-Solis, T.; Fuertes, A. B. *Materials Research Bulletin* **2006**, *41*, 2187-2197.

59. Vinu, A.; Mori, T.; Ariga, K. *Science and Technology of Advanced Materials* **2006**, *7*, 753-771.

60. Yu, C.; Tian, B.; Zhao, D. *Current Opinion in Solid State and Materials Science* **2003**, *7*, 191-197.

61. Schuth, F. In *Mesoporous Crystals and Related Nano-Structured Materials* **2004**; Vol. 148, 1-13.

62. Schuth, F.; A. Galarneau, F. F. F. D. R.; Vedrine, J. In *Studies in Surface Science and Catalysis*; Elsevier: **2001**; Vol. Volume 135, 1-12.

63. Schuth, F.; Czuryskiewicz, T.; Kleitz, F.; Linden, M.; Lu, A. H.; Rosenholm, J.; Schmidt, W.; Taguchi, A. In *Nanotechnology in Mesostructured Materials* **2003**; Vol. 146, 399-406.
64. Schuth, F.; Schmidt, W. *Advanced Materials* **2002**, *14*, 629-638.

65. Lu, A. H.; Schuth, F. *Advanced Materials* **2006**, *18*, 1793-1805.

66. Wan, Y.; Yang, H. F.; Zhao, D. Y. *Accounts of Chemical Research* **2006**, *39*, 423-432.

67. Antonelli, D. M.; Ying, J. Y. *Angewandte Chemie-International Edition in English* **1995**, *34*, 2014-2017.

68. Larsen, G.; Spretz, R.; Lotero, E. *Chem. Mater.* **2001**, *13*, 4077-4082.

69. Schwickardi, M.; Johann, T.; Schmidt, W.; Busch, O.; Schuth, F. In *Scientific Bases for the Preparation of Heterogeneous Catalysts* **2002**; Vol. 143, 93-100.

70. Schwickardi, M.; Johann, T.; Schmidt, W.; Schuth, F. *Chemistry of Materials* **2002**, *14*, 3913-3919.

71. Schwickardi, M.; Spliethoff, B.; Schmidt, W.; Schuth, F. *Zeitschrift Fur Physikalische Chemie-International Journal of Research in Physical Chemistry & Chemical Physics* **2005**, *219*, 939-948.

72. Kapoor, M. P.; Raj, A.; Matsumura, Y. *Microporous and Mesoporous Materials* **2001**, *44*, 565-572.

73. Livage, J. *Journal of Solid State Chemistry* **1986**, *64*, 322-330.

74. Livage, J.; Henry, M.; Sanchez, C. *Progress in Solid State Chemistry* **1988**, *18*, 259-341.

75. Cabrera, S.; El Haskouri, J.; Guillem, C.; Latorre, J.; Beltran-Porter, A.; Beltran-Porter, D.; Marcos, M. D.; Amoros, P. *Solid State Sciences* **2000**, *2*, 405-420.

76. Thanabodeekij, N.; Sadthayanon, S.; Gulari, E.; Wongkasemjit, S. *Materials Chemistry and Physics* **2006**, *98*, 131-137.

77. El Haskouri, J.; Cabrera, S.; Caldes, M.; Alamo, J.; Beltran-Porter, A.; Marcos, M. D.; Amoros, P.; Beltran-Porter, D.; Elsevier Sci Ltd: **2001**, 1157-1163.

78. Kao, H. M.; Cheng, C. C.; Ting, C. C.; Hwang, L. Y. *Journal of Materials Chemistry* **2005**, *15*, 2989-2992.

79. Ma, Y. R.; Qi, L. M.; Ma, J. M.; Wu, Y. Q.; Liu, O.; Cheng, H. M. *Colloids and Surfaces a-Physicochemical and Engineering Aspects* **2003**, *229*, 1-8.

80. Wang, Y.; Ma, C.; Sun, X.; Li, H. *Journal of Colloid and Interface Science* **2005**, *286*, 627-631.

81. Czuryszkiewicz, T.; Kleitz, F.; Schuth, F.; Linden, M. *Chemistry of Materials* **2003**, *15*, 3704-3709.

82. Luechinger, M.; Pirngruber, G. D.; Lindlar, B.; Laggner, P.; Prins, R. *Microporous and Mesoporous Materials* **2005**, *79*, 41-52.

83. Liang, Y. C.; Anwander, R. *Microporous and Mesoporous Materials* **2004**, *72*, 153-165.

84. Namba, S.; Mochizuki, A.; Vsp Bv: **1998**, 561-570.

85. Jana, S. K.; Nishida, R.; Shindo, K.; Kugita, T.; Namba, S. *Microporous and Mesoporous Materials* **2004**, *68*, 133-142.

86. Jana, S. K.; Mochizuki, A.; Namba, S. *Catalysis Surveys from Asia* **2004**, *8*, 1-13.

87. Barrett, E. P., Joyner, L.G., and Halenda, P.H, *J.A.C.S* **1951**, *73*, 373.

88. Atribak, I.; Bueno-Lopez, A.; Garcia-Garcia, A. *Journal of Catalysis* **2008**, *259*, 123-132.

89. Hirano, M.; Suda, A. *Journal of the American Ceramic Society* **2003**, *86*, 2209-2211.

90. Noronha, F. B.; Fendley, E. C.; Soares, R. R.; Alvarez, W. E.; Resasco, D. E. *Chemical Engineering Journal* **2001**, *82*, 21-31.

91. Kramer, E.; Forster, S.; Goltner, C.; Antonietti, M. *Langmuir* **1998**, *14*, 2027-2031.

92. Matos, J. R.; Kruk, M.; Mercuri, L. P.; Jaroniec, M.; Zhao, L.; Kamiyama, T.; Terasaki, O.; Pinnavaia, T. J.; Liu, Y. *J. Am. Chem. Soc.* **2003**, *125*, 821-829.

93. S. Horiuchi, M. I. S. Y. N. *Advanced Materials* **2000**, *12*, 1507-1511.

94. Schmidt-Winkel, P.; Glinka, C. J.; Stucky, G. D. *Langmuir* **2000**, *16*, 356-361.

95. Yang, P. D.; Zhao, D. Y.; Margolese, D. I.; Chmelka, B. F.; Stucky, G. D. *Chemistry of Materials* **1999**, *11*, 2813-2826.

96. Yu, C.; Tian, B.; Fan, J.; Stucky, G. D.; Zhao, D. *J. Am. Chem. Soc.* **2002**, *124*, 4556-4557.

97. Yu, S. Q.; Zhao, R. Y.; Liu, C. G.; Guan, C. *Abstracts of Papers of the American Chemical Society* **2003**, *226*, U263-U264.

98. Yue, Y. H.; Ma, Z.; Hua, W. M.; Gao, Z. *Acta Chimica Sinica* **2000**, *58*, 777-780.

99. Zhao, D. Y.; Feng, J. L.; Huo, Q. S.; Melosh, N.; Fredrickson, G. H.; Chmelka, B. F.; Stucky, G. D. *Science* **1998**, *279*, 548-552.

100. Zhao, D. Y.; Huo, Q. S.; Feng, J. L.; Chmelka, B. F.; Stucky, G. D. *Journal of the American Chemical Society* **1998**, *120*, 6024-6036.

101. Hukkamaki, J.; Pakkanen, T. T. *Microporous and Mesoporous Materials* **2003**, *65*, 189-196.

102. Volden, S.; Glomm, W. R.; Magnusson, H.; Oslash; ye, G.; Sj; ouml; blom, J. *Journal of Dispersion Science and Technology* **2006**, *27*, 893 - 897.

103. Larsen, G.; Lotero, E.; Marquez, M. *Chemistry of Materials* **2000**, *12*, 1513-1515.

104. Blanco, J.; Petre, A. L.; Yates, M.; Martin, M. P.; Suarez, S.; Martin, J. A. *Advanced Materials* **2006**, *18*, 1162-1165.

105. Ozawa, M.; Kimura, M. *Journal of Materials Science Letters* **1990**, *9*, 446-448.

106. Cabanas, A.; Darr, J. A.; Lester, E.; Poliakoff, M. *Chemical Communications* **2000**, 901-902.

107. Deshpande, A. S.; Niederberger, M. *Microporous and Mesoporous Materials* **2007**, *101*, 413-418.

108. Shchukin, D. G.; Caruso, R. A. *Chemistry of Materials* **2004**, *16*, 2287-2292.

109. Shi, Z.-G.; Xu, L.-Y.; Feng, Y.-Q. *Journal of Non-Crystalline Solids* **2006**, *352*, 4003-4007.

110. Yan, Y. J.; Huang, Z. R.; Dong, S. M.; Jiang, D. L. *Journal of the American Ceramic Society* **2006**, *89*, 3585-3588.

111. Ulrich Schubert; Husing, N. In *Synthesis of Inorganic Materials* 2ed.; Wiley-VCH Verlag GmbH & Co. KGaA: Weinheim, Germany, **2005**, p 305-350.

112. Aneggi, E.; Boaro, M.; Leitenburg, C. d.; Dolcetti, G.; Trovarelli, A. *Journal of Alloys and Compounds* **2006**, *408-412*, 1096-1102.

113. Kim, J. R.; Myeong, W. J.; Ihm, S. K. *Journal of Catalysis* **2009**, *263*, 123-133.

114. Ranga Rao, G.; Fornasiero, P.; Di Monte, R.; Kaspar, J.; Vlaic, G.; Balducci, G.; Meriani, S.; Gubitosa, G.; Cremona, A.; Graziani, M. *Journal of Catalysis* **1996**, *162*, 1-9.

VITA

Prince Nwabueze Anyaba was born in Owerre-Olubor, Delta State, Nigeria. He received a Bachelor of Science degree with Second Class Upper Division from the University of Lagos, Lagos, Nigeria in 1998. After graduation, he performed his National Youth Service at Anglican Grammar School, Ijare, Ondo State, Nigeria where he taught Physics, Chemistry, and Mathematics to high school students for a year. In 2002, he participated in the Shell Intensive Training Program (SITP) on oil and gas for graduates with specialization in Engineering. In 2005, he began his doctoral studies in Chemical Engineering at Clemson University. His research, *Novel Techniques for the Synthesis of Three-Way Catalytic Converter Support Materials*, was conducted under the guidance of Dr. David A. Bruce.